PREFERENTIAL OXIDATION OF CARBON MONOXIDE OVER COBALT AND PALLADIUM BASED CATALYSTS SUPPORTED ON VARIOUS METAL OXIDES

By

REINECK MHLABA

[redacted]

THESIS

Submitted in fulfilment of the requirements for the degree of

DOCTOR OF PHILOSOPHY

in

CHEMISTRY

In the

FACULTY OF SCIENCES AND AGRICULTURE

(School of Physical and Mineral Sciences)

at the

UNIVERSITY OF LIMPOPO

SUPERVISOR: Prof T Magadzu

CO-SUPERVISOR: Prof TE Mosuang

2020

IN THE LOVING MEMORY OF MY YOUNGER SISTER

(Petunia Mhlaba)

DECLARATION

I declare that PREFERENTIAL OXIDATION OF CARBON MONOXIDE OVER COBALT AND PALLADIUM BASED CATALYSTS SUPPORTED ON VARIOUS METAL OXIDES is my own work and that all the sources that I have used or quoted have been indicated and acknowledged by means of complete references and that this work has not been submitted before for any other degree at any other institution.

_____ _____

MHLABA R DATE

ACKNOWLEDGEMENTS

I would like to express my sincere gratitude to the following people and institutions whose interest and financial support made it easier for me to complete this research project.

To my supervisor, Prof T Magadzu who assisted me in shaping-up the research proposal, the execution of the results as well as the writing up.

To my Co-supervisor, Prof TE Mosuang who assisted me with the interpretation of the characterisation techniques as well as the writing up.

The University of Limpopo staff development grant and the National Research Foundation (NRF) for their financial assistance.

The office of the Dean (Faculty of Science and Agriculture University of Limpopo) for assisting with the funds for characterisation of samples (with XPS and TPR technique at CSIR and MINTEK).

The office of the director (School of Physical and Mineral Sciences) for assisting with the funds for characterisation of samples (with X-ray diffraction at WITS).

To the chemistry staff members thank you for your support.

To the department of Geology and Mining (University of Limpopo, turfloop campus) for performing the XRD analysis.

To Professor Chauke thank you for your support and for assisting with the grammar.

To my family, thank you for the support that you have shown during my studies.

Last, but not least, I would like to thank God the almighty for giving me the strength and guidance to withstand all the challenges that I have encountered during my studies, and the courage to work hard.

PUBLICATIONS AND PRESENTATIONS

PUBLICATIONS:

Reineck Mhlaba, Thuto Mosuang and Takalani Magadzu, Effect of hydrazine pre-treatment on the activity, stability and active sites of cobalt species for preferential oxidation (PROX) of CO in H_2-rich stream. Chemistry 1 (2019) 164-180.

Reineck Mhlaba, Thuto Mosuang and Takalani Magadzu, The effect of MnO_2 and the Pd-MnO_2 species on the activity of cobalt species for preferential oxidation (PROX) of CO in H_2-rich stream. We are still working on it.

ORAL PRESENTATIONS:

1. R Mhlaba, TE Mosuang, and T Magadzu, ‘’*Catalytic performance of Pd/Co_3O_4 catalyst for PROX of CO in hydrogen rich stream at low temperature*’’ FSA research day at Bolivia Lodge, Polokwane: 29-30 September 2016.
2. R Mhlaba, TE Mosuang, and T Magadzu, ‘’*Catalytic performance of Pd/Co_3O_4 catalyst for PROX of CO in hydrogen rich stream at low temperature*’’ SACI north section young chemist symposium at University of Limpopo, Turffloop campus: 23 November 2016.
3. R Mhlaba, TE Mosuang, and T Magadzu, ‘’*Reductive pre-treatment of cobalt-based catalysts towards preferential oxidation (PROX) of CO in excess hydrogen*”, FSA research day at Fusion boutique, Polokwane: 20-21 September 2018.
4. R Mhlaba, TE Mosuang, and T Magadzu, ‘’*Reductive pre-treatment of cobalt-based catalysts towards preferential oxidation (PROX) of CO in excess hydrogen*”, SACI 43 national convention 2018 at CSIR-ICC Pretoria: 2-7 December 2018.

ABSTRACT

The interest on the use of proton exchange membrane (PEM) fuel cells for vehicle application has increase due to its efficiency, high power density and rapid start up. The on-board reforming process is used to generate hydrogen; however, this process simultaneously produces 1% CO which poisons Pt-based anode catalyst. Previous studies have shown that supported Pd-based catalysts have very good stability on preferential oxidation (PROX) of CO, but these catalysts suffer from lower selectivity. Metal oxides such as Co_3O_4 and CeO_2 are known to have high oxygen vacancy which promotes CO oxidation. Furthermore, the pre-treatment of the catalysts by hydrazine as well as the addition of MnO_x species have been shown to improve the surface properties of metal/metal oxides catalysts. The study envisages that the modification of PROX catalysts will improve the CO conversion and its selectivity while maintaining higher stability.

In this work, as-prepared (Co_3O_4) and hydrazine treated cobalt (Co_3O_4(H)) based catalysts were prepared by precipitation method and investigated at temperature range of 40-220 ^oC for preferential oxidation (PROX) of CO in excess hydrogen. The FTIR and XPS data of hydrazine treated Co_3O_4 does not show peak ratio differences, indicating that usual amounts of Co^{3+} and Co^{2+} were formed. An improved surface reducibility with smaller crystallite size was noted on Co_3O_4(H) catalyst, which indicate some surface transformation. Interestingly, the in-situ treatment of standalone Co_3O_4(H) decreased the maximum CO conversion temperature ($T_{100\%}$) from 160 ^oC (over Co_3O_4) to 100 ^oC. The Co_3O_4(H) catalyst showed good stability, with approximately 85% CO conversion at 100 ^oC for 21 h, as compared to fast deactivation of the Co_3O_4 catalyst. However, the Co_3O_4(H) catalyst was unstable in both CO_2 and the moisture environment. Based on the spent hydrazine treated (CoO(H)) cobalt catalyst, the high PROX is associated with the formation of Co^{3+} species as confirmed by XRD, XPS, and TPR data.

The Pd species was incorporated on different Co_3O_4 by improved wet impregnation method and this has improved the surface area of the overall catalysts. However, the presence of Pd species on Co_3O_4(H) catalyst decreased the CO conversion due to formation of moisture. Although, the Pd on Co_3O_4(H) had lower activity, the catalyst showed better stability under both moisture and CO_2 conditions at 100 ^oC for 21 h.

The 2wt.% metal oxides (MnO_2, CeO_2, Cr_3O_4, TiO_2, MgO) on cobalt, and Pd on CeO_2-Co_3O_4 and MnO_2-Co_3O_4 were prepared by co-precipitation method and the structural composition was confirmed by XRD, FTIR, XPS and TPR data. Although, 2wt.%MnO_2 on Co_3O_4(H) showed higher activity at 80 ^oC, both MnO_2 and CeO_2 improved the activity of Co_3O_4(H) at 100 ^oC. The higher activity of MnO_2 is attributed to the higher surface area of the composite catalyst, in relation to ceria composite catalyst. Although the MnO_2 species transformed the structure of Co_3O_4 by lowering the oxidation state to Co^{2+}, the spent catalyst showed transformation from Co^{2+} to Co^{3+} during PROX, as confirmed by TPR data.

Studies on the effects of CeO_2 loading on Co_3O_4 catalysts, showed an optimum activity over 2wt.%CeO_2-Co_3O_4 as compared to other ceria loadings (i.e., 3, 5, 8, 10, 15, 30wt.%CeO_2). However, upon addition of 0.5wt.%Pd species on 2wt.%CeO_2-Co_3O_4(H) composite, the activity of the catalyst decreased slightly at 100 ^oC, which could be due to a decreased surface area. Although its activity is lower, the catalyst has shown good stability in dry, moisture and CO_2 conditions at 100 ^oC for 21 h.

In addition, studies were also undertaken on the effect of MnO_2 concentration on Co_3O_4 catalysts. The data shows that 7wt.%MnO_2 species improved the activity of Co_3O_4 catalyst at 60 ^oC, however, the catalyst could not improve the activities at higher temperatures. This low activity is associated with a decrease in surface area as concentration increases. The presence of 0.5wt.%Pd species on 7wt.%MnO_2-Co_3O_4 increased the activity at 60 and 80 ^oC, which could be due to reduction of Co^{3+} to Co^{2+} in the presence of Pd, as confirmed by XPS data. The catalyst has shown good stability in dry, moisture, and CO_2 conditions at 100 ^oC for 21 h. The hydrazine treated cobalt-based catalysts in the presence of palladium and manganese oxide is the promising catalysts for proton exchange membrane fuel cells technology.

TABLE OF CONTENTS

LIST OF FIGURES

LIST OF TABLES

LIST OF ABBREVIATIONS

BET	Brunauer-Emmet-Teller
CSIR	Council for Scientific and Industrial Research
DSC	Differential scanning
EDX	Energy dispersive X-ray analysis
FTIR	Fourier transform infrared
FWHM	Full width at half maximum
GC	Gas chromatograph
h	Hour
HRTEM	High resolution transmission electron microscopy
HT-WGS	High-temperature water-gas shift
IR	Infrared spectroscopy
LT-WGS	Low-temperature water-gas shift
PEMFC	Proton exchange membrane fuel cells
PGM	Platinum group metals
ppm	Parts per million
PROX	Preferential oxidation
SEM	Scanning electron microscopy
TCD	Thermal conductor detector
TEM	Transmission electron microscopy
TGA	Thermogravimetric analysis
TPR	Temperature programed reduction
XRD	X-ray powder diffraction
XPS	X-ray photoelectron spectroscopy
WITS	University of the Witwatersrand
WGS	Water gas shift
WHSV	Weight hourly space velocity
Wt.%	Weight percentage

THESIS OUTLINE

The thesis presents the work on PROX of CO in hydrogen rich gas stream over cobalt oxide (Co_3O_4, Co_3O_4(H), CoO, CoO(H), 2wt.%M-Co_3O_4 (M = CeO_2, MnO_2, MgO, TiO_2, and Cr_3O_4), and supported Pd based catalysts. Chapter one focuses on the background, aims and objectives of the study. Chapter two present the literature survey on the activity of different catalysts in PROX of CO in hydrogen rich gas stream. The literature review based on the operation of the fuel cell. The production of H_2 through steam reformer system and the different methods for the preparation of the samples were discussed. Chapter three present the methods which were used to prepare the samples; the cobalt oxide was prepared by precipitation method, followed by hydrazine treatment. Both samples were reduced by 5% hydrogen in helium, and Pd species were introduced on the Co_3O_4 catalysts by improved wet impregnation method. The metal oxides (CeO_2, MnO_2, MgO, TiO_2, Cr_3O_4) were incorporated to the cobalt oxide by co-precipitation method. The deposition, precipitation and the co-precipitation methods were also used to introduce the Pd species on the supports.

Chapter four present results and a detailed discussion on the role of the reductive pre-treatment of $Co(OH)_2$ species using hydrazine ($N_2H_4.H_2O$), prior to formation of Co_3O_4 by calcination. A comparison with existing methods of just calcining the $Co(OH)_2$ at a specific temperature was also investigated. The study further investigated the oxidation state and structure of as-prepared and spent catalysts, to elucidate the correlation with the observed activity/selectivity. The effects of Pd on as-prepared and hydrazine treated cobalt oxide catalyst activity/selectivity in CO PROX were investigated. Furthermore, the effects of CO_2, and moisture on the stability of the catalysts were investigated in CO PROX.

Chapter five focuses on the effects of Pd and metal oxides (CeO_2, MnO_2, MgO, TiO_2, Cr_3O_4) on the as-prepared and hydrazine treated Co_3O_4 catalyst activity and selectivity. In addition, the effects of moisture, and CO_2 on the stability of the most active catalysts were also investigated.

Finally, chapter six provides the overall conclusions of the study, as well as the recommendations for future investigations.

CHAPTER 1

1. INTRODUCTION

1.1 BACKGROUND

The preferential oxidation (PROX) of CO is an important reaction which serves as a link between low-temperature water-gas shift (LT-WGS) and the proton-exchange membrane (PEM) fuel cells. It offers an economical technique for bringing down the CO concentration from 1 % to parts per million (ppm) level from a hydrogen rich stream [1]. The preferential oxidation of CO in the hydrogen rich gas is considered as the most promising and cost-effective method with a minimal loss of hydrogen, therefore, it is highly recommended to explore catalysts with excellent performance in terms of conversion and selectivity [2]. Catalysts need to offer a wide temperature range (e.g., 80 – 180 ^{o}C) for the operation, to avoid exhaustive control temperature [3]. The flow diagram of hydrogen purification by CO PROX reaction is shown in Figure 1.1.

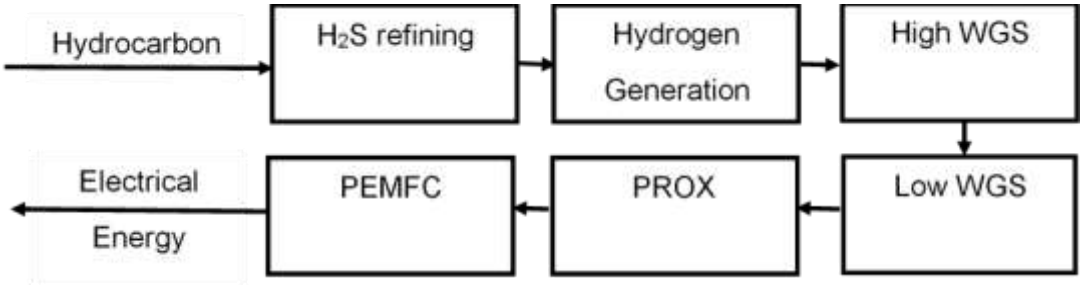

Figure 1.1 Flow diagram of hydrogen purification by CO-PROX reaction [4].

The CO oxidation is desired in PROX process (eqn. 1) while H_2 oxidation (eqn. 2) is avoided.

$$CO + ½\ O_2(g) \rightarrow CO_2 \quad (1)$$

$$H_2 + ½\ O_2 \rightarrow H_2O \quad (2)$$

For most catalysts, CO PROX is carried out in the temperature ranging from 25 to 200 ^{o}C. At higher temperatures (150 – 300 ^{o}C) oxidation may be accompanied by reverse water gas shift (eqn. 3) and/or CO methanation (eqn. 4) reactions, the latter one consuming 3 mol of H_2 for each mol of CO:

$$CO_2 + H_2 \rightarrow CO + H_2O \quad (3)$$

$$CO + 3H_2 \rightarrow CH_4 + H_2O \quad (4)$$

The disadvantage of the technology is its very strong exothermic nature, coupled with a very narrow optimal operation temperature window, and is best operated between 80 ^oC and 180 ^oC, yielding a steam loss of around 1%, it requires effective cooling. The excess dilution with nitrogen (eqn. 2) is used to minimise steam generation. Additionally, the reaction is interrupted with an intermediary cooler before proceeding to a second stage. The instrumentation and process control complexity requirements are relatively high. The advantage of this technique is the higher space velocity, which reduces the size of the required reactor. The PROX of CO is a catalytic reaction where the catalyst plays a significant role in enhancing the CO oxidation and suppressing H_2 oxidation [4-5]. A low CO concentration fuel can be achieved by synthesizing a highly active, stable, and selective catalyst for PROX reaction in H_2-rich gas mixture at the lower temperature range (80 – 120 ^oC) [6-7].

1.2 PROBLEM STATEMENT

The catalytic oxidation of carbon monoxide (CO) at low temperatures (< 100 ^oC) has attracted great attention because of its wide applications in automotive emission control, trace CO removal in the enclosed atmospheres, and CO preferential oxidation (PROX) for proton exchange membrane (PEM) fuel cells [8-9]. PROX catalysts are used for the removal of CO from fuel cell's feed gas, which is oxidised to CO_2 in the presence of hydrogen [6, 10-11]. Among various heterogeneous catalysts, noble metal catalysts such as platinum (Pt), palladium (Pd), and gold (Au) have shown excellent performance for CO oxidation at lower temperatures [6-7]. Gold-based catalysts have higher activities as compared to Pd and Pt-based catalysts, even though they suffer from poor stability and faster deactivation [10-11]. Although the activity of Pd based catalysts was lower to that of Au catalysts in the low-temperature CO oxidation, the supported Pd catalysts have shown good stability [12]. For example, recent study on 1.25wt.%Pd-5wt.%Ce/Fe$(OH)_x$ (x = 1, 2, 3, etc.) catalysts by Weiliang *et al.* [13], have shown higher stability for CO oxidation at ~40 ^oC.

The catalytic activity of Pd can be improved by the choice of the catalytic support and pre-treatment conditions (which enhances the metal-support interaction and oxygen

vacancy formation) [12, 14]. The Pd/Fe(OH)$_x$ catalysts prepared by a co-precipitation method without calcination exhibited high activity for CO oxidation at 27 ^oC [14]. This was due to a large amount of oxygen vacancies created on the surface of Fe(OH)x supports (after H_2 pre-treatment), which can act as an oxygen supply [13, 15]. However, Pd based catalysts have very low selectivity towards CO oxidation in the presence of hydrogen [16-17]. For example, the 1wt.%Pd/C catalysts showed considerably lower CO selectivity, which decreased from 32 to 23% with increasing temperature [17]. The reason for lower selectivity is that the reaction mechanism for CO oxidation over Pd/CeO_2 (without hydrogen), does not occur in exactly the same sequence in the presence of hydrogen. This is due to the formation of *β*-hydride (reaction with O_2 from both gas-phase and support sites to form water, which readily desorbed from Pd) which suppress the possibility of CO oxidation in the presence of hydrogen [16].

1.3 MOTIVATION

Research in fuel cells technology has boomed in the last decade because of the growing societal interest in energy-efficiency and environmental compatibility [18]. Among the various ranges of power demand, it is generally agreed that the earliest broad commercial adoption of fuel cell will be in transportation industries. The proton-exchange membrane (PEM) fuel cell is viewed as the most promising for these applications due to its high power density, low corrosion, rapid start-up time and low temperature operation [18-19]. An important concern for the usage of PEM fuel cells is their sensitivity to low levels (< 5 ppm) of CO. A promising method to remove trace amounts of CO (~1%) from H_2 (after hydrocarbon reforming and water-gas-shift reaction) supplied to the anode of PEM fuel cell is by preferential oxidation of CO (PROX) in the presence of excess H_2 [20]. An effective PROX catalyst should have high activity for CO oxidation as well as low activity for hydrogen oxidation, typically at low temperatures. For example, a good PROX catalyst should be able to selectively oxidize 10,000 ppm of CO to concentrations of less than 5 ppm, without decreasing the H_2 content of the reformate gas.

A finely dispersed and higher valence state of CoO_x in CeO_2 is preferable for carbon monoxide oxidation [21], ceria species promote formation of oxygen vacancies to

cobalt to retain a higher valence state of cobalt [21-22]. The metal oxides can achieve 50% conversion, with relatively low selectivity under PROX reaction at approximately 100 °C [23-24]. However, the catalyst deactivates due to surface reconstruction, which hinders the redox cycle [25-26]. Supported metal oxide catalysts such as MnO_x/Co_3O_4 have shown good PROX activity and stability (approximately 100% CO conversion) at temperatures ranging from 125 to 175 ^oC [26-27]. The use of MnO_x as promoter for Co_3O_4-CeO_2 catalysts has shown good catalytic activity/selectivity in PROX reaction at temperatures ranging from 80 to 180 ^oC, though, addition of moisture/CO_2 was unfavourable for CO removal [22]. Chang *et al.* [28], have shown that addition of a suitable amount of MgO on Au/TiO_2 might suppress H_2 oxidation and maintain CO oxidation in Au/TiO_2. Supported metal oxide catalysts such as CuO/CeO_2 have shown good PROX activity (approximately 100% CO conversion) at temperatures ranging from 110 to 160 ^oC [29-30].

Hence, the study will investigate the possibility of improving the selectivity of Pd based catalysts towards CO oxidation in the presence of hydrogen. This possibility could be achieved by using combination of metal oxides such as Co_3O_4, CeO_2, MnO_2, etc., as support materials for noble metal catalysts such as Pd [31]. This is further expected to improve the dispersity of both metal and support catalysts [32]. For example, addition of Fe into 0.8wt.%Pd/NaZSM-5 improved the dispersion of the active Pd species and 100% CO conversion temperature (T_{100}) from 180 to 47 ^oC [33].

1.4 PURPOSE OF THE STUDY

1.4.1 Aim

The aim of the study is to investigate the catalytic stability and selectivity of the cobalt and palladium-based catalysts supported on metal oxides for PROX of CO.

1.4.2 Objectives

The objectives of the study were to:

i. prepare a variety of cobalt support by precipitation method and pre-treated using either hydrazine and/or 5% H_2/He,

ii. introduce Pd species on Co_3O_4 and hydrazine treated Co_3O_4 by improved wet impregnation method,
iii. prepare 2wt.%M-Co_3O_4 (M = CeO_2, MnO_2, MgO, TiO_2, and Cr_3O_4) by co-precipitation method, and introduce Pd using different methods (improve wet impregnation, precipitation, deposition, co-precipitation) on hydrazine treated CeO_2-Co_3O_4,
iv. introduce Pd species on MnO_2-Co_3O_4 by co-precipitation method,
v. characterise all materials using the following techniques; X-ray powder diffraction (XRD), Brunauer-Emmett-Teller (BET), transmission electron microscopy (TEM), scanning electron microscopy (SEM), energy dispersive X-ray analysis (EDS), thermogravimetric analysis (TGA), Fourier transforms infrared spectroscopy (FT-IR), inductively coupled mass spectroscopy (ICP-MS), temperature programmed reduction (TPR), and X-ray photoelectron spectroscopy (XPS).
vi. evaluate the catalytic activities of all prepared catalysts for PROX of CO under H_2 rich stream within the reactor temperature range of 40 to 220 ^oC,
vii. investigate the effect of CO/O_2 ratio in CO PROX reaction,
viii. investigate the catalytic stability and effect of oxidation state of the catalysts during PROX in the presence of H_2O and CO_2 in the feed, respectively.

1.5 SCIENTIFIC CONTRIBUTIONS

The hydrazine treated catalysts such as metal oxides and palladium-based supported on cobalt will be prepared and used for preferential oxidation (PROX) of carbon monoxides in hydrogen rich gas stream. We envisage that the catalysts will be highly selective to oxidation of CO, less selective to hydrogen, and also stable at fuel cell operating temperature range (80-120 ^oC). The outcome of the study will help to promote the use of fuel cells in transportation and in the generation of electricity for the households.

1.6 ETHICAL CONSIDERATIONS

The ethical clearance is not necessary since the study does not involve the use of human specimens or animal origin.

1.7 REFERENCES

[1] M. Krumpelt, T. R. Krause, J. D. Carter, J. P. Kopasz, S. Ahmed. Fuel processing for fuel systems in transportation and portable power applications. *Catalysis Today* 77 (2002) 3-16.

[2] Z. Qu, M. Cheng, C. Sh, X. Bao. Low-temperature selective oxidation of CO in H_2-rich gases over Ag/SiO_2 catalyst. *Journal of Molecular Catalysis A: Chemical* 239 (2005) 22-31.

[3] X. Liao, W. Chu, X. Dai, V. Pitchon. Promoting effect of Fe in preferential oxidation of carbon monoxide reaction (PROX) on Au/CeO_2. *Applied Catalysis A: General* 449 (2012) 131-138.

[4] A. Mishra, R. Prasad. A Review on Preferential Oxidation of Carbon Monoxide in Hydrogen Rich Gases. *Bulletin of Chemical Reaction Engineering & Catalysis* 6 (2011) 1-14.

[5] I. López, T. Valdés-Solís, G. Marbán. An attempt to rank copper-based catalysts used in the CO-PROX reaction. *International Journal of Hydrogen Energy* 33 (2008) 197-205.

[6] M. Haruta, N. Yamada, T. Kobayashi, S. Iijima. Gold catalysts prepared by co-precipitation for low-temperature oxidation of hydrogen and of carbon monoxide. *Journal of Catalysis* 115 (1989) 301-309.

[7] C-Y. Huang, Y-Y. Chen, C-C. Su, C-F. Hsu. The clean-up of CO in hydrogen for PEMFC applications using Pt, Ru, Co, and Fe in PROX reaction. *Journal of Power Sources* 174 (2007) 294-301.

[8] S. D. Gardner, G. B. Hoflund, B. T. Upchurch, D. R. Schryer, E. J. Kielin, J. Schryer. Comparison of the performance characteristics of Pt/SnO_x and Au/MnO_x catalysts for low-temperature CO oxidation. *Journal of Catalysis* 129 (1991) 114-120.

[9] M. Haruta, S. Tsubota, T. Kobayashi, H. Kageyama, M. J. Genet, B. Delmon. Low-temperature oxidation of CO over gold supported on TiO_2, Fe_2O_3, and Co_3O_4. *Journal of Catalysis* 144 (1993) 175-192.

[10] S. Bernal, J. J. Calvino, M. A. Cauqui, J. M. Gatica, C. Larese, J. A. Perez Omil, J. M. Pintado. Some recent results on metal/support interaction effects in NM/CeO_2 (NM: noble metal) catalysts. *Catalysis Today* 50 (1999) 175-206.

[11] C. N. Costa, S. Y. Christou, G. Georgiou, A. M. Efstathiou. Mathematical modelling of the oxygen storage capacity phenomenon studied by CO pulse

transient experiments over Pd/CeO_2 catalyst. *Journal of Catalysis* 219 (2003) 259-272.

[12] M. S. Jin, J. N. Park, J. K. Shon, J. H. Kim, Z. H. Li, Y. K. Park, J. M. Kim. Low temperature CO oxidation over Pd catalysts supported on highly ordered mesoporous metal oxides. *Catalysis Today* 185 (2012) 183-190.

[13] H. Weiliang, Z. Peng, P. Xia, T. Zhicheng, L. Gongxuan. Highly active Pd/Fe based catalyst prepared with polyol-reduction method for low-temperature CO oxidation. *Journal of Environmental Chemical Engineering* 1 (2013) 189-193.

[14] B. T. Qiao, L. Liu, J. Zhang, Y. Q. Deng. Preparation of highly effective ferric hydroxide supported noble metal catalysts for CO oxidations: From gold to palladium. *Journal of Catalysis* 261 (2009) 241-244.

[15] L. Liu, F. Zhou, L. Wang, X. Qi, F. Shi, Y. Deng. Low-temperature COoxidation over supported Pt, Pd catalysts: Particular role of FeOx support for oxygen supply during reactions. *Journal of Catalysis* 274 (2010) 1-10.

[16] O. Pozdnyakova, D. Teschner, A. Wootsch, J. Kohnert, B. Stenhauer, H. Sauer, L. Toth, F. C. Jentoft, A. Knop-Gericke, Z. Paal, R. Schlogl. Preferential CO oxidation in hydrogen (PROX) on ceria-supported catalysts, part II: Oxidation states and surface species on Pd/CeO_2 under reaction conditions, suggested reaction mechanism. *Journal of Catalysis* 237 (2006) 17-28.

[17] P. V. Snytnikov, V. A. Sobyanin, V. D. Belyaev, P. G. Tsyrulnikov, N. B. Shitova, D. A. Shlyapin. Selective oxidation of carbon monoxide in excess hydrogen over Pt-, Ru- and Pd-supported catalysts. *Applied Catalysis A: General* 239 (2003) 149-156.

[18] C. Song. Fuel processing for low temperature and high temperature fuel cells challenges, opportunities for sustainable development in the 21st century. *Catalysis Today* 77 (2002) 17-49.

[19] T. V. Choudhary, D. W. Goodman. CO-free fuel processing for fuel cell applications. *Catalysis Today* 77 (2002) 65-68.

[20] O. Korotkikh, R. Farrauto. Selective catalytic oxidation of CO in H_2: Fuel cell applications. *Catalysis Today* 62 (2000) 249-254.

[21] M. Kang, M. W. Song, C. H. Lee. Catalytic carbon monoxide oxidation over CoO_x/CeO_2 composite catalysts. *Applied Catalysis A: General* 251 (2003) 143-156.

[22] Q. Guo, Y. Liu. MnOx modified Co_3O_4-CeO_2 catalysts for the preferential oxidation of CO in H_2-rich gases. *Applied Catalysis B: Environmental* 82 (2008) 19-26.

[23] D. Gu, C-J. Jia, C. Weidenthaler, H-J. Bongard, B. Spliethoff, W. Schmidt, F. Schüth. Highly ordered mesoporous cobalt-containing oxides: Structure, catalytic properties, and active sites in oxidation of carbon monoxide. *Journal of the American Chemical Society* 137 (2015) 11407-11418.

[24] L. Lukashuk, K. Föttinger, E. Kolar, C. Rameshan, D. Teschner, M. Hävecker, A. Knop-Gericke, N. Yigit, H. Li, E. McDermott, M. Stöger-Pollach, G. Rupprechter. Operando XAS and NAP-XPS studies of preferential CO oxidation on Co_3O_4 and CeO_2-Co_3O_4 catalysts. *Journal of Catalysis* 344 (2016) 1-15.

[25] J. Jansson, A. E. C. Palmqvist, E. Fridell, M. Skoglundh, L. Österlund, P. Thormählen, V. Langer. On the Catalytic Activity of Co_3O_4 in Low-Temperature CO Oxidation. *Journal of Catalysis* 211 (2002) 387–397.

[26] Q. Zhang, X. Liu, W. Fan, Y. Wang. Manganese-promoted cobalt oxide as efficient and stable non-noble metal catalyst for preferential oxidation of CO in H_2 stream. *Applied Catalysis B: Environmental* 102 (2011) 207-214.

[27] C. Liu, L. Gong, R. Dai, M. Lu, T. Sun, Q. Liu, X. Huang, Z. Huang. Mesoporous Mn promoted Co_3O_4 oxides as an efficient and stable catalyst for low temperature oxidation of CO. *Solid State Sciences* 71 (2017) 69-74.

[28] M. C. Ribeiro, G. Jacobs, U. M. Graham, K. G. Azzam, L. Linganiso, B. H. Davis. Low temperature water-gas shift: Differences in oxidation states observed with partially reduced Pt/MnO_x and Pt/CeO_x catalysts yield differences in OH group reactivity. *Catalysis Communications* 11 (2010) 1193-1199.

[29] G. Marba'n, A. B. Fuertes. Highly active and selective CuO_x/CeO_2 catalyst prepared by a single-step citrate method for preferential oxidation of carbon monoxide. *Applied Catalysis: B Environmental* 57 (2005) 43-53.

[30] X. Gong, B. Liu, B. Kang, G. Xu, Q. Wang, C. Jia, J. Zhang. Boosting Cu-Ce interaction in Cu_xO/CeO_2 nanocube catalysts for enhanced catalytic performance of preferential oxidation of CO in H_2-rich gases. *Molecular Catalysis* 436 (2017) 90-99.

[31] Y. X. Shen, G. Z. Lu, Y. Guo, Y. Q. Wang, Y. L. Guo, L. Wang, X. Zhen. An excellent support of Pd-Fe-Ox catalyst for low temperature CO oxidation: CeO_2 with rich (2 0 0) facets. *Catalysis Communication* 18 (2012) 26-31.

[32] H. J. Chun, D. B. Kim, D. H. Lim, W. D. Lee, H. I. Lee. A synthesis of CO-tolerant Na_2O_5-promoted Pt/C catalyst for direct methanol fuel cell; its physical and electrochemical characterization. *International Journal of Hydrogen Energy* 35 (2010) 6399-6408.

[33] Y. Bi, L. Chen, G. Lu. Constructing surface active centres using Pd-Fe-O on zeolite for CO oxidation. *Journal of Molecular Catalysis A: Chemical* 266 (2007) 173-179.

CHAPTER 2

2. LITERATURE REVIEW

2.1 INTRODUCTION

The Greenhouse gas emissions are ever increasing in this age where fossil fuel (gas, oil and coal) based power generations dominate. This is especially an issue when taking into consideration that the remaining reserves of oil and natural gas are rapidly dwindling as world population increases [1]. One way of combating the negative impact on the world is through the adoption of hydrogen energy generations [2]. This could be achieved through the use of hydrogen fuel cells as energy converting devices, whereby electrical and heat energy are produced in the electrochemical process with water as the only waste product [3]. Proton exchange membrane (PEM) fuel cells are ideally suitable for transport, combined heat, power, and mobile auxiliary power applications. Among the many attractive features, the high power density, rapid start up and high efficiency makes the PEM fuel cell the system of choice for the transport manufacturers [4-5]. Recent studies showed that the power densities of 680 mW cm^{-2} can be achieved for low temperature PEM fuel cells [6-7]. Though, hydrogen has high gravimetric energy density, its volumetric energy density is poor, which presents a significant barrier for the use of hydrogen for on-board fuel cells [8].

The on-board reforming of liquid fuels followed by water-gas shift (WGS) reaction is one of the alternatives source to produce hydrogen for fuel cells [9]. Generally, hydrogen can be produced from various carbon compounds, such as alkanes, alkenes, alcohols, or fossil fuel [10]. In addition to hydrogen, the reformer gas still contains a trace amount of CO (about 0.5% to 2%), which has an overwhelming effect on the energy conversion efficiency of the PEM fuel cells via CO induced poisoning of the Pt anode catalyst [11-12]. Consequently, the treatment of the hydrogen gas feed is necessary to remove the carbon monoxide for its use in the PEM fuel cell. Several methods such as hydrogen selective membranes, CO methanation, pressure swing adsorption and preferential oxidation of CO (CO PROX) have been proposed for CO removal [13].

A promising method to remove trace amounts of CO (~1%) from hydrogen rich fuel (after hydrocarbon reforming and water-gas-shift reaction) supplied to the anode of

PEM fuel cells is by preferential oxidation of CO (PROX) in the presence of excess hydrogen [14]. An effective PROX catalyst should have high activity for CO oxidation as well as low activity for hydrogen oxidation; typically, at PEM fuel cell operating temperatures of 80 to 100 ^{o}C [15-16]. For example, a good PROX catalyst should be able to selectively oxidize 10,000 ppm of CO to concentrations of less than 10 ppm, without decreasing the hydrogen content of the reformate gas [11, 14, 17]. There is a high need for an effective and cheap catalysts material for the purification of hydrogen rich stream for PEM fuel cells. The development of cheap and stable catalysts for the purification of hydrogen (through conversion of carbon monoxide (CO)), after water gas shift (WGS) reaction, is required for preferential oxidation of CO (PROX) reactions. Among various heterogeneous catalysts, noble metal catalysts such as Pt, Pd, and Au have shown excellent performance for CO oxidation at lower temperatures [18-19]. Gold-based catalysts activities seem to be superior to those of Pd and Pt-based catalysts, although they suffer from poor stability and faster deactivation [20-21]. Although the activity of Pd catalysts was lower to that of gold catalysts in the low-temperature CO oxidation, the supported Pd catalysts have shown good stability [22]. Recent studies on 1.25wt.%Pd-5wt.%Ce/Fe(OH)$_x$ catalysts by Weiliang *et al*. [23], have shown higher catalytic selectivity and stability for CO oxidation at ~40 ^{o}C. It is generally recognised that the activity of the unique performance of the catalyst is determined not only by the active component of Pd, but through interaction between Pd and support matrix of the catalyst [24-25]. Deposition of Pd stimulates the mobility of the lattice oxygen at the interface between noble metal and the support; meanwhile retaining the oxygen storage capacity of the support, which can significantly promote the catalytic activity of CO oxidation [24, 26]. Therefore, the geometric structure of the support and the dispersion of Pd nanoparticles are the key factors for highly efficient catalyst for low temperature CO oxidation [27].

The catalytic activity of Pd can be improved by the choice of the catalytic support and pre-treatment conditions, which enhances the metal-support interaction and oxygen vacancy formation [22, 28]. For example, the Pd/Fe(OH)$_x$ catalysts prepared by a co-precipitation method without calcination exhibited high activity for CO oxidation at 27 ^{o}C [28]. This was due to a large amount of oxygen vacancies created on the surface of Fe(OH)$_x$ supports (after H_2 pre-treatment); which can act as an oxygen supply [23, 29]. Luo *et al.* [30], have shown that a Co_3O_4/CeO_2 catalyst performance is further

promoted by a small amount of Pd, as a result, a remarkable improvement in CO oxidation activity is achieved even at room temperature.

However, Pd based metal catalysts have very low selectivity towards CO oxidation in the presence of hydrogen [31-32]. Zlotea *et al.* [33], have inferred an absorption of hydrogen in Pd (solid solution and hydride) as well as nano-size to induced hydrogen absorption into non-absorbing element, Ir (solid solution) in the case of supported catalysts. The adsorbed hydrogen in the nanoparticles modifies the active phase, which may promote or have detrimental effects on the catalytic performance [34-35]. The Pd nanoparticles have poor catalytic activity in PROX reaction due to formation of aggregates on the surface of the catalyst [36]. However, the overall hydrogen sorption capacity decreases strongly for Ir-Pd nano alloys as compared to pure Ir and Pd nano-particles. The Ir-Pd nanoparticles retain high activity of Pd in H_2 free CO and O reaction oxidation while preventing bulk hydrogen dissociation which result in hydride formation, which is detrimental to PROX reaction [33].

The preparation method can significantly influence the structural properties of catalysts, such as surface area, crystallite size, interface contact active component dispersion and the strength of interaction which in turn determine the redox properties and reactivity of the final catalysts [37-38]. The preparation of Pd/CeO_2 by improved wet impregnation method increased the surface area and dispersion of Pd species on the support [27]. The preparation of the noble metal catalysts by polyol reduction method showed higher dispersion and uniform size compared to the routine method (such as incipient-wetness impregnation method) [39]. Addition of Fe into 0.8wt.% Pd/NaZSM-5 improves the dispersion of the active Pd species and 100% conversion temperature (T_{100}) for CO oxidation decreased from 180 to 47 ^oC [40]. Studies on the improvement of Pd based catalysts for CO oxidation in the presence of hydrogen rich gas stream at low temperature (<100 ^oC) are limited. The inexpensive metal oxide support, such as Co_3O_4 has exhibited high catalytic activities in PROX reaction (in excess H_2) over a wide temperature range [41-42]. The Co_3O_4 has mixed oxidation states of Co^{2+} and Co^{3+}, and Co^{3+} has been reported to be more active than Co^{2+} for CO adsorption and oxidation. Omata *et al.* [43], inferred that the main factor that determines the activity and the selectivity of CO oxidation in the presence of H_2 is Co^{3+} on the surface of the catalyst. As a result, the catalytic activity is strongly dependent

on the exposed crystal facets, morphology or the amount of exposed Co^{3+} on the surface, and the crystal sizes [44-45]. The activity of the metal oxide catalysts depends on the CO adsorption strength, and the barrier of CO reacting with lattice oxygen (and redox capacity). Among metal oxides, Co_3O_4 is found to be the most active one, certifying all the three requirements [45]. The low-temperature activity of mesoporous Co_3O_4 was found to depend critically on the pre-treatment temperature, being the highest when the catalyst was pre-treated in 8%O_2 (balanced with He) at 300-500 ^oC [46]. However, the fundamental reasons for the pre-treatment temperature dependence of catalytic activity are not clear.

The finely dispersed and higher valence state of CoO_x in CeO_2 is preferable for carbon monoxide oxidation [47], ceria species promote formation of oxygen vacancies to cobalt to retain a higher valence state of cobalt [47-48]. In the process, oxygen vacancies are created in the ceria lattice. Guo *et al.* [48], have shown that interaction between Co_3O_4 and CeO_2 results in finely dispersed and high valence state of cobalt oxides species. This has contributed to higher PROX activity of Co_3O_4-CeO_2/MnO mixed oxides catalysts. Studies done using CoO_x/CeO_2 composite have resulted in a good synergy catalyst which is resistant to water vapour poisoning in CO oxidation [47].

2.2 THE PROTON EXCHANGE MEMBRANE (PEM) FUEL CELL

The PEM fuel cell was first discovered in the 1960s and was used as an auxiliary power source in the Gemini space flights [7]. Subsequently, advances in this technology were stagnant until the late 1980s when the fundamental design underwent significant reconfiguration. New fabrication methods, which have now become conventional, were adopted and optimised to a high degree. The application barrier of PEM fuel cells has to overcome the costly amount of platinum which is used as catalyst [49]. The low temperature PEM fuel cells appear to be the most suitable and commercially viable hydrogen-based fuel cell systems for static and mobile applications [7]. It has the ability to operate at lower temperature (> 90 ^oC) with fast start-up time, high current density, and it is most suitable for mobile and automotive sectors [50]. Under normal circumstances, pure hydrogen is the ideal fuel for an anode of PEM fuel cell (Figure 2.1) [51], though alternative sources are being considered. In

the case of mobile energy sources, it is not safe to store pure hydrogen on board the vehicle [52]. Figure 2.1 presents the typical PEM fuel cell system.

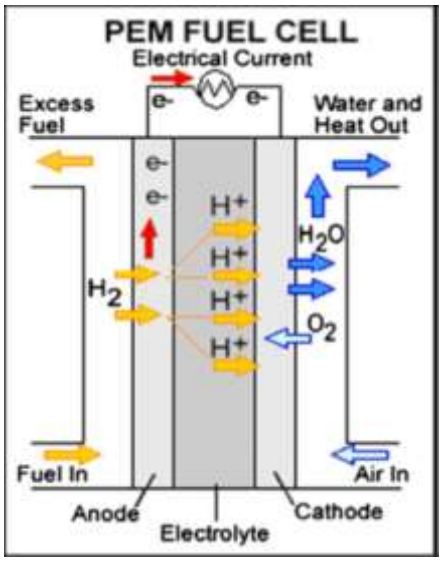

Figure 2.1 A schematic representation of a PEM fuel cell [7].

2.3 STEAM REFORMER OF HYDROCARBONS

Steam reforming has been a well-established process in the industry for more than 70 years, and it will play an important role in future applications related to a new hydrogen economy. There is also a fast growing need for more hydrogen production capacity in refineries, as the hydrogen production is low, which means that more hydrogen has to be produced at refinery or being imported [53]. Small-scale reformers for hydrogen production through steam reforming of methanol can provide an alternative solution to the demand of continuous supply of hydrogen gas for the operation of a proton exchange membrane (PEM) fuel cell [54-55].

Fuel cells need a continuous supply of hydrogen gas for their operation in portable devices. Micro reactors are used to convert hydrocarbon fuels into hydrogen gas which can be delivered to a PEM fuel cell to produce electric power. Fuel reforming on methane (CH_4), natural gas, methanol (CH_3OH) and other hydrocarbons has been a popular area of research in the recent years [54-56]. Methanol is a highly suitable liquid fuel for on board production of hydrogen, offering a high hydrogen carbon ratio (H/C),

exists as a liquid at room temperature, is biodegradable, free from sulphur, absence of C-C bonds and its reactivity allowing reformation at relatively lower temperatures (200 – 350 ^{o}C). In steam reforming, steam reacts with the feedstock in a set of reactions to produce mainly hydrogen, carbon dioxide, and carbon monoxide. The process is typically carried out in the presence of metal oxide catalyst at temperatures ranging from 195 to 260 ^{o}C [57-58]. The chemical reactions which take place during reforming process are summarised below;

$$CH_3OH + H_2O \xleftrightarrow{K_D} CO_2 + 3H_2 \qquad \Delta H^{o}_{298} = +49.4\,KJ\,mol^{-1} \qquad (1)$$

$$CH_3OH \xleftrightarrow{K_B} CO + 2H_2 \qquad \Delta H^{o}_{298} = +90.0\,KJ\,mol^{-1} \qquad (2)$$

$$CO + H_2O \xleftrightarrow{K_{WGS}} CO_2 + H_2 \qquad \Delta H^{o}_{298} = +41.1KJ\,mol^{-1} \qquad (3)$$

The low cracking temperature of methanol results in lower carbon monoxide (CO) emissions which is quite important for the operation of fuel processors [4-5]. The reformers can be attributed to small volume, small weight, low cost, long lifetime, low by product (CO), ease of manufacture, low flow resistance, low thermal resistance and short start-up time [4-5, 11-12]. Figure 2.2 shows the configuration and photograph of the assembled tubular packed bed reformer.

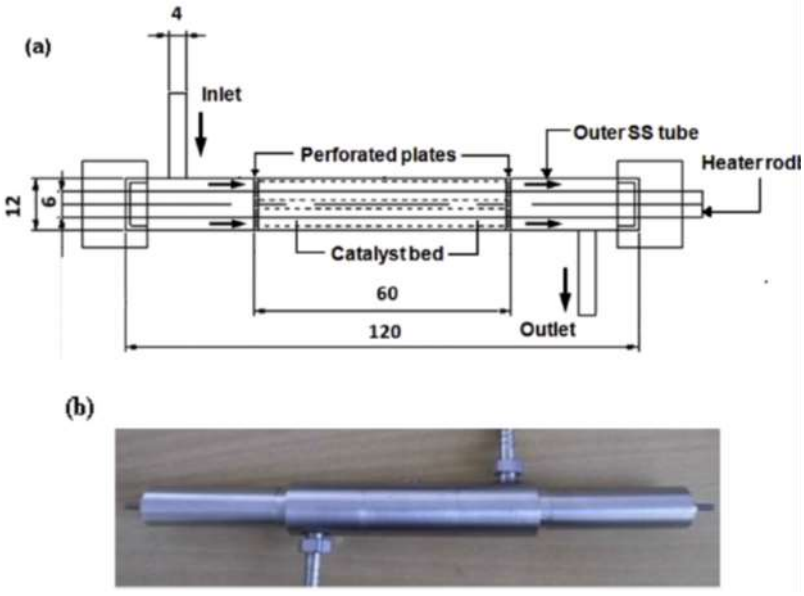

Figure 2. 2 (a) Configuration of the tubular packed bed reformer, **(b)** Photograph of the assembled reformer tube [54].

2.4 WATER-GAS SHIFT REACTION

Water-gas shift (WGS) reaction is traditionally used for production of hydrogen (H_2) from synthesis gas which is mainly used for industrial application such as ammonia production of fertilizer, petroleum refineries for a variety of operations and recently used as fuel for power generation and transportation [59-60]. The use of gasification for power generation has also increased the use of water gas shift reactors [60]. The water-gas shift (WGS) reaction is the reversible reaction of carbon monoxide with steam, leading to carbon dioxide and hydrogen, according to the reaction:

$$CO + H_2O \leftrightarrow CO_2 + H_2 \qquad -41.2 \text{ kJ mol}^{-1} \qquad (4)$$

The WGS reaction is particularly important for the utilization of the low H_2 to CO ratio syngas obtained from steam reforming or oxidation of hydrocarbons to increase the yield of the hydrogen. In recent years, there has been some interest in this reaction because of its potential use in H_2 based fuel cells for mobile and stationary applications [61]. The WGS can only reduce the level of CO from steam reformer to about 0.5-1% that poison the Pt catalyst at the anode of the fuel cell. It is then necessary to reduce the CO concentration to an acceptable level of 10 ppm [11, 17]. The promising technological solution is based on the process of catalytic preferential oxidation (PROX) of carbon monoxide [14].

2.5 PREFERENTIAL OXIDATION OF CARBON MONOXIDE

The preferential oxidation of CO in the hydrogen rich gas is considered as the most promising and cost-effective method with a minimal loss of hydrogen, therefore, it is highly recommended to explore catalysts with excellent performance in terms of conversion and selectivity [62]. It is important for catalysts to offer a wide temperature range for the operation in order to avoid exhaustive control temperature. For example, Pt supported on ceria-zirconia oxides at 10 ^oC has a maximum CO conversion. Another consideration is that when adsorption processes occur on the metal surfaces, CO is strongly adsorbed than H_2. Catalysts that are active at low temperatures are preferred in order to ensure acceptable selectivity towards CO_2 instead of H_2O [63].

Qu *et al*. [64], have shown that CO conversion increases with increasing oxygen concentration over Ag/SiO_2 catalyst. However, CO is not completely removed even in

case of 3% oxygen in the feed gas. Selectivity at low temperature does not change, but above 45 ^{o}C the selectivity decreases with an increase in O_2 gas. The same behaviour was reported when Au/TiO_2 was used as a catalyst for CO conversion, the catalyst is active at 25 ^{o}C and the activity decreases at temperature above 50 ^{o}C [65]. Au/TiO_2 has high oxidation to CO with low selectivity to O_2 [66]. Chang *et al.* [61], have shown that addition of a suitable amount of MgO on Au/TiO_2 might suppress H_2 oxidation and maintain CO oxidation in Au/TiO_2. Supported metal oxide catalysts such as CuO/CeO_2 have shown good PROX activity (approximately 100% CO conversion) at temperatures ranging from 110 to 160 ^{o}C [67-70]. It has been shown that CoO_x/CeO_2 catalysts can achieve approximately 100% CO conversion under a wide temperature range (125 to 200 ^{o}C) depending on weight hourly space velocity (WHSV) and O_2 concentration [16, 71]. The H_2 concentration has an effect on the CO oxidation rate at temperature ranging from 175 to 225 ^{o}C, and the O_2 to CO_2 selectivity decreased, which suggest that H_2 competes with CO for adsorption sites [71].

Cobalt-based catalysts such as CoO and Co_3O_4 (as standalone catalysts) have recently attracted a significant amount of interest from the scientific community, due to their promising activities in the absence [72] and presence of hydrogen [42, 73]. The CoO has exhibited good catalytic activities in PROX reaction (in excess H_2) over a wide temperature range, as compared to other transition metal oxides [73]. Such PROX activity was reported to be influenced by the tetrahedrally coordinated Co^{2+} species [73], although no supporting evidence was provided. In the absence of hydrogen, the high CO oxidation activity is attributed to the surface oxidation of octahedrally coordinated Co^{2+} species within the CoO structure [73]. The metal oxide was able to achieve 50% conversion, with relatively low selectivity under PROX reaction at approximately 100 °C [72-73]. Furthermore, the catalyst deactivates due to surface reconstruction, which hinders the redox cycle [74-75]. Supported metal oxide catalysts such as MnO_x/Co_3O_4 have shown good PROX activity and stability (approximately 100% CO conversion) at temperatures ranging from 125 to 175 ^{o}C [75-76]. The use of MnO_x as promoter for Co_3O_4-CeO_2 catalysts has shown good catalytic activity/selectivity in PROX reaction at temperatures ranging from 80 to 180 ^{o}C, though, addition of moisture/CO_2 was unfavourable for CO removal [48]. Liu *et al.* [76], have shown that the dope of appropriate amount of Mn species causes the formation of smaller sold solution particles and disorder in the spinel structure of cobalt oxide,

which result to formation of active oxygen sites. Supported MnO_x/Co_3O_4 catalysts prepared by co-precipitation method showed an improved catalytic activity and stability in PROX of CO, however, addition of moisture/CO_2 decreased the selectivity of the catalyst at temperatures less than 150 ^oC [75]. Other researchers have reported a good catalytic activity of approximately 75% CO_2 selectivity (at 80 to 120 ^oC) over bimetallic Ru-Pd/CeO_2-MnO_x catalyst [77].

The prepared catalysts can effectively weaken the adsorption of CO on Pt atoms and accelerate the adsorption of O_2 on the active sites, resulting in the high PROX activity at low temperatures. The catalytic features like low-temperature performance, stability and reproducibility are still insufficient. Thus, a highly active and stable catalyst is still required to remove CO from the H_2 rich gas stream before it reaches the PEM fuel cell [78].

2.6 EFFECT OF CO_2 AND H_2O IN THE FEED

Pack *at el.* [79], have proposed in their analysis of CuO-CeO_2 temperature programmed desorption (TPD) studies, that the main cause for the decrease in catalytic activity with CO_2 and H_2O in the feed is related to competitive CO and CO_2 adsorption as well as blockage of active sites by water at lower reaction temperature. Consequently, an increase in temperature promotes CO oxidation [80].

2.7 INCORPORATION OF PROMOTER FOR ACTIVATION OF O_2 IN CO OXIDATION

The direct way to realize the dual-site reaction pathway is to incorporate some metal or metal oxide, which are capable of oxygen (O_2) splitting. The reported formulations include CeO_3/Pt/Al_2O_3 [81], SnO_x-Pt/Al_2O_3 [82], etc. Compared with the supported monometallic Pt catalysts, the light-off temperatures are shifted to a lower range over the promoted systems in a normal CO oxidation reaction, which substantiates the contribution of activated O_2. However, CO cannot be completely removed at low temperature [32]. Further efforts have been made to prepare bimetallic system with uniform composition between Pt and promoters, to improve the cooperative effects between CO adsorption and O_2 activation sites [83]. For example, the samples which

were prepared by using organometallic precursors (Pt_5Fe_2(1.5-cyclooctadiene) $(CO)_{12}$ or $PtFe_2$(1.5-cyclooctadiene) $(CO)_8$)), the cluster derived 1wt.% $PtFe_2/SiO_2$ catalysts show a relatively uniform Fe: Pt composition and particle-size distribution. This resulted in higher activity and selectivity than the 1wt.% Fe-Pt/SiO_2 catalyst prepared by the incipient wetness impregnation methods [84].

2.8 PREPARATION METHODS OF CATALYSTS

The preparation methods have a significant effect on the structural properties of the catalysts, such as surface area, particle size, active component dispersion and strength of interaction. Hence, the preparation method determines the redox properties and the reactivity of the final catalyst [10, 38]. Zhao *et al.* [85], have shown that the performance of the supported Co_3O_4, MnO_2 and CeO_2 catalysts on activated carbon is significantly dependent on the loading method. Choosing the most suitable preparation method and pre-treatment conditions (pH, calcination temperature, etc) at the beginning of the study is a very important step. Different types of catalysts have been prepared for different reaction systems [86-87].

Palladium (Pd) is one of the most active metals for interacting with the surface of oxides as supports. According to some studies, the catalytic activity of Pd/TiO_2 catalysts depends on both the Pd crystallite size and morphology, where these catalysts with highly dispersed small Pd particles have shown to be more active concerning the strong metal-support interaction (SMSI) [88-89]. The strong interaction between the metal and support facilitates reversible spill over of the activated oxygen. They also play a crucial role in overcoming kinetic barriers to oxidation of noble metal nanoparticles at lower temperature [90].

Molina *et al.* [91], have observed higher dispersion on samples prepared by ion exchange (even at higher load) with a smaller particle size (~4-5 nm), therefore, a sample with higher surface area was obtained. The samples prepared by impregnation had higher particle size (~15-30 nm) and small surface area. In both cases, a fairly homogeneous particle size distribution was observed.

Nanostructured metal oxides and silicates are increasingly applied in catalysis, either as supports or as active species in heterogeneous catalysts, this is due to the

physicochemical properties that typically distinguish them from bulk oxides, such as higher surface area and a larger fraction of coordinatively unsaturated sites at their surface [92]. For catalytic purposes, it is generally important to optimise the exposed surface area of active sites, as a result, one has to control the degree of aggregation of the colloidal particles [93-94]. These suspensions are metastable thermodynamic systems and various operating parameters have a strong influence on the physical stability of the sol: ionic strength, addition of a stabilising agent (surfactant, polymers, and complexant), the pH of the medium, and temperature. Aggregation occurrences (or disaggregation which is generally the objective for catalytic applications), are closely related to the solubility of the oxide phase in the medium. Experimental data clearly shows that isolated particles are more easily obtained for pH conditions where solubility of the oxide solid phase is not zero. On the other hand, aggregation is more favoured when solubility of the solid phase is very low. For example, isolated PdO particles can be obtained for an acidic pH (with a re-acidification at pH < 2), whereas highly aggregated PdO particles are observed for basic pH (typically pH > 12), resulting in a low solubility of PdO. In this case, physical phenomena like electrostatic interaction seem to play a minor role with respect to chemical solubility. Variation of the pH, which is the driving force for the repulsive interaction between particles (2.5 for the acidic medium when pH = 2 and 7.5 in basic medium when pH = 12), and the ionic strength values are not able to explain the aggregation-disaggregation process [93]. The increased pH of the reaction medium promotes processes of oxidation of the reduced cobalt catalysts to form low activity cobalt hydroxide and makes them prevailing ones [95].

The morphologies and the crystallite size of the catalysts changes with an increase in the synthesis pH conditions. Mate *et al.* [96], have observed a change in the morphology of the Co_3O_4 with synthesis pH, they observed a nano-rod shape at pH 8 with a length of 10-20 nm. A change from pH 8 to 10 has resulted to the fusion and agglomeration of the rods. A further increase to pH 12, resulted to a growth of particle size in the range of 20-80 nm due to enhance agglomeration. As a result, a decrease in surface area (110-58.4 m^2g^{-1}) is observed; whereas an increase to pH 14 resulted to an increase in surface area (121.6 m^2g^{-1}) due to an increase in –OH group which might restrict aggregation of primary particles. However, an enhanced size of 25-30 nm with rather ellipsoidal-shape particles is obtained.

According to Schiavi *et al.* [97], as cobalt ion concentration (to 0.2 M) is increased the cobalt structure transforms to round nanoparticles covered by nanoflakes. Nanoflakes are formed by precipitation of cobalt hydroxide. The precipitation is induced by the pH increase that accompanies the reduction of water catalysed by cobalt nano-particles. The influence of cobalt ion concentration could be qualitatively explained by analysing the evolution of pH and cobalt ion concentration at the surface of an isolated particle (that is, in absence of overlapping diffusion layers) growing under three-dimensional mixed kinetic-diffusion control.

Calcination temperature and time also have an influence in the morphology, surface area, crystallite size of a catalyst, as well as the catalytic activity of the catalysts [98-99]. For example, Umegaki *et al.* [100], have reported good catalytic activity of Co_3O_4 catalyst calcined at 623 K, however, an increase in the calcination temperature decreased the activity of the catalyst, which was reported to be due to a decrease in the amount of surface Co^{3+} species. A decrease in catalytic activity of Co_3O_4 catalyst in liquid phase oxidation of lignin model substrates was observed due to reduction in surface areas by half (from 194.9 to 95.9 m^2g^{-1}), increase in crystallite size from 8 to 13 nm with an increase in calcination time from 1 to 6 h [98].

2.8.1 Precipitation method

Precipitation method is one of the most widely employed method to obtain man-sized materials, it is cheap and easy to scale-up for industrialisation production and commercialisation [101]. The method does not need special conditions like high temperature, special surfactant or temperature and pressure controlling [102]. Cobalt oxide catalysts prepared by precipitation method have been widely reported in methane combustion. Moreover, the parameters in the preparation process also have an important effect on the microstructure of the catalyst. Pu *et al.* [101], prepared a series of Co_3O_4 catalysts at different pH by precipitation method, and found that the aging times have a greater influence on the surface properties. As a result, aging time had a significant effect on the catalytic performance and stability of the catalyst.

2.8.2 Hydrothermal method

The hydrothermal method is one of the simplest and least expensive methods for preparation of man-size transition metal oxides with a relatively high specific surface area at low temperature (~100 to 250 ^{o}C) and higher pressure [103-104]. Nassar *et al.* [105], has synthesised cobalt carbonates microspheres in high yields by using a free-surfactant hydrothermal reaction of cobalt acetate ammonium carbonate as cheap carbonate source at 120 ^{o}C for 5 h (with 1:3, Co^{2+}: Co^{3+} mole ratio). The decomposition of the cobalt carbonates at 300 ^{o}C, formed pure Co_3O_4 spinel phase nanoparticles with 25 nm crystallite size. Generally, this methodology can as a whole be utilised in preparing other metal carbonates and their metal oxides.

2.8.3 Sol gel method

The sol-gel method is the simplest and has the ability to control the particle size and morphology through systematic monitoring of reaction parameters [106]. The process of sol-gel synthesis starts with hydrolysis and condensation step leading to the formation of a colloidal solution. Upon further condensation, the sol evolves into an integrated network per pore where solvent molecules are trapped. The gelation is generally followed by aging and drying (Figure 2.3) [107].

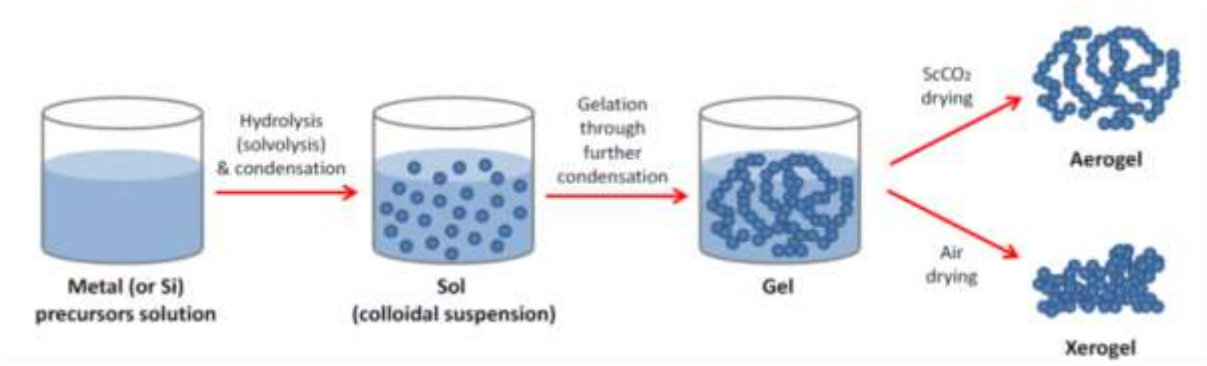

Figure 2. 3 General scheme of a sol-gel synthesis method [107].

Sol-gel method intends to desirably control the dimensions of a material on a nanometer scale from the initial stages of processing. Chemical processing, controlled

high purity, and better homogeneity can be used to enhance the property of the materials. This lower temperature processing technique is a major advantage over the conventional techniques of the nanoparticle synthesis [92]. An adequate mixing of the reaction mixture was identified as a crucial requirement for the scale-up of a sol-gel synthesis via the benzyl alcohol route. A yield of up to one gram of single-phase, highly monodisperse, and highly crystalline Co_3O_4 nanoparticles can be obtained in the developed synthesis procedure. Bubbling gas through the reaction emulsion provides sufficient mixing of the emulsion (i.e. prevents separation of the different phases and ensures the availability of water), which is identified as an oxygen source for full oxidation to Co_3O_4. An increase in the reaction temperature or the concentration of cobalt precursor can increase the crystallite sizes of cobalt oxide. However, the amount of water, associated with the additive $NH_4OH(aq)$, is the most potent parameter for size control and allows for the synthesis of highly monodisperse Co_3O_4 in the crystallite size range of 3 to 10 nm [108].

2.8.4 Deposition precipitation method

The use of deposition-precipitation method (DP) in catalyst preparation was discovered in the mid 1980's [109]. Schwarz *et al.* [110], achieved higher dispersion and homogeneous deposition of nickel on copper even at high metal load, due to the occurrence of strong precursor- support interactions. The precipitation method plays a major role in controlling the precipitates particles size and their distribution. However, this method is based on the use of precipitation combined with deposition from a liquid medium [109-110]. The method involves two processes: (i) precipitation process, it is the creation of a solid from bulk solutions or from pore fluids depending upon sufficient force of gravity (settling) to bring the solid particles together; (ii) deposition process, it is interaction of the precipitate particles with the support surface [110]. The affinity can be beneficial to the properties of homogeneously precipitated catalysts resulting in increased dispersion, improved stability against sintering and higher activity [109].

2.8.5 Impregnation method

The mounting of dissolved aqueous precursors on the oxide supports are generally accomplished by impregnation method. The volume of precursor of the active element of the catalyst is contacted with the solid support. The process is called incipient

wetness if the volume of the solution is equal to the volume of the support. When the strength of interaction between the active precursor in solution and the support is weak, the method of incipient wetness impregnation may be followed by drying to apply high loading of precursor. The maximum load depends on the solubility of the precursor in the pore filling solution, and the increase in the weight load requires higher concentration of the precursor. However, reagents such as $Ni(NO_3)_2$, results in lower solution pH and in turn cause support disruption, and substitution of ions into the support lattice. The homogenous distribution of the impregnated species on the support is usually achieved through drying of the catalyst [109].

2.9 REFERENCES

[1] C. Hui-Ming, Y. Quan-Hong, L. Chang. Hydrogen storage in carbon nanotubes. *Carbon* 39 (2001) 1447-1454.

[2] A. Mishra, S. Banerjee, S. K. Mohapatra, O. A. Graeve, M. Misra. Synthesis of carbon nanotube-TiO_2 non-tubular material for reversible hydrogen storage. *Nanotechnology* 19 (2008) 445-607.

[3] R. Orináková, A. Orinák. Recent applications of carbon nanotubes in hydrogen production and storage. *Fuel* 90 (2011) 3123-3140.

[4] C. Song. Fuel processing for low temperature and high temperature fuel cells challenges and opportunities for sustainable development in the 21st century. *Catalysis Today* 77 (2002) 17-49.

[5] T. V. Choudhary, D. W. Goodman. CO-free fuel processing for fuel cell applications. *Catalysis Today* 77 (2002) 65-68.

[6] S. Litster, G. McLean. PEM fuel cell electrodes. *Journal of Power Sources* 130 (2004) 61-76.

[7] C-C. Chen, M-S. Jeng, C-H. Leu, C-C. Yang, Y-L. Lin, S-C. King, S-Y. Wu. Low level CO hydrogen-rich gas supplied by a methanol processor for PEMFCs. *Chemical Engineering Science* 66 (2011) 5095-5106.

[8] H. T. Hwang, A. Varma. Hydrogen storage for fuel cell vehicles. *Current Option in Chemical Engineering* 5 (2014) 42-48.

[9] Y. Chen, H. Xu, Y. Wang, X. Jin, G. Xiong. Hydrogen production from liquid hydrocarbon fuels for PEMPFC application. *Fuel Processing Technology* 87 (2006) 971-978.

[10] A. Luengnaruemitchai, S. Chawla, R. Wanchanthuek. The catalytic performance of Au/La-CeOx catalyst for PROX reaction in H_2 rich stream. *International Journal of Hydrogen Energy* 39 (2014) 16953-16963.

[11] G. Sedmak, S. Hocevar, J. Levec. Kinetics of selective CO oxidation in excess of H_2 over the nanostructured $Cu_{0.1}Ce_{0.9}O_{2-y}$ catalyst. *Journal of Catalyses* 213 (2003) 135-150.

[12] H. Wang, H. Zhu, Z. Qin, F. Liang, G. Wang. Deactivation of Au/CeO_2-Co_3O_4 catalyst during CO preferential oxidation in H_2-rich stream. *Journal of Catalysis* 264 (2009) 154-162.

[13] J. D. Morse. An integrated microfluidic self-regulating and self-circulating hydrogen for fuel cells. *International Journal of Energy Resources* 31 (2007) 576-602.

[14] O. Korotkikh, R. Farrauto. Selective catalytic oxidation of CO in H_2: Fuel cell applications. *Catalysis Today* 62 (2000) 249-254.

[15] M. Watanabe, H. Uchida, K. Ohkubo, H. Igarashi. Hydrogen purification for fuel cells: Selective oxidation of carbon monoxide on Pt-Fe/zeolite catalysts. *Applied Catalysis B: Environmental* 46 (2003) 595-600.

[16] A. Arango-Diaz, J. A. Cecilia, J. Marrero-Jerez, P. Nuñez, Jiménez-Jiménez, E. Rodríguez-Castellón. Freez-dried Co_3O_4-CeO_2 catalysts for the preferential oxidation of CO with the presence of CO_2 and H_2O in the feed. *Ceramics International* 42 (2016) 7462-7474.

[17] J. W. J. Park, H. Jeong, W. L. Yoon, C. S. Kim, D. K. Lee, Y. Park, Y. W. Rhee. Selective oxidation of CO in hydrogen-rich stream over Cu-Ce catalyst promoted with transition metals. *International Journal of Hydrogen Energy* 30 (2005) 209-220.

[18] M. Haruta, N. Yamada, T. Kobayashi, S. Iijima. Gold catalysts prepared by co-precipitation for low-temperature oxidation of hydrogen and of carbon monoxide. *Journal of Catalysis* 115 (1989) 301-309.

[19] C-Y. Huang, Y-Y. Chen, C-C. Su, C-F. Hsu. The clean-up of CO in hydrogen for PEMFC applications using Pt, Ru, Co, and Fe in PROX reaction. *Journal of Power Sources* 174 (2007) 294-301.

[20] S. Bernal, J. J. Calvino, M. A. Cauqui, J. M. Gatica, C. Larese, J. A. Perez Omil, J. M. Pintado. Some recent results on metal/support interaction effects in NM/CeO_2 (NM: noble metal) catalysts. *Catalysis Today* 50 (1999) 175-206.

[21] C. N. Costa, S. Y. Christou, G. Georgiou, A. M. Efstathiou. Mathematical modelling of the oxygen storage capacity phenomenon studied by CO pulse transient experiments over Pd/CeO_2 catalyst. *Journal of Catalysis* 219 (2003) 259-272.

[22] M. S. Jin, J. N. Park, J. K. Shon, J. H. Kim, Z. H. Li, Y. K. Park, J. M. Kim. Low temperature CO oxidation over Pd catalysts supported on highly ordered mesoporous metal oxides. *Catalysis Today* 185 (2012) 183-190.

[23] H. Weiliang, Z. Peng, P. Xia, T. Zhicheng, L. Gongxuan. Highly active Pd/Fe based catalyst prepared with polyol-reduction method for low-temperature CO oxidation. *Journal of Environmental Chemical Engineering* 1 (2013) 189-193.

[24] R. V. Gulyaev, E. M. SLavinskaya, S. A. Novopashin, D. V. Smovzh, A. V. Zaikovskii, D. Yu. Osadchii, O. A. Bulavcheko, S. V. Koremnev, A. I. Boronin. Electrodeposited Cu-ZnO and Mn-Cu-ZnO nanowire/tube catalysts for higher alcohols. *Applied Catalysis B: Environmental* 147 (2014) 132-143.

[25] A. S. Ivanova, E. M. Slavinskaya, R. V. Gulyaev, V. I. Zaikovskii, O. A. Stonkus, I. G. Danilova, L. M. Plyasova, I. A. Polukhin, A. I. Boronin. Metal-support interactions in Pt/Al_2O_3 and Pd/Al_2O_3 catalysts for CO oxidation. *Applied Catalysis B: Environmental* 97 (2010) 57-71.

[26] G. Li, Q. Wang, B. Zhao, R. Zhou. The promotion effect of transition metals on the catalytic behaviour of model $Pd/Ce_{0.67}Zr_{0.33}O_2$ three-way catalyst. *Catalysis Today* 158 (2010) 385-392.

[27] L. Li, L. Li, Y. Yuan, J. Shi, Y. Yuan, Y. Li, W. Zhao, J. Shi. Highly efficient mesoporous Pd/CeO_2 catalyst for low temperature CO oxidation especially under moisture condition. *Applied Catalysis B: Environmental* 158-159 (2014) 341-347.

[28] B. T. Qiao, L. Liu, J. Zhang, Y. Q. Deng. Preparation of highly effective ferric hydroxide supported noble metal catalysts for CO oxidations: From gold to palladium. *Journal of Catalysis* 261 (2009) 241-244.

[29] L. Liu, F. Zhou, L. Wang, X. Qi, F. Shi, Y. Deng. Low-temperature CO oxidation over supported Pt, Pd catalysts: Particular role of FeO_x support for oxygen supply during reactions. *Journal of Catalysis* 274 (2010) 1-10.

[30] C. Rossignol, S. Arrii, F. Morfin, L. Piccolo, V. Caps, J. L. Rousset. Selective oxidation of CO over model gold-based catalysts in the presence of H_2. *Journal of Catalysis* 230 (2005) 476-483.

[31] O. Pozdnyakova, D. Teschner, A. Wootsch, J. Kohnert, B. Stenhauer, H. Sauer, L. Toth, F. C. Jentoft, A. Knop-Gericke, Z. Paal, R. Schlogl. Preferential CO oxidation in hydrogen (PROX) on ceria-supported catalysts, part II: Oxidation states and surface species on Pd/CeO_2 under reaction conditions, suggested reaction mechanism. *Journal of Catalysis* 237 (2006) 17-28.

[32] P. V. Snytnikov, V. A. Sobyanin, V. D. Belyaev, P. G. Tsyrulnikov, N. B. Shitova, D. A. Shlyapin. Selective oxidation of carbon monoxide in excess hydrogen over

Pt-, Ru- and Pd-supported catalysts. *Applied Catalysis A: General* 239 (2003) 149-156.

[33] C. Zlotea, F. Cuevas, V. Paul-Boncour, E. Leroy, P. Dibandjo, R. Gadiou, C. Vix-Guterl, M. Latroche. Size-Dependent Hydrogen Sorption in Ultrasmall Pd Clusters Embedded in a Mesoporous Carbon Template. *Journal of American Chemical Society* 132 (2010) 7720–7729.

[34] M. Armbrüster, M. Behrens, F. Cinquini, K. Föttinger, Y. Grin, A. Haghofer, B. Klötzer, A. Knop-Gericke, H. Lorenz, A. Ota, S. Penner, J. Prinz, C. Rameshan, Z. Révay, D. Rosenthal, G. Rupprechter, P. Sautet, R. Schlögl, L. Shao, L. Szentmiklósi, D. Teschner, D. Torres, R. Wagner, R. Widmer, G. Wowsnick. How to Control the Selectivity of Palladium-based Catalysts in Hydrogenation Reactions: The Role of Subsurface Chemistry? *Chemistry Catalysis Chemicals* 4 (2012) 1048-1063.

[35] A. Valcarcel, F. Morfin, L. Piccolo. Alkene hydrogenation on metal surfaces: Why and when are Pd overlayers more efficient catalysts than bulk Pd? *Journal of Catalysis* 263 (2009) 315-320.

[36] A. Miguel-García, Á. Berenguer-Murcia, D. Cazorla-Amorós. Preferential oxidation of CO catalyzed by supported polymer-protected palladium-based nanoparticles. *Applied Catalysis B: Environmental* 98 (2010) 161-170.

[37] Y. X. Shen, G. Z. Lu, Y. Guo, Y. Q. Wang, Y. L. Guo, L. Wang, X. Zhen. An excellent support of Pd-Fe-O_x catalyst for low temperature CO oxidation: CeO_2 with rich (2 0 0) facets. *Catalysis Communication* 18 (2012) 26-31.

[38] Z. Qu, F. Yu, X. Zhang, Y. Wang, J. Gao. Support effects on the structure and catalytic activity of mesoporous Ag/CeO_2 catalysts for CO oxidation. *Chemical Engineering Journal* 229 (2013) 522-532.

[39] H. J. Chun, D. B. Kim, D. H. Lim, W. D. Lee, H. I. Lee. A synthesis of CO-tolerant Na_2O_5-promoted Pt/C catalyst for direct methanol fuel cell; its physical and electrochemical characterization. *International Journal of Hydrogen Energy* 35 (2010) 6399-6408.

[40] Y. Bi, L. Chen, G. Lu. Constructing surface active centres using Pd-Fe-O on zeolite for CO oxidation. *Journal of Molecular Catalysis A: Chemical* 266 (2007) 173-179.

[41] P. Gawade, B. Bayram, A-M. C. Alexander, U. S. Ozkan. Preferential oxidation of CO (PROX) over CoO_x/CeO_2 in hydrogen-rich streams: Effect of cobalt loading. *Applied Catalysis B: Environmental* 128 (2012) 21-30.

[42] Y. Teng, H. Skurai, A. Ueda, T. Kobayashi. Study of oxidative coupling of methane integrated with co oxidation. *International Journal of Hydrogen Energy* 24 (1999) 355-358.

[43] K. Omata, T. Takada, S. Kasahara, M. Yamada. Active site of substituted cobalt spinel oxide for selective oxidation of CO/H_2. Part II. *Applied Catalysis A: General* 146 (1996) 255-267.

[44] Y. In Choi, H. J. Yoon, S. K. Kim, Y. Sohn. Crystal-facet depend on CO oxidation, preferential oxidation of CO in H_2-rich, water-gas shift reactions, and supercapacitor application over Co_3O_4 nano structures. *Applied Catalysis A: General* 519 (2016) 56-67.

[45] H-F. Wang, R. Kavanang, Y-L. Guo, Y. Guo, G. Lu, P. Hu. Origin of extraordinarily high catalytic activity of Co_3O_4 and its morphological chemistry for CO oxidation at low temperature. *Journal of Catalysis* 296 (2012) 110-119.

[46] Y. Ren, Z. Ma, L. P. Qian, S. Dai, H. Y. He, P. G. Bruce. Ordered crystalline mesoporous oxide as catalysts for CO oxidation. *Catalysis Letter 131* (2009) 146-154.

[47] M. Kang, M. W. Song, C. H. Lee. Catalytic carbon monoxide oxidation over CoO_x/CeO_2 composite catalysts. *Applied Catalysis A: General* 251 (2003) 143-156.

[48] Q. Guo, Y. Liu. MnOx modified Co_3O_4-CeO_2 catalysts for the preferential oxidation of CO in H_2-rich gases. *Applied Catalysis B: Environmental* 82 (2008) 19-26.

[49] S. Litster, G. McLean. PEM fuel cell electrodes. *Journal of Power Sources* 130 (2004) 61-76.

[50] Q. Li, J. O. Jensen, R. F. Savinell, N. J. Bjerrum. High temperature proton exchange membranes based on polybenzimidazoles for fuel cells. *Progress Polymer Science* 34 (2009) 440-477.

[51] Y. Wang, K. S. Chen, J. Mishler, S. C. Cho, X.C. Adroher. A review of polymer electrolyte membrane fuel cells: Technology, applications, and needs on fundamental research. *Applied Energy* 88 (2011) 981-1007.

[52] C. Galletti, S. Fiorot, S. Specchia, G. Saracco, V. Specchia. Catalytic performance of Au-TiO_2 catalysts prepared by deposition-precipitation for CO preferential oxidation in H_2-rich gases. *Chemical Engineering Journal* 134 (2007) 45-50.

[53] J. R. Rostrup-Nielsen, J. Sehested. Steam Reforming for Hydrogen. The Process and the Mechanism. *Fuel Chemistry Division Preprints* 48 (2003) 218-219.

[54] P. Nehe, V.M. Reddy, S. Kumar. Investigations on a new internally-heated tubular packed-bed methanol-steam reformer. *International Journal of Hydrogen Energy* 40 (2015) 5715-5725.

[55] P. J. deWild, M.J.F. M. Verhaak. Catalytic production of hydrogen from methanol. *Catalysis Today* 60 (2003) 3-10.

[56] H-S. Roh, K-W. Jun. Low Temperature Methane Steam Reforming for Hydrogen Production for Fuel Cells. *Bull Korean Chemistry Society* 30 (2009) 153-156.

[57] P. Nehe, S. Kumar. Methanol reformation for hydrogen production from a single channel with cavities. *Hydrogen Energy* 38 (2013) 13216-13229.

[58] B. Smith R J, M. Loganathan, M. Stha. A Review of the Water Gas Shift Reaction Kinetics. *International Journal of Chemical Reactor Engineering* 8 (2010) review 4.

[59] R. J. Rostrup-Nielsen, J. Sehested. Steam Reforming for Hydrogen. The Process and the Mechanism. *Fuel Chemistry Division Preprints* 48 (2003) 218.

[60] K. Polychronopoulou, C. M. Kalamaras, A. M. Efstathiou. Ceria-Based materials for hydrogen production via hydrocarbon steam reforming and water-gas shift reactions. *Recent Patents on Materials Science* 2011 4, 122-145.

[61] M. C. Ribeiro, G. Jacobs, U. M. Graham, K. G. Azzam, L. Linganiso, B. H. Davis. Low temperature water-gas shift: Differences in oxidation states observed with partially reduced Pt/MnO_x and Pt/CeO_x catalysts yield differences in OH group reactivity. *Catalysis Communications* 11 (2010) 1193-1199.

[62] Z. Qu, M. Cheng, C. Sh, X. Bao. Low-temperature selective oxidation of CO in H_2-rich gases over Ag/SiO_2 catalyst. *Journal of Molecular Catalysis A: Chemical* 239 (2005) 22-31.

[63] Z. Ma, S. H. Overbury, S. Dai. Au/M_xO_y/TiO_2 catalysts for CO oxidation: Promotional effect of main-group transition and rare-earth metal oxide additives. *Journal of Molecular Catalysis A: Chemicals* 273 (2007) 186-197.

[64] G. Uysal, A. N. Akin, Z. I. Onsan, R. Yildrim. Preferential CO oxidation over Pt-SnO_2/Al_2O_3 in hydrogen-rich streams containing CO_2 and H_2O (CO removal from H_2 with PROX). *Catalysis Letter* 111 (2006) 173-176.

[65] A. Mark, M. Bollinger and A. Vannice. A kinetic, DRIFTS study of low-temperature carbon monoxide oxidation over Au-TiO_2 catalysts. *Applied Catalysis B: Environmental* 8 (1996) 417-443.

[66] M. Kotobuki, A. Watanabe, H. Uchida, H. Yamashita, M. Watanabe. Reaction mechanism of preferential oxidation of carbon monoxide on Pt, Fe and Pt-Fe/mordenite catalysts. *Journal of Catalysis* 236 (2005) 262-269.

[67] G. Marba'n, A. B. Fuertes. Highly active and selective CuO_x/CeO_2 catalyst prepared by a single-step citrate method for preferential oxidation of carbon monoxide. *Applied Catalysis: B Environmental* 57 (2005) 43-53.

[68] X. Gong, B. Liu, B. Kang, G. Xu, Q. Wang, C. Jia, J. Zhang. Boosting Cu-Ce interaction in Cu_xO/CeO_2 nanocube catalysts for enhanced catalytic performance of preferential oxidation of CO inH_2-rich gases. *Molecular Catalysis* 436 (2017) 90-99.

[69] C. Zhu, T. Ding, W. Gao, K. Ma, Y. Tian, X. Li. CuO/CeO_2 catalysts synthesized from Ce-UiO-66 metal-organic framework for preferential CO oxidation. *International Journal of Hydrogen Energy* 42 (2017) 17457-17465.

[70] A. Di Benedetto, G. Landi, L. Lisi. Improved CO-PROX performance of CuO/CeO_2 catalysts by using nanometric ceria as support. *Catalysts* 8 (2018) 209-228.

[71] M. P. Woods, P. Gawade, B. Tan, U. S. Ozkan. Preferential oxidation of carbon monoxide on Co/CeO_2 nanoparticles. *Applied Catalysis B: Environmental* 97 (2010) 28-35.

[72] D. Gu, C-J. Jia, C. Weidenthaler, H-J. Bongard, B. Spliethoff, W. Schmidt, F. Schüth. Highly ordered mesoporous cobalt-containing oxides: Structure, catalytic properties, and active sites in oxidation of carbon monoxide. *Journal of the American Chemical Society* 137 (2015) 11407-11418.

[73] L. Lukashuk, K. Föttinger, E. Kolar, C. Rameshan, D. Teschner, M. Hävecker, A. Knop-Gericke, N. Yigit, H. Li, E. McDermott, M. Stöger-Pollach, G. Rupprechter. Operando XAS and NAP-XPS studies of preferential CO oxidation on Co_3O_4 and CeO_2-Co_3O_4 catalysts. *Journal of Catalysis* 344 (2016) 1-15.

[74] J. Jansson, A. E. C. Palmqvist, E. Fridell, M. Skoglundh, L. Österlund, P. Thormählen, V. Langer. On the Catalytic Activity of Co_3O_4 in Low-Temperature CO Oxidation. *Journal of Catalysis* 211 (2002) 387–397.

[75] Q. Zhang, X. Liu, W. Fan, Y. Wang. Manganese-promoted cobalt oxide as efficient and stable non-noble metal catalyst for preferential oxidation of CO in H_2 stream. *Applied Catalysis B: Environmental* 102 (2011) 207-214.

[76] C. Liu, L. Gong, R. Dai, M. Lu, T. Sun, Q. Liu, X. Huang, Z. Huang. Mesoporous Mn promoted Co_3O_4 oxides as an efficient and stable catalyst for low temperature oxidation of CO. *Solid State Sciences* 71 (2017) 69-74.

[77] R. Fiorenza, L. Spitaleri, A. Gulino, S. Scirè. Ru–Pd Bimetallic Catalysts Supported onCeO_2-MnO_X Oxides as Efficient Systems for H_2 Purification through CO Preferential Oxidation. *Catalysts* 8 (2018) 203-221.

[78] H. Yang, C. Wang, B. Li, H. Lin, K.-I. Tanaka, Y. Yuan. Doping effect of Ni-MgO on the structure and performance of carbon nanotube-supported Pt catalysts for preferential oxidation of CO in a H_2 stream. *Applied Catalysis A: General* 402 (2011) 168-175.

[79] J. W. Park, J. H. Jeong, W. L. Yoon, Y. W. Rhee. Selective oxidation of carbon monoxide in hydrogen-rich stream over Cu-Ce/-Al_2O_3 catalysts promoted with cobalt in a fuel processor for proton exchange membrane fuel cells. *Journal of Power Source* 132 (2004) 18-28.

[80] D. Gamarra, A. Martinez-Arias. Preferential oxidation of CO in rich H_2 over CuO/CeO_2: Operando-DRIFTS analysis of deactivation effect of CO_2 and H_2O. *Journal of Catalysis* 263 (2009) 189-195.

[81] Y. Tu, J. Luo, M. Meng, G. Wang, J. He. Ultrasonic-assisted synthesis of highly active catalyst Au/MnO_x-CeO_2 used for the preferential oxidation of CO in H_2-rich stream. *International Journal of Hydrogen Energy* 34 (2009) 3743-3754.

[82] J. L. Ayastuy, A. Gurbani, M. P. Gonza´lez-Marcos, M. A. Gutie´rrez-Ortiz. Selective CO oxidation in H_2 streams on CuO/$Ce_xZr_{1-x}O_2$ catalysts: Correlation between activity and low temperature reducibility. *International Journal of Hydrogen Energy 3*7 (2012) 1993-2006.

[83] C. Wieser. Novel polymer electrolyte membranes for automotive applications-requirements and benefits. *Fuel Cell* 4 (2004) 245-250.

[84] J. L. Ayastuy, A. Gurbani, M. P. Gonza´lez-Marcos, M. A. Gutie´rrez-Ortiz. Selective CO oxidation in H_2 streams on CuO/$Ce_xZr_{1-x}O_2$ catalysts: Correlation

between activity and low temperature reducibility. *International Journal of Hydrogen Energy 3*7 (2012) 1993-2006.

[85] Z. Zhao, T. Bao, Y. Li, X. Min, D. Zhao, T. Muhammad. The supported CeO_2/Co_3O_4–MnO_2/CeO_2 catalyst on activated carbon prepared by a successive-loading approach with superior catalytic activity and selectivity for CO preferential oxidation in H_2-rich stream. *Catalysis Communications* 48 (2014) 24-28.

[86] C. Guldur, F. Balikci. Catalytic oxidation of CO over Ag-Co/Alumina catalysts. *Chemical Engineering Communication* 190 (2003) 986-998.

[87] M. Thamachart, V. Meeyoo, T. Risksomboon, S. Osuwan. Catalytic activity of CeO_2-ZrO_2 mixed oxide catalysts prepared via sol-gel technique: CO oxidation. *Catalysis Today* 68 (2001) 53-61.

[88] l. Maffucci, P. Lengo, M. Di Serio, E. Santacesaria. Research note, a rapid method for the evaluation of the dispersion of palladium in supported catalysts. *Journal of Catalysis* 172 (1997) 485-487.

[89] J. Panpranot, K. Kontapakdee, P. Praserthdam. Selective hydrogenation of acetylene in excess ethylene on micron-sized and nanocrystalline TiO_2 supported Pd catalysts. *Applied Catalysis A: General* 314 (2006) 128-133.

[90] M. Todorova, E. Lundgren, V. Blum, A. Mikkelsen, S. Gray, J. Gustafson, M. Borg, J. Rogal, K. Reuter, J. N. Andersen, M. Scheffler. Photoelectrochemical studies on the monolayer assemblies of chlorophyll an on the quantum efficiency of photocurrent generation. *Surface Science* 101 (2003) 541.

[91] C. B. Molina, L. Calvo, M. A. Gilarranz, J. A. Casas, J. J. Rodriguez. Pd-Al pillared clays as catalysts for the hydrodechlorination of chlorophenol in aqueous phase. *Journal of Hazardous Materials* 172 (2009) 214-223.

[92] P. J. deWild, M. J. F. M. Verhaak. Catalytic production of hydrogen from methanol. *Catalysis Today* 60 (2003) 3-10.

[93] B. Zhou, S. Han, R. Raja, G. A. Somoraji. Nanostructure Science and Technology: Chapter 13 Synthesis of Palladium based supported catalysts by colloidal oxide chemistry. *Nanotechnology in Catalysis* 3 (2007) 255-284.

[94] A. A. Mirzaei, M. Faizi, R. Habibpour. Effect of preparation conditions on the catalytic performance of cobalt manganese oxide catalysts for conversion of synthesis gas to light olefins. *Applied Catalysis A: General* 306 (2006) 98-107.

[95] O. V. Netskina, O. V. Komova, V. I. Simagina, G. V. Odegova, I. P. Prosvirin, O.A. Bulavchenko. Aqueous-alkaline $NaBH_4$ solution: The influence of storage duration of solutions on reduction and activity of cobalt catalysts. *Renewable Energy* 99 (2016) 1073-1081.

[96] X. Liao, W. Chu, X. Dai, V. Pitchon. Promoting effect of Fe in the preferential oxidation of carbon monoxide reaction (PROX) on Au/CeO_2. *Applied Catalysis A: General* 449 (2012) 131-138.

[97] P. G. Schiavi, P. Altimari, R. Zanoni, F. Pagnanelli. Morphology-controlled synthesis of cobalt nanostructures by facile electrodeposition: transition from hexagonal nanoplatelets to nanoflakes. *Electrochemical Acta* 220 (2016) 405-416.

[98] V. R. Mate, A. Jha, U. D. Joshi, K. R. Patil, M. Shirai, C. V. Rode. Effect of preparation parameters on characterisation and activity of Co_3C_4 catalyst in liquid phase oxidation of lignin model substrates. *Applied Catalysis A: General* 487 (2014) 130-138.

[99] L. F. Liotta, G. Di Carlo, G. Pantaleo, A. M. Venezia, G. Deganello. Co_3O_4/CeO_2 composite oxides for methane emissions abatement: Relationship between Co_3O_4-CeO_2 interaction and catalytic activity. *Applied Catalysis B: Environmental* 66 (2006) 217-227.

[100] T. Umegaki, T. Inoue, Y. Kojima. Fabrication of hollow spheres of Co_3O_4 for catalytic oxidation of carbon monoxide. *Journal of Alloys and Compounds* 663 (2016) 68-76.

[101] Z. Y. Pu, H. Zhou, Y. F. Zheng, W. Z. Huang, X. N. Li. Enhanced methane combustion over Co_3O_4 catalysts prepared by a facile precipitation method: effect of aging time. *Applied Surface Science* 410 (2017) 14-21.

[102] K. Kaviyarasu, A. Raja, P. A. Devarajan. Structural elucidation and spectral characterizations of Co_3O_4 nanoflakes. *Spectrochimica Acta Part A: Molecular and Biomolecular Spectroscopy* 114 (2013) 586-591.

[103] M. Mansournia, N. Rakhshan, A. ligand-based. Hydrothermal synthesis of Co_3O_4 nanoparticles. *Journal of Molecular Structure* 1125 (2016) 714-720.

[104] F. BilgeEmre, F. Sayilkan, C. Simsek. Synthesis and characterization of nano-$BaTiO_3$ powder by a hydrothermal method. *International Journal of Latest Research in Science and Technology* 3 (2014) 190-193.

[105] M. Y. Nassar. Size-controlled synthesis of $CoCO_3$ and Co_3O_4 nanoparticles by free-surfactant hydrothermal method. *Materials Letters* 94 (2013) 112-115.

[106] H. N. Azlinaa, J. N. Hasnidawania, H. Noritaa, S. N. Surip. Synthesis of SiO_2 Nanostructures Using Sol-Gel Method. *Acta Physical Polonica* A 129 (2016) 842-844.

[107] Y. Tao, P. P. Pescarmona. Nanostructured oxides synthesis via $scCO_2^-$assisted sol-gel methods and their application in catalysis. *Catalysis* 8 (2018) 8-28.

[108] M. Wolf, N. Fischer, M. Claeys. Surfactant-free synthesis of monodisperse cobalt oxide nanoparticles of tunable size and oxidation state developed by factorial design. *Materials Chemistry and Physics* 213 (2018) 305-312.

[109] N. M. Deraz. The comparative jurisprudence of catalysts preparation methods: II. Deposition-precipitation and adsorption methods. *Journal of Indian Environment Chemistry* 2 (2018) 1-3.

[110] A. J. Schwarz. Methods for Preparation of Catalytic Materials. *Chemical Review* 95 (1995) 477-510.

CHAPTER 3

3. EXPERIMENTAL

3.1 INTRODUCTION

Catalysis plays a crucial role in the chemical industry; the use of a catalyst reduces the activation energy and increases the rate of reaction. A catalyst should be able to catalyse a reaction with the highest efficiency and the lowest energy consumption at the same time. Therefore, the main factor in selection of a catalyst for an industrial process is its activity and preparation costs of the catalyst. An equally important issue is a catalyst preparation, because a choice of a method and preparation conditions determines subsequent properties of a catalyst [1]. Methods such as impregnation, precipitation, deposition-precipitation (DP), hydrothermal (HT), strong adsorption electrostatic (SAE) are used to prepare catalysts [2-4]. Among these methods, precipitation method is widely used by industries to prepare heterogeneous catalysts (in aqueous medium at low temperature) due to its simplicity and cost-effectiveness [2-3, 5]. It is a simple method, which seems to be straightforward to scale-up, but in practice, it may cause some difficulties. Important factors such as temperature, pH of solutions, a precursor of an active phase, and precipitating agent or aging time may affect properties of the final catalytic materials [1, 4].

The characterisation of the material's surface after preparation is essential to know the evolution of different compositions in case of the catalysts. The materials are often prepared in one chemical form while their active form is completely different. Consequently, the understanding of the catalytic process requires knowledge of an active form which in addition can be susceptible to the environmental conditions. Hence, an implementation of the experimental methods which can enable the investigation of the catalyst's chemical state as close to the one existing in the reaction space is vital [6]. The in-depth understanding of metal oxide surface structure and reactivity is crucial to continue the development of the technological performance and efficiency of Co_3O_4 based materials [7].

3.2 REAGENTS AND CHEMICALS

The chemicals (and their purity in wt.%) used for the preparation of the catalysts in this work were used as received unless otherwise stated. Various catalysts (Co_3O_4, Pd/Co_3O_4, CeO_2-Co_3O_4, Pd/CeO_2-Co_3O_4, M-Co_3O_4, Pd-MnO_2/Co_3O_4) were prepared from metal oxides precursors; $Co(NO_3)_2$,$6H_2O$ (≥ 98), $Pd(NO_3)_2.H_2O$ (≥ 98), $Ce_2O_3.H_2O$ (≥ 99), $C_6H_9MnO_6.2H_2O$ (≥ 97), TiO_2 (≥ 99), $Mg(NO_3)_2.6H_2O$ (98 – 102), all purchased from Sigma Aldrich company. The $CrCl_3$ (≥ 95) metal oxide precursor was purchased from UniLAB. The NaOH, used as precipitating reagent was purchased from Sigma Aldrich Company. The $N_2H_4.H_2O$ (64 – 65) and the $NaBH_4$ (≥ 99) precursor which were used to reduce the catalysts were also purchased from Sigma Aldrich Company. The 1% O_2/He, 1% CO/He, and 50% H_2 (from pure H_2 gas cylinder) which were used as a mixture for CO PROX reactions, and 8.5% H_2/He was used as a carrier gas, all gas cylinders were purchased from Afrox Company. The 15% CO_2/He (which was used to investigate the effect of CO_2), and the pure He gas which was used to bubble water from saturator (for investigation of the effect of moisture) to the feed stream was also purchased from Afrox Company.

3.3 PREPARATION OF THE CATALYSTS

3.3.1 Preparation of Co_3O_4 by precipitation method

The Co_3O_4 was prepared by precipitation method following the procedure reported by Chen *et al,* [8]. The required amount of $Co(NO_3)_2$,$6H_2O$ was added to 100 ml of distilled water and stirred for 30 minutes at room temperature. Thereafter, a 2 M NaOH, solution was added dropwise with vigorous stirring until pH 12 is reached. The mixture was continuously stirred for 1 h at room temperature and subsequently aged at 70 ^oC for 2 h. The resulting $Co(OH)_2$ precipitates were collected by suction filtration and thoroughly washed with warm distilled water. The precipitates were dried at 80 ^oC for 24 h. A portion of the precipitates were calcined in air at 300 ^oC for 4 h to form as-prepared Co_3O_4.

Another portion was dissolved in 20 ml distilled water, and pre-treated with 100 ml of 0.1 M $N_2H_4.H_2O$ solution for 15 h. Thereafter, filtered and dried at 80 ^oC for 24 h, to form a mixture of CoO(OH) and $Co(OH)_2$, denoted as CoO_xH_y(H) [9].

A portion of a mixture of CoO(OH) and $Co(OH)_2$ was calcined at 300 ^oC in air for 4 h to form Co_3O_4(H). About 0.98 g of the three different materials were used as standalone catalysts or supports for Pd species.

A 600 mg portion of the hydrazine treated Co_3O_4 was loaded on a U-shape borosilicate glass reactor and reduced by a mixture of 5% H_2 balanced helium (30 ml/min) at 250 ^oC for 1.5 h [10].

3.3.2 Preparation of M-Co_3O_4 by co-precipitation method

A variety of metal oxides (M = CeO_2, MnO_2, MgO, TiO_2, Cr_3O_4) were supported on cobalt oxides following the co-precipitation method as reported by Chen *et al,* [8]. Approximately 2wt.% of metal oxides precursors $C_6H_9MnO_6.2H_2O$, $CrCl_3$, TiO_2, $Mg(NO_3)_2.6H_2O$, $Ce_2O_3.H_2O$ were mixed with a solution of $Co(NO_3)_2$,$6H_2O$ and stirred for 30 minutes at room temperature. Thereafter, 2 M NaOH solution was added dropwise to the mixture while vigorously stirring until pH 12 is reached. The obtained mixture was continuously stirred for 1 h at room temperature and subsequently aged at 70 ^oC for 2 h. The resulting precipitates were filtered by suction, and thoroughly washed with warm distilled water. The precipitates were dried at 80 ^oC for 24 h, a portion of the precipitates were calcined in air at 300 ^oC for 4 h. Another portion was dissolved in 20 ml distilled water, and pre-treated with 100 ml of 0.1 M $N_2H_4.H_2O$ solution for 15 h, thereafter, filtered and dried at 80 ^oC for 24 h [9]. The resulting products were calcined at 300 ^oC in air for 4 h (to form (2%M-Co_3O_4)(H)).

3.4 INCORPORATION OF Pd ON THE SUPPORT CATALYSTS

3.4.1 Preparation of (Pd/Co_3O_4) catalyst by improved wet impregnation method

The catalysts were prepared by improved wet impregnation method following the procedure reported by Li *et al,* [9]. The required amount of the $Pd(NO_3)_2.H_2O$ was dissolved in 20 ml of distilled water and the support was added to the solution with stirring. The mixture was stirred for 2 h at room temperature. Thereafter, 100 ml of 0.1 M $N_2H_4.H_2O$ solution was added slowly with stirring. The reaction was digested at room temperature for 15 h with stirring. The resulting product after 15 h was filtered and washed with warm distilled water. The product was dried at 80 ^oC for 24 h. The

resulting product was named (Pd/Co_3O_4)(H), and the untreated sample was named Pd/Co_3O_4. The sample treated with sodium borohydride was named (Pd/Co_3O_4)(B). All other catalysts were also prepared by following the same procedure, with $N_2H_4.H_2O$ used as reducing agent. The presence of the species in the composites were confirmed using inductively Coupled Plasma Mass Spectroscopy (ICP-MS) at University of Stellenbosch (Central analytical facilities).

3.4.2 Preparation of (Pd/Co_3O_4) catalyst by deposition precipitation method

The catalyst was prepared following the method reported by Shen *et al,* [11]. Two solutions were prepared; solution A was prepared by dissolving the required amount of Pd $(NO_3)_2.H_2O$ in 50 ml of 0.07 M HCL solution. Solution B was prepared by dissolving 1.5 g NaOH and 0.98 g of the Co_3O_4 in 50 ml of distilled water, the mixture was stirred at 70˚C for 2 h. Thereafter, solution A was added to solution B dropwise at 70˚C. The resulting precipitates were pre-treated with 0.1 M $N_2H_4.H_2O$ (100 ml) for 15 h at room temperature. The formed solids were filtered, washed by warm distilled water and dried at 80˚C without further calcination. The resulting sample was denoted as (Pd/Co_3O_4)(H).

3.4.3 Introduction of Pd on the support by co-precipitation method

The catalyst was prepared following the method reported by Chen *et al,* [8]. The required amount of $Pd(NO_3)_2.H_2O$ was dissolved in 50 ml of distilled water followed by the required amount of $Ce(NO_3)_2$ (or $CH_6MnO_6.2H_2O$) with stirring. The mixture was left to stir for 30 min at room temperature. Subsequently, the required amount of $Co(NO_3)_3.6H_2O$ was added to the reaction mixture with stirring, the mixture was continuously stirred for 30 min at room temperature. Thereafter, 2 M NaOH solution was added dropwise to the solution with vigorous stirring until pH 12 is reached. The obtained mixture was continuously stirred for 1 h at room temperature and subsequently aged at 70 ^oC for 2 h. The resulting precipitates were filtered by suction, and thoroughly washed with warm distilled water. The precipitates were dried at 80 ^oC for 24 h, a portion of the precipitates were calcined in air at 300 ^oC for 4 h. Another portion was dissolved in 20 ml distilled water, and pre-treated with 100 ml of 0.1 M $N_2H_4.H_2O$ solution for 15 h, thereafter, filtered and dried at 80 ^oC for 24 h [9]. The

resulting products were calcined at 300 ^{o}C in air for 4 h, and the resulting sample is denoted as (Pd-CeO_2/(Co_3O_4))(H) or (Pd-MnO_2/(Co_3O_4))(H). The presence of the species in the composites were confirmed using ICP-MS.

3.5 CHARACTERISATIONS

3.5.1 X-ray powder diffraction (XRD)

The X-ray powder diffraction (XRD) technique is used to characterise the crystallographic structure, crystallinity, crystallite size, and the dispersion of the particle and the lattice of the structure [12]. With appropriate accessories, X-ray diffraction can be used to study phase change as a function of stress or temperature, to determine lattice strain, to measure the crystalline modulus, and with the aid of molecular modelling to determine the structure of a polymer. Paterson *et al.* [13], studied the evolution of the cobalt phase reduction in the presence of water (from 0 to 1% H_2O) by in situ X-ray diffraction, the study has produced a clear transition to CoO and Co metal. The presence of water shifted the peaks to higher transition temperature and lowered the reduction process to cobalt metal.

Sample analysis

The XRD patterns of the samples were recorded on a Philips Analytical Powder X-ray B.V., PW3710 based diffractometer, equipped with a divergence slit 1/4^{o}, a receiving slit 0.1, a monochromator and using Co-Kα radiation (40 KV, 40 mA). Data were collected in the 2θ range of 5 to 75^{o} in 0.025^{o} steps, using a scan speed resulting in an equivalent counting time of 1 s per step. The average crystallite sizes, D of the as-prepared samples were calculated from (311) plane diffraction peak using the Scherrer's formula [14]:

$$D = \frac{K\lambda}{\beta \cos\theta}$$

where K is the Scherrer's constant (0.9), D is the average crystallite size (nm), λ is the wavelength of incident X-ray radiation (λ = 0.154 nm) used, β is the full width at half maximum (FWHM) of the metal oxide diffraction peaks and θ is the diffraction angle.

3.5.2 Brunauer-Emmett-Teller (BET) measurements

The Brunauer, Emmett and Teller (BET) is widely used to characterise materials for adsorption, catalysis and reactions on surfaces (as its value represents the number of potential active sites). The surface area is estimated from a specific region of a gas adsorption isotherm where monolayers of adsorbate are considered to take place. Experimentally the gas adsorption isotherm is obtained through successive doses of an adsorptive gas probe, typically N_2 at 77 K is sent to the solid material, initially dried and evacuated. The amount of gas molecules that can adsorb onto the surface of the solid is derived from the evolution of the pressure in the system [15].

Sample analysis

The BET specific surface areas (SBET expressed in m^2/g) of the sample were measured by N_2 adsorption at -196 ^oC on a Micromeritics tristar II 3020 system. The single point method was selected to analyse the samples. Before the measurements, samples were degassed under air at 200 ^oC for 2 h.

3.5.3 Thermogravimetric analysis (TGA)

The thermogravimetric analysis (TGA) is used to characterise the material's thermal stability and its fraction of volatile components by monitoring the weight change that occurs as sample is heated at constant rate. It provides evidence for the removal of associated solvent, amorphous to crystalline phase transformation and isochemical transformation (i.e., cations redistribution or migration of cations between the octahedral and tetrahedral sites) [16].

Sample analysis

The TGA profiles of the samples were determined using an STA PerkinElmer 4000 instrument. The experiments were operated from room temperature to 600 ^oC (with a heating rate of 10 ^oC/min) under N_2 atmosphere (with a flow rate of 40 ml/min). Before analysis, the samples were heated at 80 ^oC for 2 h in an oven.

3.5.4 X-ray photoelectron spectroscopy (XPS)

The X-ray photoelectron spectroscopy (XPS) analysis technique is an effective technique used to determine the surface element composition, metal oxidation states, and adsorbed oxygen species of the solid oxide materials [17]. The technique is also used to detect contamination on the surface of the sample or bulk of the sample [18]. The average depth of analysis for an XPS measurement is approximately 5 nm. The kinetic energy of the analysed electrons depends on the energy of the source (mostly < 1500 eV). It provides information about surface layers or thin film structures which is important for many industrial and research applications, where surface or thin film composition plays a role in performance including nanomaterials, photovoltaics, catalysis, corrosion, adhesion, electronics, wear environmental control, etc. [17-19].

Sample analysis

The XPS spectra were acquired with an ESCAlab-250Xi spectrometer (Shimadzu Co. Ltd) equipped with Al kα X-ray exciting source (1486.7 eV) operating at 10 kV and 10 mA. All the elemental binding energies were referenced to C (1s) line situated at 285.0 eV.

3.5.5 Energy-dispersive spectroscopy (EDS)

The energy dispersive (EDS) X-ray analysis is a technique used to analyse near-surface elements and estimate their proportion at different position, thus giving an overall mapping of the sample. The EDS can be used to estimate the composition or the amount of nanoparticles near the surface, provided they contain some heavy metal ions. For example, the presence of Au, Pd and Ag nanoparticles on the surface can easily be identified using EDS [18].

Sample analysis

The compositions of the prepared catalysts were obtained by EDS using a Noran-X-ray detector on the JEOL JSM-6100 scanning electron microscope. The accelerating

voltage used in the EDS analysis was 5 kV. Four different areas of each sample were scanned to obtain the average C, O, Pd, Ce, Mn, and Co ratios.

3.5.6 Inductively coupled mass spectroscopy (ICP-MS)

Inductively coupled plasma mass spectrometry (ICP-MS) is an attractive way to perform elemental analysis, particularly in high sample volume facilities, where turnaround time is critical. It features a multi-elemental capability, good precision, a long linear dynamic range, simple spectra, low detection limits, and the ability to do rapid isotopic analysis [20]. It has found wide application to analysis of a variety of samples, including water and food, as well as geochemical, environmental, and biological samples. However, it has some limitations, such as matrix effects, which can be important, and the need to keep the concentration of dissolved solids low to avoid clogging problems [20-21].

Sample analysis

Multi-element determination was performed on an Agilent 7900 inductively coupled Mass Spectroscopy (ICP-MS), equipped with 0.4 ml/min Micro mist nebulizer. The samples (~0.03 g) were added in a solution mixture (of 6 ml HNO_3 and 1 ml H_2O_2), and digested using microwave (1600 W, 100%) at ramp time of 25 min, pressure of 800 psi and hold time of 10 min. Solution was then introduced into the instrument via autosampler by peristaltic pump. Plasma gas flow rate was a 5 ml/min and collision and reaction gases flow rates were 5 ml/min and 6 ml/min for He and H_2, respectively. Analysis was optimised at 1600 W forward power and 0.83 L/min carrier gas flow (Ag) with a make-up gas of 0.15 L/min. Sample depth (10 mm) and lens parameter were optimised for highest signal and optimum peak shapes while maintaining low oxides.

3.5.7 Temperature programmed reduction (TPR)

The temperature programmed reduction (TPR) is a useful technique for the characterisation of metal oxide catalysts. It is a highly sensitive method for discriminating the reducibility of different species, providing information about its chemical state, as well as its dispersion state. Analysis of catalysts are performed by

placing the catalyst in a fixed bad reactor, exposed to reducing mixture which continuously passes through the catalytic bed. The reactor temperature is increased according to a linear temperature programme. The difference between the inlet and outlet concentration of the gas mixture is measured as a function of time using a thermal conductivity detector (TCD). The resulting TPR profile contains qualitative and quantitative information on the oxidation state of the reducible species present and in that sense, it is a fingerprint. The technique is basically quantitative and the information obtained is kinetic, consequently, directly corresponds to the catalytic behaviour [19, 22].

Sample analysis

Hydrogen temperature-programmed reduction (H_2-TPR) of the samples were carried out on a Micromeritiscs Autochem II 2920 equipped with a thermal conductive detector. The TPR analysis began by conditioning the sample, flowing oxygen and helium mixture through approximately 0.035 g of a sample for 1 h. The TPR analysis was done by flowing analysis gas (10% H_2/Ar) through the sample while the temperature was increased linearly up to 900 ^oC at 10 ^oC/min. The consumption of the hydrogen was monitored using a thermal conductivity detector (TCD).

3.5.8 Fourier transform infrared spectroscopy (FTIR)

The infrared spectroscopy has the ability to monitor the vibrations of the functional groups (at room temperature) for the molecular structure which govern the course of chemical reactions. It offers continuous operation and low maintenance compared to gas chromatography, and low cost and structural specificity compared to mass spectroscopy. The term ‘’infrared’’ generally refers to any electromagnetic radiation falling in the region from 0.7 to 1000 mm. The region between 2.5 and 25 mm (4000 to 400 cm^{-1}) is most attractive for chemical analysis [19, 23].

Sample analysis

The FTIR spectra of the samples were recorded using a Spectrum II spectrophotometer (PerkinElmer). Measurements were done using 100 scans at 16

cm^{-1} resolutions, units of log (1/R) (absorbance), over the mid IR region of 400-4000 cm^{-1}. The small powder sample was centred on the glass plate crystal surface, and pressure clamps were used to apply pressure on the filter.

3.5.9 Scanning electron microscope (SEM)

The scanning electron microscopy (SEM) is used to check the morphology of the materials [24]. It can produce a very high resolution images of a sample surface, revealing details about 1-5 nm in size in its primary detection mode. i.e., secondary electron imaging [18].

Sample analysis

The morphologies of the samples were observed using a Zeiss Auriga Field Emission scanning electron microscope (SEM). Samples were secured to the stubs using double sided conductive carbon tape. Samples were then coated with chromium using the Quorum Q 150 T ES coater and inserted into the microscope for viewing. Images were captured using the SmartSEM software.

3.5.10 Transmission electron microscope (TEM)

The transmission electron microscopy (TEM) analysis technique is used to investigate the microstructure of the materials, it provides the crystallographic information and composition at a nanometer scale. A high energy beam of electrons is shone through a very thin sample, and the interactions between the electrons and the atoms can be used to observe features such as crystal structure, dislocations and grain boundaries. High resolution transmission electron microscopy (HRTEM) can be used to analyse the quality, shape, size and density of quantum wells, wires and particles. It operates on the same basic principles as that of the light microscope, but uses electrons instead of light. It can reveal the finest details of internal structure, as small as an individual atom, because the wavelength of electrons is much smaller than that of light. The optimal resolution attainable for TEM images is in many orders of magnitude better than that from a light microscope [18, 24].

Sample analysis

The TEM images were obtained using JEOL JEM 2100 high resolution transmission electron microscope operated at 120 kV. Small spatula tip of the sample was dispersed in the liquid ethanol (~3 ml) to create a very lightly dispersed solution. The mixture was then sonicated for 30 min in an ultra sonicator at room temperature. The carbon coated Cu grid was dipped on the solution and left to dry overnight.

3.6 EXPERIMENTAL SETUP FOR PROX OF CO

The catalytic test for CO PROX in hydrogen rich stream was carried out in a continuous flow fixed bed U-shape borosilicate glass (inner diameter of 5 mm) reactor system. Prior to all catalytic tests, the samples were heated in a flowing pure He gas (20 ml/min) at 40 ^{o}C for 30 min, as a standard pre-treatment. The catalyst weight was 200 mg and the total flow rate of the reaction mixture was 100 ml/min, yielding a mass flow of 30000 ml g^{-1} h^{-1}. The feed contained 1% CO, 1% O_2, 50% H_2, and 48% He. The reactor temperature was monitored using a K-type thermocouple placed next to the catalyst bed and controlled with a temperature controller. The effect of CO_2 was examined with the addition of 15% CO_2 in the feed. In order to examine the effect of water vapour on the reaction, the carrier gas (with the flow rate of 20 ml/min) was bubbled through the water kept in the saturator at room temperature. The copper sulphate powder was used to trap excess water downstream of the reactor and before GC analysis. The resulting product and reactant analysis was carried out by a gas chromatography (DANN-GC) equipped with a thermal conductive detector (TCD).

The schematic diagram of the reactor system used for PROX of CO in hydrogen rich gas stream is shown in Figure 3.1.

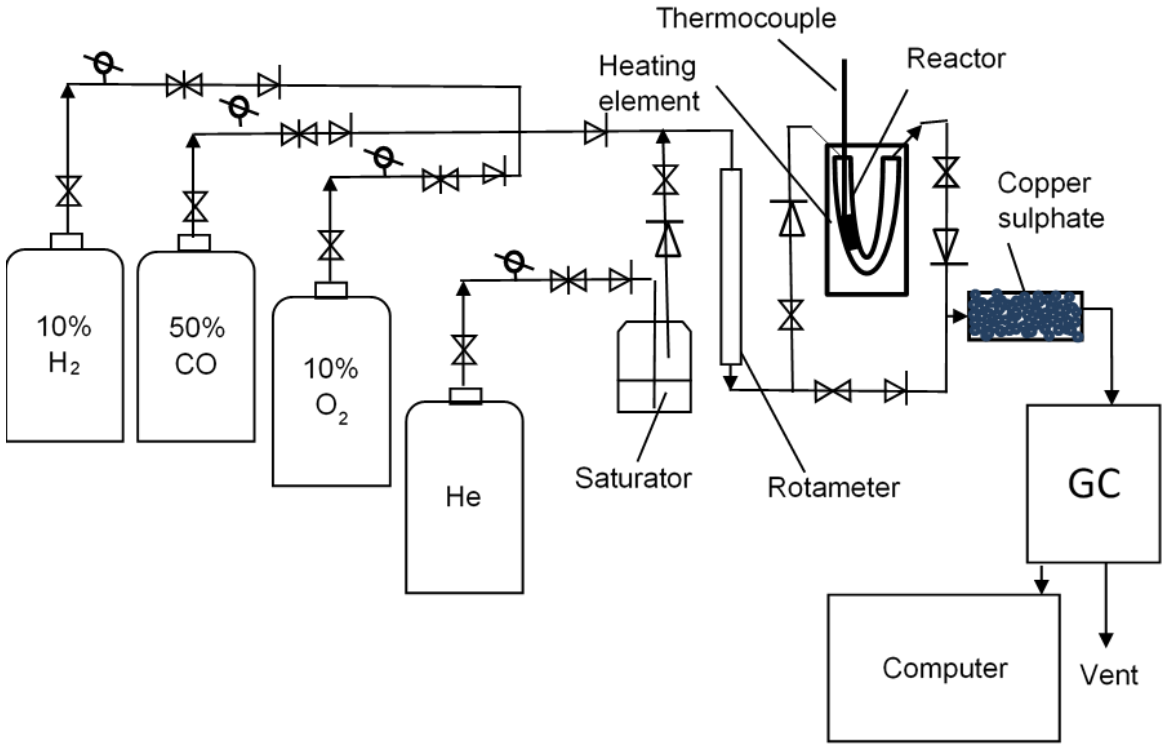

Figure 3.1 A schematic representation of a U-shape tube reactor system used on PROX of CO reaction (= Pressure gauge, = Shut-off valve, = Needle valve, = One-way valve, GC = Gas chromatograph).

The components of the reaction mixture were identified by injection of the standard samples of the expected products. The components detected by GC are shown in Appendix A (for the standard) and Appendix B (for PROX). The separation of the components was achieved by the use of Porapack-Q and the molecular sieve columns. The catalytic activity data were reported as CO and H_2 conversion, CO and H_2 selectivity as illustrated below. The percentage of CO conversion was calculated using equation 3.1.

$$x_{CO} = \frac{[CO]_{in} - [CO]_{out}}{[CO]_{in}} \times 100\% \qquad 3.1$$

The percentage of H_2 conversion was calculated using equation 3.2.

$$x_{H_2} = \frac{[H_2]_{in} - [H_2]_{out}}{[H_2]_{in}} \times 100\% \qquad 3.2$$

The percentage of CO selectivity was calculated using equation 3.3.

$$s_{CO_2} = 0.5 \times \left(\frac{[CO]_{in} - [CO]_{out}}{[O_2]_{in} - [O_2]_{out}} \right) \times 100\% \quad 3.3$$

The percentage of H_2O selectivity was calculated using equation 3.4.

$$s_{H_2O} = 0.5 \times \left(\frac{[H_2]_{in} - [H_2]_{out}}{[O_2]_{in} - [O_2]_{out}} \right) \times 100\% \quad 3.4$$

The percentage of O_2 selectivity was calculated using equation 3.5.

$$\lambda = \frac{2 \times [O_2]_{in}}{[CO]_{in}} \times 100\% \quad 3.5$$

The catalytic activity for the selected catalysts in PROX of CO in hydrogen rich gas stream (at dry condition) are presented in Table 3.1.

Table 3.1 The catalytic activity of the prepared catalysts in PROX of CO at temperature range of 40 to 220 ^oC (under dry condition).

Catalyst	**CO conversion at 100 ^oC**	**T_{max} (^oC)[a]**	**Maximum CO conversion (%)[a]**
Co_3O_4	47.9	160	100
Co_3O_4(H)	100	100	100
CoO(H)	100	100	100
1wt.%Pd/(Co_3O_4(H))	47.3	220	79.5
2wt.%Pd/(Co_3O_4(H))	51.4	220	72.8
2wt.%CeO_2-Co_3O_4	87.2	120	98.5
(2wt.%CeO_2-Co_3O_4)(H)	99.4	100	99.4
(0.5wt.%Pd/(2wt.%CeO_2-Co_3O_4))(H)	88.2	220	100
0.5wt.%Pd-2wt.%CeO_2/(Co_3O_4))(H)	98.7	220	100
(7wt.%MnO_2-Co_3O_4)(H)	98.1	100	98.1
(0.5wt.%Pd-7wt.%MnO_2/(Co_3O_4))(H)	97.8	100	97.8

[a] T_{max} is the temperature achieving the maximum CO conversion.

3.7 REFERENCES

[1] A. Tarka, M. Zybert, Z. Kindler, J. Szmurlo, B. Mierzwa, W. Rarog-Pilecka. Effect of precipitating agent on the properties of cobalt catalysts promoted with cerium and barium for NH_3 synthesis obtained by co-precipitation. *Applied Catalysis A: General* 532 (2017) 19-25.

[2] K. Klaigaew, C. Samart, C. Chaiya, Y. Yoneyama, N. Tsubaki, P. Reubroycharoen. Effect of preparation methods on activation of cobalt catalyst supported on silica fiber for Fischer-Tropsch synthesis. *Chemical Engineering Journal* 278 (2015) 166-173.

[3] F. Giovannelli, V. Marsteau, M. Zaghrioui, C. Autret, F. Delorme. Low temperature synthesis of Co_3O_4 and $(Co_{1-x}Mn_x)_3O_4$ spinels Nanoparticles. *Advanced Powder Technology* 28 (2017) 1325-1331.

[4] N. Pernicone, Chapter 8 Scale-up of catalyst production. *Catalysis Today* 34 (1997) 335-547.

[5] Z. Y. Pu, H. Zhou, Y. F. Zheng, W. Z. Huang, X. N. Li. Enhanced methane combustion over Co_3O_4 catalysts prepared by a facile precipitation method: effect of aging time. *Applied Surface Science* 410 (2017) 14-21.

[6] A. Sarnecki, P. Adamski, A. Albrecht, A. Komorowska, M. Nadziejko, D. Moszyński. XPS study of cobalt-ceria catalysts for ammonia synthesis-The reduction process. *Vacuum* 155 (2018) 434-438.

[7] S. C. Petitto, M. Langell. Surface composition and structure of Co_3O_4 (110) and the effect of impurity segregation. *Journal of Vac Science Technology* 22 (2004).

[8] Y. Chen, D. Liu, L. Yang, M. Meng, J. Zhang, L. Zheng, S. Chu, T. Hu. Ternary composite oxide catalysts CuO/Co_3O_4-CeO_2 with wide temperature-window for the preferential oxidation of CO in H_2-rich stream. *Chemical Engineering Journal* 234 (2013) 88-98.

[9] G. Li, L. Li, Y. Yuan, j. Shi, Y. Yuan, Y. Li, W. Zhao, J. Shi. Highly efficient mesoporous Pd/CeO_2 catalyst for low temperature CO oxidation especially under moisture condition. *Applied Catalysis B: Environmental* 158-159 (2014) 341-347.

[10] D. Gu, C-J. Jia, C. Weidenthaler, H-J. Bongard, B. Spliethoff, W. Schmidt, F. Schüth. Highly ordered mesoporous cobalt-containing oxides: Structure, catalytic properties, and active sites in oxidation of carbon monoxide. *Journal of the American Chemical Society* 137 (2015) 11407-11418.

[11] Y. Shen, G. Lu, Y. Wang, Y. Guo, L. Wang, X. Zhen. An excellent support of Pd-Fe-Ox catalyst for low temperature CO oxidation: CeO_2 with rich (200) facets. *Catalysis Communications* 18 (2012) 26-31.

[12] E. Kramer, E. Meiwei. Synthesis and characterisation of cobalt-substituted hydroxyapatite powders. *Ceramics International* 40 (2014) 13471-13480.

[13] J. Paterson, M. Peacock, E. Ferguson, M. Ojeda, J. Clarkso. In situ X-ray diffraction of Fischer-Tropsch catalysts-Effect of water on the reduction of cobalt oxides. *Applied Catalysis A: General* 546 (2017) 103-110.

[14] S. L. Sharifi, H. R. Shakur, A. Mirzaei, A. Salmani, M. H. Hosseini. Characterization of Cobalt oxide Co_3O_4 nanoparticles prepared by various methods: Effect of calcination temperatures on size, dimension and catalytic decomposition of hydrogen peroxide. *International Journal of Nanoscience Nanotechnology* 9 (2013) 51-58.

[15] K. S. W. Sing, D. H. Everett, R. A. W. Haul. L. Moscou L., R. A. Pierotti, J. Rouquérol, T. Siemieniewska. IUPAC Recommendations: Reporting Physisorption Data for Gas Solid Systems with Special Reference to the Determination of Surface Area and Porosity. *Pure and Applied Chemistry* 57 (1984) 603-619.

[16] S. Rana, J. Philip, B. Raj. Micelle based synthesis of cobalt ferrite nanoparticles and its characterization using Fourier Transform Infrared Transmission Spectrometry and Thermogravimetry. *Material Chemistry and Physics* 124 (2010) 264-269.

[17] X. Zhang, J. Ye, J. Yuan, T. Cai, B. Xiao, Z. Liu, K. Zhao, L. Yang, D. He. Excellent low-temperature catalytic performance of nan sheet Co-Mn oxides for total benzene oxidation. *Applied Catalysis A: General* 566 (2018) 104-112.

[18] M. Joshi, A. Bhattachary, S. Wazed. Characterisation techniques for nanotechnology applications in textiles. *Indian Journal of Fibre and Textile Research* 33 (2008) 304-317.

[19] D. Brune, R. Hellborg, H. J. Whitlow, O. Hunderi. Surface characterisation. Wiley-VCH, 1997.

[20] L. Poirier, J. Nelson, D. Leong, L. Berhane, P. Hajdu, F. Lopez-Linares. Application of ICP-MS and ICP-OES on the Determination of Nickel, Vanadium, Iron, and Calcium in Petroleum Crude Oils via Direct Dilution. *Energy and Fuels* 30 (2016) 3783−3790.

[21] D. Beauchemin. Inductively Couple Plasma Mass Spectrometry Methods. Elsevier Ltd. Queen's University, Kingston, ON, Canada. 2017.

[22] S. Trivedi, R. Prasad. Reactive calcination route for synthesis of active Mn–Co_3O_4 spinel catalysts for abatement of CO-CH_4 emissions from CNG vehicles. *Journal of Environmental Chemical Engineering* 4 (2016) 1017-1028.

[23] W. M. Doyle. Principles and Applications of Fourier Transform Infrared (FTIR) Process Analysis. *Technical Note AN-906 Rev C* 1-24.

[24] A. Sarnecki, P. Adamski, A. Albrecht, A. Komorowska, M. Nadziejko, D. Moszyński. XPS study of cobalt-ceria catalysts for ammonia synthesis-The reduction process. *Vacuum* 155 (2018) 434-438.

CHAPTER 4

4. RESULTS AND DISCUSSIONS

REDUCTIVE PRE-TREATMENT OF COBALT BASED CATALYSTS TOWARDS PREFERENTIAL OXIDATION (PROX) OF CO IN EXCESS HYDROGEN

4.1 INTRODUCTION

The activity of Co_3O_4 in the presence of excess hydrogen deactivates due to the transformation of the Co_3O_4 to metallic cobalt [1-3]. A variety of prepared metal oxides supported catalyst have shown that pre-treatment conditions play a crucial role towards the formation of desired species and improved catalytic activities [4-6]. The role of reductive pre-treatment of Co_3O_4 samples by hydrazine shown catalytic improvement of Co_3O_4 in CO PROX from this work. The $Co(OH)_2$ was prepared by precipitation method and used as a precursor for the preparation of Co_3O_4. The $Co(OH)_2$ was pre-treated by hydrazine prior to calcination (to form Co_3O_4(H)) and compared with as-prepared catalysts. Samples were further reduced by 5% H_2/He to form CoO and CoO(H) at 250 ^oC. The Pd species were supported on different cobalt by improved impregnation. Samples were characterised using XRD, BET, TGA, XPS, TPR, FTIR, EDS, SEM, and TEM techniques. An improvement in the structural transformation to higher surface area was observed over the hydrazine treated catalyst. As a result, the catalytic activity improved by decreasing the maximum CO conversion temperature in CO PROX reaction.

The PROX activity was investigated at a temperature ranging from 40 to 220 ^oC, and the CO/O_2 ratio of 1 (λ). The effect of oxidation state in the activity of cobalt oxide was investigated by reductive pre-treatment of the Co_3O_4(H), by 5% H_2/He. The spent catalyst of CoO(H) in CO PROX is transformed to Co_3O_4 due to the presence of oxygen vacancies.

The chapter further focus on the role of Pd based metal catalysts on different Co_3O_4 support. It was found that Pd species suppress the activity of the catalyst in CO PROX, due to formation of *β* hydrides which form moisture, a similar observation was reported

previously [7-8]. However, introduction of the Pd species over hydrazine treated Co_3O_4 improved the catalytic activity at lower temperature (40-80 ^oC).

Furthermore, this chapter reports on the role of the reductive pre-treatment of $Co(OH)_2$ species using hydrazine, prior to formation of Co_3O_4 by calcination. A comparison with existing methods of calcining the $Co(OH)_2$ at specific temperatures was also investigated. The role of Pd species on different Co_3O_4 supports was also discussed. The study further account on the oxidation state and structure of as-prepared and spent catalysts, to elucidate the correlation with the observed activity/selectivity. Furthermore, the stability of the catalysts under dry, 15% CO_2, and moisture (by bubbling He gas through water vessel at 20 ml/min, at room temperature) were investigated in CO PROX at 100 ^oC for 21 h.

4.2 CHARACTERISATION OF CATALYSTS

The as-prepared catalysts were characterised using XRD, BET, TGA, XPS, TPR, FTIR, EDS, SEM, and TEM techniques. The results based on these techniques are discussed in the following sections.

4.2.1 X-ray powder diffraction (XRD) analysis

4.2.1.1 The role of hydrazine treatment on Co_3O_4

The data in Figure 4.1 shows the XRD patterns of $Co(OH)_2$, $CoO_xH_y(H)$, as-prepared Co_3O_4, hydrazine treated Co_3O_4, CoO(H), and CoO(H) spent catalysts. The XRD profile of as-prepared Co_3O_4 (Figure 4.1(c)), revealed the diffraction peaks with 2θ values at 19.2, 31.2, 36.9, 38.9, 45.1, 55.7, and 59.5^o that are assigned to the (111), (220), (311), (222), (400), (422), and (511) crystal planes of the crystalline Co_3O_4 phase, respectively. This is in agreement with previous investigations [9-11]. The diffraction peaks of the sample are in good agreement with the JCPDS file of the cubic spinel type Co_3O_4 phase (JCPDS Card No. 76-1802) [12-14]. The XRD profile of the mixture shows two overlapping peaks at 2θ values of 19.2 and 38.9^o; this confirms that transformation process from $Co(OH)_2$ to CoO(OH) phases has occurred (Figure 4.1(b)) [15], due to the oxidation of $Co(OH)_2$ (Figure 4.1(a)).

Interestingly, the peak intensity at 36.6^o 2θ of hydrazine treated Co_3O_4 (Figure 4.1(d)), has decreased substantially as compared to the as-prepared Co_3O_4 sample. The peak

reduction is attributed to the treatment of $Co(OH)_2$ with hydrazine solution, prior to catalyst calcination at 300 ^oC. The reduction of the hydrazine treated Co_3O_4 by 5% H_2 has resulted to CoO(H) species (Figure 4.1(e)) [16]. However, the spent catalyst in PROX of CO resulted to the formation of Co_3O_4 species (Figure 4.1(f)), due to the oxygen vacancy from the feed [17]. The average crystallite sizes, D of the as-prepared samples were calculated from (311) plane diffraction peak using the Scherrer's formula (section 3.5.1).

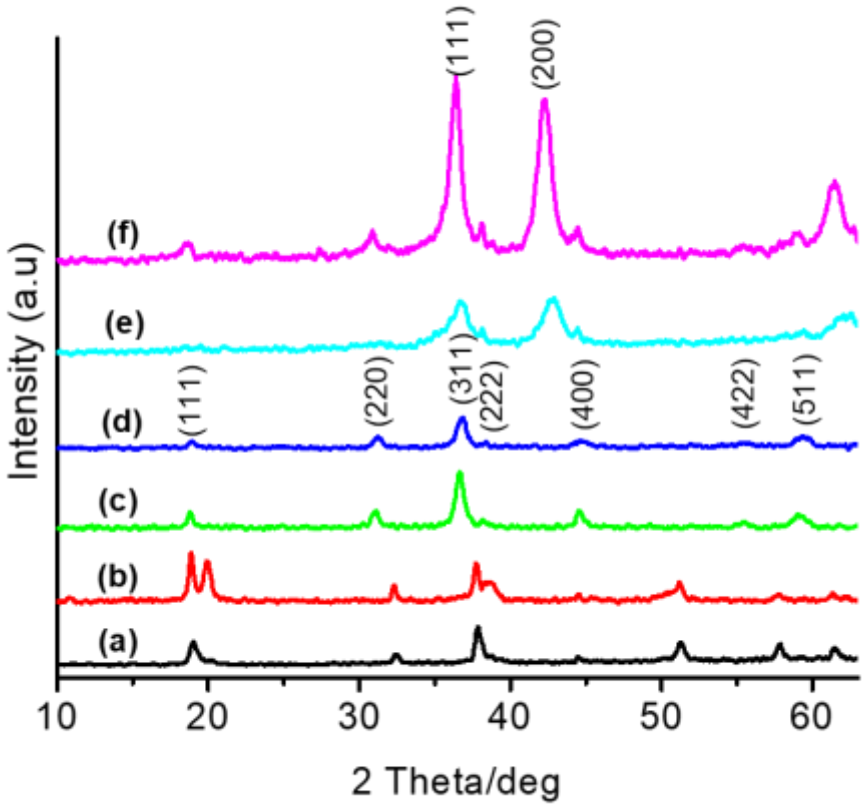

Figure 4.1 The XRD patterns of **(a)** $Co(OH)_2$, **(b)** $CoO_xH_y(H)$, **(c)** Co_3O_4, **(d)** $Co_3O_4(H)$, **(e)** CoO(H), and **(f)** CoO(H) spent catalysts.

The estimated average crystallite sizes using the Scherrer's equation reveals the effects of hydrazine treatment on the crystallite sizes of the formed Co_3O_4 phase (Table 4.1). This clearly suggests that some surface rearrangements have occurred, as evidenced by an increase in surface area (from 47.9 to 62.2 m^2/g), after hydrazine treatment. Furthermore, this finding correlates with the surface roughness formation

as depicted by SEM and TEM data. This finding correlates with the reported improved surface area of Co_3O_4, upon calcination of CoO(OH) [15].

4.2.1.2 The role of Pd species on Co_3O_4

The data in Figure 4.2 shows the XRD patterns of 2wt.%Pd/Co_3O_4, (2wt.%Pd/Co_3O_4)(H), (2wt.%Pd/Co_3O_4*)(H) and 2wt.%Pd/(Co_3O_4(H)) catalysts. The introduction of the Pd on the support base does not change the structure of the support. It must be noted that the peaks for Pd are missing from the patterns (Figure 4.2), which may suggest that Pd is in its amorphous phase [18]. This could also suggest a good synergy between the support (Co_3O_4) and the Pd species [19].

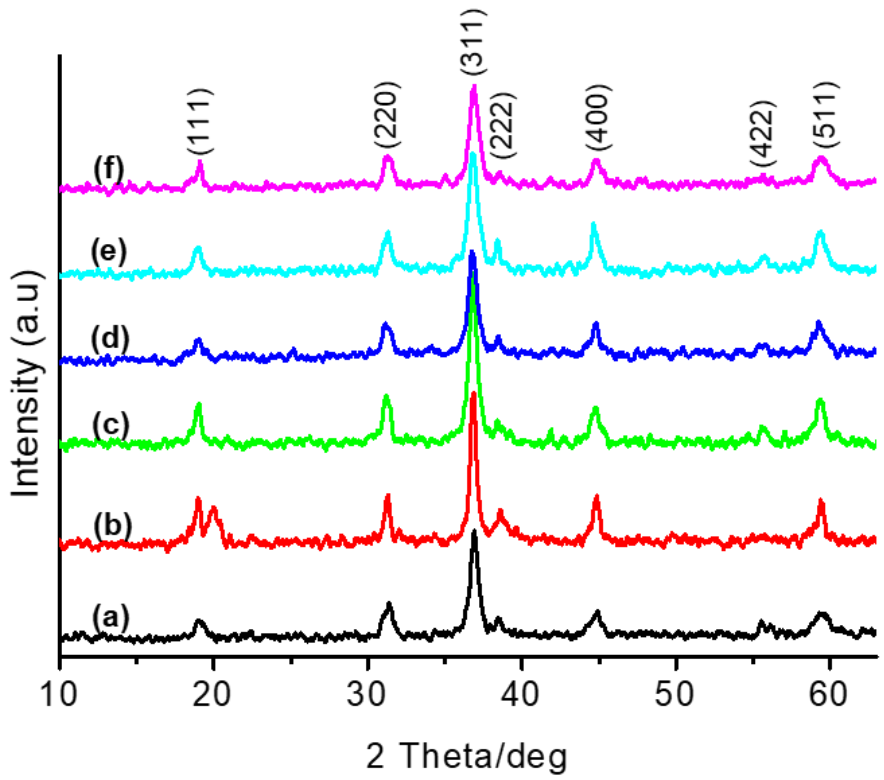

Figure 4.2 The XRD pattern for **(a)** 2wt.%Pd/Co_3O_4 80 ^oC, **(b)** (2wt.%Pd/Co_3O_4-CoO(OH)(H) 80 ^oC, **(c)** (2wt.%Pd/Co_3O_4)(H) 300 ^oC, **(d)** (2wt.%Pd/Co_3O_4*)(H) 300 ^oC, **(e)** 2wt.%Pd/(Co_3O_4(H)) 300 ^oC, **(f)** (2wt.%Pd/Co_3O_4*)(B) 300 ^oC, catalysts.

The preparation method has an effect on the structure of the Pd/Co_3O_4 sample, the introduction of the Pd on the calcined sample (Co_3O_4) resulted in a broad peak with

low intensities (Figure 4.2(a)). Two overlapping peaks were observed at 2θ values of 19.2 and 20.0^{o} when the 2wt.%Pd/Co_3O_4 sample was reduced by hydrazine, which denotes the formation of CoO(OH) species (Figure 4.2(b)) [20]. However, pure Co_3O_4 phase was obtained when the sample is calcined at 300 ^{o}C (Figure 4.2(c)). The introduction of the Pd species to $Co(OH)_2$ (denoted as Co_3O_4*) and a reduced Co_3O_4 (denoted as Co_3O_4(H)) prior to calcination, respectively, has resulted in a pure Co_3O_4 phase (Figure 4.2(d) and (e)). The reduction of the 2wt.%Pd/Co_3O_4* has resulted in a lower broadened peaks (Figure 4.2(d)), compared to (2wt.%Pd/Co_3O_4)(H) and 2wt.%Pd/(Co_3O_4(H)) samples (Figure 4.2(c) and (e)).

A further decrease in the diffraction peaks (with 2θ values of 19.2, and 38.9^{o}) was observed when 0.10 M sodium borohydride ($NaBH_4$) solution was used as a reducing agent (Figure 4.2(f)). The observed results suggest that $NaBH_4$ is a good reducing agent compared to hydrazine ($N_2H_4.H_2O$). The calculated average crystallite sizes for the as-prepared samples according to Figure 4.2 are presented in Table 4.1.

4.2.2 Brunauer-Emmett-Teller (BET) analysis

The surface area of the catalysts was confirmed using the BET analysis and is presented in Table 4.1. The surface area of the calcined Co_3O_4 catalyst is lower than the one for the reductive pre-treated Co_3O_4 catalyst. The introduction of 2wt.%Pd species on the calcined Co_3O_4 resulted in a decreased surface area, however, an increase in the surface area was observed when Pd species was introduced on the reduced Co_3O_4 prior to calcination (Table 4.1). The nitrogen adsorption-desorption isotherm data further indicates an increase in porosity and pore volume of hydrazine treated Co_3O_4, following the in-situ reduction and the mesoporous nature of Co_3O_4 phase remained intact (Table 4.1). This finding correlates with the report by Li *et al.* [21], on mesoporous CeO_2 support, which was not affected by the in-situ reduction process.

The surface area of the 2wt.%Pd/Co_3O_4 has increased from 44.2 m^2/g to 53.4 m^2/g after reductive pre-treatment by hydrazine. Calcination of the reduced 2wt.%Pd/Co_3O_4 catalyst showed a decrease in the surface area to 45.9 m^2/g. However, when the 2wt.%Pd is added on hydrazine treated Co_3O_4 prior to calcination, an increase in the surface area to 63.0% was observed. Further reduction of the catalyst by 0.1 M

hydrazine decreased the surface area to 58.1 m^2/g. The 2wt.%Pd/Co_3O_4* catalyst which was reduced by sodium borohydride, had a higher surface area than those pre-treated by hydrazine (Table 4.1).

Table 4.1 The effect of pre-treatment on the crystallite size and surface area of the as-prepared samples.

Catalyst	**S_{BET} (m^2/g)**	**Pore volume ($cm^3\ g^{-1}$)**	**Pore size (nm)**	**Average crystallite size (nm)[a]**
Co_3O_4(H)	62.2	0.158	9.95	20.0
Co_3O_4	49.7	0.137	11.3	23.2
CoO_xH_y(H)	126.5	0.142	7.82	7.74
$Co(OH)_2$				18.0
CoO(H)	56.6	0.184	13.0	11.4
(2wt.%Pd/Co_3O_4*)(B) 300 ^oC	71.3	0.174	9.76	20.9
2wt.%Pd/Co_3O_4 80^oC	44.2	0.164	15.5	23.6
(2wt.%Pd/Co_3O_4-CoO(OH))(H) 80^oC	53.4	0.132	15.6	32.6
(2wt.%Pd/Co_3O_4)(H) 300 ^oC	45.9	0.197	17.9	26.4
(2wt.%Pd/Co_3O_4*)(H) 300 ^oC	64.7	0.206	12.5	24.9
(1wt.%Pd/(Co_3O_4(H)) 300 ^oC	70.0	0.185	10.4	
(2wt.%Pd/(Co_3O_4(H)) 300 ^oC	63.0	0.170	10.1	22.5
(2wt.%Pd/(Co_3O_4(H))(H) 80 ^oC	58.1	0.161	14.4	
(3wt.%Pd/(Co_3O_4(H)) 300 ^oC	309.5	0.660	5.00	

[a] Average crystallite sizes were estimated from (311) plane of XRD patterns. Co_3O_4* = $Co(OH)_2$, Co_3O_4 = calcined $Co(OH)_2$, Co_3O_4(H) or CoO_xH_y(H) = hydrazine treated $Co(OH)_2$

An increase in surface area to 309.5 m^2/g was observed when 3wt.% Pd is loaded on the Co_3O_4, and cause for an increase could not be confirmed by EDS or ICP (the techniques only analyse the species on the catalyst surface). The results showed that synthesis method of the support prior to introduction of the Pd species affected the subsequent surface area. Lojewska *et al.,* [22] reported that the difference in surface

area of Co_3O_4 species can be due to change in the bulk structure, such as variations in Co^{3+} distribution in the defect spinel structure.

4.2.3 Thermogravimetric analysis (TGA)

The transformation of $Co(OH)_2$ (by in-situ reduction) as well as the stability of formed $CoO_xH_y(H)$, Co_3O_4, $Co_3O_4(H)$, 2wt.%Pd/($Co_3O_4(H)$) and CoO(H) catalysts were investigated by TGA under a nitrogen atmosphere at a heating rate of 10 ^oC/minute, as shown in Figure 4.3. The TGA profile of a $Co(OH)_2$ (Figure 4.3(a)) shows a weight loss of ~15% at 210 ^oC, due to structural transformation to Co_3O_4 species. A similar trend was observed with the $CoO_xH_y(H)$ (Figure 4.3(b)), which shows a weight loss of ~12.3% at 240 ^oC, which indicates transformation to Co_3O_4 species. The structural transformation of $Co(OH)_2$, and/or $CoO_xH_y(H)$ to Co_3O_4 species was further confirmed by DSC results (Figure 4.3 inset).

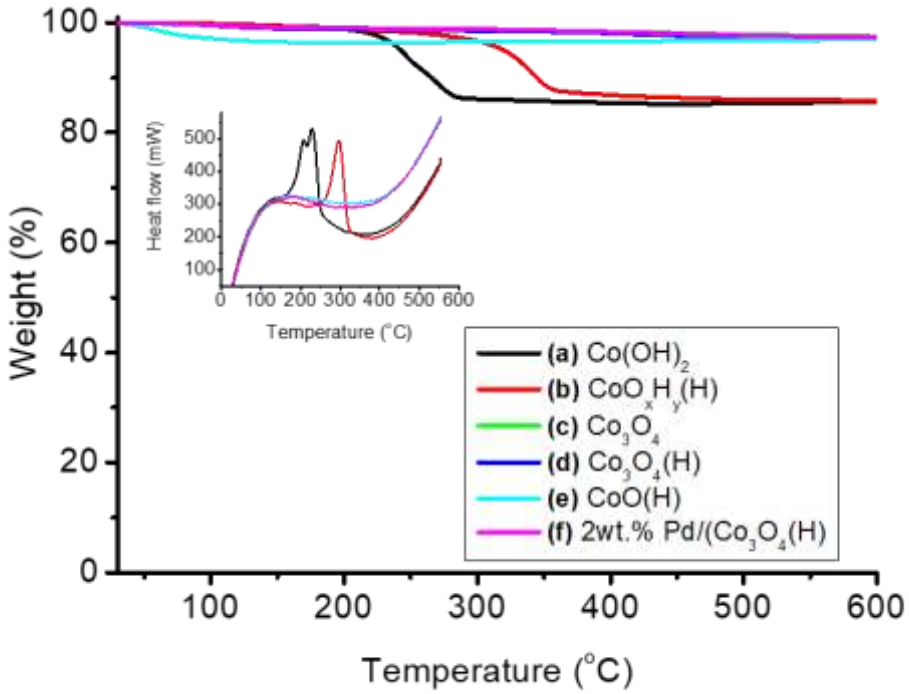

Figure 4.3 Thermogravimetric analysis of **(a)** $Co(OH)_2$, **(b)** $CoO_xH_y(H)$, **(c)** Co_3O_4, **(d)** Co_3O_4 (H), **(e)** CoO(H), and **(f)** 2wt.%Pd/($Co_3O_4(H)$) catalysts. Inset DSC results for the catalysts.

Similar behaviour was reported elsewhere [18, 23], during the transformation of $CoO(OH)/Co(OH)_2$ to Co_3O_4 in the presence of ambient air/helium. However, the as-prepared Co_3O_4, hydrazine treated Co_3O_4, and 2%Pd/(Co_3O_4(H)) samples remained stable up to 600 ^oC (Figure 4.3(c), (d), and (f)). This clearly indicates that the calcination process undertaken after in-situ reduction has completely transformed all the cobalt species to a spinel Co_3O_4 phase. As a result, the structure remained stable even in the presence of Pd species (Figure 4.3(f)). The TGA profile of CoO(H) (Figure 4.3(e)) initially showed a weight loss of 3.6% at 100 ^oC (the catalyst was not treated prior to analysis, and hence, the weight loss is due to the presence of moisture) which remained relatively stable up to 600 ^oC.

4.2.4 X-ray photoelectron spectroscopy (XPS) analysis

The oxidation state of various Co species formed over Co_3O_4, hydrazine treated Co_3O_4 (Co_3O_4(H)), and the CoO(H) sample are presented in Figure 4.4. The XPS survey spectra confirm the coexistence of C, Co and O over Co_3O_4, Co_3O_4(H), and CoO(H)), catalysts (Figure 4.4A). Two prominent peaks (at approximately 780.8 and 796.2 eV) with the absence of satellite peak at 786 eV, are due to the presence of Co^{3+} and Co^{2+} species within the Co_3O_4 spinel (Figure 4.4B(a) and (b)) [19, 24].

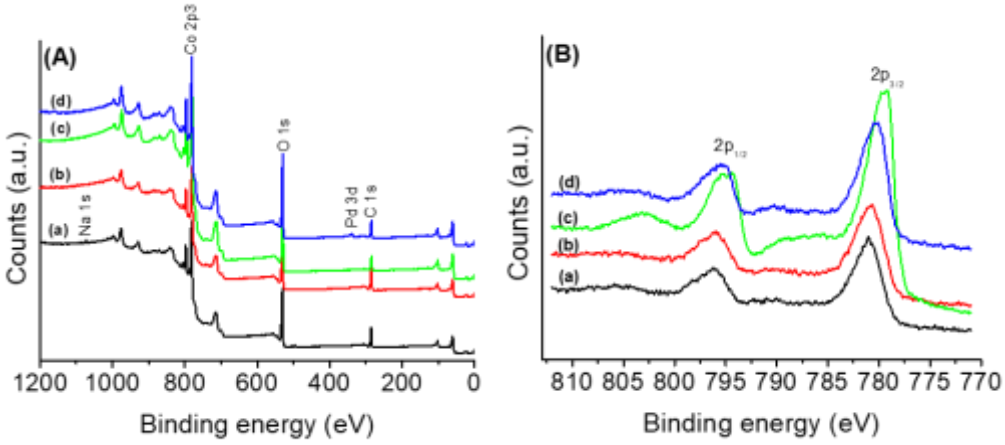

Figure 4.4 The XPS spectra of **(a)** Co_3O_4, **(b)** Co_3O_4(H), **(c)** CoO(H), and **(d)** 2wt.%Pd/(Co_3O_4(H)) catalysts. XPS survey spectra **(A)** and oxidation state **(B)** of samples.

The XPS data of as-prepared Co_3O_4 and hydrazine treated Co_3O_4 catalysts shows similar features, which suggests that the treatment with hydrazine did not alter oxidation state. The presence of Pd species is also confirmed by the survey spectra (Figure 4.4A(d)), and the structure has similar features like that of as-prepared and hydrazine treated Co_3O_4 samples (Figure 4.4B(a), (b) and (d)). The observed results suggest that Pd did not alter the structure of the Co_3O_4(H), as confirmed by XRD data. In the case of CoO(H) sample (Figure 4.4B(c)), a slight shift in the binding energy was observed at 779.5 and 794.7 eV, with the spin orbit splitting of 15.2 eV. The presence of a small satellite peak at 786 eV (Figure 4.4(c)) confirmed the presence of CoO [25]. The structural composition of 2wt.% Pd/Co_3O_4 catalysts was also confirmed by EDS data (see Appendix C).

In order to understand the role of Co^{3+}, the activities of CoO(H) catalysts were monitored during PROX reaction at different temperatures. The XPS spectra for Co 2p (A) and O 1s (B) from the CoO(H) and its spent catalysts (used in CO PROX reaction starting from 40 to 160 ^oC with an interval of 20 ^oC) are presented in Figure 4.5.

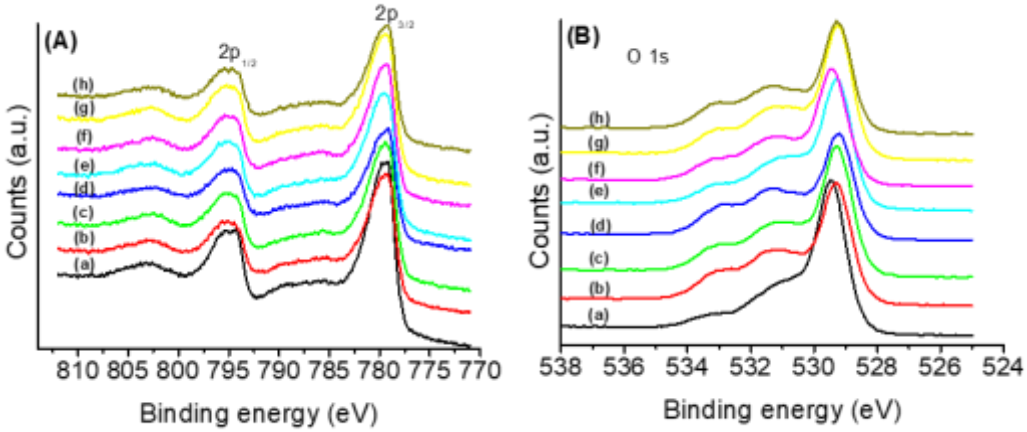

Figure 4.5 The XPS spectra of **(A)** Co 2p, and **(B)** O 1s of CoO (hydrazine treated) catalyst, for pure CoO and spent catalysts obtained at different temperatures in CO PROX.

The observed main peak of Co $2p_{3/2}$ at 779.4 eV and its satellite peak at 785.5 eV (Figure 4.5A(a)), indicates that the surface phase of the catalyst is CoO [24]. A

decrease in intensity of the Co 2p peak and its satellite peak was observed when the catalyst was used for PROX at 40 ^{o}C (Figure 4.5A(b)), and further decreased with an increase in reactor temperature (up to 100 ^{o}C). The XPS data of the catalyst at 100 ^{o}C shows the absence of the satellite peak, which confirms the formation of a Co_3O_4 spinel structure. These XPS data (Figure 4.5A) suggests that a transformation from Co^{2+} to Co^{3+} species has occurred, which supports the XRD data (Figure 4.1(f)). These findings are further supported by the data recorded by Nguyen *et al*. [26], who noted the presence of Co_3O_4 spinel structure during PROX. This structural change was also suggested elsewhere under CO oxidation [16]. Interestingly, above 120 ^{o}C under PROX the satellite peak seems to re-emerge, which could be due to the effects of temperature.

The O 1s spectra of CoO(H) (Figure 4.5B) showed one sharp peak at 529.5 eV, and two weak shoulder peaks at 531.2 and 533.3 eV. The high binding energy shoulders are assigned to nonstoichiometric oxygen atoms [27-28] and were defined to be oxygen atoms around oxygen vacancies in the surface lattice [26]. The main peak at 529.5 eV is due to the stoichiometric oxygen atoms of the catalyst surface [26]. Upon exposure to PROX gases, the two shoulder peaks became more visible and remain the same even at higher temperatures. Interestingly, the catalyst spent at 100 ^{o}C (Figure 4.5B(e)) shows that the shoulder peak at 531.2 eV has broadened, while that at 533.0 eV has weakened. This can easily be linked with the formation of spinel structure, as indicated above. The observed results suggest that the surface oxygen vacancies have increased during PROX, which differs from the results reported by Nguyen *et al*., [26]. This could be due to H_2 pre-treatment temperature, as well as hydrazine treatment effects.

4.2.5 Temperature programmed reduction (TPR) analysis

The TPR profile of Co_3O_4, Co_3O_4(H), CoO(H), and spent CoO(H) catalysts are presented in Figure 4.6. The transformation of the catalysts was investigated using H_2-TPR, as shown in Figure 4.6. The as-prepared Co_3O_4 (Figure 4.6(a)) exhibited two main broad peaks at 263 (with an area of 1260, as shown by deconvolution of TPR peak, insert) and 326 ^{o}C (with an area 1590), which belong to the stepwise reduction of $Co_3O_4 \rightarrow CoO \rightarrow Co$ [29]. Other researchers have reported similar reduction trend

of Co_3O_4, and this was found to depend on the calcination temperature and the morphology of the materials [30-31].

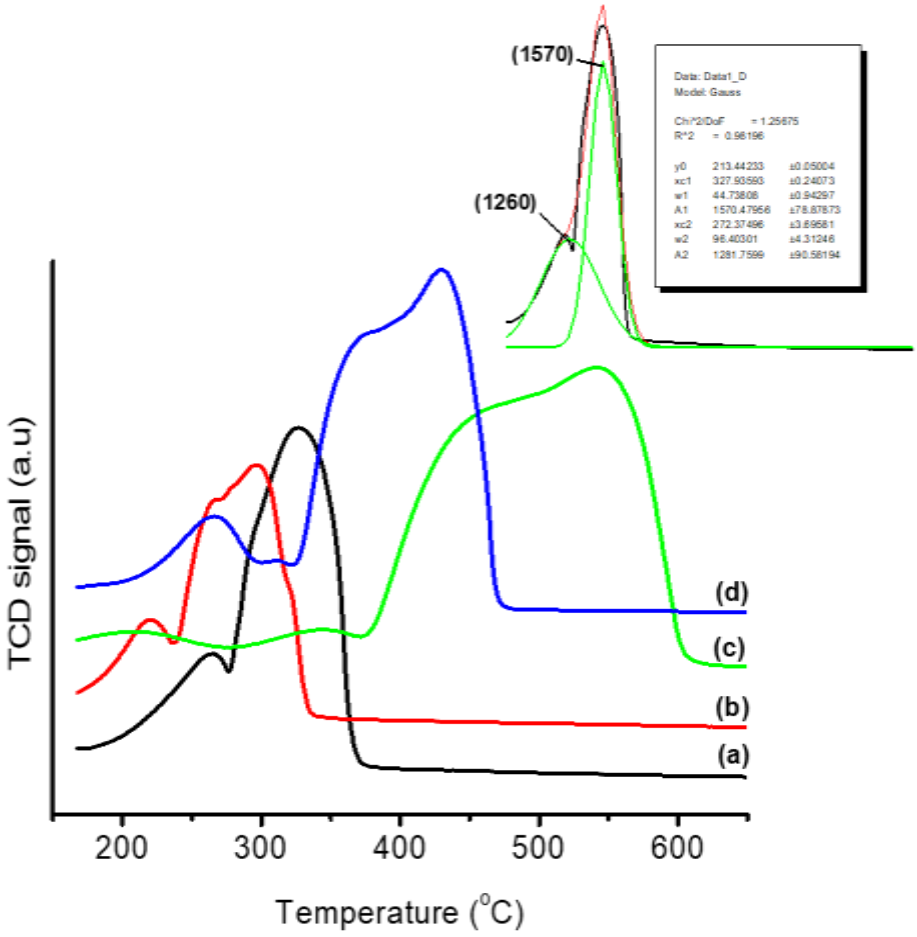

Figure 4.6 The TPR profiles of **(a)** Co_3O_4, **(b)** Co_3O_4(H), **(c)** CoO(H), and **(d)** CoO(H) spent catalyst. Inset example of deconvoluted TPR peak profiles of Co_3O_4.

The reductive pre-treatment of the Co_3O_4 by hydrazine (Figure 4.6(b)), lowered the reduction maxima from 263 to 220 ^oC ($Co_3O_4 \rightarrow CoO$). This clearly demonstrated that hydrazine did not eliminate the higher oxidation state of Co_3O_4; but rather change the surface reducibility of the catalyst. A slight decrease in the peak area (884) of the hydrazine treated Co_3O_4 (Figure 4.6(b)), suggests that a smaller amount of Co^{3+} species was reduced.

The CoO(H) catalyst (Figure 4.6(c)), shows an initial broad peak at 204 ^oC, which can be attributed to the reduction of octahedrally coordinated Co^{3+} species and the second broad peak with a maximum at 338 ^oC is attributed to the reduction of tetrahedrally

coordinated Co^{2+} species [29]. The TPR of CoO(H) (Figure 4.6(c)) indicated the absence of a Co_3O_4 peak as determined by deconvolution of its peak profile (which gave a negligible amount of area under the peak). The last intense broad peak which shows a reduction from 373 to 612 ^oC is attributed to octahedrally coordinated Co^{2+} species within CoO(H) catalyst. This indeed confirms that CoO(H) was successfully prepared, and the data is well supported by both XRD and XPS profiles. The TPR profile of a spent CoO(H) (Figure 4.6(d) shows a lower reducibility of the catalyst (at approximately 267 ^oC, with an area of 1656), which clearly resembles the reduction profile of Co_3O_4 spinel structure. The overall results suggest that some Co^{2+} (octahedral sites) were converted to Co^{3+} (octahedral sites) during PROX reaction (as relatively confirmed by XRD data). This support the reported results on CO oxidation [16].

4.2.6 Fourier transform infrared spectroscopy (FTIR) analysis

The FTIR spectra of $Co(OH)_2$, CoO_xH_y(H), Co_3O_4, Co_3O_4(H), 2wt.%Pd/(Co_3O_4(H)), and the CoO(H) samples are shown in Figure 4.7. The FTIR profile of Co_3O_4 and Co_3O_4(H) samples (Figure 4.7(c), (d), and (e)), displayed two distinct and sharp bands at 547 and 651 cm^{-1}, which originate from the stretching vibrations of the metal oxygen bonds (Co-O) [13, 18]. The band at 547 cm^{-1} is assigned to the octahedral arrangement of Co^{3+}, while the band at 651 cm^{-1} is due to Co^{2+} in the tetrahedral site [18], such arrangements of Co^{3+} and Co^{2+} ions at octahedral and tetrahedral positions respectively, confirms the formation of spinel Co_3O_4 phase [20]. This indicates that the same Co_3O_4 phase has been formed upon transformation of CoO_xH_y(H) by calcination, which is consistent with the XRD data. The structure of Co_3O_4 did not change after introduction of 2wt.%Pd species (Figure 4.7(e)). The intensive broad bands at 1631 cm^{-1} and 3347 cm^{-1} are due to O-H stretching vibrations interacting through H bonds [13]. The FTIR profile of $Co(OH)_2$ (Figure 4.7(a)), and that of CoO_xH_y(H) (Figure 4.7(b)), shows a sharp band at 3613 cm^{-1}, assigned to the non-hydrogen bonded hydroxyl group [7]. The 468 and 565 cm^{-1} bands are ascribed to Co-O stretching and Co-OH bending vibrations respectively, of either $Co(OH)_2$ or CoO(OH) (Figure 4.7(a) and (b)) [7, 32].

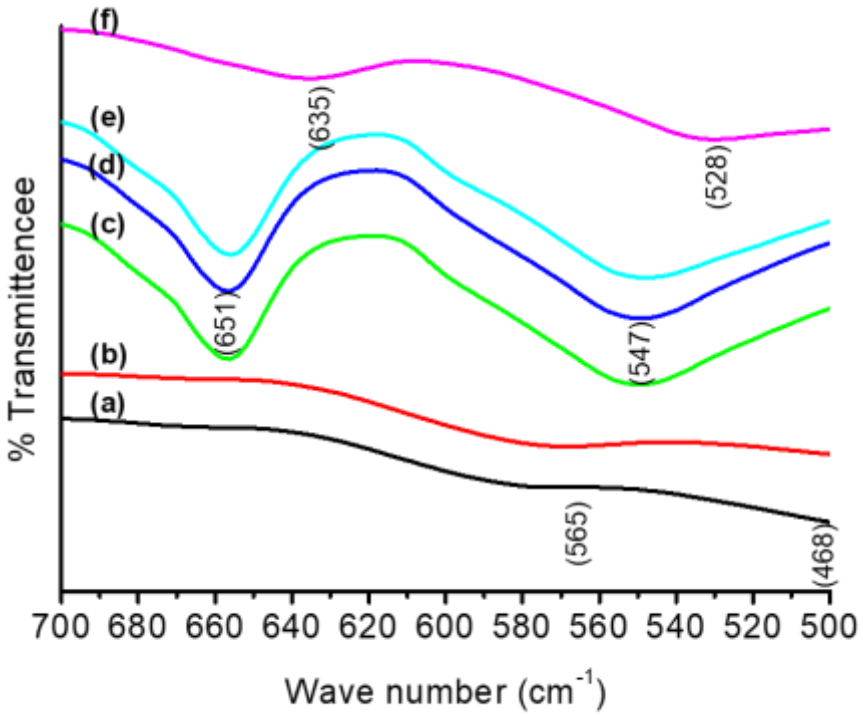

Figure 4.7 The FTIR spectra of **(a)** $Co(OH)_2$, **(b)** $CoO_xH_y(H)$, **(c)** Co_3O_4, **(d)** $Co_3O_4(H)$, **(e)** 2wt.%Pd/($Co_3O_4(H)$), and **(f)** CoO(H) catalysts.

The reduction of $Co_3O_4(H)$ by 5% H_2 balanced Helium at 250 ^oC partially convert the Co_3O_4 to CoO species (Figure 4.7(f)). The formation of CoO(H) is confirmed by the formation of weak bands at 528 and 635 cm^{-1} (Figure 4.7(f)), which originate from the stretching vibrations of the metal oxygen bonds (Co-O) [18]. The transformation of the structure was also confirmed by XPS and XRD data.

4.2.7 Scanning electron microscope (SEM) analysis

The SEM images of $CoO_xH_y(H)$, Co_3O_4, $Co_3O_4(H)$, CoO(H), and 2wt.%Pd/($Co_3O_4(H)$) samples are shown in Figure 4.8. The SEM images of $CoO_xH_y(H)$ (Figure 4.8(a)), indicate the presence of hexagonal platelets and rod-like morphology with agglomerations [33]. The SEM image of hydrazine treated Co_3O_4 (Figure 4.8(c)), indicates even more formation of hexagonal platelets upon calcination. This image resembles the SEM image of Co_3O_4 (Figure 4.8(b)), although its image shows the presence of some few rod-like morphology.

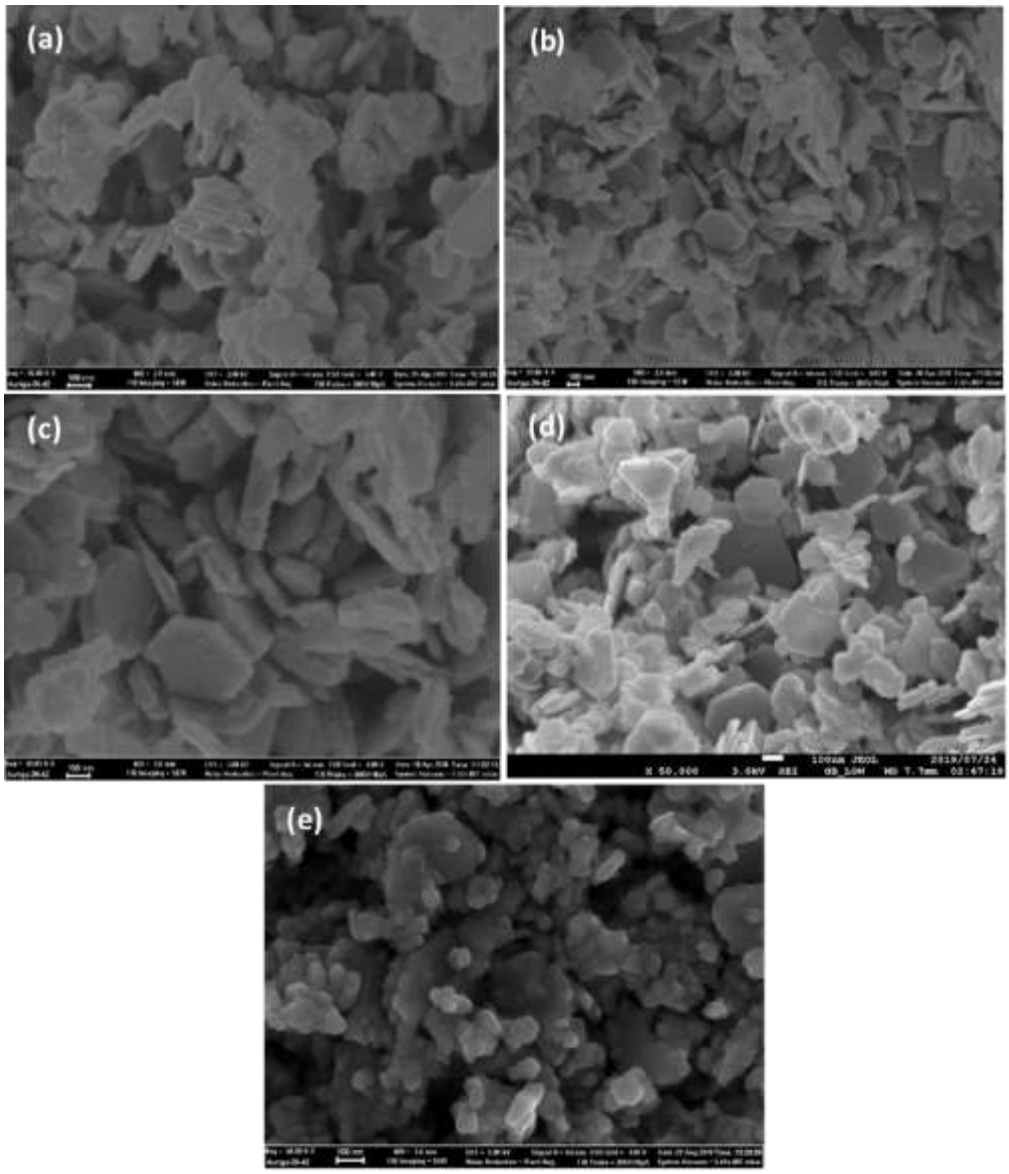

Figure 4.8 The SEM images of **(a)** CoO_xH_y(H), **(b)** Co_3O_4, **(c)** Co_3O_4(H), **(d)** CoO(H), and **(e)** 2wt.%Pd/(Co_3O_4 (H)) samples.

This suggests somehow that the in-situ reduction might have assisted in the transformation of rod-like to hexagonal platelets morphology during calcination. The overall structure remained intact, upon reduction by hydrazine, which correlates with the report by Chen *et al,* [33]. The SEM image of CoO(H) indicate the presence of hexagonal platelets like morphology (Figure 4.8(d)). The introduction of Pd species on the hydrazine treated sample did not change the structure of the Co_3O_4 (Figure 4.8(e)), as confirmed by XRD, FTIR and XPS data.

4.2.8 Transmission electron microscope (TEM) analysis

The TEM images of CoO_xH_y(H), Co_3O_4, Co_3O_4(H), CoO(H), 2wt.%Pd/(Co_3O_4(H)), and 3wt.%Pd/(Co_3O_4(H)) samples are shown in Figure 4.9.

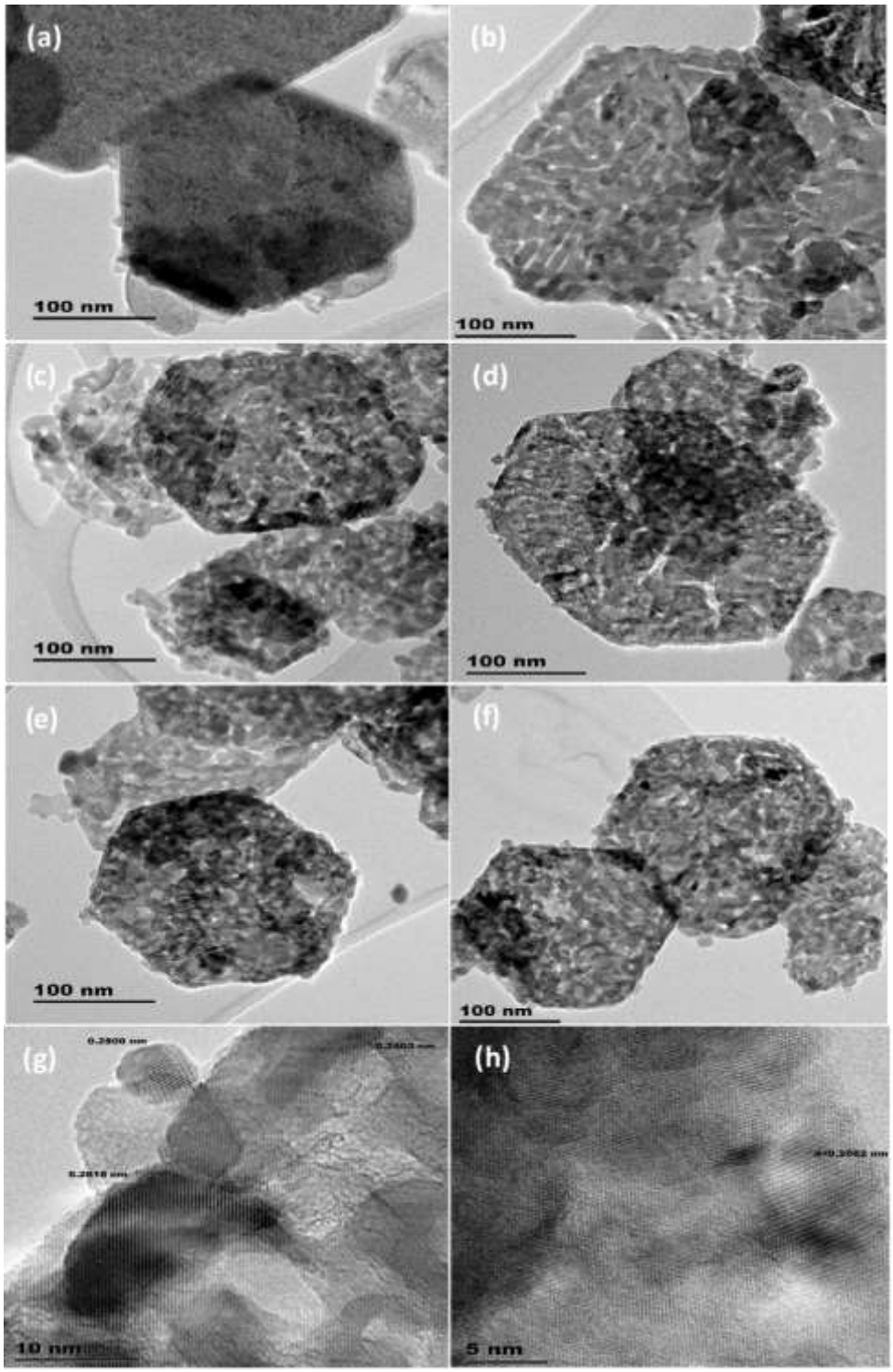

Figure 4.9 The TEM images of **(a)** CoO_xH_y(H), **(b)** Co_3O_4, **(c)** Co_3O_4(H), **(d)** CoO(H), **(e)** 2wt.%Pd/(Co_3O_4(H)), **(f)** 3wt.%Pd/(Co_3O_4(H)), and HRTEM image of **(g)** 2wt.%Pd/(Co_3O_4(H)), and **(h)** CoO(H), samples.

The TEM image (Figure 4.9(a)) clearly indicates the presence of hexagonal like morphology (possibly Co_3O_4 phases) that is over-shadowed by some porous layers [20, 33, 34], that could easily be associated with $CoO(OH)/Co(OH)_2$, in agreement with XRD data. The report by Liu *et al.* [15], noted an increase in surface roughness of as-prepared Co_3O_4, which is in agreement with this work (SEM and TEM data). Furthermore, the TEM image of Co_3O_4, Co_3O_4(H), 2wt.%Pd/(Co_3O_4(H)), and 3wt.%Pd/(Co_3O_4(H)) samples (Figure 4.9(b), (c), (e) and (f)), show some highly porous aggregates of nanoparticles with relatively uniform size distribution between 15 and 20 nm. This distribution is well aligning with the XRD data of the three samples.

The reductive treated 2wt.%Pd/Co_3O_4 by $NaBH_4$ resulted to pure hexagonal structure with rod-like morphology. Chen *et al.,* [33] have also observed pure hexagonal morphologies when Co_3O_4 is reduced by aqueous $NaBH_4$, the Co_3O_4 maintains its morphology. Moreover, the phase identification as shown on the HRTEM image, indicates the presence of lattice fringe spacing of 0.24 nm (311) (Figure 4.9(g)) [35-36], and 0.28 nm (220), which confirms the characteristic lattice structure of Co_3O_4 [34, 36]. Similar observation on the lattice spacing over Co_3O_4 species was reported by Hu *et al,* [37]. Although Pd particles cannot be observed in the TEM images, the EDS and XPS data shows that the 2wt.%Pd/Co_3O_4 catalysts contain the following elements Co, C, O, and Pd, which indicate that the Pd species are highly dispensed on the cobalt support. A similar observation on the dispersion of Pd on the pure Co_3O_4 support was reported by Xu *et al*. [38], and Wang *et al*, [39].

The diameters for pure Co_3O_4 were measured to be in the range of 5-500 nm, and the subsequence catalysts were having diameters in the range 10-500 nm indicating the minor influence of Pd loading on the morphology. The TEM image for CoO(H) (Figure 4.9(d)) shows hexagonal like morphology as indicated by SEM data. The HRTEM indicate the lattice fringe spacing of 0.206 nm (200) (Figure 4.9(h)), which denote a cubic face of a CoO [40].

4.3 CATALYTIC ACTIVITY FOR PROX OF CO REACTION

All catalysts were tested for CO PROX at the reaction temperature of 40 to 220 ^{o}C, the feed contained 1% CO, 1% O_2, 50% H_2, and 48% He. The 200 mg of the samples was loaded in a U-shape borosilicate glass reactor and conditioned at 40 ^{o}C in helium flow at 20 ml/min for 30 min, prior to catalytic tests. The stability of the catalysts was investigated under dry, 15% CO_2 and moisture conditions at 100 ^{o}C for 21 h.

4.3.1 Effects of hydrazine pre-treatment as compared to as-prepared Co_3O_4 and mixture of CoO(OH) and $Co(OH)_2$

The data in Figure 4.10 shows the temperature dependence catalytic activities of CoO_xH_y(H), Co_3O_4 and Co_3O_4(H) catalysts for PROX of CO. The CoO_xH_y(H) catalyst (Figure 4.10A(a)) showed 18% CO conversion at 40 ^{o}C, which drastically increased to 72% as the temperature was increased. The catalyst had a maximum CO conversion of 100% at 120 ^{o}C, however, the activity was accompanied by a decrease in selectivity as temperature increases (Figure 4.10B(a)). The Co_3O_4 catalyst (Figure 4.10A(b)) showed a lower activity at lower temperature; however, its activity improved with temperature. Eventually, the catalyst achieved a maximum CO conversion at 160 ^{o}C. Such an increase is attributed to a transformation of $Co(OH)_2$ into a spinel Co_3O_4 phase by calcination at 300 ^{o}C, as evidenced by structural changes on TEM and SEM data. The TGA profile of Co_3O_4 also showed a stable phase within the temperature range, explored on PROX reaction. The catalyst had a slight decrease in conversion and selectivity (Figure 4.10B (b)) above 160 ^{o}C, which can be associated with small moisture formation [41].

Interestingly, the Co_3O_4(H) catalyst (Figure 4.10A(c)) showed an exponential increase from 40 to 80 ^{o}C and a drastic change to 100% conversion at 100 ^{o}C, with good selectivity. The in-situ reduction decreased the maximum CO conversion temperature ($T_{100\%}$) from 160 ^{o}C (over Co_3O_4 catalyst) to 100% at 100 ^{o}C (Figure 4.10A(c)). The $T_{100\%}$ of standalone Co_3O_4(H) catalyst is well comparable/above (with) the activity of CuO-ceria catalyst [42-45], and better off in terms of selectivity. An average of 98% CO conversion falls within the fuel cells operating temperature window [46]. The PROX activity of Co_3O_4(H) catalyst is consistent with the suggestion made by Boyd *et al.* [4], though on a different system (i.e., for the need of partially reduced gold state).

Although, some in-situ reduction has occurred, on Co_3O_4(H) catalyst, the FTIR data did not show peak ratio differences. Similarly, the XPS results do not provide clear dependents of PROX reaction on oxidation state of cobalt. However, the TPR data indicates that hydrazine did not completely eliminate the higher oxidation state of Co_3O_4 but improved the surface reducibility/properties of the catalyst.

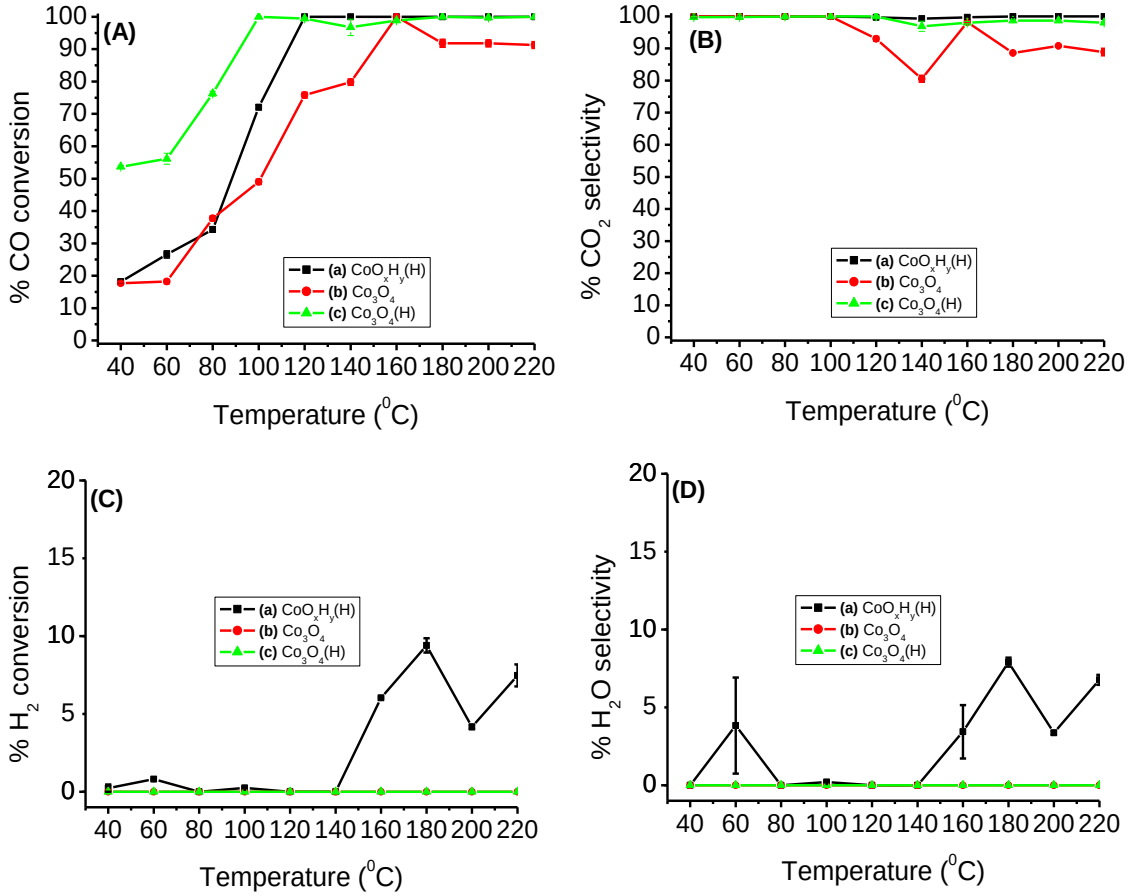

Figure 4.10 The CO conversion **(A)**, CO_2 selectivity **(B)**, H_2 conversion **(C)**, H_2O selectivity **(D)** of **(a)** CoO_xH_y(H) 80 ^oC (■), **(b)** Co_3O_4 300 ^oC (●), and **(c)** Co_3O_4 (H) 300 ^oC (▲) catalysts.

Several studies [47-48] and a recent finding [33], has attributed to an enhanced activity of *p*-nitrophenol reduction over the reduced Co_3O_4 catalyst, to the oxygen vacancies created during surface reduction process. It is therefore expected that the high PROX activity observed over Co_3O_4(H) could easily be associated with the created oxygen vacancies [48]. In addition to the oxygen vacancies created, the BET data showed an improved specific surface area and pore volume (Table 4.1), upon reduction. The

catalyst had almost 100% selectivity to CO_2 from 40 to 120 ^oC, which was followed by almost 6% decrease at 140 ^oC (Figure 4.10B(c)). The catalyst showed almost zero H_2 conversion and selectivity towards moisture (Figure C and D(c)). The Co_3O_4(H) catalyst outperformed the PROX activity of the Co_3O_4-CeO_2 catalyst reported by Arango-Diaz *et al,* [46]. This reduces the need of bi-metallic oxides catalysts; which could result in lower catalytic costs.

To further evaluate the role of the CoO(OH) formed due to in-situ reduction of prepared $Co(OH)_2$, resulted in a mixture of CoO(OH) and $Co(OH)_2$, a portion of as-prepared CoO(OH) was reduced by hydrazine, calcined at 300 ^oC for 4 h. The PROX reaction data of the catalyst produced similar activities to that of the hydrazine treated Co_3O_4 catalyst (CO conversion and selectivity), which indicate the independence of route taken.

4.3.2 PROX of CO over Co_3O_4 and Co_3O_4 (H) catalysts pre-treated with 5% H_2

The effect of the oxidation state of cobalt in the PROX of CO in hydrogen rich stream was investigated by reducing both Co_3O_4 and Co_3O_4(H) by 5% H_2 balanced He at 250 ^oC for 1.5 h to form CoO and CoO(H) species [16]. The CoO and CoO(H) catalysts were tested for PROX of CO in excess H_2 feed stream at 40-220 ^oC. Figure 4.11 present the results for CO PROX in excess H_2 over CoO, CoO(H), Co_2O_4, and Co_3O_4(H) catalysts, respectively.

The CoO(H) catalyst (Figure 4.11(d)) has shown a slight improvement in CO conversion with temperature, when compared with the CoO (Figure 4.11A(b)) and Co_3O_4(H) catalyst (Figure 4.11A(c)), at low temperature region. The CO conversion at 80 ^oC has improved from 73.4% (over Co_3O_4(H) catalyst) to 87.5% over CoO(H) catalyst (Figure 4.11A(b) and (c)). However, the activities of the three catalysts were comparable at higher temperatures. The activity of CoO(H) can easily be traced back to the surface profile of the catalyst upon exposure to PROX gases. This has been clearly demonstrated by XPS data, which indicated a transformation of octahedrally coordinated Co^{2+} species to octahedrally coordinated Co^{3+} species [16]. This was further confirmed by TPR and XRD profiles of spent CoO(H) catalyst. This behaviour supports the reported oxidation of an octahedral Co^{2+} species, which resulted in high CO oxidation [16]. However, the catalytic selectivity of CO to CO_2 species has

improved over CoO(H) catalyst, when compared to CoO and Co_3O_4(H) catalyst. The CoO(H) catalyst has shown a lower H_2 conversion than Co_3O_4(H) catalyst, as a result, the selectivity of H_2 to moisture is lower over CoO(H) catalyst.

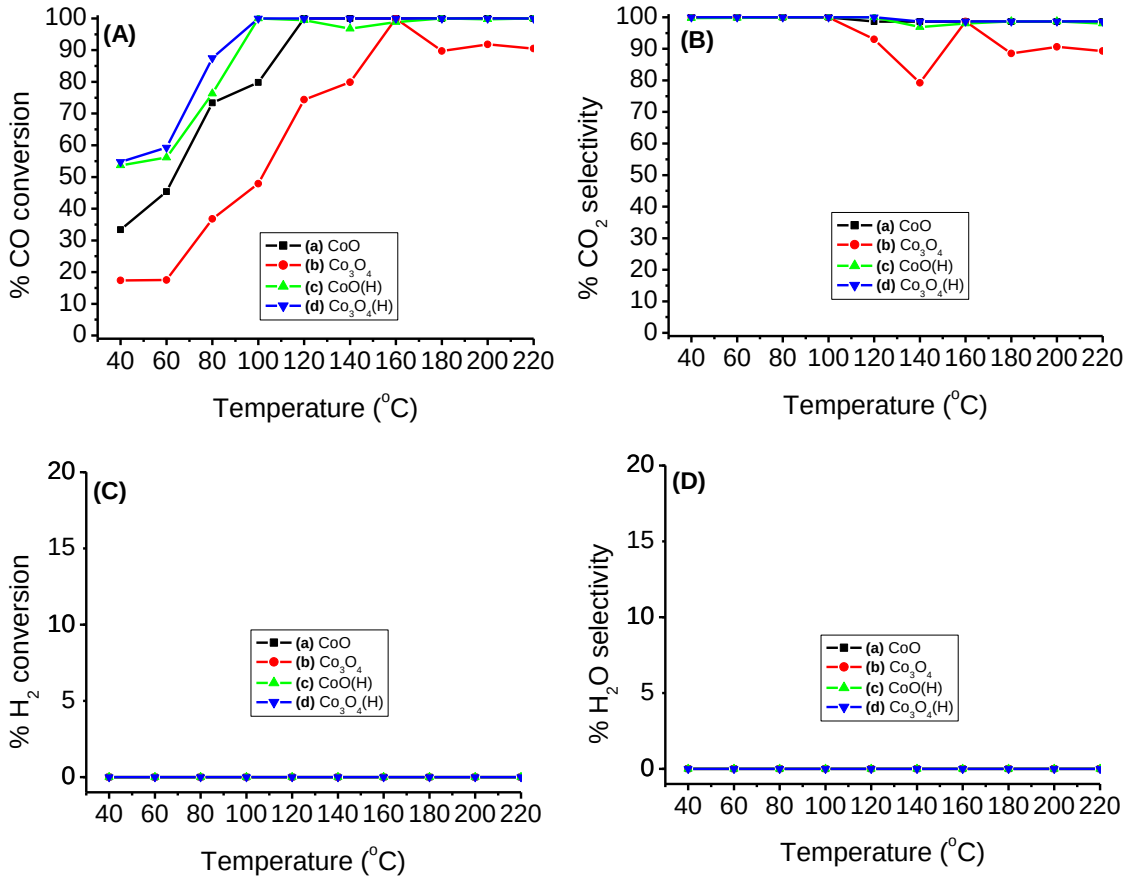

Figure 4.11 The CO conversion **(A)**, CO_2 selectivity **(B)**, H_2 conversion **(C)**, H_2O selectivity **(D)** of **(a)** Co_3O_4 (■), **(b)** CoO (●), **(c)** Co_3O_4 (H) (▲), and **(d)** CoO (H) (▼) catalysts.

Gu *et al.,* [16] have shown that oxidation of Co^{2+} to Co^{3+} during catalytic activity results to a higher catalytic activity of cobalt. Other researchers have concluded that the main factor that determines the activity and selectivity for CO oxidation in the presence of hydrogen is Co^{3+} species (at the octahedral) on the surface of the catalyst, while other secondary factors also contribute to the activity [49]. A good catalytic performance of the metal oxide containing tetrahedrally coordinated Co^{2+} was observed by other researchers [1, 16]. The CoO catalyst can be easily oxidised to Co_3O_4 under an oxidative atmosphere, and such unique catalysis of CoO can be observed only in a

reductive atmosphere [1, 16]. The XRD data for the spent catalyst has shown the transition of the CoO(H) catalysts to Co_3O_4(H) phase (Figure 4.1(f)). That conclude the findings by other researchers that Co^{3+} play a major role in the activity of the cobalt oxide in CO oxidation [16, 49].

4.3.3 The role of CO/O_2 ratio (λ), moisture, and activation energy on the activity of Co_3O_4(H) catalysts

4.3.3.1 Effect of CO/O_2 ratio (λ)

The effect of CO/O_2 ratio (λ) in CO PROX in H_2 rich stream over Co_3O_4(H) catalyst was conducted at 40-220 ^oC and the results are presented in Figure 4.12. The oxidation for both CO and H_2 species increases with an increase in the CO/O_2 ratio (λ) (Figure 4.12A). Higher CO/O_2 ratio (λ) favoured catalytic selectivity to H_2 conversion, and the formation of moisture (Figure 4.12C and 4.12D). As a result, selectivity of CO to CO_2 decreases as the excess oxygen increases (Figure 4.12B).

The high density of oxygen vacancies gives high activity for PROX in terms of high conversion of CO in H_2 [50]. However, the catalyst is also selective to H_2 conversion to moisture. The observed results are in good agreement with the results reported by Marino *et al.* [32], under PROX of CO in excess H_2 over Pt/CeO_2-ZrO_2 and Ir/CeO_2-ZrO_2 catalysts, respectively. Reina *et al.,* [51] have shown that an increase in the mobility of oxygen increases the oxidation of hydrogen. The reactor temperature gives different optimum selectivity to CO conversion with respect to the CO/O_2 ratio (λ). Marino *et al.,* [32] have reported an optimum CO oxidation at a temperature below 100 ^oC, a decreased CO oxidation is ascribed to higher oxidation of hydrogen at a higher temperature.

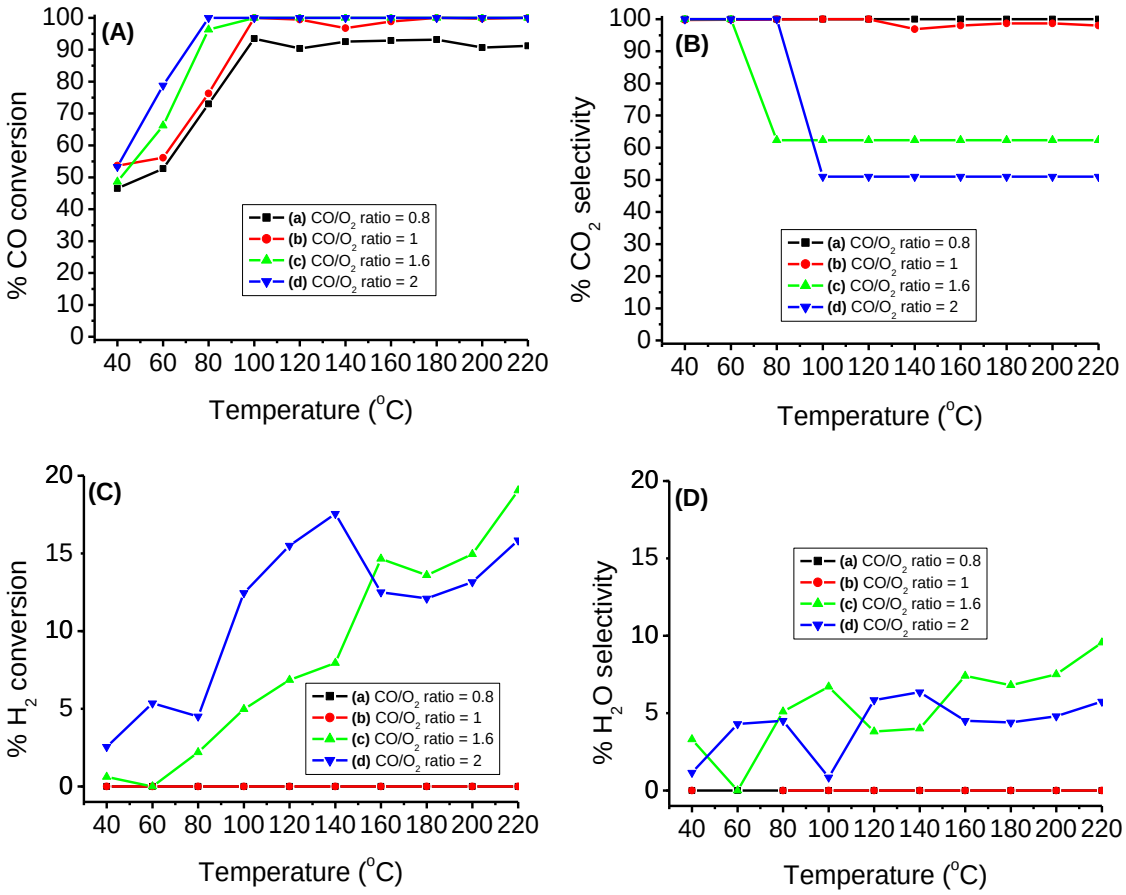

Figure 4.12 The CO conversion **(A)**, CO_2 selectivity **(B)**, H_2 conversion **(C)**, H_2O selectivity **(D)** of Co_3O_4(H) catalyst effect of CO/O_2 ratio (λ); **(a)** 0.8 (■), **(b)** 1.0 (●), 1.6 **(c)** (▲), and **(d)** 2.0 (▼).

4.3.3.2 Stability of catalysts as function of temperature

The CO PROX in excess H_2 was investigated over Co_3O_4 (H) in the presence of moisture at 40-220 °C. Figure 4.13 present the results obtained in PROX of CO in excess H_2 feed under dry, and moisture condition (~10%), respectively. The catalyst had the CO conversion of 46.1% at 40 °C and 49.3% at 60 °C under moisture condition (Figure 4.13A(b)), which is lower compared to PROX under dry condition. However, the activity in CO oxidation improves with reactor temperature, as a result, a 65.5% of CO conversion was observed at 80 °C. The catalyst gave almost the same activity to that of the dry condition at temperatures above 80 °C. A slight decrease in the selectivity of CO to CO_2 was observed with temperature (Figure 4.13B(b)). The

catalytic activity of the Co_3O_4(H) catalyst had shown an increase in conversion of H_2 species with temperature, under moisture condition (Figure 4.13C(b)).

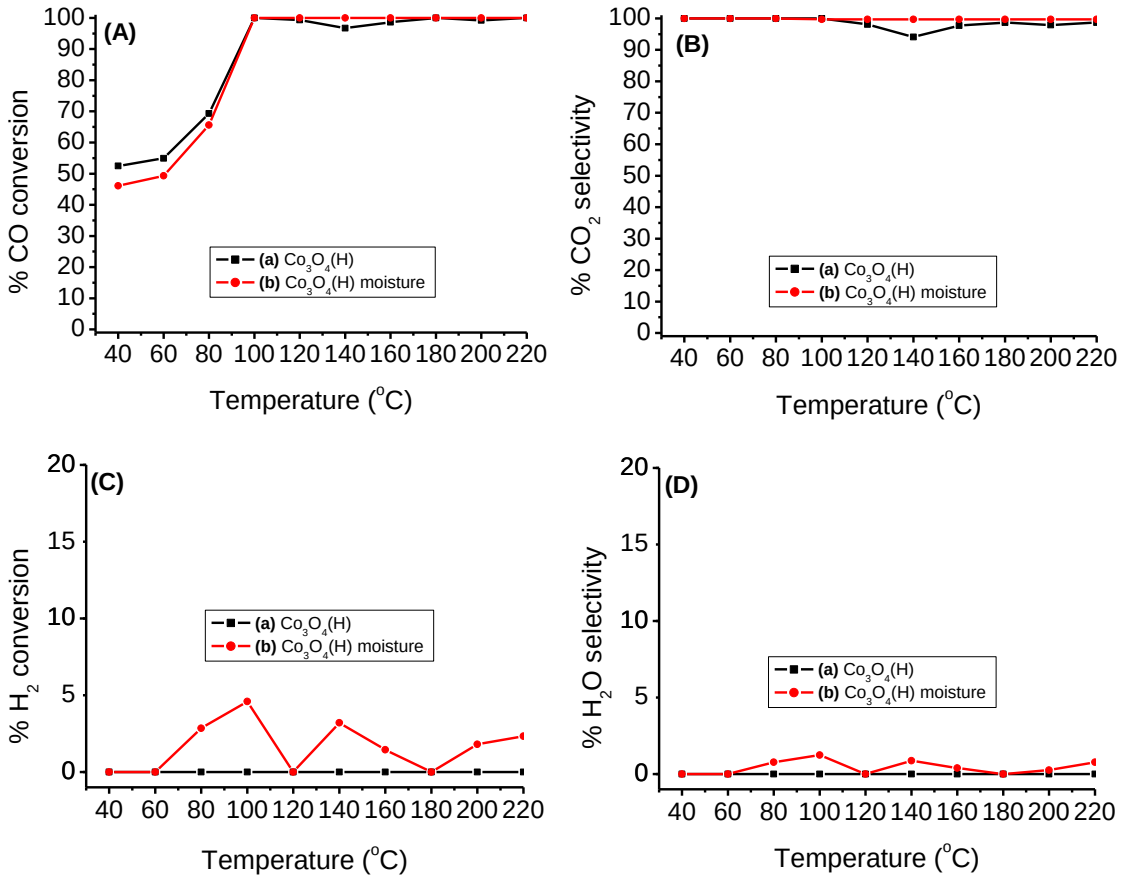

Figure 4.13 The CO conversion **(A)**, CO_2 selectivity **(B)**, H_2 conversion **(C)**, H_2O selectivity **(D)** of Co_3O_4(H) catalyst under; **(a)** dry (■), and (**b)** moisture condition (●).

Li *et al.,* [21] have shown that the deactivation is unlikely to occur due to the physical and textural changes in the catalyst system, which may be attributed to the relatively high moisture concentration, and that can lead to H_2O capillary condensation in the smaller pores of the catalyst. Consequently, by preventing the access of the reactants to the catalyst surface. Generally, increasing the temperature can remove the occurrence of H_2O capillary condensation. As a result, the activity of the Co_3O_4(H) catalyst is higher at higher temperature under moisture condition.

4.3.3.3 Effect of Activation energy

The comparative study on the activation energy required for CO PROX in excess H_2 under dry, and moisture condition was investigated over Co_3O_4(H) catalyst at 40-70 ^oC, respectively. The activation energies for CO conversion was calculated from Arrhenius plots, as shown in Figure 4.14. A decrease in the specific reaction rate from 2.98 x 10^{-3} $mol_{CO}/g_{Cat}/h$ (under dry condition) to 1.32 x 10^{-3} $mol_{CO}/g_{Cat}/h$ (under moist condition) at 40 ^oC was observed.

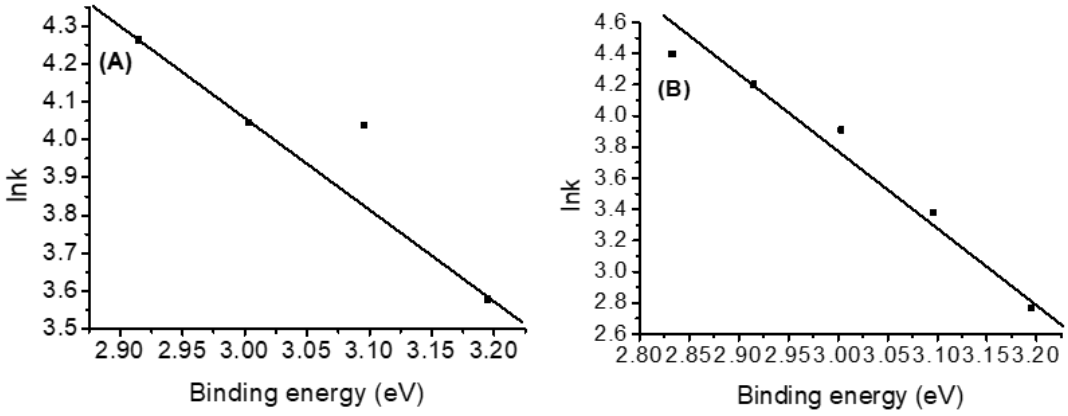

Figure 4.14 Arrhenius plots for the reaction rate of PROX reaction (activation energy, E_a) over Co_3O_4(H) catalyst under **(A)** dry, and **(B)** moisture condition.

The catalyst activation energies for CO PROX reactions under dry and moisture conditions were found to be 21.5 kJ/mol and 42.1 kJ/mol, respectively (Figure 4.14A and B). This increase in the activation suggest that the active sites of the catalyst are impeded by water molecules and lower the adsorption of CO on the active sites on the catalyst surface. Similar findings were reported by Li *et al.* [21], they suggested that water molecules condense on the surface of the catalysts and block access of the reactant movement to the active sites. Thus, the presence of moisture in the feed stream during PROX increased the activation energy for the activity and selectivity of the Co_3O_4(H) catalyst (Figure 4.14B).

4.3.4 The stability test of the catalysts in CO PROX reaction

The stability of the catalysts was investigated over the Co_3O_4 and Co_3O_4(H) catalysts at 100 ^oC for 21 h. Effect of moisture and CO_2 in CO PROX was also investigated over the most stable catalyst (Co_3O_4(H)) at 100 ^oC for 21 h, respectively. Figure 4.15 shows the results for the stability tests, effect of moisture and CO_2 in the feed.

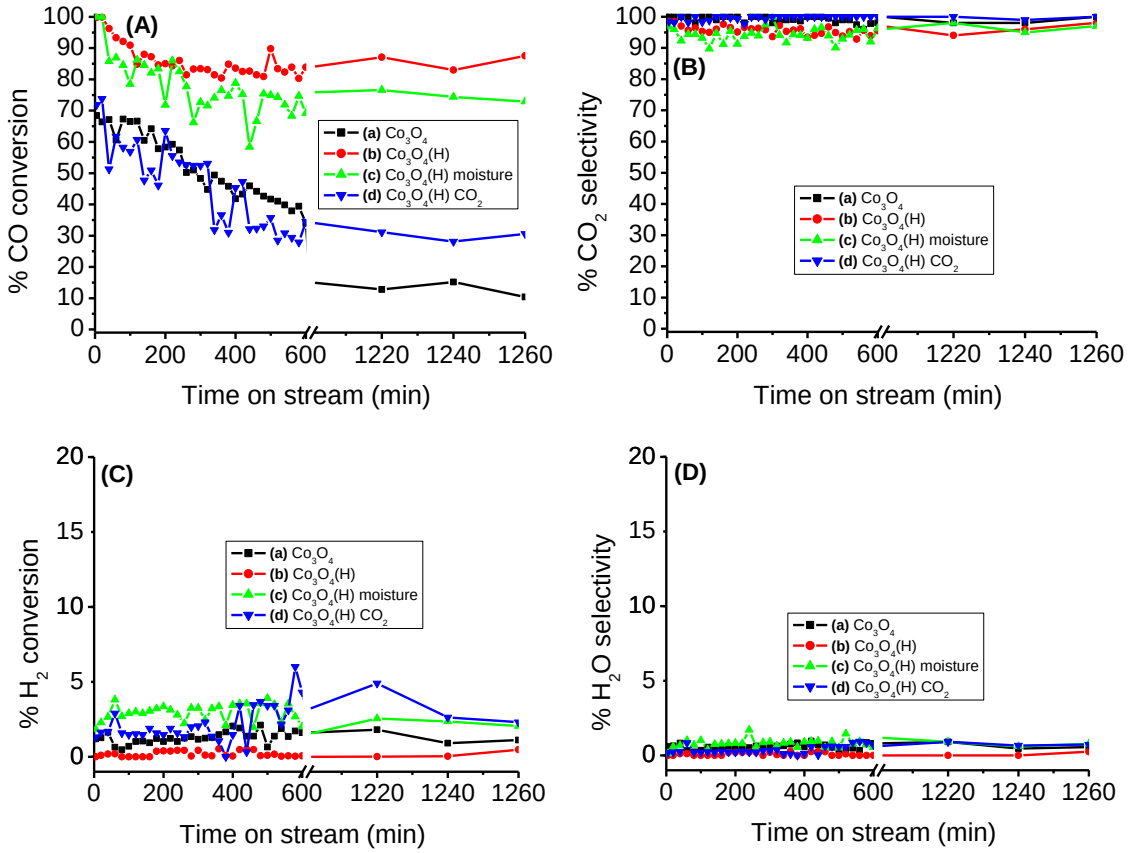

Figure 4.15 The CO conversion **(A)**, CO_2 selectivity **(B)**, H_2 conversion **(C)**, H_2O selectivity **(D)** of **(a)** Co_3O_4 (■), **(b)** Co_3O_4(H) (●), **(c)** Co_3O_4(H) moisture (▲), and **(d)** Co_3O_4(H) CO_2 (▼) catalysts with time on stream.

The Co_3O_4 catalyst gave approximately 68% CO conversion, which deactivated with time on stream at 100 ^oC for 21 h (Figure 4.15A(a)). Other researchers have reported Co_3O_4 as an excellent candidate for CO oxidation in the presence of hydrogen [52-53]. They have shown that excess amount of hydrogen under PROX condition may result in lower oxidation state cobalt phases, including metallic cobalt, which may promote side reactions [54-55]. However, the Co_3O_4(H) catalyst produced 100% CO

conversion, which remained the same for almost an hour (Figure 4.15A(a)). Thereafter, the catalyst activity decreased to 85% (after 160 min), which was accompanied by steady fluctuations for almost 21 h (Figure 4.15A(b)). Interestingly, upon the introduction of moisture in the feed, the Co_3O_4(H) gave almost the same activity as that of the dry condition (Figure 4.15A(a) and (b)). The activities of this catalyst remained almost unchanged for 21 h, which indicates very good stability, especially under moisture condition. This data is consistent with the report by Li *et al.* [21], who have noted a stable and high CO oxidation at higher temperature; hence, avoiding the phenomenon of H_2O capillary condensation. The stability of hydrazine treated Co_3O_4 under dry condition can well be attributed to the in-situ reduction as compared to as-prepared Co_3O_4 catalyst which seems to loose activities much faster.

The catalytic activity of hydrazine treated Co_3O_4 catalyst in the presence of 15% CO_2 in the feed showed a sudden decrease from 75% CO conversion within 5 min at 100 ^oC. As time progressed, a steady decrease to 27% CO conversion was observed. The decrease in CO conversion can be associated with a competitive effect between CO and CO_2 that hinders the redox circle Co^{3+}-Co^{2+} [41, 46]. Other researchers have reported that Co_3O_4 catalyst deactivates in excess H_2 due to the formation of CoO and low tolerance for CO_2 and H_2O [46].

4.3.5 Effect of reduction of Pd/Co_3O_4 catalyst in CO PROX reaction

Effect of reduction of 2wt.%Pd/Co_3O_4 catalyst in CO PROX reaction was investigated by introducing Pd species on a calcined Co_3O_4 support, and a portion of the prepared catalyst was reduced by 0.1 M hydrazine solution and dried at 80 ^oC. Figure 4.16 present the results obtained in PROX of CO in excess H_2 over the prepared catalysts. The introduction of Pd species on the calcined Co_3O_4 catalysts suppressed the catalytic activity of Co_3O_4 in CO PROX reaction (Figure 4.16A(a)). It can be clearly seen that the catalyst is good in the conversion of H_2 species to moisture (Figure 4.16C(a)). Nguyen *et al.,* [5] reported the poor activity of Pd/CeO_2 catalyst in terms of CO conversion and the selectivity to CO_2 in PROX. This was previously ascribed to hydrogen absorption by Pd, leading to preferential formation of moisture [56-58].

However, the hydrazine treated 2wt.%Pd/Co_3O_4–CoO(OH) showed an improvement in CO conversion from 11% (over 2wt.%Pd/Co_3O_4) to 46% at 100 ^oC (Figure 4.16A(a) and (b)). The reductive pre-treatment improved the surface area of the catalyst from 44.1 to 53.4 m^2/g (as indicated by BET data). As a result, the catalyst activity in PROX of CO has improved. The selectivity of CO to CO_2 increased with temperature (Figure 4.6B(b)), the catalyst had the highest selectivity of 71% at 180 ^oC. The selectivity to moisture was minimized (Figure 4.16D(b)), though, the activity is still lower compared to that of the cobalt oxide support alone.

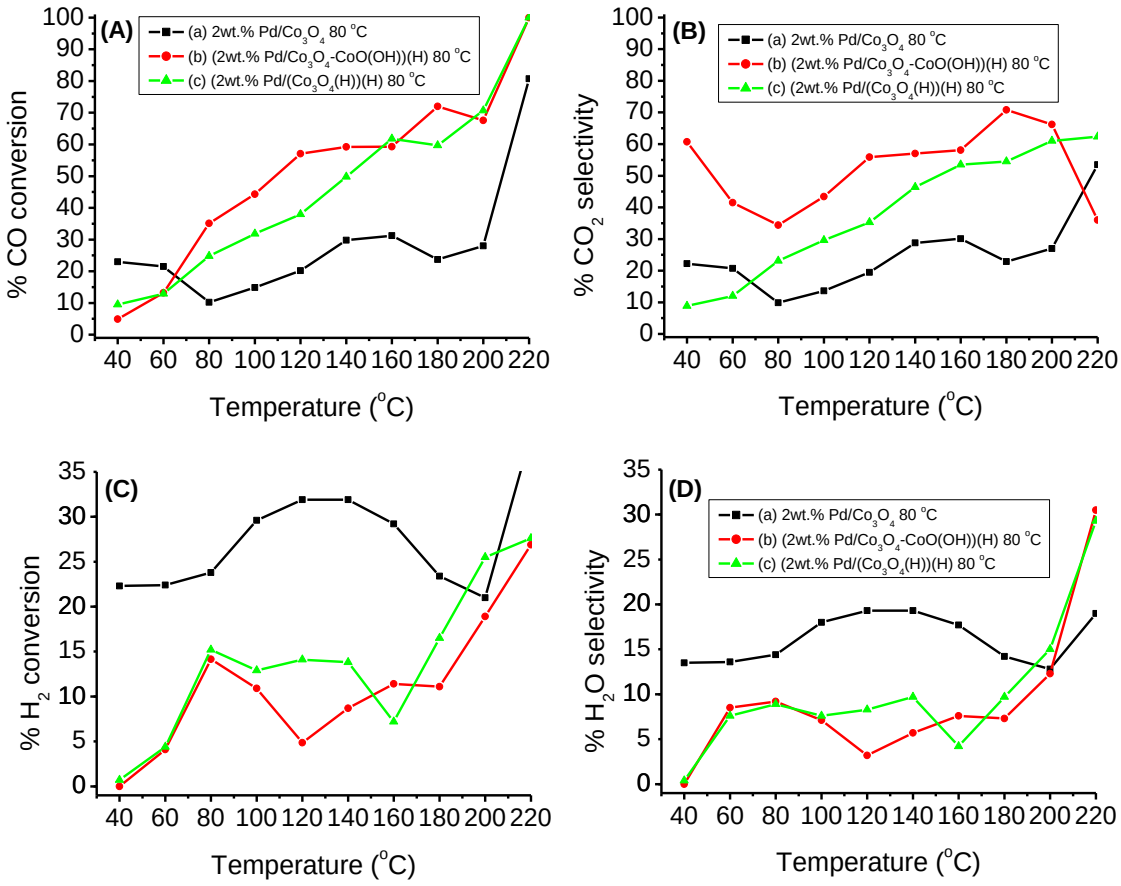

Figure 4.16 The CO conversion **(A)**, CO_2 selectivity **(B)**, H_2 conversion **(C)**, H_2O selectivity **(D)** of **(a)** (2wt.%Pd/Co_3O_4) 80 ^oC (■), **(b)** (2wt.%Pd/Co_3O_4-CoO(OH))(H) 80 ^oC (●), and **(c)** (2wt.%Pd/(Co_3O_4(H))(H) 80 ^oC (▲).

We have noted that even when (2wt.%Pd/Co_3O_4*)(H) catalyst is calcined at 300 ^oC the activity is still the same (see Appendix D). When the support is reduced for the

second time the activity of the catalyst has decreased from 46% CO conversion (over 2wt.%Pd/(Co_3O_4(H)), to 34% at 100 ^oC (Figure 4.16A(c)). The results suggest that Pd species which is not reduced (Figure 4.16C(a)) promote the conversion of H_2 to moisture, and hydrazine treated Pd species (Figure 4.16A(b) and C(b)) favour conversion of CO and less of the H_2 species.

4.3.6 The effect of pre-treatment atmosphere prior to CO PROX reaction

The effect of pre-treatment prior to CO PROX reaction was investigated over (2wt.%Pd/Co_3O_4*)(H) catalyst, which was prepared by calcination of a reduced 2wt.%Pd/$Co(OH)_2$ catalyst. The catalyst was divided into three portions and conditioned at 200 ^oC for 30 min in the (i) helium flow at 20 ml/min, (ii) the second portion was oxidised by flushing 10% O_2, (iii) and the last portion was reduced by flushing 50% H_2 species, respectively. The reactor temperature was allowed to cool down to 40 ^oC before catalytic tests. Figure 4.17 present the results obtained in PROX of CO over (2wt.%Pd/Co_3O_4*)(H) catalysts, conditioned at different atmospheric environments.

The catalyst which was conditioned in 50 % H_2 balanced helium atmosphere resulted to a bit lower activity of 13.7% at 100 ^oC in CO PROX (Figure 4.17A(b)), compared to other pre-treatment conditions. The catalyst favour formation of moisture at higher temperature (Figure 4.17C(b)). Teng *et al.* [1], have shown that at higher reductive condition most metal oxides are reduced to lower valence oxides or metallic phases. Hence, such irreversible changes of the catalysts leading to the higher selectivity of the H_2 oxidation and/or formation of CH_4 gas [1-2]. An improvement in the activity to 36.9% CO conversion was observed over the catalyst which was conditioned in O_2 atmosphere (Figure 4.17(c)). Although the catalyst favour conversion of H_2 to moisture at lower temperatures (40 to 80 ^oC).

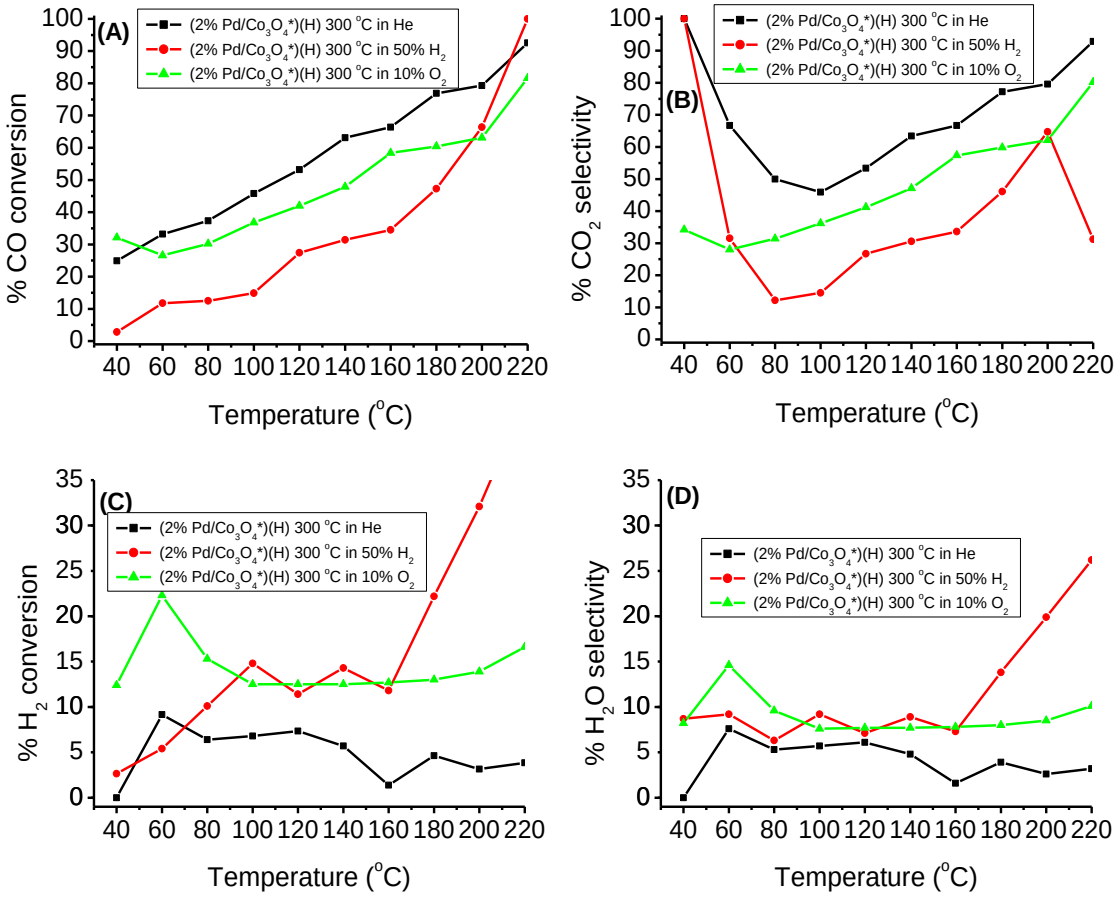

Figure 4.17 The CO conversion **(A)**, CO_2 selectivity **(B)**, H_2 conversion **(C)**, H_2O selectivity **(D)** of **(a)** (2wt.%Pd/Co_3O_4*)(H) He treated (■), **(b)** (2wt.%Pd/Co_3O_4*)(H) 50 % H_2 treated (●), and **(c)** (2wt.%Pd/Co_3O_4*)(H) 10 % O_2 treated (▲).

Interestingly the catalyst which was conditioned at 200 ºC inflow of He(Figure 4.17A(a)), showed CO conversion of 42.6 % at 100 ºC, with better selectivity compared the other catalysts. The conversion and selectivity of H_2 to moisture is lower and decreased with temperature (Figure 4.17C(a) and Figure 4.17D(a)). Sadykov *et al.* [59], have reported that pre-treatment in helium could result in surface reconstruction of Co_3O_4 to enhance the formation of weakly bound oxygen species, hence, the catalytic activity improves. Pre-treatment enhance the formation of surface oxygen vacancies, where weakly bound molecular oxygen species are formed to react with CO adsorb on Co^{3+} site [60].

4.3.7 The CO PROX reaction over Pd/Co_3O_4 pre-treated by different reducing agents

A comparative study on the activity of 2wt.%Pd/Co_3O_4 catalyst which was prepared by reduction pre-treatment of 2wt.%$Pd/Co(OH)_2$ by hydrazine (H) or sodium borohydride solution (B), respectively, was investigated for PROX of CO in excess H_2. Figure 4.18 present the results obtained in PROX of CO in excess H_2 over the prepared samples.

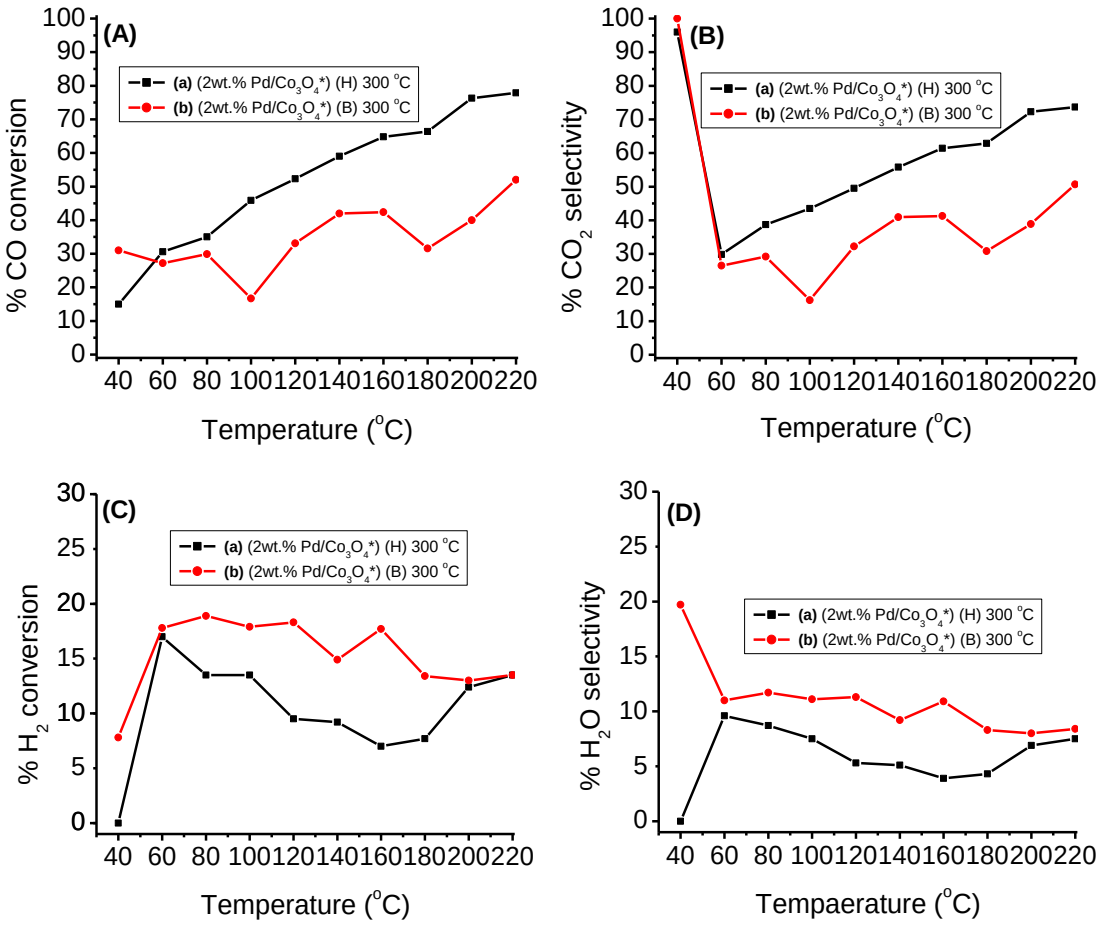

Figure 4.18 The CO conversion **(A)**, CO_2 selectivity **(B)**, H_2 conversion **(C)**, and H_2O selectivity **(D)** of **(a)** (2wt.%Pd/Co_3O_4*)(H) (■), and **(b)** (2wt.%Pd/Co_3O_4*)(B) (●) catalysts.

Though, the (2wt.%Pd/Co_3O_4*)(B) catalyst (Figure 4.18A(b)) had a higher surface area of 71.3 m^2/g compared to (2wt.%Pd/Co_3O_4*)(H) with a surface area of 64.7 m^2/g

(Figure 4.18A(a)). The (2wt.%Pd/Co_3O_4*)(B) catalyst showed CO conversion of 17.4% at 100 ^oC, with low selectivity in CO conversion, the catalyst favour conversion of H_2 to moisture. However, the (2wt.%Pd/Co_3O_4*)(H) catalyst (Figure 4.18A(a)) showed an improved activity of 44.5% at 100 ^oC in CO conversion. We have further noted that the CO conversion increases with the reaction temperature over (2wt.%Pd/Co_3O_4*)(H) catalyst (Figure 4.18A(a)). The conversion of H_2 is lower over (2wt.%Pd/Co_3O_4*)(H) compared to (2wt.%Pd/Co_3O_4*)(B) catalyst. The results suggest that the catalytic activity of 2wt.%Pd/Co_3O_4* depends on the type of the pre-treatment precursor.

4.3.8 The CO PROX over Pd/Co_3O_4 prepared over different supports

The 2wt.% Pd species was introduced to: (a) Co_3O_4, and (b) CoO_xH_y(H) species, respectively. Sample (a) was reduced by 0.1 M hydrazine solution, all samples were dried at 80 ^oC, and sample (b) was calcined at 300 ^oC. The Pd species was also introduced on the Co_3O_4 by co-precipitation method prior to hydrazine treatment and calcined at 300 ^oC. All samples were tested for CO PROX reaction in excess H_2, and the results are presented in Figure 4.19. The 2wt.%Pd/Co_3O_4)(H) catalyst (Figure 4.19A(a)) showed CO conversion of 4.9% at 40 ^oC, which increased to 59.3% at 160 ^oC, and the highest conversion of 100% was observed at 220 ^oC. The catalytic selectivity of CO to CO_2 decreased from 60.7% at 40 ^oC to 34.4% at 60 ^oC, and subsequently increased to 70.5% at 180 ^oC (Figure 4.19B(a)). The catalyst selectivity to CH_4 gas was observed from 180 ^oC, due to higher H_2 conversion. Other scientists have shown that the presence of Pd species on the support promotes oxidation and reduction of the catalyst [7, 19, 61].

The introduction of the Pd species by co-precipitation (Figure 4.19A(c)) improved the catalyst activity, a CO conversion of 22.6% at 40 ^oC, which improved with temperature to 55% at 80 ^oC observed. We also observed that CO conversion decreased to 39.6% at 100 ^oC, followed by a gradual increase to 100% at 200 ^oC. As a result, the catalyst selectivity to CO dropped from 100% at 40 ^oC to 40% at 100 ^oC, followed by an increase to 100% at 200 ^oC (Figure 4.19B(c)). Thus, conversion of H_2 increased from 2.6% at 40 ^oC to 30% at 220 ^oC (Figure 4.19C(c)).

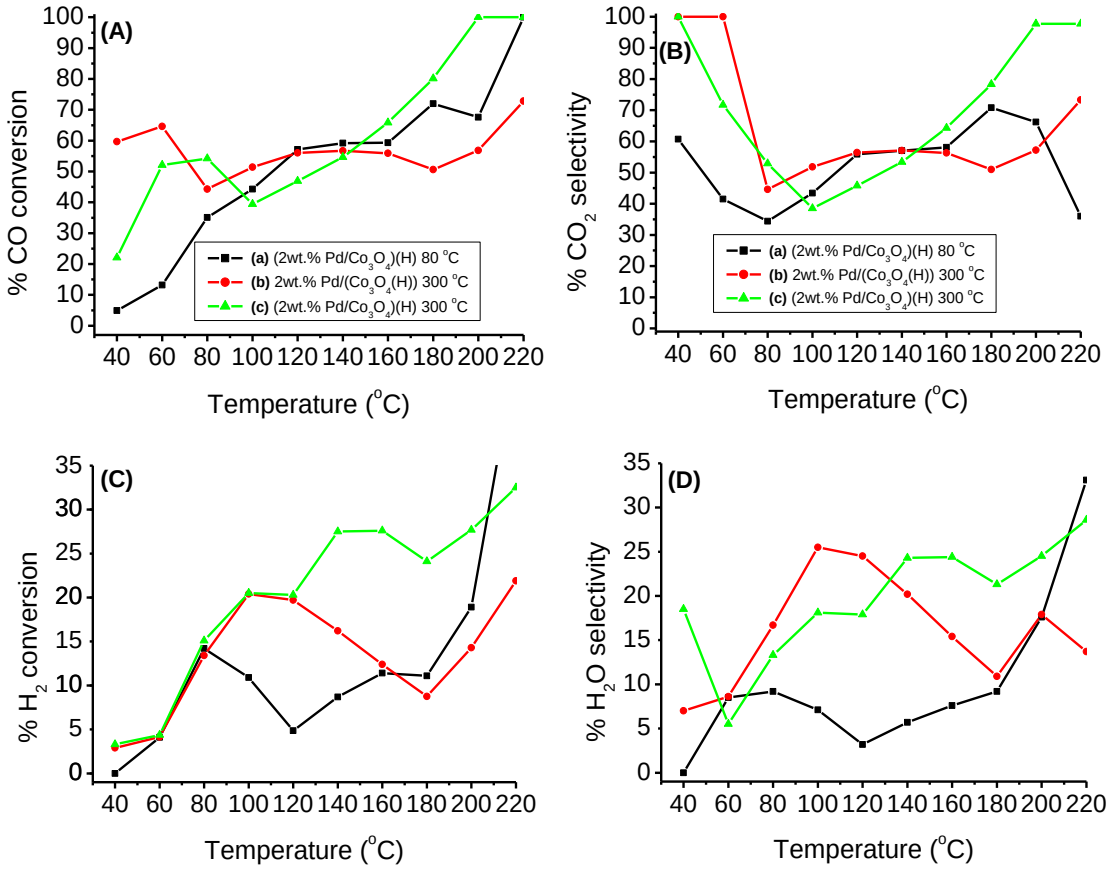

Figure 4.19 The CO conversion **(A)**, CO_2 selectivity **(B)**, H_2 conversion **(C)**, and H_2O selectivity **(D)** of **(a)** (2wt.%Pd/Co_3O_4)(H) 80 °C (■), **(b)** (2wt.%Pd/(Co_3O_4(H)) 300 °C (●), and **(c)** (2wt.%Pd/Co_3O_4)(H) 300 °C (▲) catalysts.

Interestingly, the introduction of 2wt.% Pd species on the CoO_xH_y(H), followed by calcination improves CO conversion at lower temperature (from 40 to 80 °C, Figure 4.19A(b)), an increase in CO conversion from 59.7 at 40 °C to 64.6% at 60 °C was observed. Conversion decreased from 64.6% at 60 °C to 44.3% at 80 °C, however, an increase in CO conversion with temperature from 80 °C to 140 °C observed. Selectivity of CO to CO_2 decreased from 96.0% at 40 °C to 29.8% at 60 °C, followed by a gradual increase to 73.7% at 220 °C (Figure 4.19B(b)). The higher activity over 2wt.%Pd(Co_3O_4(H)) could be due to the higher surface area when compared with other catalysts. The pre-treatment of the Pd species lower activity at lower temperature.

4.3.9 Effect of Pd load in CO PROX reaction over a reduced support

The effects of the amount of Pd in CO PROX reaction was investigated by varying the Pd load at 1%, 2%, and 3wt.% on the Co_3O_4(H) catalyst support, respectively. Figure 4.20 present the results in CO PROX reaction which was obtained over Pd/(Co_3O_4(H)) catalysts.

The catalyst with a 3wt.% Pd load (Figure 4.20A(c)) had the lowest CO conversion of 36.3% at 40 ^oC, which decreased to 29.2% at 80 ^oC. A gradual increase in CO conversion was observed from 29.2% at 80 ^oC to 33.3% at 140 ^oC, followed by a steady decrease to 29.1% at 200 ^oC. A highest CO conversion of 47.1% was observed at 220 ^oC. The catalyst had the lowest selectivity of CO to CO_2, compared to the 1 and 2wt.% Pd load (Figure 4.20B(c)). The catalyst favour conversion of H_2 to moisture (Figure 4.20C(c)).

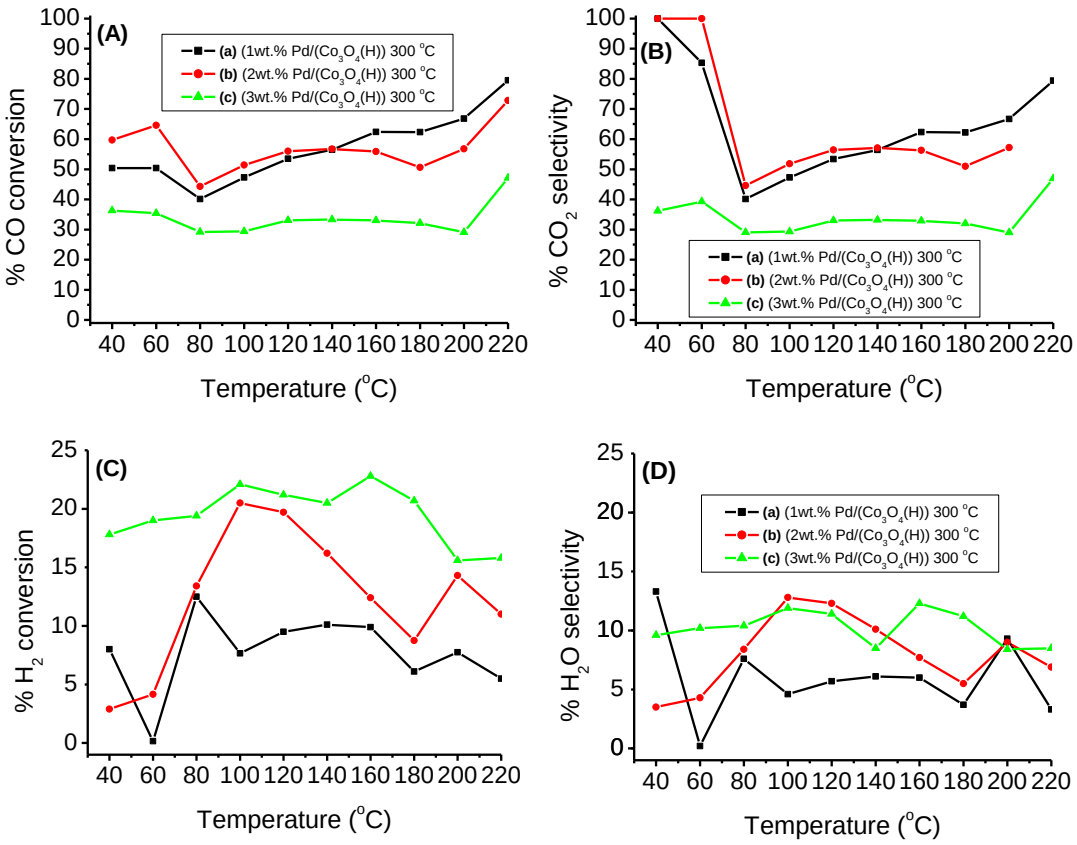

Figure 4.20 The CO conversion **(A)**, CO_2 selectivity **(B)**, H_2 conversion **(C)**, and H_2O selectivity **(D)** of **(a)** 1wt.%Pd/(Co_3O_4(H)) 300 ^oC (■), **(b)** 2wt.%Pd/(Co_3O_4(H)) 300 ^oC (●), and **(c)** 3wt.%Pd/(Co_3O_4(H)) 300 ^oC (▲) catalysts.

An improved catalytic activity was observed over 1wt.%Pd/Co_3O_4(H) catalyst (Figure 4.20A(a)) which showed CO conversion of 50.4% at 40 ^oC, which drops with reactor temperature to 40.1% at 80 ^oC, followed by a gradual increase to 79.5% at 220 ^oC. A catalytic selectivity of CO to CO_2 dropped from 100% at 40 ^oC to 40.1% at 80 ^oC (Figure 4.20B(a)). However, an increase in temperature resulted in a gradual increase of CO_2 selectivity to 79.5% at 220 ^oC. Interestingly, the 2wt.% load (Figure 4.20A(b)) had the highest CO conversion of 64.6% at 60 ^oC, followed by a decrease to 44.3% at 80 ^oC. However, an increase in the conversion of CO after 80 ^oC to 56.7% at 140 ^oC was observed. The catalyst had the highest CO conversion of 72.8% at 220 ^oC. The catalytic selectivity of CO to CO_2 decreased from 100% at 60 ^oC to 44.6% at 80 ^oC. However, a gradual increase in CO_2 selectivity was observed from 44.6% at 80 ^oC to 57.1% at 140 ^oC (Figure 4.20B(b).

Other researchers have also reported poor catalytic performance of supported Pd, due to formation of hydride and formation of moisture in CO PROX [7-8]. The increase in the amount of Pd species increased the amount of absorbed oxygen on the surface [21]. As a result, a catalyst with 3wt.% Pd species showed a higher surface area of 309.5 m^2/g and favour conversion of H_2 to moisture.

4.3.10 Activation energy for CO PROX reaction over 1wt.%Pd/(Co_3O_4(H)) catalyst

The comparative study on the activation energy required for CO PROX in excess H_2 under dry, and moisture condition was investigated over 1wt.%Pd/(Co_3O_4(H)) catalyst at 40-80 ^oC, respectively. The activation energies for CO conversion was calculated from Arrhenius plots, as shown in Figure 4.21. An increase in the specific reaction rate from 9.83 x 10^{-5} $mol_{CO}/g_{Cat}/h$ (under dry condition) to 4.867 x 10^{-4} $mol_{CO}/g_{Cat}/h$ (under moist condition) at 40 ^oC was observed. The catalyst activation energies for CO PROX reactions under dry and moisture conditions were found to be 13.3 kJ/mol and 7.80 kJ/mol, respectively (Figure 4.21A and 4.21B). Other researchers have reported a decrease in the activation energy of the catalysts in CO PROX when Pd species is supported on the catalytic support in the presence of moisture [21, 62]. The decrease in the activation energy suggests that the presence of Pd species on the catalyst promotes the active sites for H_2O dissociation [62]. As a result, the selectivity of CO to

CO_2 has improved in the presence of H_2O species in the feed, the improvement was also noted with time on stream at 100 ^oC (section 4.3.11.2, Figure 4.23A). It has been reported in the literature that the increase in CO conversion in the presence of moisture is due to water gas shift [2, 50].

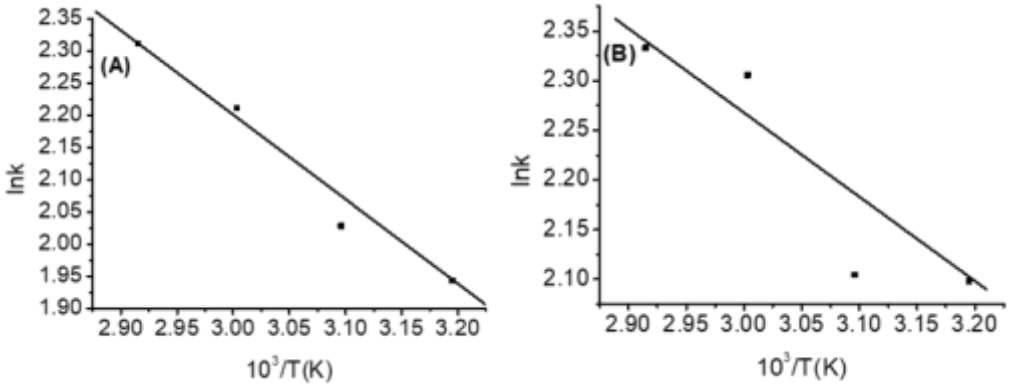

Figure 4.21 Arrhenius plots for the reaction rate of CO PROX (activation energy, E_a) over 1wt.%Pd/(Co_3O_4(H)) catalyst under **(A)** dry, and **(B)** moisture condition.

4.3.11 The effects of moisture and CO_2 on the stability of 1wt.%Pd/(Co_3O_4(H))

4.3.11.1 Stability of catalysts as a function of temperature

The effect of moisture and CO_2 species was investigated at a reactor temperature of 40 to 220 ^oC over 1wt.%Pd/(Co_3O_4(H)) catalyst, respectively. The moisture and 15% CO_2 were introduced in the feed stream (1% CO, 1% O_2, and 50% H_2, mixture) during PROX reaction over 1wt.%Pd/(Co_3O_4(H)) catalyst, respectively, Figure 4.22 present the results obtained.

A decrease in the conversion of CO at lower temperature is observed at 40 and 60 ^oC, the conversion dropped by 5.8% at 40 ^oC and by 11% at 60 ^oC, compared to the conversion in dry condition (Figure 4.22A(a) and (b)). A steady increase in CO conversion with reactor temperature was observed over the feed with moisture (from 60 to 220 ^oC). Introduction of moisture in the feed during PROX reaction can suppress the activity at a lower temperature, due to coverage of the surface of the catalyst which hinders the adsorption of the adsorbing species on the catalyst [3, 63]. Selectivity of CO to CO_2 has improved over the feed with moisture than the moisture free feed stream (Figure 4.22B(a) and (b)). The conversion of H_2 species increased with

temperature from 40 to 80 ^{o}C in both conditions, and a decrease in the H_2 conversion was observed after 80 ^{o}C (Figure 4.22C(a) and (b)). The selectivity of H_2 to moisture is lower, when moisture is introduced in the feed stream.

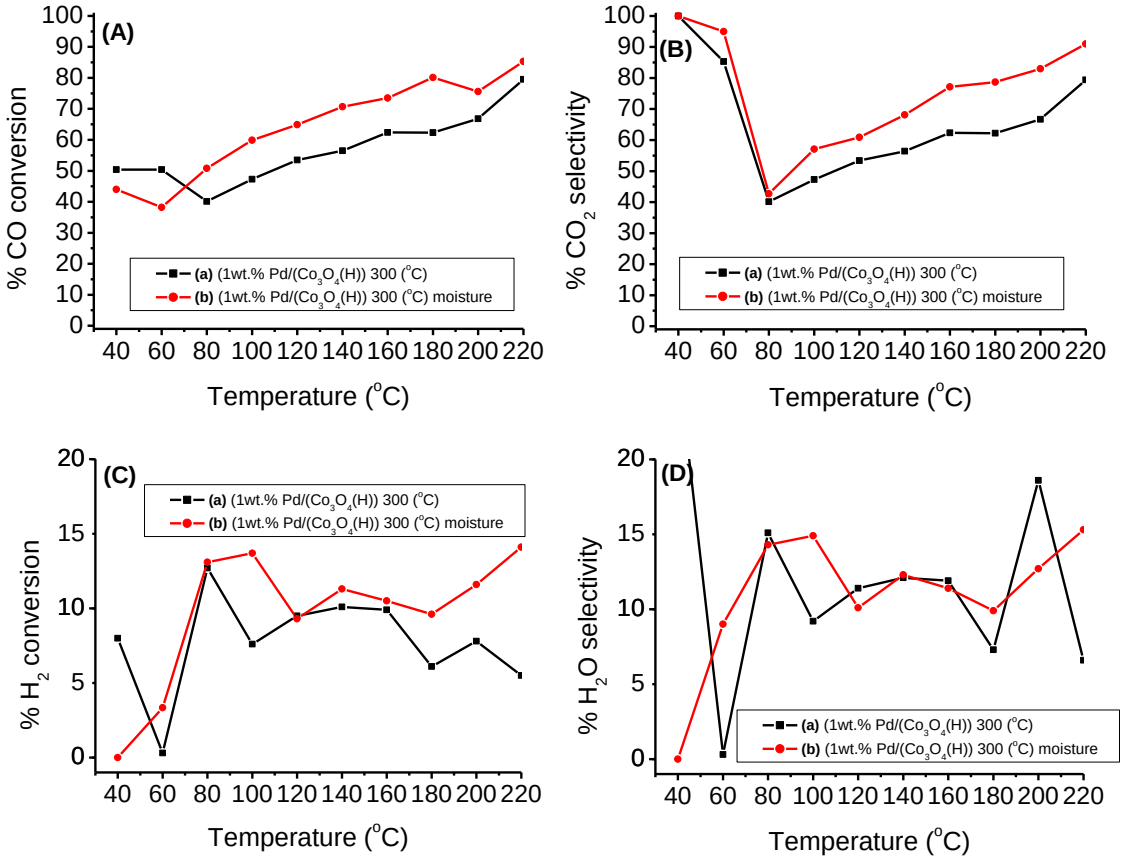

Figure 4.22 The CO conversion **(A)**, CO_2 selectivity **(B)**, H_2 conversion **(C)**, and H_2O selectivity **(D)** of 1wt.%Pd/(Co_3O_4(H)) catalyst under; **(a)** dry (■), and **(b)** moisture condition (●).

4.3.11.2 Stability of catalysts as function of time on stream

The stability of the catalysts was investigated over 1wt.%Pd/(Co_3O_4(H)) catalyst at 100 ^{o}C for over 21 h. The feed stream consists of 1% CO, 1% O_2, and 50% H_2 feed. The effect of moisture or CO_2 atmosphere in the feed was also investigated at 100 ^{o}C for 21 h, respectively. Figure 4.23 present the results obtained on stability, effect of moisture, and effect of CO_2 in excess H_2 over 1wt.%Pd/(Co_3O_4(H)) catalyst, respectively. The catalysts (Figure 4.23A(a)) showed a steady increase with fluctuation in the conversion of CO species with time on stream in dry condition. The selectivity of CO to CO_2 (Figure 4.24B(a)) also increased steadily with increasing time

on stream. The conversion of H_2 of about 14.5% was observed with time on stream (Figure (4.23C(a)). The selectivity of H_2 to moisture of about 19.5% was also observed with time on stream (Figure 4.23D(a)). The accumulation of moisture on the catalyst surface resulted in water-gas shift, which in turn resulted in an increase in CO conversion with time on stream. Similar observation was reported by Marino *et al,* [32]., where the conversion of CO to CO_2 increases due to the accumulated moisture at higher temperature via the water gas shift reaction (WGSR) at higher temperature and excess O_2.

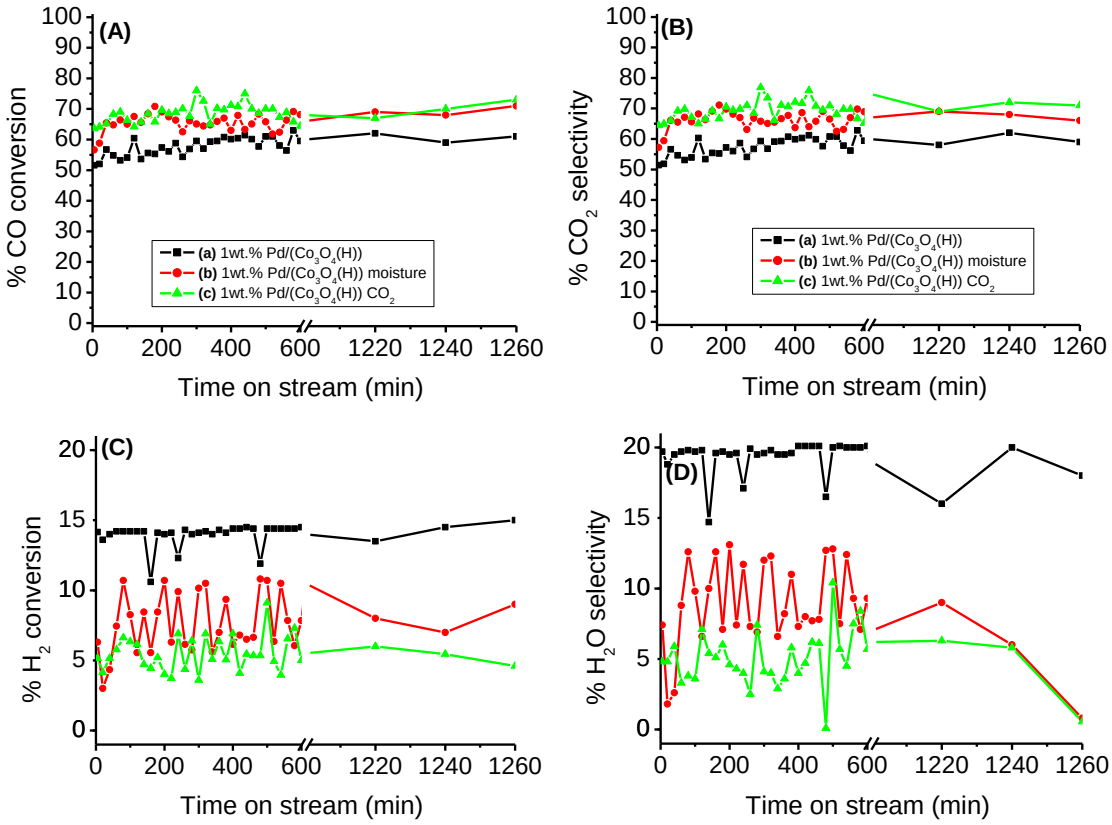

Figure 4.23 The CO conversion **(A)**, CO_2 selectivity **(B)**, H_2 conversion **(C)**, and H_2O selectivity **(D)** of **(a)** 1wt.% Pd/(Co_3O_4(H)) (■), **(b)** 1wt.%Pd/(Co_3O_4 (H)) moisture (●), and **(c)** 1wt.%Pd/(Co_3O_4(H)) in CO_2 (▲) catalysts with time on stream.

The introduction of moisture on the feed resulted to a steady increase in the CO conversion (Figure 4.23A(b)), and its selectivity to CO_2 (Figure 4.23B(b)) with time on stream. A decrease in H_2 conversion (Figure 4.23C(b) was observed in PROX reaction

in moisture condition. As a result, the selectivity of H_2 to moisture (Figure 4.23D(b)) fluctuates with time on stream with the highest selectivity of 0.66%. Saavedra *et al.,* [64], have shown that when water is added on the feed, there is no deactivation for 21 h over Au/Al_2O_3 catalyst, and O_2 selectivity remains constant and high (~80%). They have shown that when water is removed O_2 selectivity immediately drops and the CO oxidation activity begins to degrade over time.

The introduction of CO_2 in the feed stream has also shown an improvement in the conversion of CO (Figure 4.23A(a) and (c)), when compared with a moisture free feed. The selectivity of CO to CO_2 (Figure 4.23B(c)) has also improved with time on stream. The conversion of H_2 is lower in the presence of CO_2, as a result, the selectivity of H_2 to moisture is lower compared to the other conditions (moisture and dry conditions). An improvement in the catalytic selectivity of O_2 to CO_2, and a decrease in consumption of H_2 in the presence of H_2O or CO_2, confirms that a decrease in CO conversion does not cause reverse water gas shift reaction [65]. A similar observation on the improvement of CO conversion in the presence of moisture over Pd/CeO_2 catalyst was reported by Li *et al,* [21]. The presence of Pd species promotes the active sites for H_2O dissociation [62].

4.4 CONCLUSIONS

The Co_3O_4 and Co_3O_4(H) catalysts were successfully prepared using the precipitation method prior to calcination at 300 ^oC. Both CoO and CoO(H) catalysts were prepared by reducing Co_3O_4 and Co_3O_4(H) by 5% H_2/He, respectively. The Pd species were successfully introduced on different Co_3O_4 by improved wet impregnation method. The structural compositions of the catalysts were confirmed by XRD, FTIR, XPS, TPR, and TGA data; with the activity of the catalysts investigated under PROX reaction. The XRD and TPR of Co_3O_4(H) catalyst indicated that a surface transformation occurred, as confirmed by an increase in the BET surface area. Interestingly, the mesoporous structure of the catalyst remained intact, as compared to that of Co_3O_4 catalyst. Though an in-situ reduction has occurred prior to calcination of CoO_xH_y(H), the FTIR data did not show peak ratio differences, which indicates that a usual amount of Co^{3+} and Co^{2+} were formed; which is consistent with the XRD, XPS and TPR data. Introduction of Pd species on the cobalt oxide did not change the structure of Co_3O_4 as indicated by XRD, XPS and TEM data. However, an increased surface area was observed with respect to the type of cobalt species; Co_3O_4, $Co(OH)_2$ (denoted as Co_3O_4*), and Co_3O_4(H) gave a surface area of 64.7, 53.4 and 63.0%. The hydrazine treated 2wt.%Pd/Co_3O_4 catalyst resulted to a mixture of CoO(OH) and Co_3O_4 species, due to oxidation of Co^{2+} to Co^{3+}, as confirmed by XRD and FTIR data. The surface area of Co_3O_4 species increased with the Pd species load, as confirmed by BET surface area. Reduction of 2wt.%Pd/Co_3O_4 catalysts by sodium borohydride showed the highest BET surface area with an intact structure from Co_3O_4 (as confirmed by SEM and TEM data).

During PROX the oxidation of both CO and H_2 species increased with CO/O_2 ratio (λ), and a higher CO/O_2 ratio (λ) favoured formation of moisture. The PROX data of Co_3O_4(H) catalyst gave 85% CO conversion (with good selectivity) at 100 ^oC under dry conditions, which remained stable for 21 h. The catalyst activity increased with temperature, especially within the fuel cells temperature window. This activity correlates with the surface properties of the catalyst and showed a very low moisture formation at temperatures above 120 ^oC. A relatively similar activity with good stability was observed under moisture-rich condition, avoiding the H_2O capillary condensation phenomenon. The data indicated that the Co_3O_4 catalyst is unstable and deactivated with time on stream at 100 ^oC. The PROX activity of the Co_3O_4(H) catalyst in the

presence of moisture deactivated from 100 to 70% and remained fluctuating steadily for almost 21 h. The Co_3O_4(H) produced almost 75% CO conversion in the presence of CO_2, which deactivate as time increased. Surprisingly, the PROX of CoO(H) indicated that the catalyst is highly active at a low temperature range, which correlated with the formation of Co^{3+} species as confirmed by TPR and XRD data.

Unfortunately, the addition of Pd species on Co_3O_4(H) suppressed the activity of the catalyst, and favour conversion of H_2 to moisture. The data shows that activation energy of Co_3O_4(H) catalyst decreased from 21.5 to 13.3 kJ/mol upon the addition of Pd species under dry condition, which is due to splitting of H_2 to form moisture. A decrease in CO conversion from 85% (over Co_3O_4(H)) to 51% (over 1wt.%Pd on Co_3O_4(H)) at 100 ^oC was observed, CO conversion increased with time on stream for 21 h, due to water gas shift of the accumulated moisture. Similarly, the catalyst showed better stability under both moisture and CO_2 conditions for 21 h. The Pd species over other different Co_3O_4 catalysts showed a lower activity in CO conversion. The 2wt.%Pd on Co_3O_4 showed the CO conversion of 14.9% at 100 ^oC, an improvement in CO conversion from 14.9 to 44.3% was observed over the 2wt.%Pd on Co_3O_4 catalyst which was pre-treated with hydrazine. The 2wt.%Pd on Co_3O_4* catalyst showed CO conversion of 39.4% at 100 ^oC.

4.5 REFERENCES

[1] Y. Teng, H. Skurai, A. Ueda, T. Kobayashi. Oxidative removal of CO contained in hydrogen by using metal oxide catalysts. *International Journal of Hydrogen Energy* 24 (1999) 355-358.

[2] P. Gawade, B. Bayram, A-M. C. Alexander, U. S. Ozkan. Preferential oxidation of CO (PROX) over $CoOx/CeO_2$ in hydrogen rich stream. *Applied Catalysis B: Environmental* 128 (2012) 21-30.

[3] Y. Yu, T. Takei, H. Ohashi, H. He, X. Zhang, M. Haruta. Pretreatments of Co_3O_4 at moderate temperature for CO oxidation at 80 ^oC. *Journal of Catalysis* 267 (2009) 121-128.

[4] D. Boyd, S. Golunski, G.R. Hearne, T. Magadzu, K. Mallick, M.C. Raphulu, A. Venugopal, M.S. Scurrell. Reductive routes to stabilized nanogold and relation to catalysis by supported gold. *Applied Catalysis A: General* 292 (2005) 76-81.

[5] T.-S. Nguyen, F. Morfin, M. Aouine, F. Bosset, J. –L. Rousset, L. Piccolo. Trends in the CO oxidation and PROX performances of the platinum group metals supported on ceria. *Catalysis Today* 253 (2015) 106-114.

[6] P. Lakshmanan, J. E. Park, B. Kim, E. D. Park. Preferential oxidation of CO in a hydrogen rich stream over $Au/MO_x/Al_2O_3$ (M = La, Ce, and Mg) catalysts. *Catalysis Today* 265 (2016) 19-26.

[7] O. Pozdnyakova, D. Teschner, A. Wootsch, J. Krohnert, B. Steinhauer, H. Sauer, L. Toth. Preferential CO oxidation in hydrogen (PROX) on ceria-supported catalysts, part II: Oxidation states and surface species on Pd/CeO_2 under reaction conditions, suggested reaction mechanism. *Journal of Catalysis* 237 (2006) 17-28.

[8] C. Zlotea, F. Morfin, T.S. Nguyen, N.T. Nguyen, J. Nelayah, *C.* Ricolleau, M. Latroche, L. Piccolo. Nanoalloying bulk-immiscible iridium and palladium inhibits hydride formation and promotes catalytic performances. *Nanoscale* 0 (2014) 1-5.

[9] G. Li, L. Li, J. Shi, Y. Yuan, Y. Li, W. Zhao. One-pot pyrolytic synthesis of mesoporous $MCo_2O_4(4.5)$ (M = Mn, Ni, Fe, Cu) spinels and its high efficient catalytic properties for CO oxidation at low temperature. *Journal of Molecular Catalysis A: Chemical* 390 (2014) 97-104.

[10] S. Farhadi, K. Pourzare, S. Sadeghinejad. Synthesis and characterization of Co_3O_4 nanoplanes by simple thermolysis of the $[Co(NH_3)_6]_2(C_2O_4)_3.4H_2O$ complex. *Polyhedron* 67 (2014) 104-110.

[11] Y. Chen, D. Liu, L. Yang, M. Meng, J. Zhang, L. Zheng, S. Chu, T. Hu. Ternary composite oxide catalysts CuO/Co_3O_4-CeO_2 with wide temperature window for the preferential oxidation of CO in H_2 rich stream. *Chemical Engineering Journal* 234 (2013) 88-98.

[12] C-W. Tang, L-C. Hsu, S-W. Yu, C-B. Wang, S-H. Chien. In situ FT-IR and TPD-MS study of carbon monoxide oxidation over a CeO_2/Co_3O_4 catalyst. *Vibrational Spectroscopy* 65 (2013) 110-115.

[13] T. Ozkaya, A. Baykal, M. S. Toprak, Y. Koseoglu, Z. Durmus. Reflux synthesis of Co_3O_4 nano particles and magnetic characterization. *Journal of Magnetism and Magnetic Materials* 321 (2009) 2145-2149.

[14] R. S. Jayashree, P. V. Kamath. Electrochemical synthesis of a-cobalt hydroxide. *Journal of Material Chemistry* 9 (1999) 961-963.

[15] Y-C. Liu, J. A. Koza, J. A. Switzer. Conversion of electrodeposited $Co(OH)_2$ to CoOOH and Co_3O_4, and comparison of their catalytic activity for the oxygen evolution reaction. *Electrochimica Acta* 140 (2014) 359-365.

[16] D. Gu, C-J. Jia, C. Weidenthaler, H-J. Bongard, B. Spliethoff, W. Schmidt, F. Schüth. Highly ordered mesoporous cobalt-containing oxides: Structure, catalytic properties, and active sites in oxidation of carbon monoxide. *Journal of the American Chemical Society* 137 (2015) 11407-11418.

[17] L. Lukashuk, K. Föttinger, E. Kolar, C. Rameshan, D. Teschner, M. Hävecker, A. Knop-Gericke, N. Yigit, H. Li, E. McDermott, M. Stöger-Pollach, G. Rupprechter. Operando XAS and NAP-XPS studies of preferential CO oxidation on Co_3O_4 and CeO_2-Co_3O_4 catalysts. *Journal of Catalysis* 344 (2016) 1-15.

[18] C. W. Tang, C. B. Wang, S. H. Chien. Characterization of cobalt oxides studied by FT-IR, Raman, TPR and TG-MS. *Thermochemical Acta* 473 (2008) 68-73.

[19] J-Y. Luo, M. Meng, X. Li, X-G. Li, Y-Q. Zha, T-D. Hu, Y-N. Xie and J. Zhang. Mesoporous Co_3O_4-CeO_2, Pd/Co_3O_4-CeO_2 catalysts: Synthesis, characterisation and mechanistic study of their catalytic properties for low-temperature CO oxidation. *Journal of Catalysis* 254 (2008) 310-324.

[20] J. Yang, H. Liu, W. N. Martens, R. L. Fronst. Synthesis and characterization of Cobalt Hydroxide, Cobalt Oxyhydroxide, and Cobalt Oxide Nanodiscs. *Journal of Physical Chemistry C* 114 (2010) 111-119.

[21] G. Li, L. Li, Y. Yuan, j. Shi, Y. Yuan, Y. Li, W. Zhao, J. Shi. Highly efficient mesoporous Pd/CeO_2 catalyst for low temperature CO oxidation especially under moisture condition. *Applied Catalysis B: Environmental* 158-159 (2014) 341-347.

[22] J. Lojewska, A. Kolodziej, J. Zak, J. Stoch. Pd/Pt promoted Co_3O_4 catalysts for VOCs combustion: Preparation of active catalyst on metallic carrier. *Catalysis Today* 105 (2005) 655-661.

[23] F. Barde´, M.-R. Palacin, B. Beaudoin, A. Delahaye-Vidal, J. –M. Tarascon. New approaches for synthesizing *Y*III-CoOOH by soft chemistry. *Chemical Mater* 16 (2004) 299-306.

[24] V. R. Mate, A. Jha, U. D. Joshi, K. R. Patil, M. Shirai, C. V. Rode. Effect of preparation parameters on characterisation and activity of Co_3O_4 catalyst in liquid phase oxidation of lignin model substrates. *Applied Catalysis A: General* 487 (2014) 130-138.

[25] M. M. Natile, A. Glisenti. CoO_x/CeO_2 Nanocomposite Powders: Synthesis, Characterization, and Reactivity. *Chemistry of Materials* 17 (2005) 3403-3414.

[26] L. Nguyen, S. Zhang, S. J. Yoon and F. Tao. Preferential Oxidation of CO in H_2 on Pure Co_3O_{4-x} and Pt/Co_3O_{4-x}. *Chemistry Catalysis Chemicals* 7 (2015) 2346-2353.

[27] S. Zhang, J-j. Shan, Y. Zhu, A. I. Frenkel, A. Patlolla, W. Huang, S. J. Yoon, L. Wang, H. Yoshida, S. Takeda, F. (Feng) Tao. WGS Catalysis and in Situ Studies of CoO_{1-x}, PtCon/Co_3O_4, and PtmCom′/CoO_{1-x} Nanorod Catalysts. *Journal of American Chemistry Society* 135 (2013) 8283-8293.

[28] L. Wang, S. Zhang, Y. Zhu, A. Patlolla, J. Shan, H. Yoshida, S. Takeda, A. I. Frenkel, F. (Feng) Tao. Catalysis and in Situ Studies of Rh1/Co_3O_4 Nano rods in Reduction of NO with H_2 Lei. *Acta Catalysis* 3 (2013) 1011-1019.

[29] O. O. James, S. Maity. Temperature programme reduction (TPR) studies of cobalt phases in alumina supported cobalt catalysts. *Journal of Petroleum Technology and Alternative Fuel* 7 (2016) 1-12.

[30] T. Chang, Z. Shen, Y. Huang, J. Lu, D. Ren, J. Cao, H. Liu. Post-plasma-catalytic removal of toluene using MnO_2-Co_3O_4 catalysts and their synergistic mechanism. *Chemical Engineering Journal* 348 (2018) 15-25.

[31] V. A. de la Pena O'Shea, N. Homs, E. B. Pereira, R. Nafria, P. R. de la Piscina. X-ray diffraction study of Co_3O_4 activation under ethanol steam-reforming. *Catalysis Today* 126 (2007) 148-152.

[32] F. Mariño, C. Descorme, D. Duprez. Noble metal catalysts for the preferential oxidation of carbon monoxide in the presence of hydrogen (PROX). *Applied Catalysis B: Environmental* 54 (2004) 59-66.

[33] H. Chen, M. Yang, S. Tao, G. Chen. Oxygen vacancy enhanced catalytic activity of reduced Co3O4 towards p-nitrophenol reduction. *Applied Catalysis B: Environmental* 209 (2017) 648-656.

[34] J. Yang, S. Quaresma, S. Mei, J. M. F. Ferreira. Hydrothermal synthesis of free-standing Co_3O_4 nanocubes. *Key Engineering Mater* 280-283 (2005) 713-716.

[35] S. K. Mahammadunnisa, T. Akanksha, K. Krushnamurty, C. H. Subrahmanyam. Catalytic decomposition of N_2O over CeO_2 supported Co_3O_4 catalysts. *Journal of Chemical Science* 128 (2016) 1795-1804.

[36] Z. P. Xu, H. C. Zeng. Interconversion of Brucite-like and hydrotalcite-like phases in cobalt hydroxide compounds. *Chemistry Maters* 11 (1999) 67-74.

[37] L. Hu, Q. Peng, Y. Li. Selective synthesis of Co_3O_4 nanocrystal with different shape and crystal plane effect on catalytic property for methane combustion. *Journal of American Chemical Society* 130 (2008) 16136-16137.

[38] W. Xu, X. Liu, J. Ren, P. Zhang, Y. Wang, Y. Guo, Y. Guo, G. Lu. A novel mesoporous Pd/cobalt aluminate bifunctional catalyst for aldol condensation and following hydrogenation. *Catalysis Communications* 11 (2010) 721-726.

[39] Y. Wang, C. Zhanga, Y. Yua, R. Yueb, H. Hea. Ordered mesoporous and bulk Co_3O_4 supported Pd catalysts for catalytic oxidation of o-xylene. *Catalysis Today* 242 (2015) 294-299.

[40] N. Tang, W. Wang, H. You, Z. Zhai, J. Hilario, L. Zeng, L. Zhang. Morphology of pours CoO nanowalls enhanced electrochemical performance as supercapacitors electrodes. *Catalysis Today* 330 (2019) 240-245.

[41] C-J. Jia, M. Schwickardi, C. Weidenthaler, W. Schmidt, S. Korhonen, B. M. Weckhuysen, F. Schüth. Co_3O_4-SiO_2 Nanocomposite: A Very Active Catalyst for CO Oxidation with Unusual Catalytic Behavior. *Journal of American Chemistry Society* 133 (2011) 11279-11288.

[42] G. Marba'n, A. B. Fuertes. Highly active and selective CuO_x/CeO_2 catalyst prepared by a single-step citrate method for preferential oxidation of carbon monoxide. *Applied Catalysis: B Environmental* 57 (2005) 43-53.

[43] X. Gong, B. Liu, B. Kang, G. Xu, Q. Wang, C. Jia, J. Zhang. Boosting Cu-Ce interaction in Cu_xO/CeO_2 nanocube catalysts for enhanced catalytic performance of preferential oxidation of CO inH_2-rich gases. *Molecular Catalysis* 436 (2017) 90-99.

[44] C. Zhu, T. Ding, W. Gao, K. Ma, Y. Tian, X. Li. CuO/CeO_2 catalysts synthesized from Ce-UiO-66 metal-organic framework for preferential CO oxidation. *International Journal of Hydrogen Energy* 42 (2017) 17457-17465.

[45] A. Di Benedetto, G. Landi, L. Lisi. Improved CO-PROX performance of CuO/CeO_2 catalysts by using nanometric ceria as support. *Catalysts* 8 (2018) 209-228.

[46] A. Arango-Diaz, J. A. Cecilia, J. Marrero-Jerez, P. Nuñez, J. Jiménez-Jiménez, E. Rodríguez-Castellón. Freeze-dried Co_3O_4–CeO_2 catalysts for the preferential oxidation of CO with the presence of CO_2 and H_2O inthefeed. *Ceramics International* 42 (2016) 7462-7474.

[47] L. F. Liotta, G. Di Carlo, G. Pantaleo, A. M. Venezia and G. Deganello. Co_3O_4/CeO_2 composite oxides for methane emissions abatement: Relationship between Co_3O_4-CeO_2 interaction, catalytic activity. *Applied Catalysis B: Environmental* 66 (2006) 217-227.

[48] J-b. Li, Z-q. Jiang, K. Qianb, W-x. Huang. Effect of calcination temperature on surface oxygen vacancies and catalytic performance towards CO oxidation of Co_3O_4 nanoparticles supported on SiO_2. *Journal of Chines Chemical Physics* 25 (2012) 103-109.

[49] K. Omata, T. Takada, S. Kasahara, M. Yamada. Active site of substituted cobalt spine1 oxide for selective oxidation of CO/H_2. Part II. *Applied Catalysis A: General* 146 (1996) 255-267.

[50] L. Nguyen, S. Zhang, S. J. Yoon and F. Tao, S. Varghese, M. G. Cutrufello, E. Rombi, C. Cannas, R. Monaci, I. Ferino. CO oxidation and preferential oxidation of CO in the presence of hydrogen over SBA-15-templated CuO-Co_3O_4 catalysts. *Applied Catalysis A: General* 443-444 (2012) 161-170.

[51] T. R. Reina, C. Megías-Sayago, A. Pérez Florez, S. Ivanova, M. Á. Centeno, J. A. Odriozola. H_2 oxidation as criterion for PROX catalyst selection: Examples

based on Au–CoOx-supported systems. *Journal of Catalysis* 326 (2015) 161-171.

[52] Q. Zhang, X. Liu, W. Fan and Y. Wang. Manganese-promoted cobalt oxide as efficient, stable non-noble metal catalyst for preferential oxidation of CO in H_2 stream. *Applied Catalysis B: Environmental* 102 (2011) 207-214.

[53] M. J. Pollard, B. A. Weinstock, T.E. Bitterwolf, P. R. Griffiths, A. P. Newbery, J. B. Paine III. A mechanistic study of the low-temperature conversion of carbon monoxide to carbon dioxide over a cobalt oxide catalyst. *Journal of Catalysis* 254 (2008) 218-225.

[54] K. Omata, Y. Kobayashi, M. Yamada. Artificial neural network-aided development of supported Co catalyst for preferential oxidation of CO in excess hydrogen. *Catalysis Communications* 6 (2005) 563-567.

[55] Z. Zhao, M. M. Yung, U. S. Ozkan. Effect of support on the preferential oxidation of CO over cobalt catalysts. *Catalysis Communications* 9 (2008) 1465 -1471

[56] O. Pozdnyakova-Tellinger, D. Teschner, J. Krohnert, F. C. Jentoft, A. Knop-Gericke. R. Schlo, A. Woods. Surface Water-Assisted Preferential CO Oxidation on Pt/CeO_2 Catalyst. *Journal of Physical Chemistry C* 111 (2007) 5426-5431.

[57] F. Morfin, S. Nassreddine, J. L. Rousset, L. Piccolo. Nanoalloying Effect in the Preferential Oxidation of CO over Ir−Pd Catalysts. *ACS catalysis* 2 (2012) 2161-2168.

[58] C. Zlotea, F. Morfin, T. S. Nguyen, N. T. Nguyen, J. Nelayah, C. Ricolleau, M. Latroche, L. Piccolo. Nanoalloying bulk-immiscible iridium and palladium inhibits hydride formation and promotes catalytic performances. *Nanoscale* 6 (2014) 9955-9959.

[59] V. A. Sadykov, S. F. Tikhov, S. V. Tsybulya, G. N. Kryukova, S. A. Veniaminov, V. N. Kolomiichuk, N. N. Bulgakov, E. A. Paukshtis, V. P. Ivanov, S. V. Koshcheev, V. I. Zaikovskii, L. A. Isupova, L. B. Burgina. Role of defect structure in structural sensitivity of the oxidation reactions catalyzed by dispersed transition metal oxides. *Journal of Molecular Catalysis A: Chemical* 158 (2000) 361-365.

[60] Y. Yu, T. Takei, H. Ohashi, H. He, X. Zhang, M. Haruta. Pretreatments of Co_3O_4 at moderate temperature for CO oxidation at 80 ^oC. *Journal of Catalysis* 267 (2009) 121-128.

[61] S. H. Oh, R. M. Sinkevitch. Carbon monoxide removal from hydrogen-rich fuel cell feedstreams by selective catalytic oxidation. *Journal of Catalysis* 142 (1993) 254-262.

[62] J. Kugai, J. T. Miller, N. Guo, C. Song. Role of metal components in Pd–Cu bimetallic catalysts supported on CeO_2 for the oxygen-enhanced water gas shift. *Applied Catalysis B: Environmental* 105 (2011) 306-316.

[63] Q. Guo, Y. Liu, T. Caputo, L. Lisi, R. Pirone, G. Russon. Preferential oxidation of CO in H_2 over Co_3O_4-CeO_2 catalysts. *Reaction Kinetics and Catalysis Letter* 92 (2007) 19-25.

[64] J. Saavedra, T. Whittaker, Z. Chen, C. J. Pursell, R. M. Rioux. Controlling Activity and Selectivity Using Water in the Au-catalysed Preferential Oxidation of CO in H_2. *Nature Chemistry* 8 (2016) 584-589.

[65] T. Cwele, N. M, S. Singh, H. B. Friedrich. Effect of Cu additives on the performance of a cobalt substituted ceria ($Ce_{0.90}Co_{0.10}O_2$) catalyst in total and preferential CO oxidation. *Applied Catalysis B: Environmental* 182 (2016) 1-14.

CHAPTER 5

5. RESULTS AND DISCUSSIONS

THE ROLE OF VARIOUS METAL OXIDE ON CATALYTIC ACTIVITY OF Pd/Co_3O_4 IN CO PROX REACTION

5.1 INTRODUCTION

The metal oxide as support for the catalyst can improve the oxygen vacancies, surface area, dispersion of the catalyst, the catalytic activity, and selectivity to CO PROX reaction [1-4]. The role of various metal oxides (CeO_2, MnO_2, MgO, TiO_2, and Cr_3O_4) on the PROX activity of Co_3O_4, and the corresponding effects of Pd nanoparticles were investigated. The study was conducted to improve catalytic activity, selectivity and stability in PROX, and it was conducted as follows: All metal oxides were introduced on Co_3O_4 by co-precipitation method prior to hydrazine treatment and calcined at 300 ^oC, unless stated otherwise (for more details see section 3.3.2 and 3.4.3). Based on the data generated the effects of concentration of CeO_2, MnO_2 and Pd were investigated. This was followed by evaluating the methods of loading Pd nanoparticles on 2wt.% CeO_2-Co_3O_4 composite. The samples were characterised using XRD, BET, TGA, XPS, TPR, FTIR, EDS, SEM, and TEM techniques.

Both MnO_2 and CeO_2 improved the activity of Co_3O_4(H) at 100 ^oC, and MnO_2-Co_3O_4 composite showed higher activity at lower temperature. The higher activity of MnO_2 composite could be due to the higher surface area compared to that of ceria composite. The presence of 0.5wt.%Pd on either MnO_2 or CeO_2 composite showed good activity, selectivity and stability at the fuel operating temperature window.

Lastly, the stability under dry, 15% CO_2 and moisture (by bubbling He gas through water vessel at 20 ml/min, at room temperature) effects were investigated for PROX of CO in excess hydrogen over the most active catalysts at 100 ^oC for 21 h.

5.2 CHARACTERISATION OF METAL OXIDES ON Co_3O_4 CATALYSTS

The as-prepared catalysts were characterised using XRD, BET, TGA, XPS, TPR, FTIR, EDS, SEM, and TEM techniques. The results based on these techniques are discussed in the following sections.

5.2.1 X-ray powder diffraction (XRD) analysis of metal oxides on Co_3O_4 catalysts

The XRD patterns of various metal oxides (CeO_2, MnO_2, TiO_2, MgO, and Cr_3O_4) supported on Co_3O_4 are shown in Figure 5.1 and appendix (Figure 7.3). All the diffraction peaks are in good agreement with the JCPDS file of the cubic spinel type Co_3O_4 phase (JCPDS Card No. 76-1802) [5, 6, 7]. The diffraction peaks appear broadened due to the small size effect of the nano-plates [5].

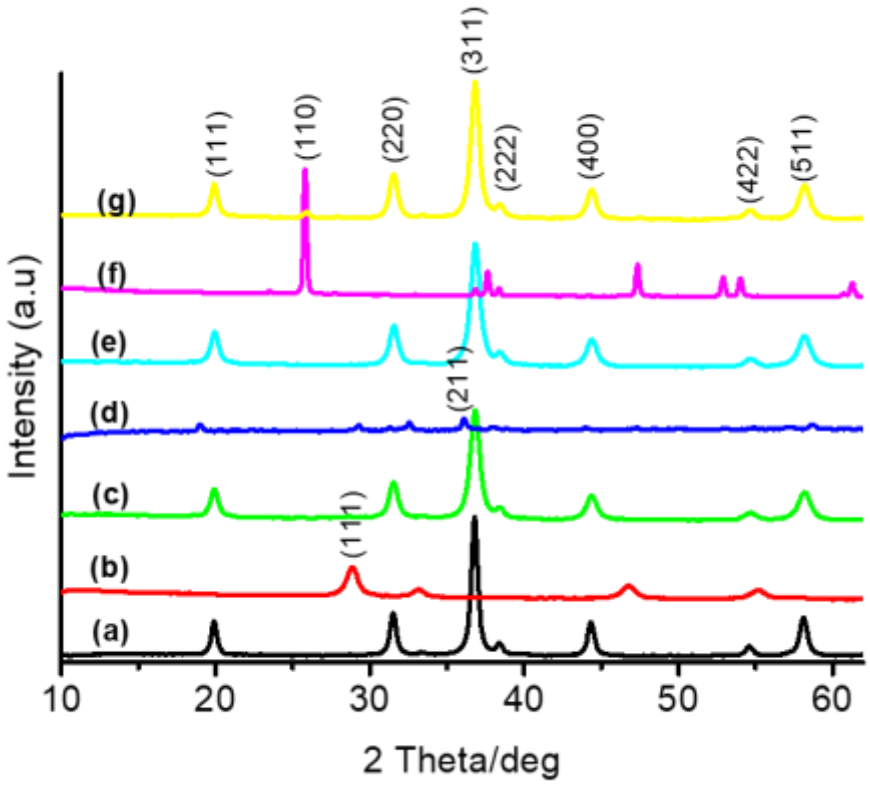

Figure 5.1 The XRD patterns of **(a)** Co_3O_4 (H), **(b)** CeO_2, **(c)** (2%CeO_2-Co_3O_4)(H), **(d)** MnO_2, **(e)** (2%MnO_2-Co_3O_4)(H), **(f)** TiO_2, **(g)** (2%TiO_2-Co_3O_4)(H), catalysts.

The introduction of the 2wt.% of metal oxides (CeO_2, MnO_2, MgO, TiO_2, and Cr_3O_4) on Co_3O_4 could not alter its structural phase, due to small amount of the metal oxide

species on Co_3O_4 (Figure 5.1(c) and (e); and Appendix E(i) and E(k)), except in the case of TiO_2 (Figure 5.1(g)). The peak at 2θ value of 25.9^o correspond to TiO_2 species on the composite (Figure 5.1(g)) [8].

5.2.2 Thermogravimetric analysis (TGA) of metal oxides on Co_3O_4 catalysts

The stability of formed (2wt.%CeO_2-Co_3O_4)(H), (2wt.%MnO_2-Co_3O_4)(H), (2wt.%TiO_2-Co_3O_4)(H), (2wt.%MgO-Co_3O_4)(H) and (2wt.%Cr_3O_4-Co_3O_4)(H) catalysts were investigated by means of TGA, as shown in Figure 5.2.

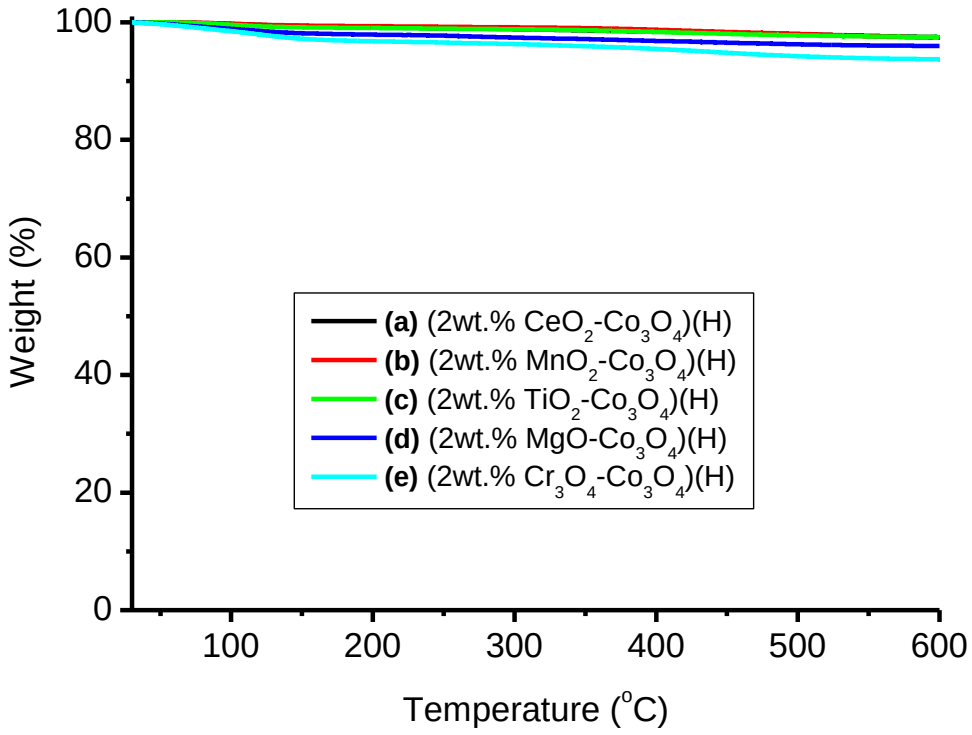

Figure 5.2 TGA profiles of **(a)** (2wt.%CeO_2-Co_3O_4)(H), **(b)** (2wt.%MnO_2-Co_3O_4)(H), **(c)** (2wt.%TiO_2/Co_3O_4)(H), **(d)** (2wt.%MgO-Co_3O_4), and **(e)** (2wt.%Cr_3O_4-Co_3O_4)(H), catalysts.

The TGA profile for all the samples remained stable up to 600 ^{o}C. This clearly indicates that the introduction of the metal oxide did not alter the structure of the Co_3O_4 and calcination process undertaken after in situ reduction completely transformed both cobalt and the metal oxide species to a spinel Co_3O_4 and expected metal oxide phase. Further studies on the characterisation of metal oxide load and Pd species on the

cobalt oxide was conducted over CeO_2-Co_3O_4 and MnO_2-Co_3O_4 catalysts due to their better catalytic activity in PROX of CO.

5.3 CHARACTERISATION OF CeO_2-Co_3O_4 CATALYSTS

5.3.1 X-ray diffraction (XRD) analysis

5.3.1.1 Effects of CeO_2 loading on Co_3O_4 phase

The data in Figure 5.3 shows the XRD patterns of Co_3O_4, CeO_2, 2wt.% CeO_2-Co_3O_4, 5wt.% CeO_2-Co_3O_4, 8wt.% CeO_2-Co_3O_4, 10wt.% CeO_2-Co_3O_4, and 30wt.% CeO_2-Co_3O_4 catalysts (all catalysts were not pre-treated by hydrazine).

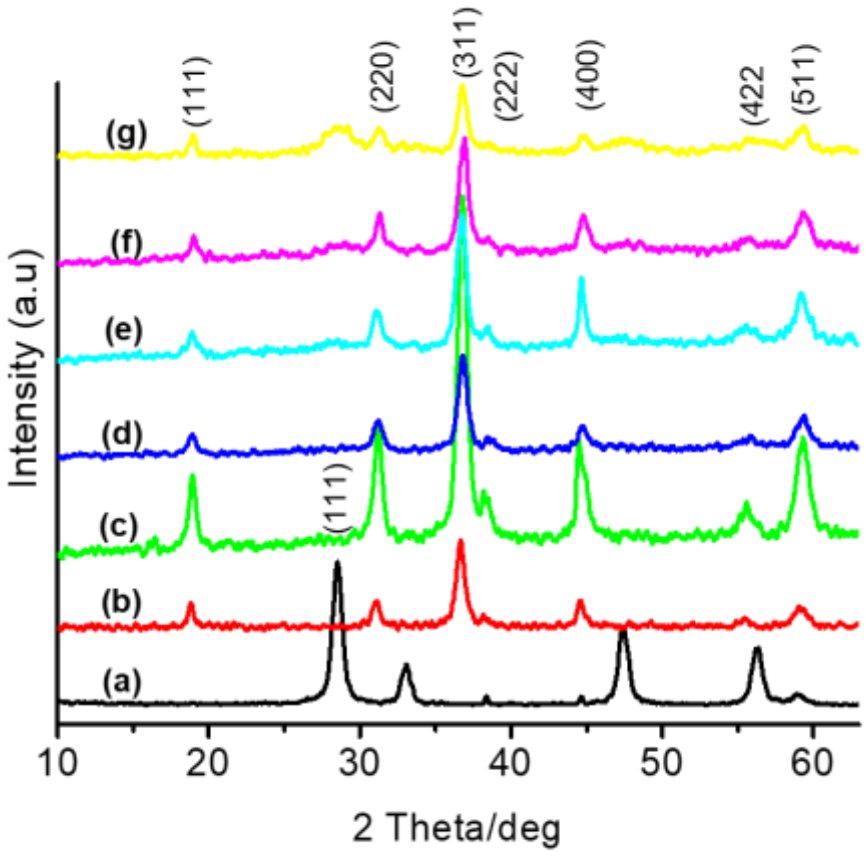

Figure 5.3 The XRD patterns of **(a)** CeO_2, **(b)** Co_3O_4, **(c)** 2wt.%CeO_2-Co_3O_4, **(d)** 5wt.%CeO_2-Co_3O_4, **(e)** 8wt.%CeO_2-Co_3O_4, **(f)** 10wt.%CeO_2-Co_3O_4, and **(g)** 30wt.%CeO_2-Co_3O_4, catalysts.

The XRD profile confirms the CeO_2 (a) and the corresponding Co_3O_4 (b) patterns, based on their prominent peaks at 2θ value of 28.3 (111) and 36.8° (311) plane, respectively [5]. Upon loading 2wt.% of CeO_2 on Co_3O_4 the intensity of (311) plane decreased. This trend continued with an increase of CeO_2 loading, until the peak at 2θ value of 28.3° emerges (see Figure 5.3(g)). The average crystallite size of Co_3O_4 decreased when 2wt.% CeO_2 was added, and then started to increase with the CeO_2 loading (Table 5.1). Similar trend was reported by Lu *et al* [9]. The decrease in crystallite size with 2wt.% CeO_2 was found to correspond to a higher BET surface area of the overall catalyst (see Table 5.1, section 5.2.2.5). Hence, the optimum loading of ceria was kept at 2wt.% on the surface of Co_3O_4.

5.3.1.2 Effect of preparation method of 1wt.%Pd on 2%CeO_2-Co_3O_4 support

The effect of Pd species on the hydrazine treated 2wt.% CeO_2-Co_3O_4 was investigated by introducing the Pd species using different methods. Figure 5.4 present the XRD patterns of (2wt.%CeO_2-Co_3O_4)(H), and that of 1wt.%Pd/(2wt.%CeO_2-Co_3O_4(H)) prepared by precipitation, deposition, and improved wet impregnation methods.

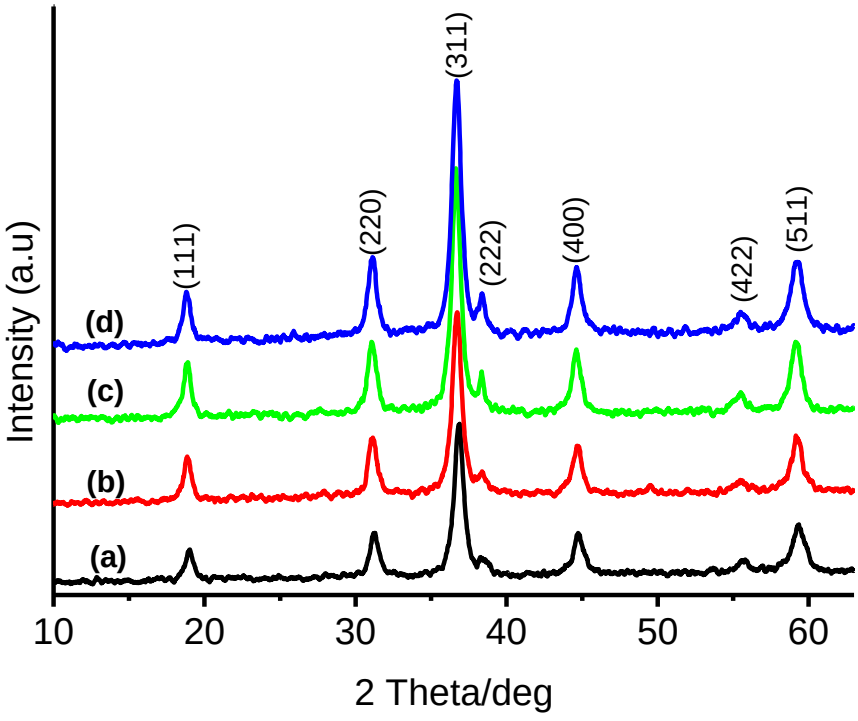

Figure 5.4 The XRD patterns of **(a)** (2wt.% CeO_2-Co_3O_4)(H), **(b)** 1wt.%Pd/(2wt.%CeO_2-Co_3O_4(H)) precipitation, **(c)** 1wt.%Pd/(2wt.%CeO_2-Co_3O_4(H)) deposition, and **(d)** 1wt.%Pd/(2wt.%CeO_2-Co_3O_4(H)) impregnation, catalysts.

The XRD patterns for the 1wt.% Pd on the reduced 2wt.%CeO_2-Co_3O_4 samples did not change the structure feature of 2wt.%CeO_2-Co_3O_4 catalyst (Figure 5.4(b), (c), and (d)). A decrease in the XRD peak intensities was observed over all the three catalysts, however, the peak for Pd species is missing from the XRD patterns (Figure 5.4(b), (c), and (d)). This could suggest a good synergy between the support (2wt.%CeO_2-Co_3O_4) and the 1wt.%Pd species [5]. An increased BET surface area of the 1wt.%Pd/(2wt.%CeO_2-Co_3O_4(H)) catalysts (Table 5.2) as a result of the preparation method was observed (wet impregnation method < deposition < precipitation). Preparation method plays an important role on the structural composition of the catalysts [10, 11]. However, an improved surface area was noted when the Pd species is introduced on the support by co-precipitation method. Hence, co-precipitation method was considered for further investigation on effect of Pd load on 2wt.%CeO_2-Co_3O_4 catalyst.

5.3.1.3 Effect of Pd loading on 2wt.% CeO_2-Co_3O_4

Figure 5.5 presents the XRD patterns of 2wt.% CeO_2-Co_3O_4, 0.5wt.%Pd-2wt.%CeO_2/Co_3O_4 and 1wt.%Pd/2wt.%CeO_2-Co_3O_4 catalysts. The peak for Pd species is missing from the XRD pattern, which suggests a good synergy between Pd and the support [5, 12]. These findings correlate with the work reported by Luo *et al* [5], where Pd species was supported on Co_3O_4-CeO_2 by impregnation method. The presence of the 0.5wt.%Pd decreased the surface area of the CeO_2-Co_3O_4 composite, however, and increase in the surface area was observed with an increasing load of Pd to 1wt.% (Table 5.1). The crystallite size of the catalyst decreased from 22.3 to 20.7 nm with an increased Pd loading. The XRD peak intensities of the catalysts increased with an increased Pd load on the support (Figure 5.5).

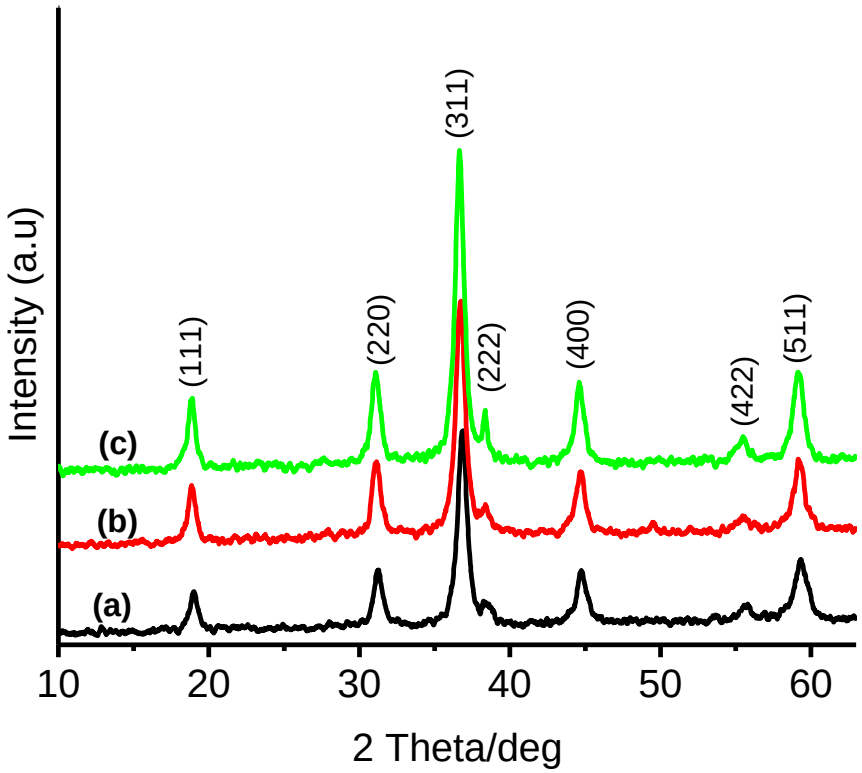

Figure 5.5 The XRD patterns of **(a)** 2wt.%CeO_2-Co_3O_4, **(b)** 0.5wt.%Pd-2wt.%CeO_2/Co_3O_4, and **(c)** 1wt.%Pd/2wt.%CeO_2-Co_3O_4, catalysts.

5.3.2 Brunauer-Emmett-Teller (BET) analysis

The data in Table 5.1 shows the BET surface area analysis of Co_3O_4(H), 2wt.% CeO_2-Co_3O_4, 5wt.%CeO_2-Co_3O_4, 8wt.%CeO_2-Co_3O_4, 0.5wt.%Pd-2wt.%CeO_2/Co_3O_4, and 1wt.%Pd/2wt.%CeO_2-Co_3O_4. The introduction of ceria species on the cobalt oxide resulted in a decrease in the surface area, from 2 to 5wt.% ceria load. However, an optimum ceria load of 8% increased the surface area to 65.3 m^2/g. interestingly, the treatment of the 2wt.%CeO_2-Co_3O_4 by hydrazine has further increased the surface area, pore volume and pore size of the catalyst (Table 5.1). Other researchers have reported an increase in the dispersion and the surface area of cobalt oxide due to optimum ceria load [13]. The introduction of 1wt.%Pd species by co-precipitation method resulted in a surface area of 83.6 m^2/g, which is a bit higher when compared with the samples prepared by deposition, precipitation, and improved wet impregnation method, respectively. Consequently, preparation method plays an important role in the subsequent type of the end product required [10, 13].

Table 5.1 The effect of CeO_2 and Pd species on the crystallite size and surface area of the as-prepared samples.

Catalyst	S_{BET} (m^2/g)	Pore volume ($cm^3\ g^{-1}$)	Pore size (nm)	Average crystallite size (nm)[a]
CeO_2				6.6
Co_3O_4(H)	62.2	0.158	9.95	20.0
2wt.%CeO_2-Co_3O_4	63.5	0.177	10.8	21.8
5wt.%CeO_2-Co_3O_4	56.2	0.175	12.6	22.3
8wt.%CeO_2-Co_3O_4	65.3	0.202	12.1	28.1
(2wt.%CeO_2-Co_3O_4)(H)	81.8	0.253	11.9	22.9
(0.5wt.%Pd-2wt.%CeO_2/Co_3O_4)(H) cppt	70.9	0.332	18.2	22.3
(0.5wt.%Pd/2wt.%CeO_2-Co_3O_4)(H) cppt	76.7	0.245	12.5	
(1wt.%Pd/2wt.%CeO_2-Co_3O_4)(H) cppt	83.6	0.280	13.3	20.7
(1wt.%Pd/(2wt.%CeO_2-Co_3O_4(H)) dep	80.8	0.227	10.9	22.3
(1wt.%Pd/(2wt.%CeO_2-Co_3O_4(H)) adv	75.8	0.220	11.4	22.3
(1wt.%Pd/(2wt.%CeO_2-Co_3O_4(H)) ppt	81.1	0.261	10.6	22.1

[a] Average crystallite sizes were estimated from (311) plane of XRD patterns. ppt = precipitation method, dep = deposition method, imp = improved wet impregnation method, co-ppt = co-precipitation method.

5.3.3 Thermogravimetric analysis (TGA)

The stability of the formed (2wt.%CeO_2-Co_3O_4)(H) and (0.5wt.%Pd-2wt.%CeO_2/Co_3O_4)(H) catalysts were investigated by TGA, as shown in Figure 5.6. The TGA profile for all the samples remained stable up to 600 ^oC. This clearly indicates that the calcination process undertaken after in-situ reduction has completely transformed both cobalt and ceria species to a spinel Co_3O_4 and CeO_2 phase. The introduction of Pd species did not alter the structure of CeO_2-Co_3O_4, as confirmed by XRD data.

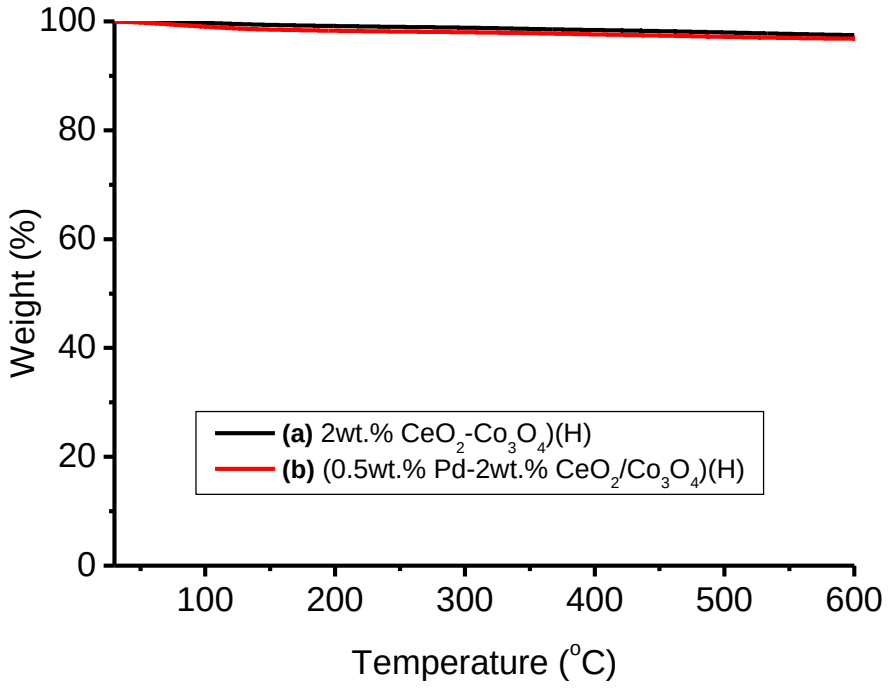

Figure 5.6 Thermogravimetric analysis of **(a)** (2wt.%CeO_2-Co_3O_4)(H), and **(b)** (0.5wt.%Pd-2wt.%CeO_2/Co_3O_4)(H), catalysts.

5.3.4 X-ray photoelectron spectroscopy (XPS) analysis

The oxidation state of various Co species and structural composition formed over (2wt.%CeO_2-Co_3O_4) (H), and (0.5wt.%Pd-2wt.%CeO_2/Co_3O_4) (H) samples, prepared by co-precipitation method are presented in Figure 5.7.

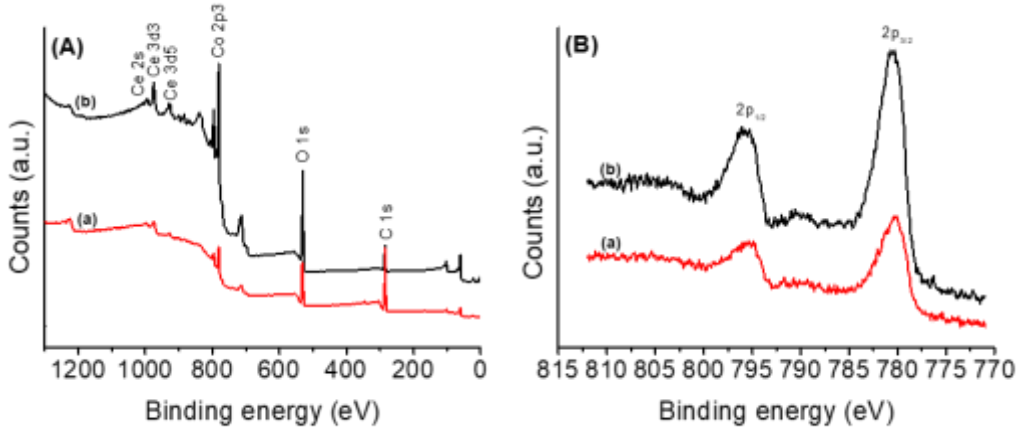

Figure 5.7 The XPS spectra of **(a)** (0.5wt.%Pd-2wt.%CeO_2/Co_3O_4) (H), and **(b)** (2wt.%CeO_2-Co_3O_4) (H) catalysts. XPS survey spectra **(A)** and oxidation state **(B)** of samples.

The XPS survey spectra confirm the coexistence of C, Co, Ce, and O over 2wt.%CeO_2-Co_3O_4(H), and 0.5wt.%Pd-2wt.%CeO_2/Co_3O_4(H) samples (Figure 5.7A). The chemical structural composition of the catalysts was also confirmed by EDS data (see Appendix F). As shown in the previous studies, two peaks were observed overall samples and are due to Co $2p_{3/2}$ and Co $2p_{1/2}$ species, as shown in Figure 5.7B. The binding energy of 780.4 and 795.6 eV, and spin orbit splitting of 15.8 eV was also observed over 2wt.%CeO_2-Co_3O_4 sample (Figure 5.7B(b)) [14]. The results suggest that the cobalt species are present mainly as Co^{3+} and Co^{2+} species [15], though, cannot be quantified. A decreased intensity of the peaks due to reduction was also observed, as confirmed by XRD data. The shift in the binding energy of the reduced samples was observed when 0.5wt.%Pd-2wt.%CeO_2 species is introduced on the Co_3O_4 species prior to reduction (Figure 5.7B(a)). The presence of Pd species on the 2wt.%CeO_2-Co_3O_4 decreased the intensity of the peaks, which imply an increase in the Co^{3+}/Co^{2+} atomic ratio [16].

5.3.5 Fourier transform infrared spectroscopy (FTIR)

The FTIR spectra of (2wt.%CeO_2-Co_3O_4) (H), and (0.5wt.%Pd-2wt.%CeO_2/Co_3O_4) (H) samples are shown in Figure 5.8. Just like in the previous chapter, the FTIR profile of CeO_2-Co_3O_4 sample (Figure 5.8(b)), displays two distinct and sharp bands at 547 and 651 cm^{-1}, which originate from the stretching vibrations of the metal-oxygen bonds (Co-O) [14, 17-18]. The band at 547 cm^{-1} is assigned to the octahedral arrangement of Co^{3+}, with the band at 651 cm^{-1} due to Co^{2+} in a tetrahedral position [18], which confirms the formation of spinel Co_3O_4 (Figure 5.8(a)). This indicates that CeO_2 species did not have an effect on the structural profile of Co_3O_4 phase, which is consistent with the XRD data. However, a decrease in the peak intensity was observed, which could explain the surface area transformation of the materials (Table 5.1, section 5.2.2.5). The intensive broadband at 1631 and 3347 cm^{-1} are due to O-H stretching vibration interacting through H bonds [17].

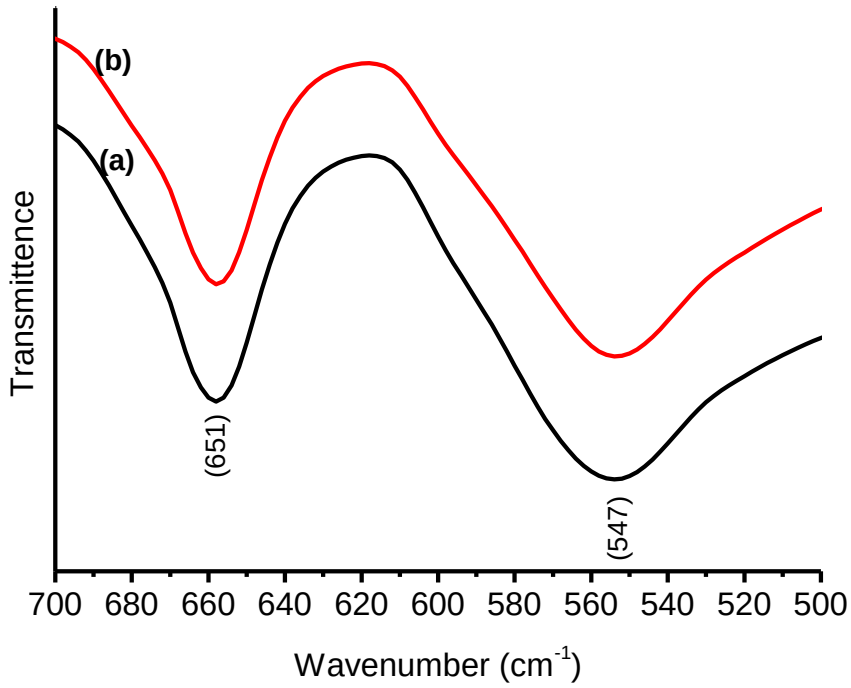

Figure 5.8 The FTIR spectra of **(a)** (2wt.%CeO_2-Co_3O_4) (H), and **(b)** (0.5wt.%Pd-2wt.%CeO_2/Co_3O_4) (H), catalysts.

The FTIR profile of CeO_2 alone shows the absorption bands at 1304 and 1631 cm^{-1} which correspond to physical absorbed water molecule (see Appendix G(a)) [17, 19]. The bands at 886 and 547 cm^{-1} are produced by CeO_2, which is a typical peak for Ce-O stretching vibrations [19]. The structure of the catalysts is further confirmed by TEM analysis.

5.3.6 Scanning electron microscope (SEM) analysis

The SEM images of a (2wt.%CeO_2-Co_3O_4)(H), (0.5wt.%Pd-2wt.%CeO_2/Co_3O_4)(H) catalysts are shown in Figure 5.9.

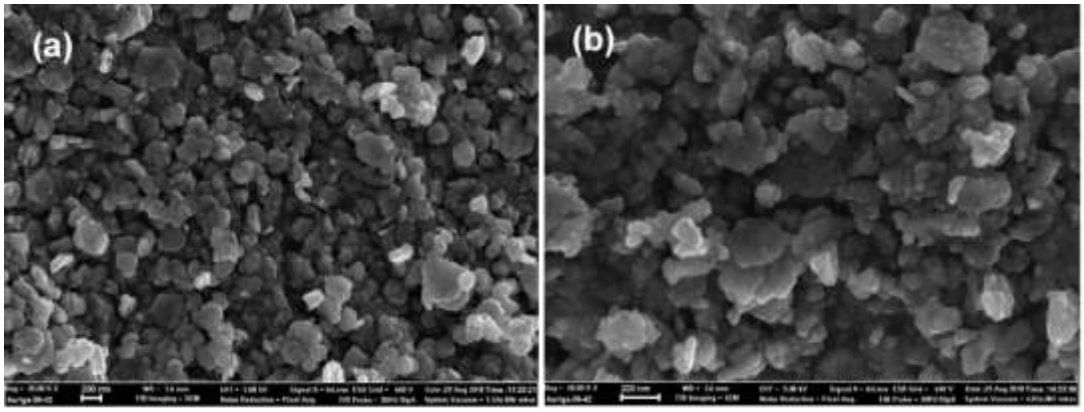

Figure 5.9 The SEM images of **(a)** (2wt.%CeO_2-Co_3O_4) (H), and **(b)** (0.5wt.%Pd-2wt.%CeO_2/Co_3O_4) (H) catalysts.

The introduction of 2wt.%CeO_2 on Co_3O_4 sample shows a mixture of hexagonal platelets and rod-like morphologies with agglomerations (Figure 5.9(a)) compared to that of Co_3O_4 (section 4.2.7, Figure 4.8(c)). The introduction of 0.5wt.%Pd-2wt.%CeO_2 on the Co_3O_4 sample promotes the formation of more agglomerates spheroids attached to the hexagonal platelets and rods like morphology (Figure 5.9(b)).

5.3.7 Transmission electron microscope (TEM) analysis

The TEM images of a 2wt.%CeO_2-Co_3O_4, (2wt.%CeO_2-Co_3O_4)(H), and (0.5wt.%Pd-2wt.%CeO_2/Co_3O_4)(H) catalysts are presented in Figure 5.10. Like the SEM, the TEM images of the 2wt.%CeO_2-Co_3O_4 sample showed hexagonal platelets and rod-like morphologies (Figure 5.10(a)). The reductive pre-treatment of the 2wt.%CeO_2-Co_3O_4 sample resulted in the mixture of hexagonal platelets, cubic and rod-like morphologies (Figure 5.10(b)). The introduction of the 0.5wt.%Pd-2wt.%CeO_2 species on the Co_3O_4 disrupted its structure (Figure 5.10(c)). The (0.5wt.%Pd-2wt.%CeO_2/Co_3O_4) (H) sample consists of spheroids and rod-like morphologies. This distribution is well aligning with the XRD data of the two samples and SEM results. Moreover, the phase identification as shown on the HRTEM (Figure 5.10(d)) indicates the presence of lattice fringe spacing of 0.48 nm (311) and 0.28 nm (111), which confirms the characteristic lattice structure of Co_3O_4 [7, 20-21]. The presence of the Pd species is not visible on the TEM images which indicate that the Pd are highly dispersed on the CeO_2-Co_3O_4 support [22].

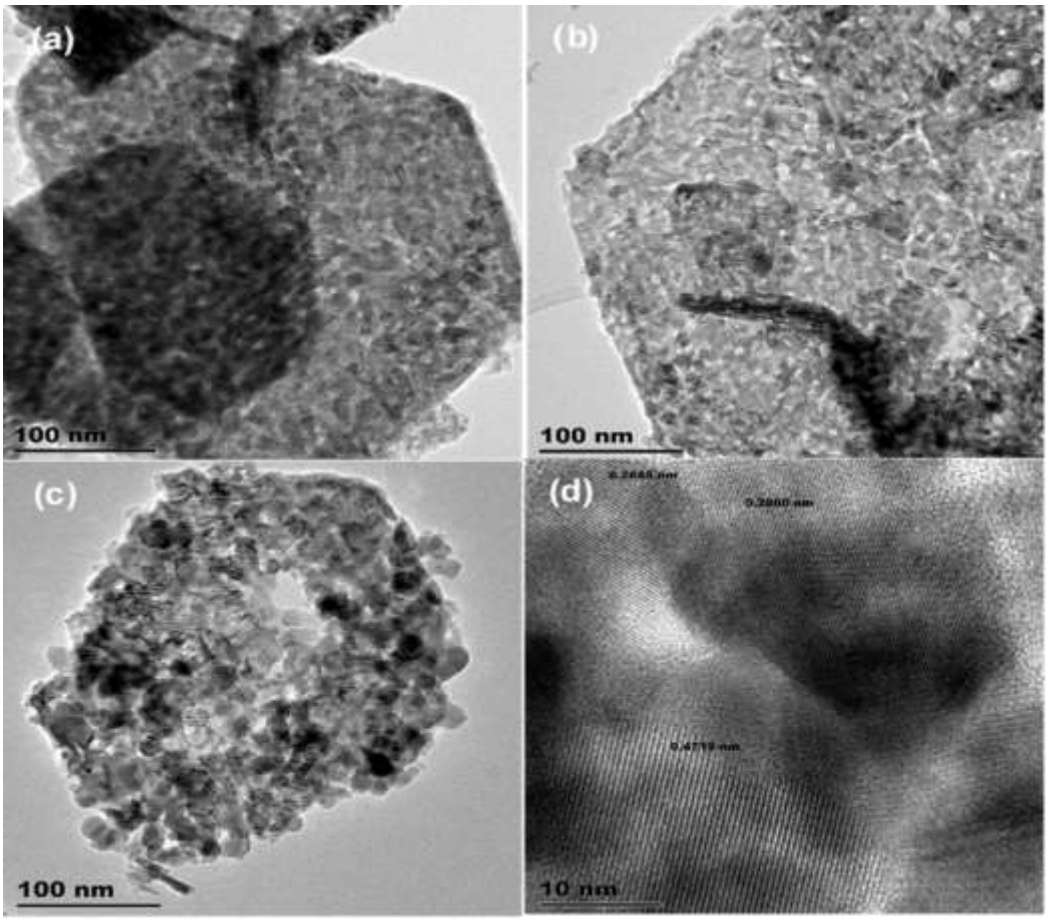

Figure 5.10 The TEM images of **(a)** 2wt.%CeO_2-Co_3O_4, **(b)** (2wt.%CeO_2-Co_3O_4)(H), **(c)** (0.5wt.%Pd-2wt.%CeO_2/Co_3O_4)(H), and **(d)** HRTEM of (0.5wt.%Pd-2wt.%CeO_2/Co_3O_4)(H), catalysts.

5.4 CHARACTERISATION OF MnO_2-Co_3O_4 CATALYSTS

5.4.1 XRD profile of various MnO_2 on Co_3O_4

The effect of Mn load over the Co_3O_4 was investigated by varying the amount of Mn on Co_3O_4, the samples were prepared by co-precipitation method and treated by hydrazine. The XRD patterns for the prepared samples are presented in Figure 5.11.

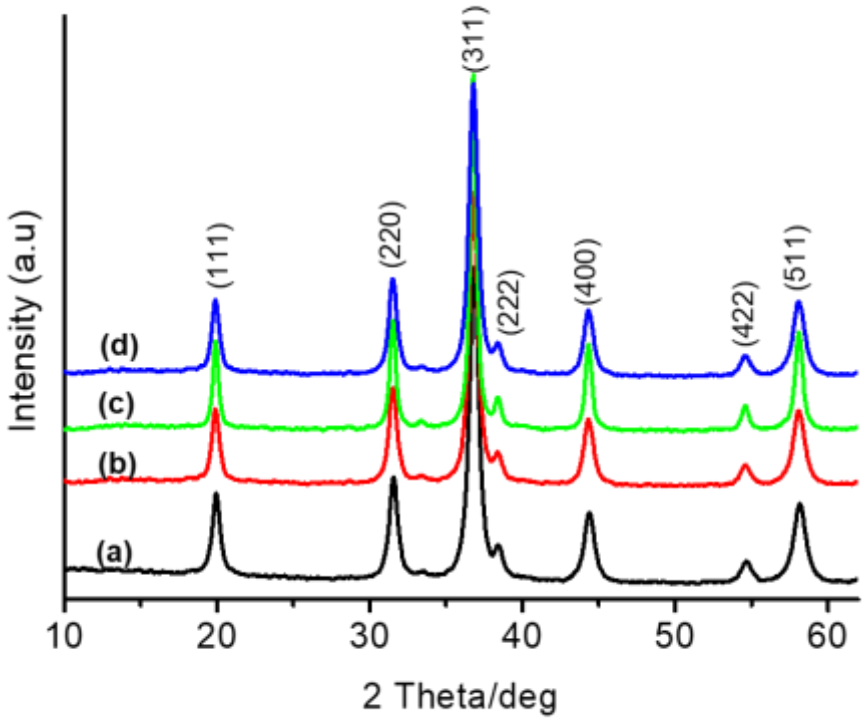

Figure 5.11 The XRD patterns of **(a)** (2wt.%MnO_2-Co_3O_4)(H), **(b)** (5wt.%MnO_2-Co_3O_4)(H), **(c)** (7wt.%MnO_2-Co_3O_4)(H), and **(d)** (10wt.%MnO_2-Co_3O_4)(H), catalysts.

The product reveals diffraction peaks with 2θ values of 19.8, 31.3, 32.9, 36.8, 38.9, 44.9, 54.5, and 58.5° that are assigned to the (111), (220), (113), (311), (222), (400), (422), and (511) crystal planes of (Co, Mn) (JCPDS Card No. 18-0408), respectively (Figure 5.11(a)) [23]. A typical diffraction peak at 2θ value of 36.8° for MnCoOs (Figure 5.11(a) to (d)) sample is due to formation of spinel structure (Co, Mn) [24], the diffractions at 2θ values of 31.3, 44.9, and 58.5° correspond to Co_3O_4 (JCPDS Card No. 76-1802) are visible [25-26]. The typical diffractive peak at 2θ values of 19.2°, 32.9, 38.2, 44.9 and 54.5° could be assigned to Mn structure (PDF-65-2776JCPDS file) which implied the good dispersion of Mn into lattice of Co_3O_4 [27]. A slight shift of the Co_3O_4 reflections to smaller 2θ angles is detected, as a result of the formation of the Mn-Co-O catalyst [28]. The results show that much smaller samples of 5 nm as compared to Co_3O_4 with 10 nm crystallite are formed, indicating that the addition of Mn suppressed the growth of the crystal [28]. The average crystallite size, D of the as-prepared samples was calculated from (311) plane diffraction peak using the Scherrer's formula (as shown in section 3.4.1).

5.4.2 Brunauer-Emmett-Teller (BET) analysis

The BET analysis of the hydrazine treated 2wt. %MnO_2-Co_3O_4, 5wt.%MnO_2-Co_3O_4, 7wt.%MnO_2-Co_3O_4, and 0.5wt.%Pd-7wt.%MnO_2/Co_3O_4, 1wt.%Pd-7wt.%MnO_2/Co_3O_4, and 2wt.%Pd-7wt.%MnO_2/Co_3O_4 samples are shown in Table 5.2. The introduction of the Mn species on Co_3O_4 samples prior to reduction by $N_2H_4.H_2O$ solution improved the surface area of the Co_3O_4. The surface area decreased with an increase in the Mn load. Liu *et al.* [2], showed that the use of Mn as promoter can result in a Co_3O_4 spinel phase with the highest surface area, smallest nano-size crystallites and highly dispersed oxygen deficiency and structural defect morphology. An increase in the amount of manganese resulted in a decrease in the surface area of cobalt oxide, from 249 (at 2wt.%MnO_2 load) to 81.8 m^2/g (at 7wt.% MnO_2). The negative effect of the surface area of the cobalt, due to higher manganese load is reported in the literature [28]. The introduction of the 0.5wt.%Pd-7wt.%MnO_2 species on the cobalt oxide catalysts resulted in a decrease in the surface area of the catalyst, from 81.8 to 63.1 m^2/g. However, an increase in the surface area of the composite was observed with an increasing amount of the Pd species. The increased surface area may be due to increased roughness of the surface Pd species [29].

Table 5.2 The effect of Mn and Pd on the crystallite size and surface area of the as-prepared samples.

Catalyst	**S_{BET} (m^2/g)**	**Pore volume ($cm^3\ g^{-1}$)**	**Pore size (nm)**	**Average crystallite size (nm)[a]**
2wt.%MnO_2-Co_3O_4(H)	249	0.562	5.28	23.0
5wt.%MnO_2-Co_3O_4(H)	235	0.600	5.92	33.9
7wt.%MnO_2-Co_3O_4(H)	81.8	0.253	11.9	47.6
(0.5wt.%Pd-7wt.%MnO_2/Co_3O_4)(H)	63.1	0.346	23.0	37.5
(1wt.%Pd-7wt.%MnO_2/Co_3O_4)(H)	71.2	0.324	19.1	35.4
(2wt.%Pd-7wt.%MnO_2/Co_3O_4)(H)	69.9	0.422	25.7	37.7

[a] Average crystallite sizes were estimated from (311) plane of XRD patterns.

5.4.3 Thermogravimetric analysis (TGA)

The thermal stability of hydrazine treated 7wt.%MnO_2-Co_3O_4, and 0.5wt.%Pd-7wt.%MnO_2/Co_3O_4 samples were investigated by TGA in a static nitrogen atmosphere at a heating rate of 10 ^oC/min, as shown in Figure 5.12.

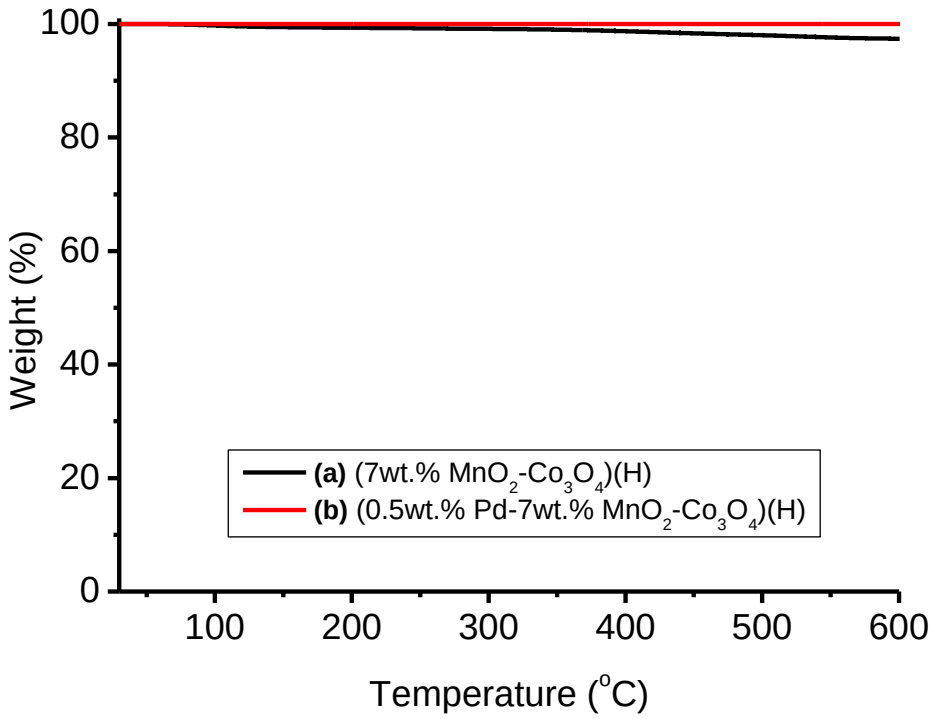

Figure 5.12 Thermogravimetric analysis of **(a)** (7wt.%MnO_2-Co_3O_4)(H), and **(b)** (0.5wt.%Pd-7wt.%MnO_2/Co_3O_4)(H) catalysts.

The TGA profile of hydrazine treated 7wt.%MnO_2-Co_3O_4 samples showed a slight steady decrease in the composition of the structure with temperature (Figure 5.12(a)). The introduction of 0.5wt.%Pd-7wt.%MnO_2 species on the Co_3O_4 prior to reduction and calcination at 300 ^oC, resulted in hydrothermal stable samples up to 600 ^oC (Figure 5.12(b)). This clearly indicates that the calcination process undertaken after in situ reduction has completely transformed all cobalt species to a spinel Co_3O_4 phase and the Mn phase species.

5.4.4 X-ray photoelectron spectroscopy (XPS) analysis

The oxidation state of various Co and Mn species formed over (7wt.%MnO_2-Co_3O_4)(H), (0.5wt.%Pd-7wt.%MnO_2/Co_3O_4)(H), (1wt.%Pd-7wt.%MnO_2/Co_3O_4)(H), and (2wt.%Pd-7wt.%MnO_2/Co_3O_4)(H) catalysts which were prepared by co-precipitation method are presented in Figure 5.13. The XPS survey spectra confirm the coexistence of C, Co, O, and Mn over (7wt.%MnO_2-Co_3O_4)(H), (0.5wt.%Pd-7wt.%MnO_2/Co_3O_4)(H), (1wt.%Pd-7wt.%MnO_2/Co_3O_4)(H), and (2wt.%Pd-7wt.%MnO_2/Co_3O_4)(H) catalysts (Figure 5.13A). Two peaks were observed overall samples and are due to Co $2p_{3/2}$ and Co $2p_{1/2}$ species as shown in (Figure 5.13B). The (7wt.%MnO_2-Co_3O_4)(H) sample has the binding energy of 781.6 and 796.6 eV (Figure 5.13B(a)). Moreover, the sample has the spin orbit splitting of 15 eV, which denote the presence of Co_3O_4 [14]. The increase in the binding energy of Co $2p_{3/2}$ (from 180.2 eV) after addition of MnO_2 to Co_3O_4 suggest an increase in fraction of Co^{3+}/Co^{2+} in MnO_2-Co_3O_4 catalyst [28].

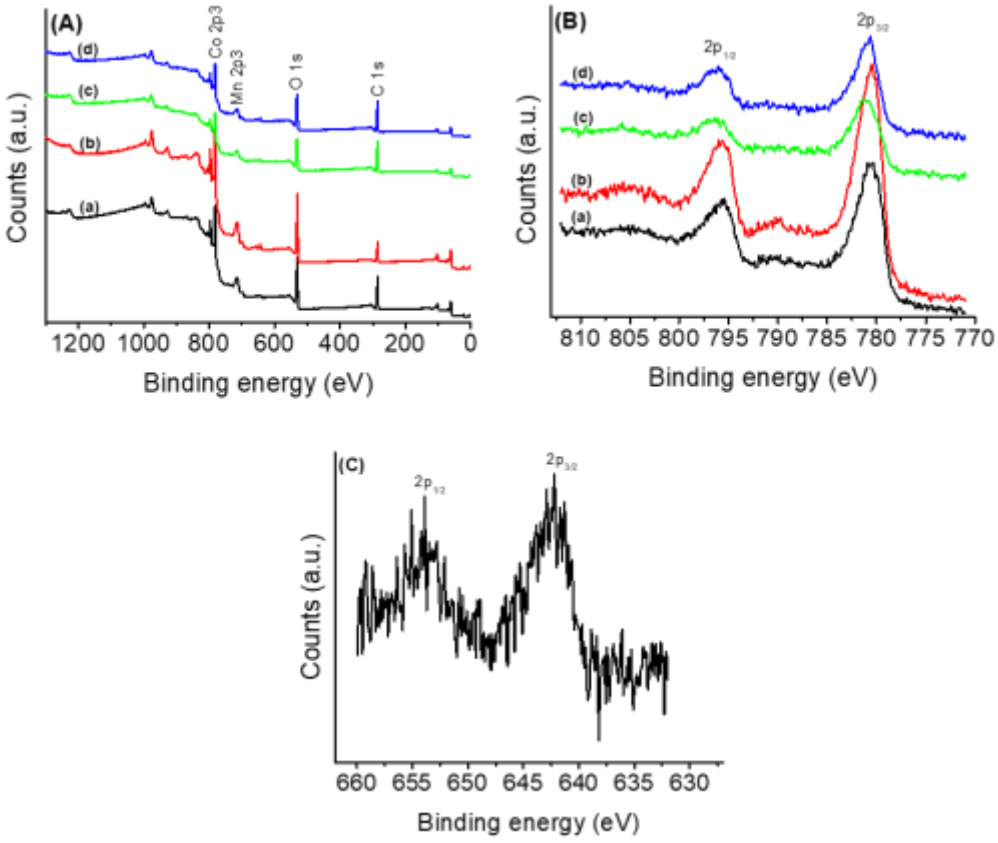

Figure 5.13 The XPS spectra of **(a)** (7wt.%MnO_2-Co_3O_4)(H), **(b)** (0.5wt.%Pd-7wt.%MnO_2/Co_3O_4)(H), **(c)** (1wt.%Pd-7wt.%MnO_2/Co_3O_4) (H), and **(d)** (2wt.%Pd-7wt.%MnO_2/Co_3O_4) (H), catalysts. XPS survey spectra **(A)** and oxidation state **(B, C)** of samples.

The peak intensity of (7wt.%MnO_2-Co_3O_4)(H) decreased with an increase in the amount of Pd load. The shake-up satellite peak at 790 eV belong to Co $2p_{1/2}$ and it shows the presence of Co^{2+} [30]. The electronic interaction between MnO_x and CoO_x is an important influencing factor for enhancing the redox properties of the sample [23, 31]. Zhanga *et al.* [32], reported have reported that the presence of Mn^{2+} can promote the regeneration of Co^{3+} (i.e. $Co^{3+} \rightarrow \%Co^{2+}$). The XPS spectrum for Mn $2p_{3/2}$ indicate two high intensity asymmetric peaks with binding energies of 642.2 and 653.9 eV, for Mn $2p_{3/2}$ and Mn $2p_{1/2}$, respectively (Figure 5.13C) [32]. The sample has the spin orbit splitting of 11.7 eV, which denote the presence of the MnO_2 [33]. The structural composition for (0.5wt.% Pd-7wt.% MnO_2/Co_3O_4)(H) catalyst was also confirmed by EDS data, see Appendix H).

5.4.5 Temperature programmed reduction (TPR) analysis

The transformation of the as-prepared and spent (7wt.% MnO_2-Co_3O_4)(H) catalysts, and (0.5wt.%Pd-7wt.%MnO_2/Co_3O_4)(H) catalyst was further investigated using H_2-TPR, as shown in Figure 5.14. The hydrazine treated Co_3O_4 exhibited two main broad peaks at reduction maxima of 228 ^oC (with a peak area of 816, insert) and 326 ^oC (with a peak area of 1351, inset), which belong to the stepwise reduction of $Co_3O_4 \rightarrow CoO \rightarrow Co$ [24]. The (7wt.%MnO_2-Co_3O_4)(H) catalyst (Figure 5.14(a)), compared with the peak characteristic of Co species increased reduction maxima from 228 to 256 ^oC ($Co_3O_4 \rightarrow CoO$, which gave a negligible amount of area under the peak), and increased reduction maxima from 326 to 367 ^oC ($CoO \rightarrow Co$). This phenomenon could have resulted from mutual effect of Co and Mn species and confirmed the addition of Mn to Co which resulted to a shift in the area of the peaks [2], which is in agreement with the XRD data. The TPR profile of a spent (7wt.%MnO_2-Co_3O_4)(H) catalyst (Figure 5.14(B)(b)) shows a reducing maxima which is higher (at approximately 290 ^oC, with an area of 346) than that of Co_3O_4 spinel structure. Liu *et al* [2] have reported similar reduction behaviour with the higher reduction maxima when 5wt.% MnO_x is doped on Co_3O_4. A sharp reduction maxima peak at 220 ^oC was observed over (0.5wt.% Pd-7wt.%MnO_2/Co_3O_4)(H) catalyst, and both peaks (256 and 365 ^oC, which gave a negligible amount of area under the peak) are shifted to lower reduction maxima of 220 and 349 ^oC (Figure 5.14(a) and (c)). Wang *et al.* [22], have shown that the shift in reduction maxima is due to PdO which facilitate the reduction of Co_3O_4 due to the H_2

spillover effect. Ercolino *et al.* [34], reported a decrease in the reduction maxima of Co_3O_4 in the presence of palladium, maximum reduction depends on the amount of palladium load.

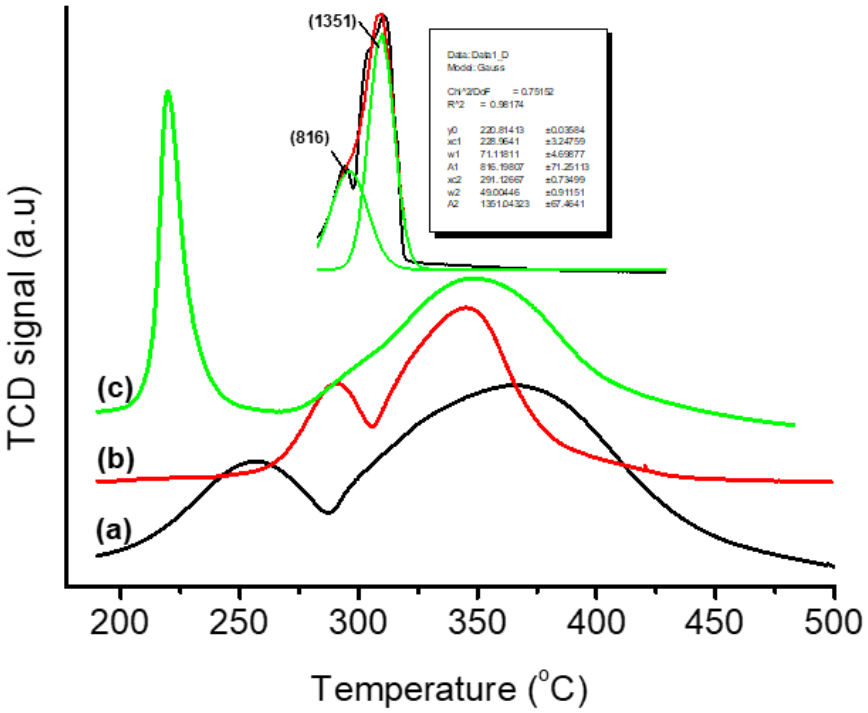

Figure 5.14 The TPR profile of **(a)** (7wt.%MnO_2-Co_3O_4)(H), **(b)** (7wt.%MnO_2-Co_3O_4)(H) spent catalyst, **(c)** (0.5wt.%Pd-7wt.%MnO_2/Co_3O_4)(H) catalysts. Inset: example of deconvoluted TPR peak profile of Co_3O_4(H).

5.4.6 Fourier transform infrared spectroscopy (FTIR)

The FTIR spectra of hydrazine treated 7wt.%MnO_2-Co_3O_4, and 0.5wt.%Pd-7wt.%MnO_2/Co_3O_4, catalysts are shown in Figure 5.15. The FTIR spectra for all the samples displays two distinct and sharp bands at 547 and 651 cm^{-1}, which originate from the stretching vibrations of the metal oxygen bonds (Co-O) [14, 17-18]. The band at 547 cm^{-1} is assigned to the octahedral arrangement of Co^{3+}, while the band at 651 cm^{-1} is assigned to Co^{2+} placed in the tetrahedral site [18], which confirms the formation of spinel Co_3O_4 phase. The intensive broadband at 1631 cm^{-1} and 3347 cm^{-1} are due to O-H stretching vibration interacting through H bonds [17]. The peak of Mn-O bond was not observed and that indicates the dispersion of the Mn in the catalyst sample, which is consistent with the XRD data [27].

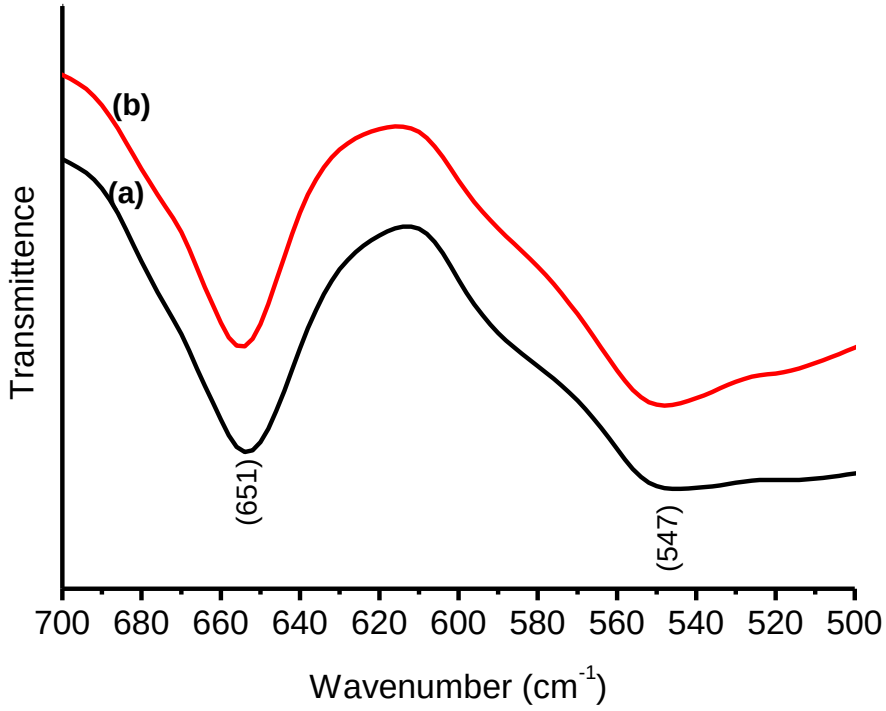

Figure 5.15 The FTIR spectra of **(a)** (7wt.%MnO_2-Co_3O_4)(H), and **(b)** (0.5wt.%Pd-7wt.%MnO_2/Co_3O_4)(H), catalysts.

5.4.7 Scanning electron microscope (SEM) analysis

The SEM images of a hydrazine treated 7wt.%MnO_2-Co_3O_4, and 0.5wt.%Pd-7wt.%MnO_2/Co_3O_4 catalysts are shown in Figure 5.16. The SEM images for (7wt.%MnO_2-Co_3O_4)(H) and (0.5wt.%Pd-7wt.%MnO_2/Co_3O_4)(H) catalysts show hexagonal platelets, rod-like and granular like morphology with agglomerations (Figure 5.16(a) and (b)). The observed results show that Mn somehow disrupt the conventional structural arrangement as confirmed by the TEM data.

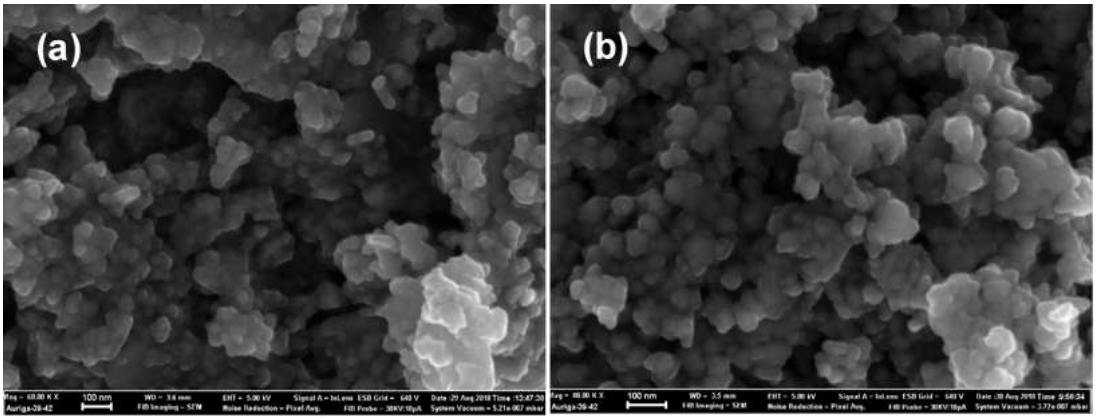

Figure 5.16 The SEM images of **(a)** (7wt.%MnO_2-Co_3O_4)(H), and **(b)** (0.5wt.%Pd-7wt.%MnO_2/Co_3O_4)(H) samples.

5.4.8 Transmission electron microscope (TEM) analysis

The TEM images of the hydrazine treated 7wt.%MnO_2-Co_3O_4, 0.5%Pd-7wt.%MnO_2/Co_3O_4, and 1wt.%Pd-7wt.%MnO_2/Co_3O_4 catalysts are shown in Figure 5.17. The TEM image of Co_3O_4(H) in (see section 4.2.7 Figure 4.7(c)) shows the agglomerates of hexagonal-like features. Upon loading Mn species on the Co_3O_4 prior to reduction by $N_2H_4.H_2O$ solution, resulted to a complete disrupted Co_3O_4 structure with granular like particles, with agglomerations of Mn species (Figure 5.17(a)). Liu *et al.* [2], reported that an appropriate amount of manganese can cause the formation of small solid solution particles and disorder in the spinel structure of cobalt oxides, which enhances the formation of active oxygen ion species for CO oxidation. The 0.5wt.%Pd-7wt.%MnO_2 on the Co_3O_4 had shown structural features similar to that of 7wt.%MnO_2-Co_3O_4 (Figure 5.17(b) and (c)). The Pd load from 0.5 to 1wt.% did not have an effect on the structural changes, all samples had granular particles and rod-like morphology (Figure 5.17(b) and (d)). The HRTEM images (Figure 5.17(d)) show a distinct lattice fringe with an interplanar spacing of 0.248 and 0.286 nm, which matches well with the spacing between the (311) and (220) planes of Mn-Co spinel phase [28]. The lattice d-spacing of 0.467 nm is also measured in Figure 5.17(d) which corresponds to (111) plane of Co_3O_4 spinel phase. Similar observations were reported by Luo *et al,* [23].

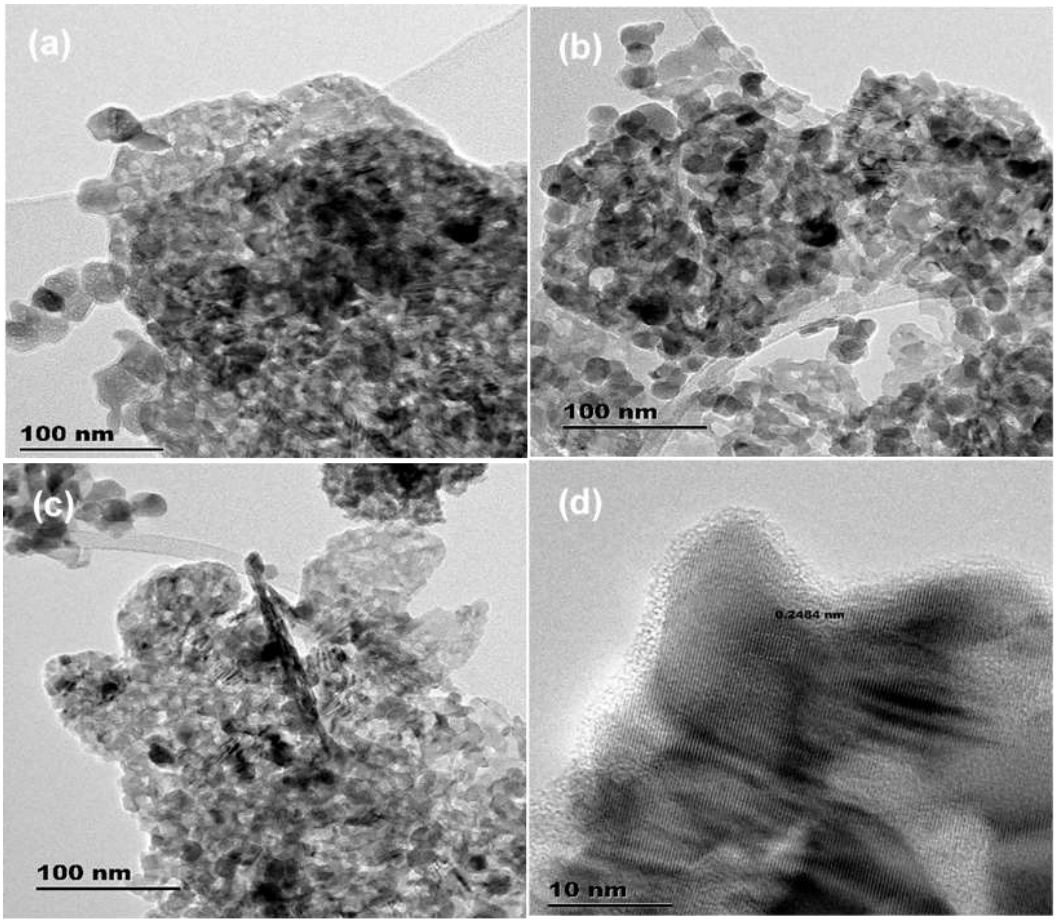

Figure 5.17 The TEM images of **(a)** (7wt.%MnO_2-Co_3O_4)(H), **(b)** (0.5wt.%Pd-7wt.%MnO_2/Co_3O_4)(H), **(c)** (1wt.%Pd-7wt.%MnO_2/Co_3O_4)(H), and **(d)** HRTEM (0.5wt.%Pd-7wt.%MnO_2/Co_3O_4)(H), catalysts.

5.5 CATALYTIC ACTIVITY FOR CO PROX REACTION

All catalysts were tested for CO PROX at the reaction temperature of 40 to 220 ^oC, the feed contained 1% CO, 1% O_2, 50% H_2, and 48% He. The 200 mg of the samples was loaded in a U-shape borosilicate glass reactor and conditioned at 40 ^oC in helium flow at 20 ml/min for 30 min, prior to catalytic tests. The stability of the catalysts was investigated under dry, 15% CO_2 and moisture conditions at 100 ^oC for 21 h.

5.5.1 Catalytic activity of various metal oxide supported on Co_3O_4 catalysts

The effect of a metal oxide on PROX of CO conversion in excess hydrogen was investigated over hydrazine treated 2wt.%M-Co_3O_4 (M = MnO_2, CeO_2, Cr_3O_4, MgO,

and TiO_2) catalysts, prepared by co-precipitation method (Figure 5.18). The 2wt.%MgO-Co_3O_4 catalyst (Figure 5.18A(d)) showed a lower CO conversion of 28.8% at 100 °C, and the highest conversion of 97% was observed at 220 °C.

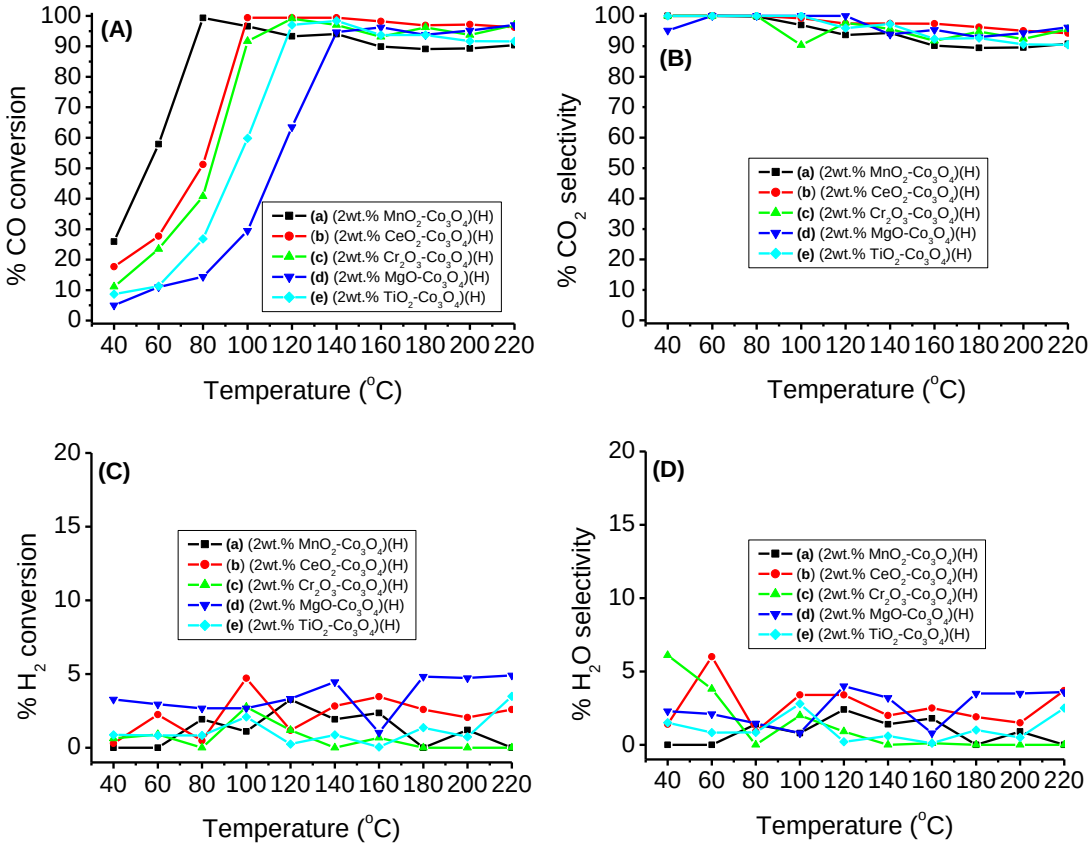

Figure 5.18 The CO conversion **(A)**, CO_2 selectivity **(B)**, H_2 conversion **(C)**, and H_2O selectivity **(D)** of **(a)** (2wt.%MnO_2-Co_3O_4) (H) (■), **(b)** (2wt.%CeO_2-Co_3O_4) (H) (●), **(c)** (2wt.%Cr_2O_4-Co_3O_4) (H) (▲), **(d)** (2wt.%MgO-Co_3O_4) (H) (▼), and **(e)** (2wt.%TiO_2-Co_3O_4) (H) (♦), catalysts.

However, the addition of 2wt.%TiO_2 on Co_3O_4 catalyst (Figure 5.18A(e)) improved the activity to 59.2% at 100 °C, and the highest conversion of 98.4% was observed at 140 °C. A further improvement was observed over 2wt.%Cr_2O_3-Co_3O_4 catalyst (Figure 5.18A(c)) which showed a 91.7% CO conversion at 100 °C, and the highest conversion of 99.1% at 120 °C. Interestingly, the 2wt.%CeO_2-Co_3O_4 catalyst (Figure 5.18A(b)) showed the highest activity of 99.4% at 100 °C, and a stable activity was maintained

with temperature. It has been reported in the literature that supported CeO_2 on Co_3O_4 catalysts improved the catalytic activity of Co_3O_4 catalysts in CO PROX [7, 36]. Lukashuk *et al.* [7], reported a decrease in CO conversion maximum temperature in CO PROX from 90% at 170 ^oC (over Co_3O_4) to 90% at 142 ^oC over CeO_2-Co_3O_4.

Although, the 2wt.%MnO_2-Co_3O_4 catalyst (Figure 5.18A(a)) showed 57.9% CO conversion at 60 ^oC, and the highest conversion of 99.3% at 80 ^oC. The catalyst activity decreased with temperature after 80 ^oC. The catalyst had a 100% selectivity of CO to CO_2 at the reaction temperature of 40 to 80 ^oC (Figure 5.18B(a)), and the selectivity decreased steadily with temperature. The higher activity of MnO_2 composite could be due to the higher surface area of 246.8 m^2/g of the catalyst and structural defects as confirmed by SEM and TEM, in relation to 2wt.%CeO_2-Co_3O_4 catalyst with the surface area of 81.8 m^2/g. Liu *et al.* [2], reported a higher surface area, smaller crystallite size and higher oxygen dispersion with structural defect Co_3O_4 catalyst when Mn is used as a promoter. Fiorenza *et al.* [35], have shown that reducible oxides such as CeO_2 and MnO_x weaken the CO adsorption on the metal active sites and provide additional sites for adsorption or activation of O_2. All catalysts showed a lower H_2 conversion and selectivity to moisture, with temperature. The catalytic activity of the prepared catalysts increased in the following order: 2wt.%MgO-Co_3O_4 < 2wt.%TiO_2-Co_3O_4 < 2wt.%Cr_2O_4-Co_3O_4 < 2wt.%CeO_2-Co_3O_4 < 2wt.%MnO_2-Co_3O_4. Therefore, studies were performed to investigate the effect of CeO_2 loading on Co_3O_4 catalysts (the catalysts were not treated by hydrazine). Furthermore, the PROX reactions over MnO_2-Co_3O_4 with different MnO_2 loading were investigated.

5.5.2 The effect of ceria loading on activity of Co_3O_4

A series of CeO_2-Co_3O_4 mixed oxides catalysts with different Ce/Co ratios were prepared by co-precipitation method and calcined at 300 ^oC in air. All catalysts were tested for PROX of CO in excess hydrogen at the temperature range of 40 to 220 ^oC. Figure 5.19 shows the CO conversion (see Appendix I, for other results) and the selectivity of CO to CO_2 during PROX of CO at different temperature over the as-prepared catalysts. These catalysts were not treated by hydrazine. The CeO_2 catalyst had the lowest activity in CO PROX reaction, the highest CO conversion of 19.4% was obtained at 220 ^oC (Figure 5.19A(b)). The CeO_2 nanoparticles alone can thus not

account for the enhanced activity [3]. The Co_3O_4 catalyst has shown better activity in CO conversion when compared with the CeO_2 species, the activity of 96.7% in CO conversion was obtained at 160 ^oC (Figure 5.19A(a)).

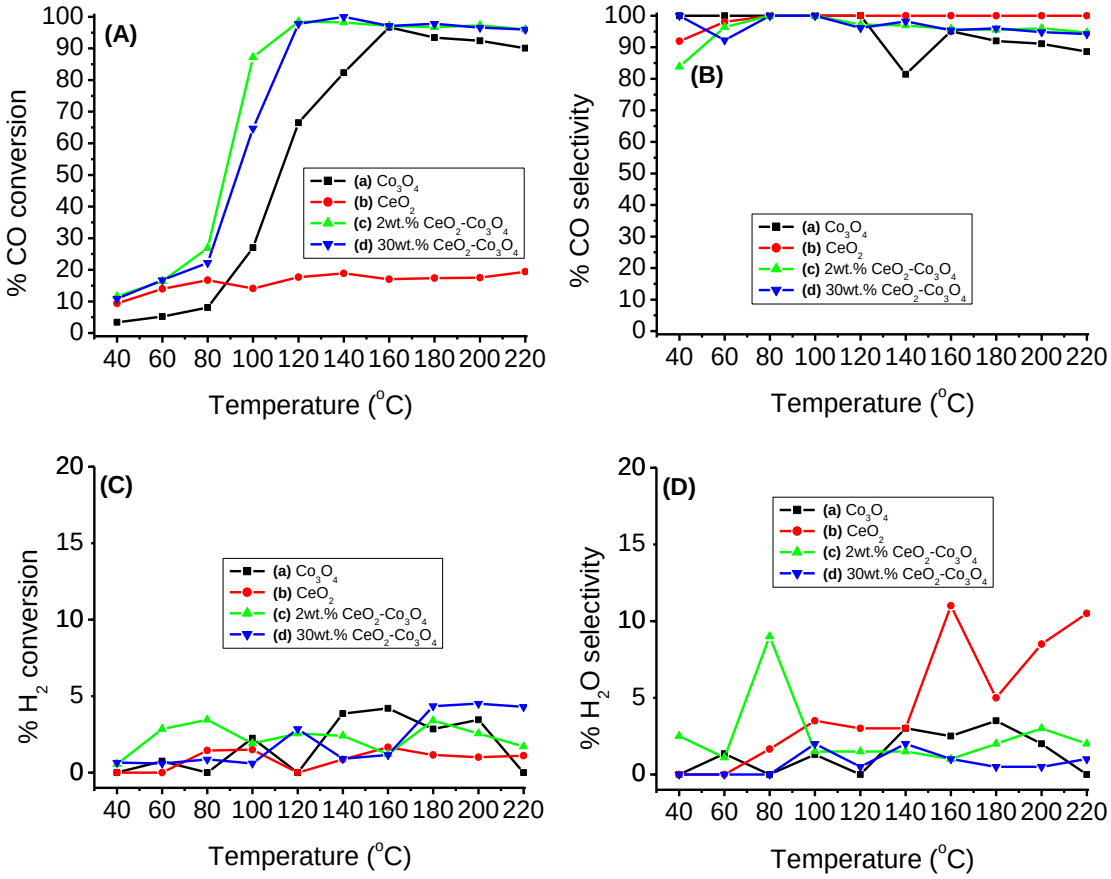

Figure 5.19 The CO conversion **(A)**, CO_2 selectivity **(B)**, H_2 conversion **(C)**, and H_2O selectivity **(D)** of **(a)** Co_3O_4 (■), **(b)** CeO_2 (●), **(c)** 2wt.%CeO_2-Co_3O_4 (▲), **(d)** 30wt.%CeO_2-Co_3O_4 (▼), catalysts.

The Co_3O_4 is known to be good in CO conversion in excess H_2 species, though, its activity decreases with time on stream [37]. However, introduction of CeO_2 species on the Co_3O_4 catalyst improved its catalytic activity in CO PROX reaction [3]. It has been reported that a strong synergy between ceria and cobalt oxides retained cobalt at the higher valence state [13, 38]. The CeO_2-Co_3O_4 catalyst with 30wt.% CeO_2 load showed CO conversion of 64.7% at 100 ^oC and the highest conversion of 100% at 140 ^oC (Figure 5.19(d)). However, the CeO_2-Co_3O_4 catalyst with 2wt.% of CeO_2 load had

the CO conversion of 87% at 100 ^{o}C, and the highest conversion of 98.2% at 120 ^{o}C (Figure 5.19A(c)).

Interestingly, the results showed that the CeO_2-Co_3O_4 catalyst with CeO_2 load of 8wt.% (See Appendix I(f)) and J) has the highest activity in CO conversion at fuel cells temperature range of 80 to 120 ^{o}C. The catalyst higher activity could be due to the higher surface area of 65.3 m^2/g, in relation to 2wt.% CeO_2 composite with the surface area of 63.5 m^2/g. However, the 8wt.%CeO_2-Co_3O_4 catalyst activity decreases with temperature in CO conversion. The catalyst with 2wt.% CeO_2 load exhibited second best results in CO conversion (Figure 5.19(c)), and has shown better stability and selectivity of CO to CO_2 with temperature. All catalysts have higher selectivity of CO to CO_2, as a result, they have lower H_2 conversion to moisture (Figure 5.19D). The catalyst with a 2wt.% CeO_2 load is considered for further tests with other catalytic parameters.

Research has shown that the addition of CeO_2 to Co_3O_4 creates Co-O-Co-O-Ce interfacial active sites that exhibit easier oxygen activation and/or oxygen vacancy formation [7]. Moreover, Lu *et al.* [9], reported that strong interaction between CeO_2 and Co_3O_4 result to a unique redox property, which enhanced the available surface active oxygen and led to high valence state of cobalt oxide species. That may contribute to the catalytic performance improvement [3]. The results infer that addition of CeO_2 to the Co_3O_4 catalyst improves both catalytic and selectivity at a lower temperature, the catalytic performance being higher than that exhibited by Co_3O_4 or CeO_2 catalysts. It is reported that the Co_3O_4-CeO_2 catalyst possess rather good catalytic oxidation performance for CO removal in H_2 rich stream [39-40], and Co^{3+} ions were identified as the main active sites for CO oxidation. It has been reported that the optimal Co and Ce ratio is essential to obtaining a good catalyst, and excess cobalt load can lead to the decrease in catalytic activity due to poor dispersion of active species [41].

5.5.3 The effects of hydrazine pre-treatment on activity of CeO_2-Co_3O_4 catalysts

The comparative study on the effect of hydrazine on 2wt.%CeO_2-Co_3O_4 catalysts are shown in Figure 5.20. The catalyst was pre-treated by 0.1 M hydrazine solution and calcined at 300 ^{o}C, and their catalytic activity was investigated at temperature range

of 40 to 220 °C. The reductive pre-treatment improved the surface area of the CeO_2-Co_3O_4 catalyst from 63.5 to 81.8 m^2/g, as confirmed by BET data. As a result, the activity of 2wt.%CeO_2-Co_3O_4 catalyst in CO conversion has improved from 98.5% at 120 °C (over untreated 2wt.%CeO_2-Co_3O_4, Figure 5.20(a)) to 99.4% at 100 °C over (2wt.%CeO_2-Co_3O_4)(H) catalyst (Figure 5.20A(b)). However, a slight steady decrease in CO conversion was observed with reactor temperature after 140 °C. A 100% catalytic selectivity of CO to CO_2 was observed from 40 to 100 °C, which followed by a slight decrease with temperature (Figure 5.20B(b)). The (2wt.%CeO_2-Co_3O_4)(H) catalyst (Figure 5.20D(b)) has a lower hydrogen conversion, and the selectivity to moisture. Tang *et al.* [42], reported that optimized pre-treatment under low temperature is suitable for CeO_2/Co_3O_4 catalysts for CO conversion process. The 2wt.%CeO_2-Co_3O_4 hydrazine treated catalyst outperformed the PROX activity of the CeO_2-Co_2O_4 catalysts reported by other researchers [7, 36].

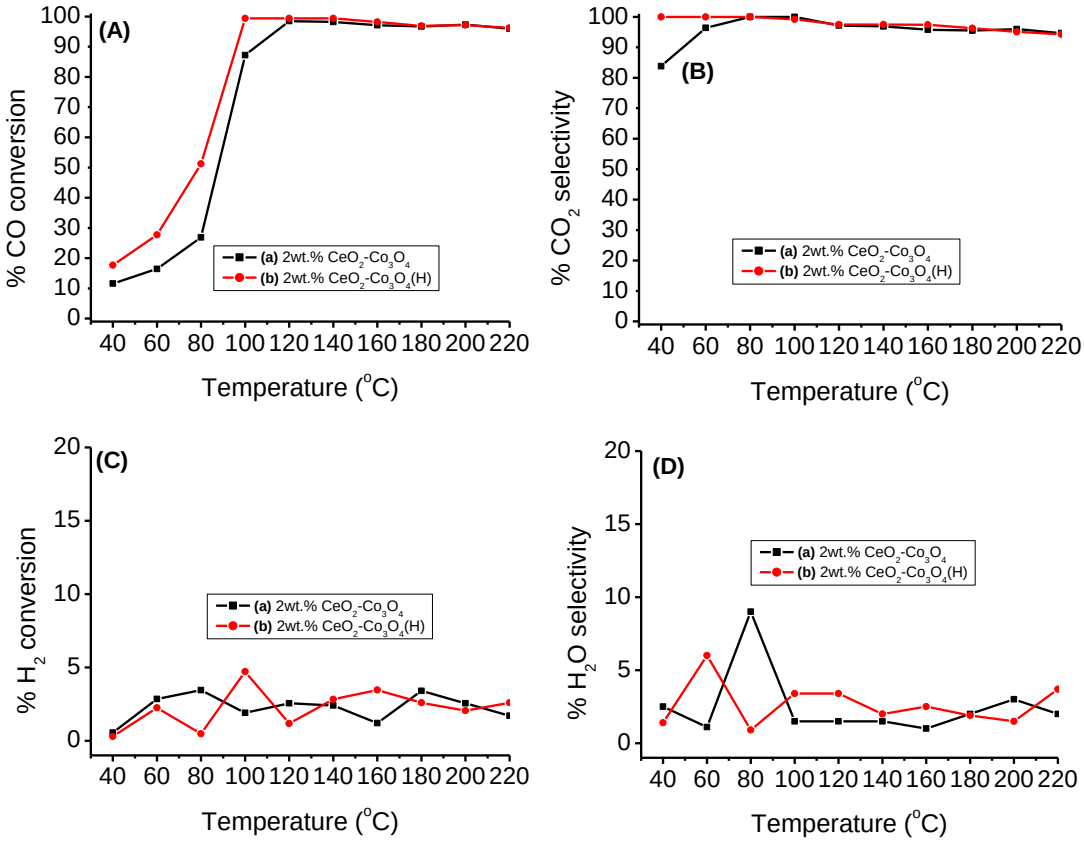

Figure 5.20 The CO conversion **(A)**, CO_2 selectivity **(B)**, H_2 conversion **(C)**, and H_2O selectivity **(D)** of **(a)** 2wt.% CeO_2-Co_3O_4 (■), and **(b)** (2wt.% CeO_2-Co_3O_4)(H) (●), catalysts.

5.5.4 The CO PROX over Pd/(2wt.%CeO_2-Co_3O_4) catalysts prepared with different methods

The 1wt.% Pd based metal was introduced on a hydrazine treated mixture of CeO_2 and Co_3O_4 (i.e., (2wt.%CeO_2-Co_3O_4)(H)), by improved wet impregnation, precipitation and deposition method, respectively. Another 1wt.%Pd based metal was introduced on a 2wt.%CeO_2-Co_3O_4 by co-precipitation method and later reduced by hydrazine solution. Figure 5.21 present the results for PROX of CO in excess hydrogen over the prepared catalysts.

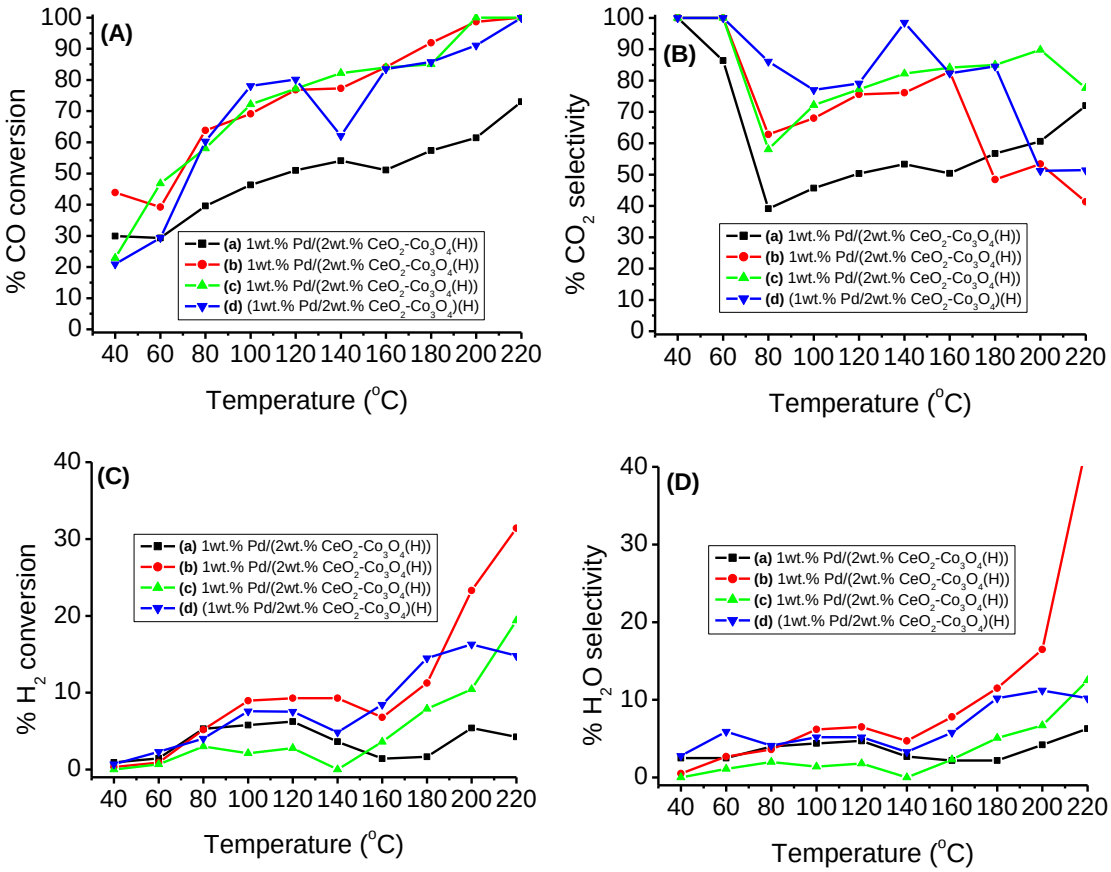

Figure 5.21 The CO conversion **(A)**, CO_2 selectivity **(B)**, H_2 conversion **(C)**, and H_2O selectivity **(D)** of **(a)** 1wt.%Pd/(2wt.%CeO_2-Co_3O_4(H)) impregnation (■), **(b)** 1wt.%Pd/(2wt.%CeO_2-Co_3O_4(H)) deposition (●), **(c)** 1wt.%Pd/(2wt.%CeO_2-Co_3O_4(H)) precipitation (▲), and **(d)** (1wt.%Pd/2wt.%CeO_2-Co_3O_4)(H) co-precipitation (▼), catalysts.

The 1wt.%Pd/(2wt.%CeO_2-Co_3O_4(H)) catalyst (Figure 5.21A(a)) prepared by improved wet impregnation (with surface area of 75.8 m^2/g) showed CO conversion of 46.3% at 100 ^oC, the highest CO conversion of 73.0% was obtained at 220 ^oC (Figure 5.19A(a)). The 1wt.%Pd/(2wt.%CeO_2-Co_3O_4(H)) catalyst (Figure 5.21A(b)) which was prepared by deposition method (with surface area of 80.8 m^2/g) showed an improvement in CO conversion of 69.1% at 100 ^oC, and the highest conversion of 100% was observed at 220 ^oC. The higher conversion at 220 ^oC was due to formation of CH_4 gas (see equations 3 and 4 in chapter one). Varghese *et al.* [43], have also reported a decrease in CO selectivity over Cu-containing catalyst at temperature of 160 ^oC and above in PROX due to formation of CH_4 gas.

The introduction of 1wt.%Pd species on 2wt.%CeO_2-Co_3O_4(H) composite (Figure 5.21A(c)) by precipitation method improved the activity at 100 ^oC to 72.2%, and the highest conversion of 100% was attained at 200 ^oC. The higher conversion was due to H_2 dissociation and formation of CH_4 gas (Figure 5.21C(c)) [42, 44]. The higher activity could be due to the improved surface area (i.e., 81.1 m^2/g) of the catalysts. Interestingly, based on the better activity of the sample prepared by precipitation of Pd on 2wt.%CeO_2-Co_3O_4(H) (similar better activity was also observed when the Pd species is precipitated on 2wt.%CeO_2-Co_3O_4 prior to hydrazine treatment and calcination (see Appendix K)), we have decided to prepare the catalysts by co-precipitation, prior to hydrazine treatment and calcination (Figure 5.21(d)).

The preparation of the catalyst by co-precipitation method has improved the surface area from 81.1 m^2/g (catalyst prepared by precipitation method) to 83.2 m^2/g for the catalyst which was prepared by co-precipitation. As a result, the catalyst (Figure 5.21A(d)) showed CO conversion of 78.1% at 100 ^oC, with the highest activity of 99.9% at 220 ^oC. However, higher reactor temperature resulted in a decrease in CO selectivity of 51% at 220 ^oC, due to hydrogen dissociation and the formation of CH_4 gas [42, 44].

The catalytic activity with respect to preparation method increased in the following order; advance wet impregnation < deposition < precipitation < co-precipitation method. The preparation method has an effect on the surface area and the activity of the catalysts [20]. The catalyst which was prepared by co-precipitation methods showed higher surface area of 83.2 m^2/g, the crystallite size of 20.7 nm and the highest

pore volume, therefore, its activity is the highest in CO PROX reaction. As a result, the co-precipitation method was considered for further investigation on the effect of Pd load over 2wt.%CeO_2-Co_3O_4 in PROX.

5.5.5 The effect of Pd loading on 2wt.%CeO_2-Co_3O_4 catalyst

The effect of Pd load over 2wt.%CeO_2-Co_3O_4 catalyst in PROX of CO in excess H_2 was investigated on catalysts prepared by co-precipitation method. Figure 5.22 present the results obtained over the prepared samples in PROX of CO.

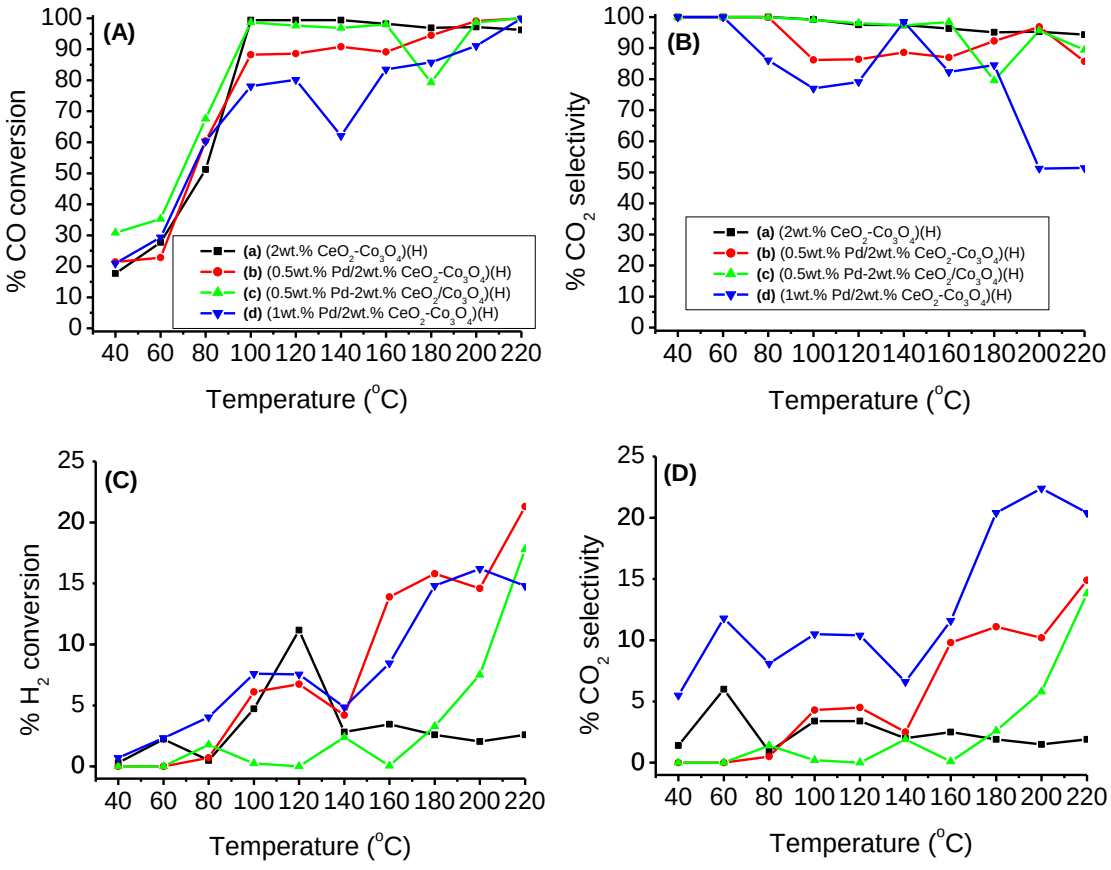

Figure 5.22 The CO conversion **(A)**, CO_2 selectivity **(B)**, H_2 conversion **(C)**, and H_2O selectivity **(D)** of **(a)** 2wt.%CeO_2/Co_3O_4 (■), **(b)** 0.5wt.%Pd/2wt.%CeO_2-Co_3O_4 (●), and **(c)** 0.5wt.%Pd-2wt.%CeO_2/Co_3O_4 (▲), **(d)** 1wt.%Pd/2wt.%CeO_2-Co_3O_4 (▼), catalysts.

The introduction of 1wt.% Pd load over the 2wt.%CeO_2-Co_3O_4 catalysts (Figure 5.22A(d)) showed 78.1% at 100 ^oC, and the highest activity of 99.9% at 220 ^oC. The catalyst is selective to CH_4 gas at higher temperature. Although, the surface area of the catalyst decreased with the Pd concentration from 83.6 (over 1wt.%Pd on composite) to 76.7 m^2/g over 0.5wt.%Pd on the composite. The 0.5wt.%Pd/2wt.%CeO2-Co2O4 catalyst showed CO conversion of 88.2% at 100 ^oC, and the highest activity of 100% was observed at 220 ^oC. However, the catalyst is also selective to CH4 gas at higher temperature.

Interestingly, the preparation of the catalyst by introducing 0.5wt.%Pd-2wt.%CeO_2 species on Co_3O_4 improved the catalytic activity of Co_3O_4 (Figure 5.22A(c)). Although, the surface area of the catalyst decreased to 70.9 m^2/g. The 0.5wt.%Pd-2wt.%CeO_2/Co_3O_4 catalyst has a bigger pore size and pore volume than the other catalysts. And the XPS data has shown an increase in the Co^{3+}/Co^{2+} atomic ratio. The 0.5%Pd-2wt.%CeO_2/Co_3O_4 catalyst showed CO conversion of 98.7% at 100 ^oC, and the highest activity of 100% was observed at 220 ^oC. The catalytic selectivity of CO to CO_2 decreased from 100% at 40-80 ^oC, to 99.1% at 100 ^oC, and 79.6% at 180 ^oC, followed by an increase to 95.8% at 200 ^oC (Figure 5.22B(c)). A further increase in temperature after 200 ^oC resulted in a decrease in the CO selectivity to 89.4% at 220 ^oC. An improvement on the catalytic activity of the nan alloys was reported in the literature [14, 17-18]. The presence of Pd on the catalyst increased the active sites for H_2O dissociation [14]. All catalysts have shown an increase in the selection to moisture with temperature.

The observed activities in this study indicates that introduction of Pd species on the support enhances both the reduction and oxidation performance of the catalysts, due to hydrogen spill over [35]. Zlotea *et al.* [17], reported an improved catalytic activity of Ir-Pd nanoalloys in PROX reaction, they have noted that the catalyst can prevent bulk hydrogen dissociation which can result in (*β* hydrides formation) formation of moisture.

5.5.6 The effects of moisture and/or CO_2 on the stability of 2wt.% CeO_2-Co_3O_4 and 0.5wt.%Pd-2wt.% CeO_2/Co_3O_4 catalysts

5.5.6.1 Stability of catalysts as function of temperature

The effect of moisture (by bubbling He gas through water vessel at 20 ml/min, at room temperature) over hydrazine treated 0.5wt.%Pd-2wt.%CeO_2/Co_3O_4 catalyst was investigated for CO PROX reaction in excess H_2 at a reactor temperature of 40 to 220 ^oC. Figure 5.23 present the results obtained for CO PROX under dry and moisture condition over 0.5wt.%Pd-2wt.%CeO_2/Co_3O_4 catalyst.

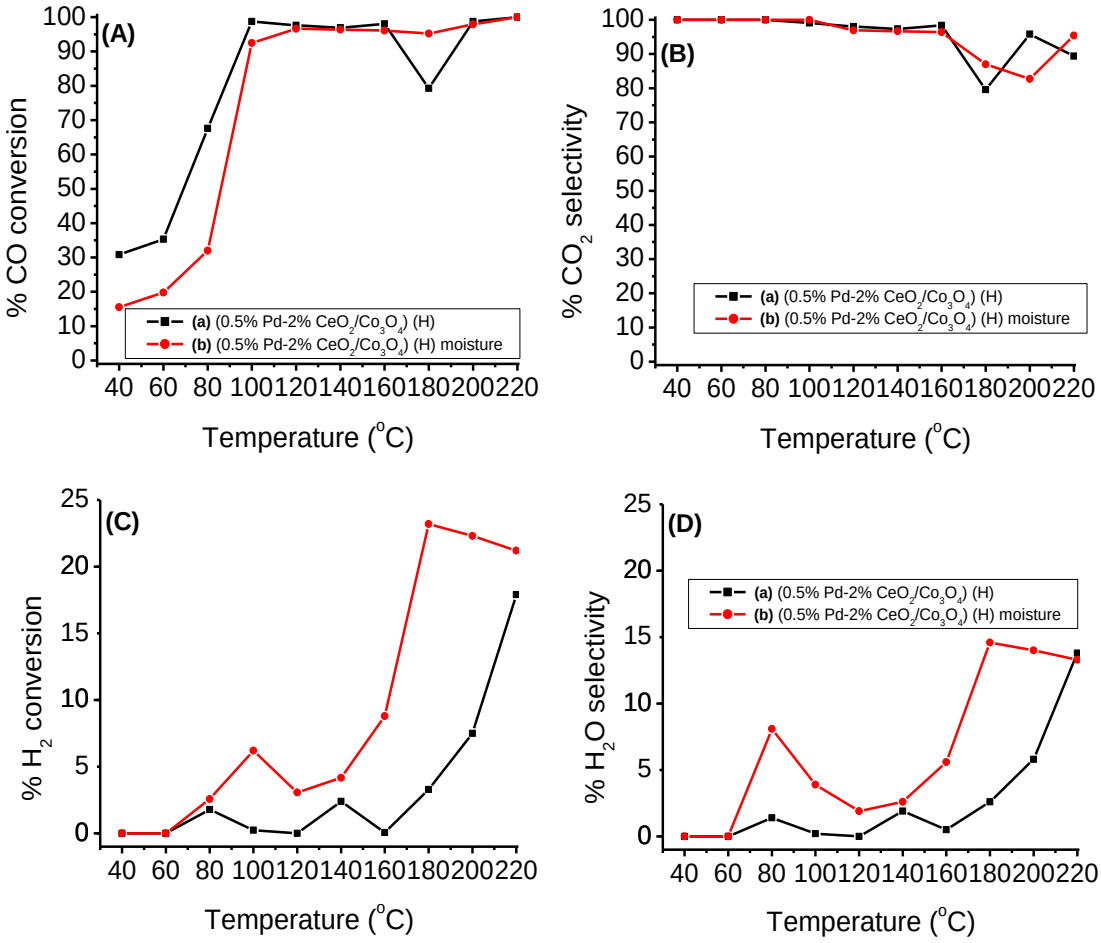

Figure 5.23 The CO conversion **(A)**, CO_2 selectivity **(B)**, H_2 conversion **(C)**, and H_2O selectivity **(D)** of 0.5wt.%Pd-2wt.%CeO_2/Co_3O_4 catalyst under **(a)** dry (■), and **(b)** moisture (●).

The catalyst showed CO conversion of 16% at 40 ^{o}C (Figure 5.23), which increases to 31% at 60 ^{o}C and 92% at 100 ^{o}C in the presence of moisture. A 100% selectivity of CO to CO_2 from 40 to 100 ^{o}C, with a slight decrease to 96.9% at 120 ^{o}C was observed (Figure 5.23B(b)). Other researchers reported a drastic decrease in CO selectivity after 100 ^{o}C in CO PROX reaction [44-45]. Formation of CH_4 gas was observed from the temperature of 180 ^{o}C and above, similar observation was reported in the literature during PROX [46]. The moisture suppressed the activity of the catalyst at a lower temperature (from 40 to 100 ^{o}C), however, an improvement was noted at a temperature higher than 120 ^{o}C, (Figure 5.23A(b)).

5.5.6.2 Stability of catalysts as function of time on stream

The stability of the catalysts was investigated over the hydrazine treated 2wt.%CeO_2-Co_3O_4 and 0.5wt.%Pd-2wt.%CeO_2/Co_3O_4 catalysts at 100 ^{o}C for 21 h. The effect of moisture, and CO_2 in CO PROX was also investigated over 0.5wt.%Pd-2wt.%CeO_2/Co_3O_4 catalyst at 100 ^{o}C for 21 h, respectively. The results for the stability tests, effect of moisture and CO_2 in the feed are presented in Figure 5.24. The 2wt.%CeO_2-Co_3O_4 catalyst (Figure 5.24A(a)) showed a good stable activity with fluctuation in CO conversion of about 99%. A stable catalytic selectivity of about 99% of CO to CO_2 was observed (Figure 5.24B(a)), and it fluctuates with time on stream. The introduction of 0.5wt.%Pd-2wt.%CeO_2 on Co_3O_4 suppressed the activity and selectivity of the catalyst (Figure 5.24A(b) and 5.24B(b)). The 0.5wt.%Pd-2wt.%CeO_2/Co_3O_4 catalyst has shown a drop (Figure 5.24A(b)) in CO conversion from 99% over 2wt.%CeO_2-Co_3O_4 to about 94%. However, the catalyst stability is still maintained with time on stream for over 21 h. The catalytic selectivity of CO to CO_2 is also stable and fluctuates with time on stream (Figure 5.24B(b)).

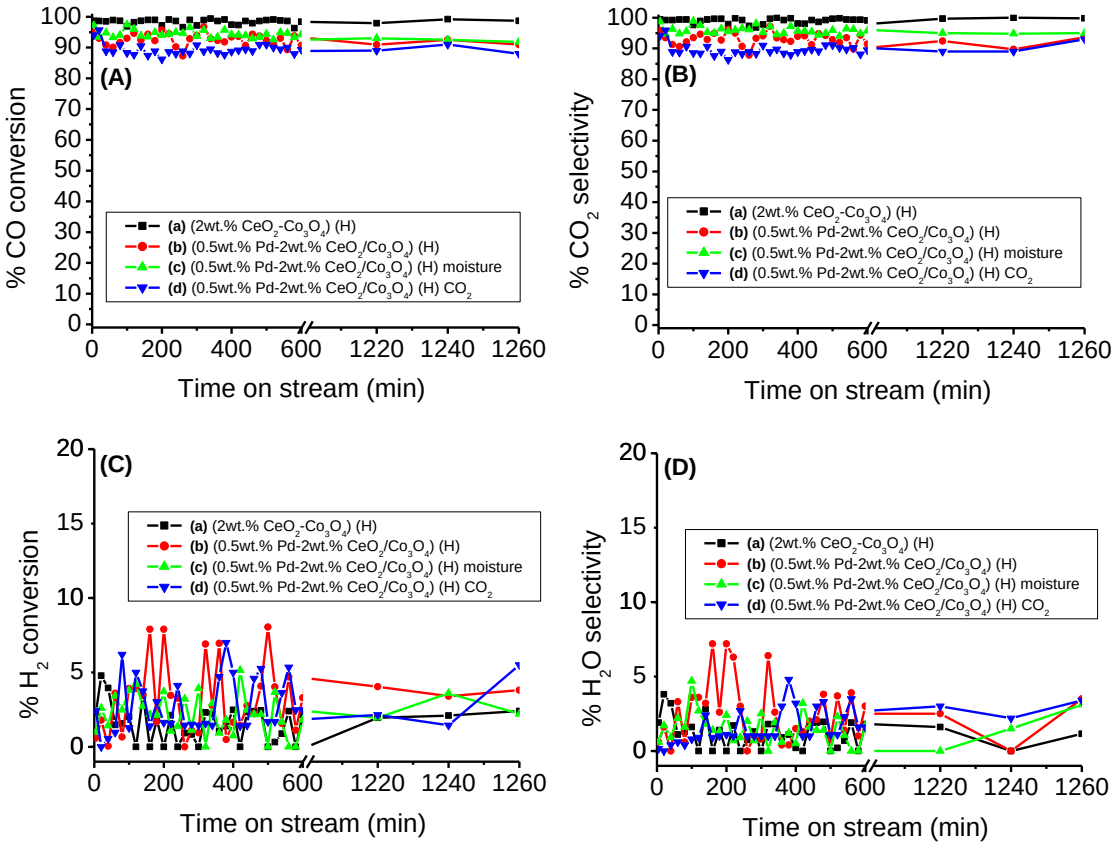

Figure 5.24 The CO conversion **(A)**, CO_2 selectivity **(B)**, H_2 conversion **(C)**, and H_2O selectivity **(D)** of **(a)** 2wt.%CeO_2-Co_3O_4 (■), **(b)** 0.5wt.%Pd-2wt.%CeO_2/Co_3O_4 (●), **(c)** 0.5wt.%Pd-2wt.%CeO_2/Co_3O_4 moisture (▲), **(d)** 0.5wt.%Pd-2wt.%CeO_2/Co_3O_4 CO_2 (▼), catalysts with time on stream.

Introduction of moisture in the feed stream somehow improved the catalytic activity of the catalyst (Figure 5.24A(c)). The conversion of CO fluctuates with time on stream and did not show any deactivation. Moisture also improved the selectivity of CO to CO_2 species (Figure 5.24B(c)), and the selectivity fluctuates with time on stream. Both the conversion and selectivity of H_2 to moisture fluctuated with time on stream and are slightly lower when compared with the CO PROX under dry condition on 0.5wt.%Pd-2wt.%CeO_2/Co_3O_4 catalyst (Figure 5.24(c)). Gawade *et al.* [4], reported lower H_2 selectivity and higher CO selectivity at lower temperature (< 125 ^oC) in the presence of H_2O over 10wt.%CoO/CeO_2 in PROX, due to lower O_2 selectivity.

The introduction of CO_2 on the feed suppressed the activity of the catalyst (Figure 5.24A(d)). A lower CO conversion of 88% (from 96%) was observed at 100 ^oC,

however, the catalyst stability is somehow conserved by the catalyst with time on stream (Figure 5.24A(d)). The catalyst has shown a stable fluctuation in catalytic selectivity of CO to CO_2 species (approximately 88%) with time on stream. The conversion of H_2 fluctuates with time on stream and is slightly higher compared to activities in the presence of moisture (Figure 5.24C(c) and (d)). The catalytic selectivity of H_2 to moisture is lower and fluctuates with time on stream, with the highest selectivity of 3.5%. However, the introduction of 15% CO_2 in the feed stream slightly suppressed the activity and the selectivity of the catalyst. Gawade *et al.* [4], reported that CoO_x/CeO_2 catalyst demonstrated better moisture or CO_2 tolerance at higher cobalt loading.

5.5.7 Effects of different MnO_2 loading on PROX of CO over Co_3O_4

The catalysts were prepared by co-precipitation methods and the amount of MnO_2 species were varied as follows: 2, 5, 7 and 10wt.% MnO_2 on the MnO_2-Co_3O_4 catalysts. Figure 5.25 present the results obtained in CO PROX in excess H_2 over the as-prepared catalysts. The MnO_2-Co_3O_4 catalyst with 10wt.% MnO_2 load (Figure 2.25A(d)) showed CO conversion of 27.9% at 40 ^oC, which increased to 49% at 60 ^oC. The catalyst had the highest CO conversion of 100% at 100 ^oC, which followed by a decrease with temperature to 77.9% at 200 ^oC. We have noted a 100% selectivity of CO to CO_2 (Figure 5.25B(d)) at the temperature ranging from 40 to 80 ^oC, which was followed by a steady decrease to 77.9% at 200 ^oC. The catalyst had the highest conversion and selectivity of H_2 to moisture (of 7.0% and 6.2% at 140 ^oC) compared to other catalysts. The catalyst with 10wt.% MnO_2 load had the lowest catalytic activity in PROX reaction, due to blockage of the cobalt sites by higher Mn load [2, 45]. Liu *et al.* [2], reported a decrease in the activity of the MnCo with 20wt.% Mn load in CO conversion. However, the MnO_2-Co_3O_4 catalyst with 5wt.% MnO_2 loading (Figure 5.25A(b)) showed 22.1% CO conversion at 40 ^oC, which drastically increased to 95.8% at 80 ^oC, and the highest CO conversion of 100% was obtained at 100 ^oC. Similarly, the catalyst with a 2wt.% load showed 25.9% CO conversion at 40 ^oC (Figure 5.25(a)), which drastically increased to a maximum CO conversion of 99.3% at 80 ^oC. This was followed by steady decrease with temperature after 80 ^oC to 82.5% at 220 ^oC. The catalyst had a 100% selectivity to CO_2 from 40 to 80 ^oC, which decreased with temperature to 89.5% at 180 ^oC (Figure 5.25B(a)).

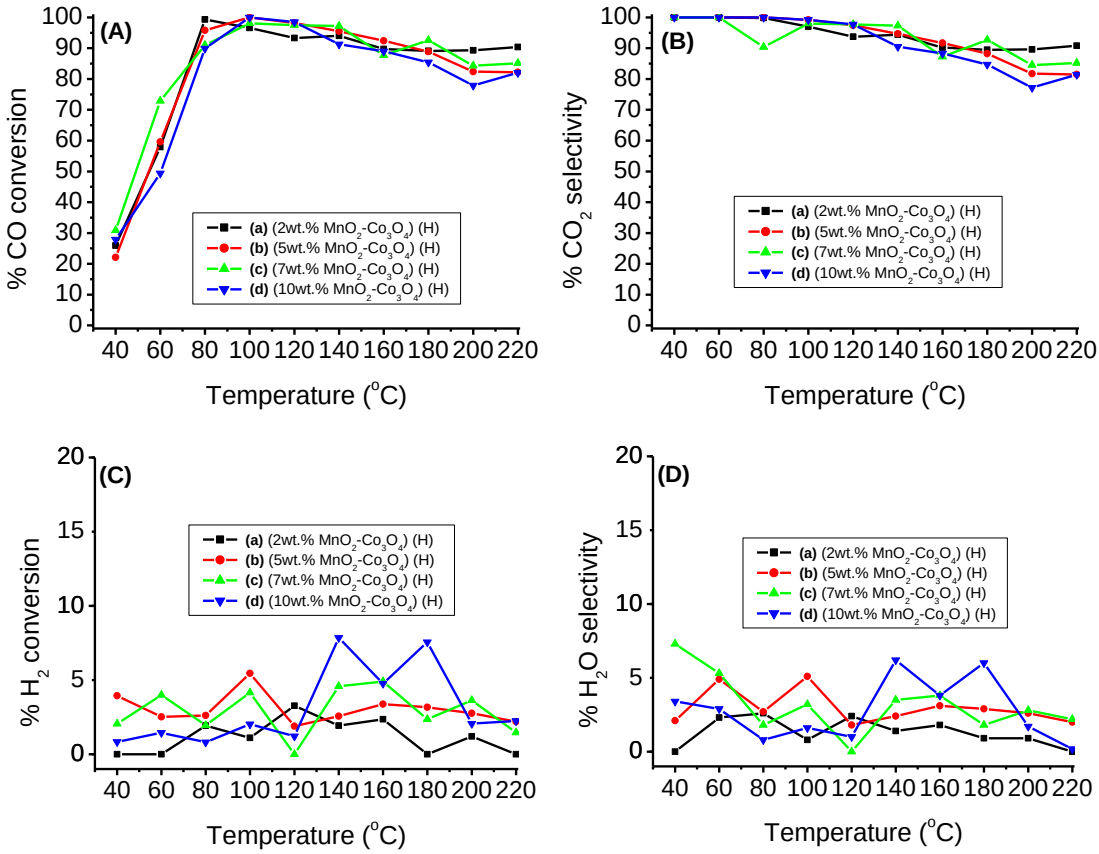

Figure 5.25 The CO conversion **(A)**, CO_2 selectivity **(B)**, H_2 conversion **(C)**, and H_2O selectivity **(D)** of **(a)** 2wt.% MnO_2-Co_3O_4 (■), **(b)** 5wt.% MnO_2-Co_3O_4 (●), **(c)** 7wt.%MnO_2-Co_3O_4 (▲), and **(d)** 10wt.%MnO_2-Co_3O_4 (▼), catalysts.

Interestingly, the MnO_2-Co_3O_4 catalyst with 7wt.% MnO_2 load (Figure 5.25A(c)) showed higher activity in CO conversion of 30.9% at 40 °C, which increased to 72.9% at 60 °C. The catalyst had the highest CO conversion of 98.1% at 100 °C, which followed by a steady decrease with the lowest CO conversion of 84.4% at 200 °C. A 100% catalytic selectivity of CO to CO_2 species (Figure 2.25B(c)) was observed at temperature ranging from 40 to 60 °C. A further increase in temperature resulted in a steady decrease in CO_2 selectivity, and the lowest selectivity of 84.5% was observed at 200 °C. A lower conversion and selectivity of H_2 to moisture which fluctuate with temperature was observed over all catalysts. Although, the surface area of the catalysts decreased with the MnOx concentration, the optimum loading of 7wt.% with surface area of 81.8 m^2/g gave better activity at lower temperature of 40 to 60 °C. However, catalyst activity at temperature above 60 °C is lower than that of 2wt.% MnO_2

load. The XPS data for 7wt.% load showed an increased binding energy which suggest an increase in the fraction of Co^{3+}/Co^{2+}. Other researchers have shown that an optimum amount of Mn is required to promote the mobility of surface oxygen vacancies of the catalyst [2, 45]. The hydrazine treated 7wt.%MnO_2-Co_3O_4 catalyst has outperformed the PROX activity of 10wt.%Mn/Co reported by Zhang *et al* [16]. Further investigation on the effect of Pd load was conducted over the catalyst with a 7wt.% MnO_2 load in CO PROX reaction.

5.5.8 The effect of Pd loading on 7wt.% MnO_2-Co_3O_4 catalyst

The effect of Pd loading on 7wt.% MnO_2-Co_3O_4 catalyst was investigated by varying the amount of Pd species and the catalysts, were prepared by co-precipitation method and reduced by 0.1 M hydrazine solution. Figure 5.26 present the results obtained in CO PROX in excess H_2 over the catalysts, respectively. The CO conversion over 2wt.%Pd-7wt.%MnO_2/Co_3O_4 catalyst has drastically decreased from 85.9% at 40 ^oC to 52.9% at 80 ^oC (Figure 5.26A(d)). A further increase in temperature resulted in a steady increase in CO conversion from 52.9% to 86.5% at 220 ^oC. The selectivity of CO to CO_2 over the catalyst decreased from 98.9% at 40 ^oC to 51.7% at 80 ^oC, followed by a steady increase to 75.5% at 220 ^oC (Figure 5.26B(d)). The higher catalytic activity at lower temperature could be related to the higher surface area as confirm by BET data (Table 5.2). The catalyst showed an increase in the H_2 selectivity with temperature, the highest selectivity of 17.2% was attained at 220 ^oC (Figure 5.26D(d)). The CO PROX over 1wt.%Pd-7wt.%MnO_2/Co_3O_4 catalyst improved at lower temperature, a CO conversion increased from 36.2% at 40 ^oC to 92.4% at 60 ^oC. A further increase in temperature resulted in a gradual decrease in CO conversion from 92.4% to 87.6% at 160 ^oC (Figure 5.26A(c)). The catalytic selectivity of CO to CO_2 decreased gradually with temperature from 100% at 40 ^oC to 66.2% at 220 ^oC (Figure 5.26B(c)). An increase in CO conversion after 160 ^oC was observed and was accompanied by the formation of moisture and CH_4 gas. The catalyst had the highest selectivity of H_2 to moisture (approximately 21.7%) at 200 ^oC (Figure 5.26C(c)).

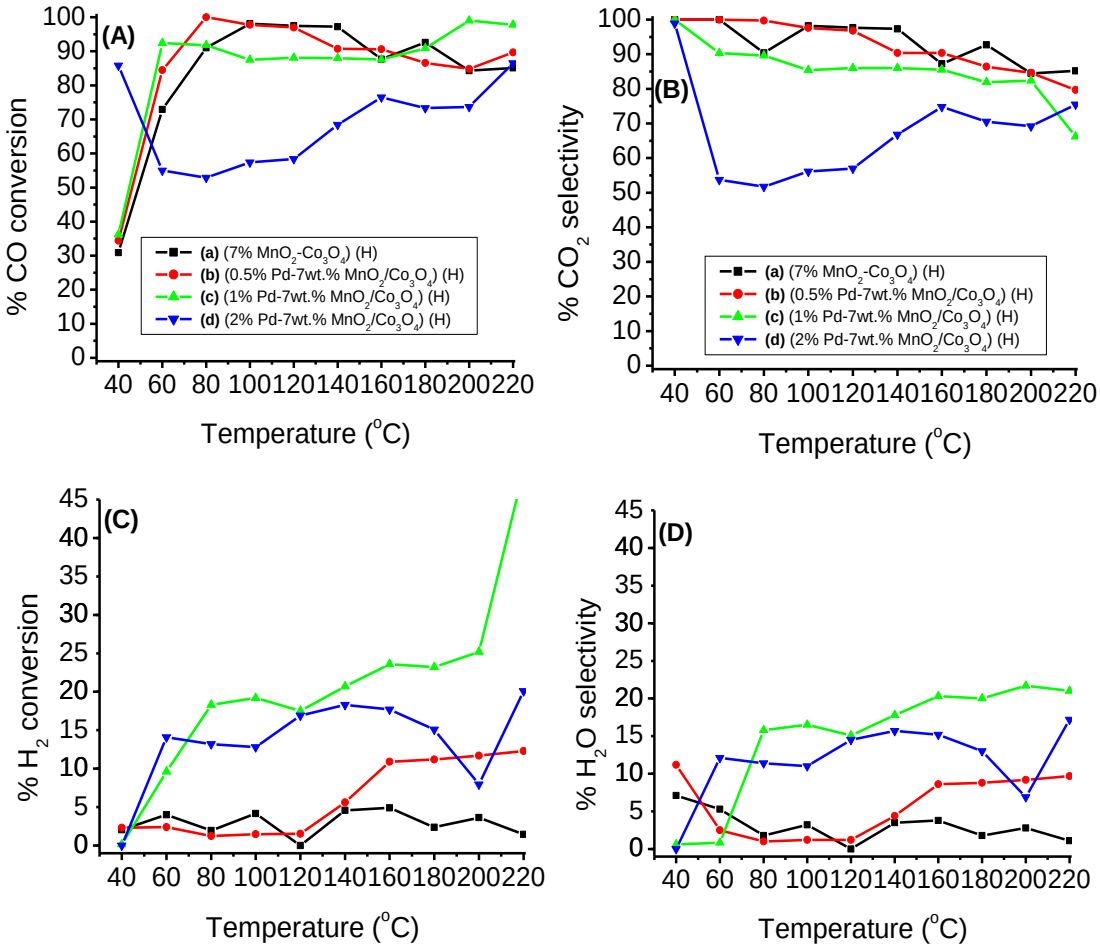

Figure 5.26 The CO conversion **(A)**, CO_2 selectivity **(B)**, H_2 conversion **(C)**, and H_2O selectivity **(D)** of **(a)** 7wt.%MnO_2-Co_3O_4 (■), **(b)** 0.5wt.%Pd-7wt.%MnO_2/Co_3O_4 (●), **(c)** 1wt.%Pd-7wt.%MnO_2/Co_3O_4 (▲), and **(d)** 2wt.%Pd-7wt.%MnO_2/Co_3O_4 (▼) catalysts.

The data indicates that 0.5wt.%Pd-7wt.%MnO_2/Co_3O_4 catalyst had the CO conversion of 39.2% at 40 °C, and 100% conversion at 80 °C (Figure 5.26A(b). This shows that the presence of Pd improves the CO conversion, as compared to 7wt.% MnO_2-Co_3O_4 catalyst. However, introduction of Pd species did not change the structure of the catalyst as confirmed by SEM and TEM data (section 5.2.4.7 and 5.2.4.8). Further increase in temperature resulted in a decrease in the conversion of CO to 89% at 220 °C. The catalyst had 100% selectivity of CO to CO_2 at temperature ranging from 40 to 80 °C (Figure 5.26B(b)), which decreased steadily with temperature to 79.7% at 220 °C. The selectivity of H_2 to moisture increases steadily with temperature and the

highest selectivity is attained at 220 ^{o}C (Figure 5.26D(b)). This suggests that the addition of Pd promotes the formation of moisture, as compared to 7wt.% MnO_2-Co_3O_4 catalyst. The Pd species has high affinity towards H_2 which could result to formation of *β* hydrides and moisture [47-49].

An increase in Pd load suppresses the catalytic activity of the Pd-7wt.%MnO_2/Co_3O_4 catalyst at higher temperature. The Pd species encourages the conversion of H_2 to moisture and the formation of CH_4 gas at higher temperature over the catalysts. Luo *et al.* [5], have shown that Pd species can promote the reduction and oxidation of cobalt phase to a greater extent, due to hydrogen or oxygen spillover effects. As a result, higher Pd load promote CO PROX at lower temperature and suppresses the activity at higher temperature due to higher hydrogen splitting which increases with temperature [47]. The catalyst favour conversion of H_2 to moisture and the formation of methane gas at temperature above 160 ^{o}C.

5.5.9 Activation energy for CO PROX reaction over 7wt.%MnO_2-Co_3O_4 catalyst

The comparative study on the activation energy required for CO PROX in excess H_2 under dry, and moisture condition was investigated over 7wt.%MnO_2-Co_3O_4 catalyst at 40-80 ^{o}C, respectively. The activation energies for CO conversion was calculated from Arrhenius plots, as shown in Figure 5.27.

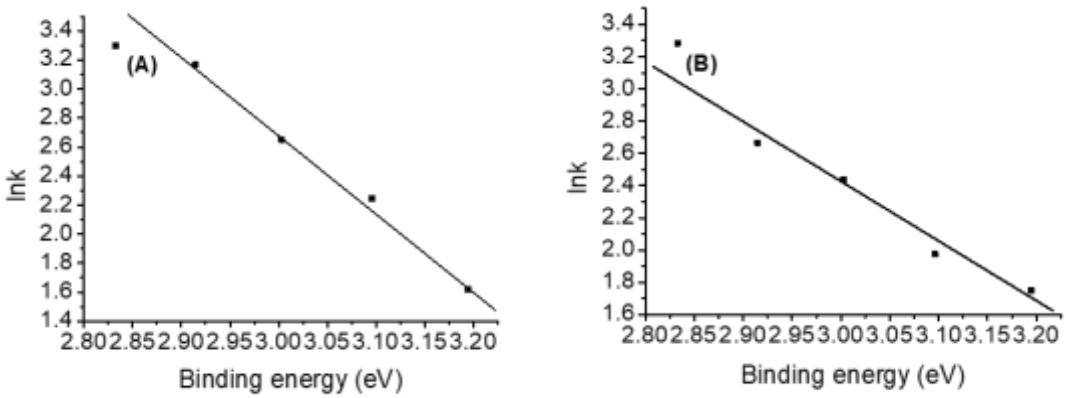

Figure 5.27 Arrhenius plots for the reaction rate of PROX (activation energy, E_a) over (7wt.%MnO_2-Co_3O_4)(H) catalyst under **(A)** dry, and **(B)** moisture condition.

An increase in the specific reaction rate from 6.158 x 10^{-3} $mol_{CO}/g_{Cat}/h$ (under dry condition) to 5.379 x 10^{-3} $mol_{CO}/g_{Cat}/h$ (under moist condition) at 40 ^{o}C was observed. The catalyst activation energies for CO PROX reactions under dry and moisture conditions were found to be 33.1 kJ/mol and 42.6 kJ/mol, respectively (Figure 5.27A and 5.27B). The activation energy increased due to the coverage of the active site by moisture molecule [23, 46]. Tang *et al.* [46], described the decrease in catalytic activity in benzene oxidation as a result of the occupied active sites by water vapour molecule which compete with benzene molecules or oxygen molecules and further reduce the number of active sites.

5.5.10 The effects of moisture and/or CO_2 on the stability of 7wt.% MnO_2-Co_3O_4 and 0.5wt.%Pd-7wt.% MnO_2/Co_3O_4 catalysts

5.5.10.1 Stability of catalysts as function of temperature

The effects of moisture (by bubbling He gas through water vessel at 20 ml/min, at room temperature) on the catalytic activity of 0.5wt.%Pd-7wt.%MnO_2/Co_3O_4 catalyst for PROX CO in excess of H_2, was investigated at different temperatures, as shown in Figure 5.28. The catalyst showed a decrease in CO conversion to 23.9% at 40 ^{o}C under moisture (Figure 5.28A(b)), which is lower than 39.2% conversion under dry condition. The decrease is clearly seen at 60 ^{o}C in which a 66.0% conversion was recorded under moisture condition (Figure 5.28A(b)). The activity of the catalyst remained almost unchanged (at temperatures above 80 ^{o}C), which indicates very good stability. The observation is similar/related to the report by Gamarra *et al* [50], on CuO/CeO_2 catalyst. Interestingly, the selectivity of CO to CO_2 was already 100% at temperature range from 40 and 60 ^{o}C and the selectivity decreased steadily with temperature from 100% to 82.3% at 180 ^{o}C. At lower temperature, the data suggests that the moisture blocks the surface active sites of the catalyst, and impede the binding of CO [3- 4, 16]. The presence of moisture in the feed stream during CO PROX in excess H_2 suppresses the activity of 0.5wt.%Pd-7wt.%MnO_2/Co_3O_4 catalyst at lower temperature (40-60 ^{o}C).

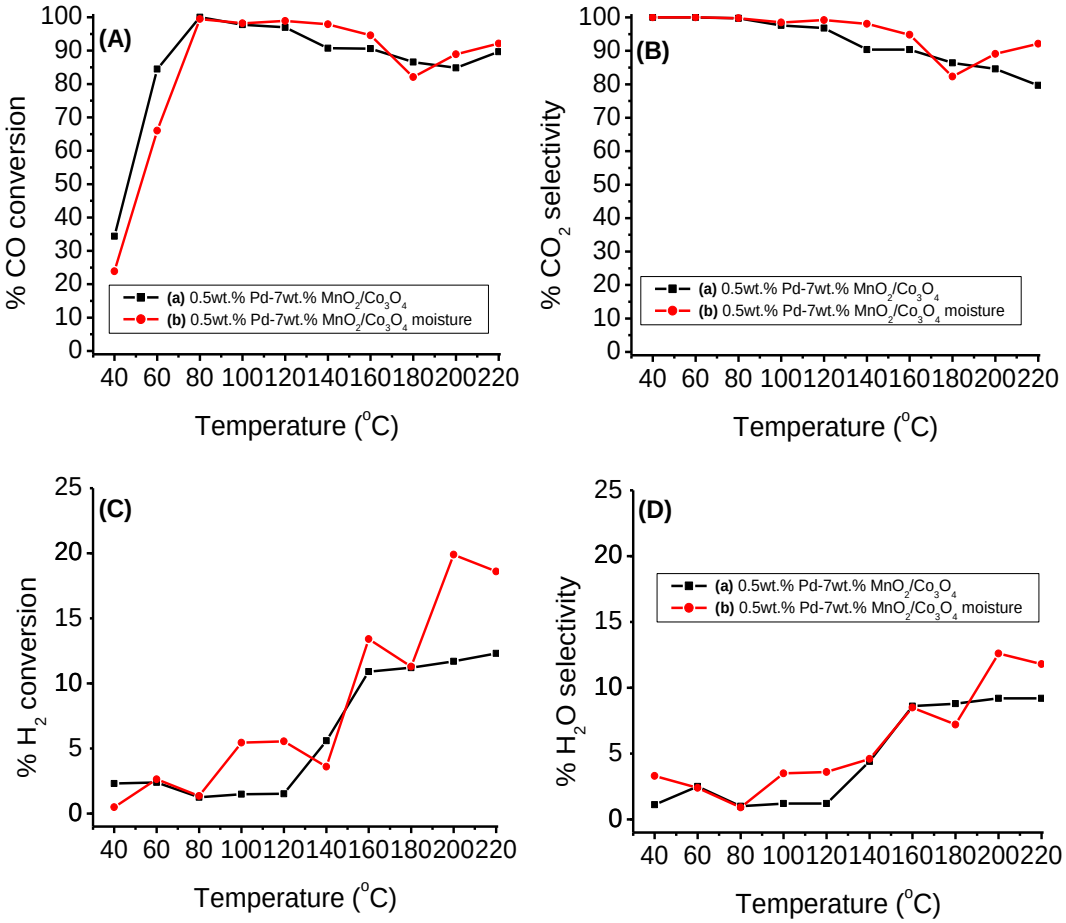

Figure 5.28 The CO conversion **(A)**, CO_2 selectivity **(B)**, H_2 conversion **(C)**, and H_2O selectivity **(D)** of 0.5wt.%Pd-7wt.%MnO_2/Co_3O_4 catalyst; **(a)** dry (■), and **(b)** moisture condition (●).

5.5.10.2 Stability of catalysts as function of time on stream

The stability of the catalysts was investigated over the hydrazine treated 7wt.%MnO_2-Co_3O_4 and 0.5wt.%Pd-7wt.% MnO_2/Co_3O_4 catalysts at 100 ºC for 21 h. The effect of moisture, and CO_2 in CO PROX was also investigated over 0.5wt.%Pd-7wt.% MnO_2/Co_3O_4 catalyst at 100 ºC for 21 h, respectively. The results for the stability tests, effect of moisture and CO_2 in the feed are presented in Figure 5.29.

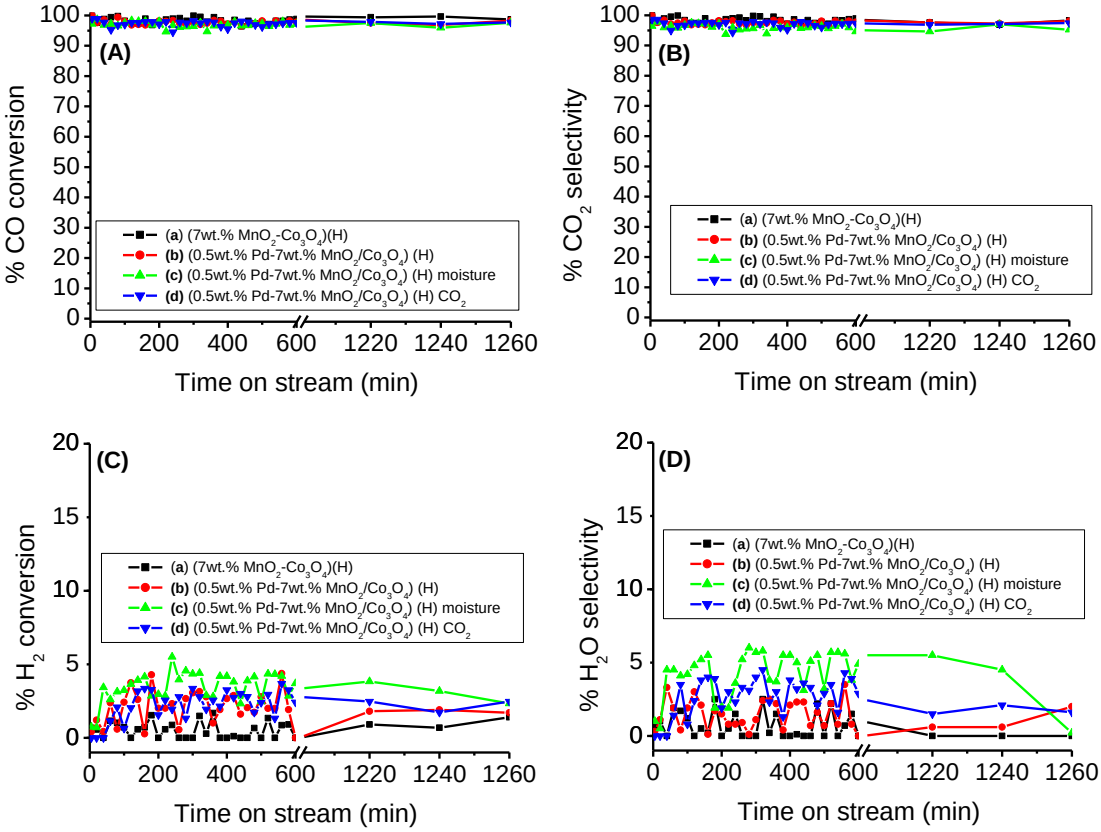

Figure 5.29 The CO conversion **(A)**, CO_2 selectivity **(B)**, H_2 conversion **(C)**, and H_2O selectivity **(D)** of **(a)** 7wt.%MnO_2-Co_3O_4 (■), **(b)** 0.5wt.%Pd-7wt.%MnO_2/Co_3O_4 (●), **(c)** 0.5wt.%Pd-7wt.%MnO_2/Co_3O_4 moisture (▲), **(d)** 0.5wt.%Pd-7wt.%MnO_2/Co_3O_4 CO_2 (▼), catalysts with time on stream.

The 7wt.%MnO_2-Co_3O_4 catalyst (Figure 5.29A(a)) showed a good stable activity of about 98.8% CO conversion for 21 h. A stable catalytic selectivity of about 98% of CO to CO_2 was observed (Figure 5.29B(a)), and it fluctuates with time on stream. The data are consistent with the report by Zhang *et al* [16], who noted a stable activity of MnO_x/Co_3O_4 catalyst at a temperature ranging from 100 to 125 ^oC. The 0.5wt.%Pd-7wt.%MnO_2/Co_3O_4 catalyst (Figure 5.29A(b)) gave approximately 98.0% CO conversion (with good CO_2 selectivity), which remained stable for 21 h. The catalyst has shown lower H_2 conversion and selectivity to moisture (Figure 5.29C(b)). Hydrazine treatment and the presence of 0.5wt.%Pd-7wt.% MnO_2 species improved the catalytic activity and stability of the catalyst. Fiorenza *et al.* [35], have shown that the supported bimetallic catalyst can improve the activity/selectivity of the catalyst in CO PROX reaction.

The 0.5wt.%Pd-7wt.%MnO_2/Co_3O_4 catalyst (Figure 5.29A(c)) in the presence of moisture in the feed showed a stable activity of about 98.0% in CO PROX for 21 h. The catalyst (Figure 5.29B(c)) had a good stability in the selectivity of CO to CO_2, though the selectivity was a bit lower when compared with that of moisture free atmosphere. The selectivity of H_2 to moisture was a bit higher compared to that of dry condition.

The catalytic activity of the 0.5wt.%Pd-7wt.%MnO_2/Co_3O_4 catalyst (Figure 5.29A(d)) in the presence of CO_2 showed a stable activity for 21 h. The CO conversion in the presence of CO_2 in the feed stream did not really show any effect in the suppression of the catalytic activity of the 0.5wt.%Pd-7wt.%MnO_2/Co_3O_4 catalyst. The catalytic stability in CO PROX is still maintained in the presence of CO_2 in the feed stream, CO conversion in the presence of CO_2 is better than that in the presence of moisture, with good selectivity of CO to CO_2 (Figure 5.29B(d)). The conversion of H_2 is lower when compared with the activity of the catalyst in the presence of moisture (Figure 5.29C(d)). The hydrazine treated 0.5wt.%Pd-7wt.%MnO_2/Co_3O_4 catalyst outperformed the PROX activity of the MnO_x/Co_3O-CeO_2 and MnO_x/Co_3O_4 catalysts reported in the literature [16, 36]. It has been reported that the presence of Mn^{2+} on the catalyst can promote the regeneration of Co^{3+} (i.e., $Co^{2+} \rightarrow Co^{3+}$) [51].

5.6 CONCLUSIONS

The 2wt.% of metal oxides (CeO_2, MnO_2, MgO, Cr_3O_4, and TiO_2) on cobalt, and Pd supported on CeO_2-Co_3O_4 and MnO_2-Co_3O_4 were successfully prepared by co-precipitation method. The morphology and structural compositions of the composites were confirmed by XRD, BET, TGA, XPS, TPR, FTIR, SEM, TEM data. The XRD data shows that introduction of the metal oxide on Co_3O_4 did not alter its structural phase, except for the composite with TiO_2 species. The TGA profile for all the samples showed thermal stability up to 600 ^oC. The XRD peaks intensity broadens with an increase in the amount of ceria load. The 2wt.%CeO_2-Co_3O_4 composite showed an improved surface area of 81.8 m^2/g compared to Co_3O_4(H). However, introduction of 0.5wt.%Pd-2wt.%CeO_2 species on Co_3O_4 resulted in a decreased surface area to 70.9 m^2/g. The presence of Pd species on the catalyst decreased the Co^{3+}/Co^{2+} atomic ratio XPS peak intensity. The HRTEM indicate the presence of lattice fringe spacing of 0.48 nm (311) and 0.28 nm (111), which confirm the characteristic lattice structure of Co_3O_4. An increase in the MnO_2 load on Co_3O_4 showed a decreased in XRD peaks intensity. A decrease in BET surface area of the composites from 249 (2wt.%MnO_2-Co_3O_4) to 81.8 m^2/g (7wt.% MnO_2-Co_3O_4) was observed. The presence of MnO_2 transformed the structure of Co_3O_4 as confirmed by SEM and TEM data. The presence of 0.5wt.%Pd on 7wt.%MnO_2-Co_3O_4 decreased the surface area to 63.1 m^2/g.

The catalysts were evaluated for PROX of CO in excess hydrogen at the temperature range of 40 to 220 ^oC. Although, 2wt.%MnO_2 on Co_3O_4(H) showed higher activity 99.3% at 80 ^oC, both MnO_2 and CeO_2 improved the activity of Co_3O_4(H) at 100 ^oC. The CO conversion over supported metal oxide on Co_3O_4(H) catalysts increased in the following order: MgO < TiO_2 < Cr_3O_4 < CeO_2 < MnO_2. The higher activity of MnO_2 is attributed to the higher surface area of the composite catalyst (i.e., 249 m^2/g, 2wt.%MnO_2-Co_3O_4(H)), in relation to ceria composite catalyst (i.e., 81.8 m^2/g). Although the MnO_2 species disrupted the structure of Co_3O_4 by lowering the oxidation state to Co^{2+}, the spent catalyst showed transformation from Co^{2+} to Co^{3+} during PROX, as confirmed by TPR data.

Further studies were undertaken on the effects of CeO_2 loading on Co_3O_4 composite catalysts. The data shows that an optimum activity is obtained while using 2wt.%CeO_2 on Co_3O_4 as compared to other ceria loadings (i.e., 3, 5, 8, 10, 15, 30wt.%CeO_2). However, upon addition of 0.5wt.%Pd-2wt.%CeO_2 species on Co_3O_4, the activity of

the catalyst decreased slightly at 100 ^{o}C, which could be associated with a decrease in the surface area. The 0.5wt.%Pd-2wt.%CeO_2 species on Co_3O_4 lowered H_2 conversion, and the creation of oxygen vacancies by ceria species resulted in redox reaction of Co^{2+} to Co^{3+} as confirmed by XPS. Although its activity is lower, the catalyst has shown good stability in dry, moisture and CO_2 conditions at 100 ^{o}C for 21 h.

In addition, studies were also undertaken on the effect of MnO_2 concentration on Co_3O_4 composite catalysts. The data shows that 7wt.%MnO_2 species improved the activity of Co_3O_4 catalyst at 60 ^{o}C, however, the catalyst could not improve the activities at higher temperatures. This low activity is associated with a decrease in surface area as concentration increases. The presence of 0.5wt.%Pd-7wt.%MnO_2 species on Co_3O_4 increased the activity at 60 and 80 ^{o}C, which could be due to reduction of Co^{3+} to Co^{2+} in the presence of Pd, as confirmed by XPS data. The catalyst has shown good stability in dry, moisture and CO_2 conditions at 100 ^{o}C for 21 h. The hydrazine treated cobalt-based catalysts in the presence of palladium and manganese oxide is the promising catalysts for proton exchange membrane fuel cells technology.

5.7 REFERENCES

[1] P.S. Barbato, S. Colussi, A. Di Benedettoc, G. Landi, L. Lisi, J. Llorca, A. Trovarelli. CO preferential oxidation under H_2-rich streams on copper oxide supported on Fe promoted CeO_2. *Applied Catalysis A: General* 506 (2015) 268-277.

[2] C. Liu, L. Gong, R. Dai, M. Lu, T. Sun, Q. Liu, X. Huang, Z. Huang. Mesoporous Mn promoted Co_3O_4 oxides as an efficient and stable catalyst for low temperature oxidation of CO. *Solid State Sciences* 71 (2017) 69-74.

[3] Y. Chen, D. Liu, L. Yang, M. Meng, J. Zhang, L. Zheng, S. Chu, T. Hu. Ternary composite oxide catalysts CuO/Co_3O_4-CeO_2 with wide temperature-window for the preferential oxidation of CO in H_2-rich stream. *Chemical Engineering Journal* 234 (2013) 88-98.

[4] P. Gawade, B. Bayram, A-M. C. Alexander, U. S. Ozkan. Preferential oxidation of CO (PROX) over CoO_x/CeO_2 in hydrogen-rich streams: Effect of cobalt loading. *Applied Catalysis B: Environmental* 128 (2012) 21-30.

[5] J-Y. Luo, M. Meng, X. Li, X-G. Li, Y-Q. Zha, T-D. Hu, Y-N. Xie, J. Zhang. Mesoporous Co_3O_4-CeO_2 and Pd/Co_3O_4-CeO_2 catalysts: Synthesis, characterization and mechanistic study of their catalytic properties for low-temperature CO oxidation. *Journal of Catalysis* 254 (2008) 310-324.

[6] Y. Shen, G. Lu, Y. Wang, Y. Guo, L. Wang, X. Zhen. An excellent support of Pd-Fe-Ox catalyst for low temperature CO oxidation: CeO_2 with rich (200) facets. *Catalysis Communications* 18 (2012) 26-31.

[7] L. Lukashuk, K. Föttinger, E. Kolar, C. Rameshan, D. Teschner, M. Hävecker, A. Knop-Gericke, N. Yigit, H. Li, E. McDermott, M. Stöger-Pollach, G. Rupprechter. Operando XAS and NAP-XPS studies of preferential CO oxidation on Co_3O_4 and CeO_2-Co_3O_4 catalysts. *Journal of Catalysis* 344 (2016) 1-15.

[8] J. Zhang, P. Tang, T. Liu, Y. Feng, C. Blackman, D. Li. Facile synthesis of mesoporous hierarchical Co_3O_4-TiO_2 P-n heterojunctions with greatly enhanced gas sensing performance. *Journal of Material Chemical* A 5 (2017) 10387-10397.

[9] S. Lu, F. Wang, C. Chen, F. Huang, K. Li. Catalytic oxidation of formaldehyde over CeO_2-Co_3O_4 catalysts. *Journal of Rare Earths* 35 (2017) 867-874.

[10] A. Luengnaruemitchai, S. Chawla, R. Wanchanthuek. The catalytic performance of Au/La-CeOx catalyst for PROX reaction in H_2 rich stream. *International Journal of Hydrogen Energy* 39 (2014) 16953-16963.

[11] Z. Qu, F. Yu, X. Zhang, Y. Wang, J. Gao. Support effects on the structure and catalytic activity of mesoporous Ag/CeO_2 catalysts for CO oxidation. *Chemical Engineering Journal* 229 (2013) 522-532.

[12] C. W. Tang, C. B. Wang, S. H. Chien. Characterization of cobalt oxides studied by FT-IR, Raman, TPR and TG-MS. *Thermochemical Acta* 473 (2008) 68-73.

[13] S. K. Mahammadunnisa, T. Akanksha, K. Krushnamurty, C. H. Subrahmanyam. Catalytic decomposition of N_2O over CeO_2 supported Co_3O_4 catalysts. *Journal of Chemical Science* 128 (2016) 1795-1804.

[14] J. Kugai, J. T. Miller, N. Guo, C. Song. Role of metal components in Pd-Cu bimetallic catalysts supported on CeO_2 for the oxygen-enhanced water gas shift. *Applied Catalysis B: Environmental* 105 (2011) 306-316.

[15] M. P. Woods, P. Gawade, B. Tan, U. S. Ozkan. Preferential oxidation of carbon monoxide on Co/CeO_2 nanoparticles. *Applied Catalysis: B Environmental* 97 (2010) 28-35.

[16] Q. Zhang, X. Liu, W. Fan, Y. Wang. Manganese-promoted cobalt oxide as efficient and stable non-noble metal catalyst for preferential oxidation of CO in H_2 stream. *Applied Catalysis B: Environmental* 102 (2011) 207-214.

[17] C. Zlotea, F. Morfin, T.S. Nguyen, N.T. Nguyen, J. Nelayah, C. Ricolleau, M. Latroche, L. Piccolo. Nanoalloying bulk-immiscible iridium and palladium inhibits hydride formation and promotes catalytic performances. *Nanoscale* 0 (2014) 1-5.

[18] Y. Ren, S. Zhang, H. Li. Electro-oxidation of methanol on SnO_2-promoted Pd/MWCNTs catalysts in alkaline solution. *International Journal of Hydrogen Energy* 39 (2014) 288-296.

[19] S. L. Sharifi, H. R. Shakur, A. Mirzaei, A. Salmani, M. H. Hosseini. Characterization of Cobalt oxide Co_3O_4 nanoparticles prepared by various methods: Effect of calcination temperatures on size, dimension and catalytic decomposition of hydrogen peroxide. *International Journal of Nanoscience Nanotechnology* 9 (2013) 51-58.

[20] S. O. Soloviev, P. I. Kyriienko, N. O. Popovych. Effect of CeO_2 and Al_2O_3 on the activity of Pd/Co_3O_4/cordierite catalyst in the three-way catalysis reactions (CO/NO/C_nH_m). *Journal of Environmental Sciences* 24 (2012) 1327-1333.

[21] K. Kaviyarasu, A. Raja, P. A. Devarajan. Structure elucidation and spectral characterizations of Co_3O_4 nanoflakes. *Spectrochimica Acta Part A: Molecular and Biomolecular Spectroscopy* 114 (2013) 586-591.

[22] Y. Wang, C. Zhang, Y. Yu, R. Yue, H. He. Ordered mesoporous and bulk Co_3O_4 supported Pd catalysts for catalytic oxidation of o-xylene. *Catalysis Today* 242 (2015) 294-299.

[23] Y. Luo, Y. Zheng, J. Zuo, X. Feng, X. Wang, T. Zhang, K. Zhang, L. Jiang. Insights into the high performance of Mn-Co oxides derived from metalorganic frameworks for total toluene oxidation. *Journal of Hazardous Materials* 349 (2018) 119-127.

[24] T. Chang, Z. Shen, Y. Huang, J. Lu, D. Rena, J. Sun, J. Cao, H. Liu. Post-plasma-catalytic removal of toluene using MnO_2–Co_3O_4 catalysts and their synergistic mechanism. *Chemical Engineering Journal* 348 (2018) 15-25.

[25] C-W. Tang, L-C. Hsu, S-W. Yu, C-B. Wang, S-H. Chien. In situ FT-IR and TPD-MS study of carbon monoxide oxidation over a CeO_2/Co_3O_4 catalyst. *Vibrational Spectroscopy* 65 (2013) 110-115.

[26] R. S. Jayashree, P. V. Kamath. Electrochemical synthesis of a-cobalt hydroxide. *Journal of Material Chemistry* 9 (1999) 961-963.

[27] H. Chen, M. Yang, S. Tao, G. Chen. Oxygen vacancy enhanced catalytic activity of reduced Co_3O_4 towards *p*-nitrophenol reduction. *Applied Catalysis B: Environmental* 209 (2017) 648-656.

[28] T. Chang, Z. Shen, Y. Huang, J. Lu, D. Ren, J. Sun, J. Cao, H. Liu. Post-plasma-catalytic removal of toluene using MnO_2–Co_3O_4 catalysts and their synergistic mechanism. *Chemical Engineering Journal* 348 (2018) 15-25.

[29] L. Jia, Y. Guo, T. P. Tran, M. Sakurai, H. Kameyama. Synergistic effect of copper and cobalt in Cu-Co bulk oxide catalyst for catalytic oxidation of volatile organic compounds. *Journal of Chemical engineering of Japan, Advanced publication,* April 19, 2012.

[30] Y. Chen, Y. Zhang, S. Fu. Synthesis and characterization of Co_3O_4 hollow spheres. *Materials Letters* 61 (2007) 701-705.

[31] T. Ozkaya, A. Baykal, M. S. Toprak, Y. Koseoglu, Z. Durmus. Reflux synthesis of Co_3O_4 nano particles and magnetic characterization. *Journal of Magnetism and Magnetic Materials* 321 (2009) 2145-2149.

[32] X. Zhanga, J. Yea, J. Yuanb, T. Caia, B. Xiao, Z. Liu, K. Zhao, L. Yangb, D. Hea. Excellent low-temperature catalytic performance of nanosheet Co-Mn oxides for total benzene oxidation. *Applied Catalysis A: General* 546 (2017) 103-110.

[33] Y. Zhang-Steenwinkel, J. Beckers, A. Bliek. Surface properties and catalytic performance in CO oxidation of cerium substituted lanthanum manganese oxides. *Applied Catalysis A: General* 235 (2002) 79-92.

[34] G. Ercolino, P. Stelmachowski, G. Grzybek, A. Kotarba, S. Specchia. Optimization of Pd catalysts supported on Co_3O_4 for low-temperature lead combustion of residual methane. *Applied Catalysis B: Environmental* 206 (2017) 712-725.

[35] R. Fiorenza, L. Spitaleri, A. Gulino, S. Scirè. Ru-Pd Bimetallic Catalysts Supported on CeO_2-MnO_X Oxides as Efficient Systems for H_2 Purification through CO Preferential Oxidation, *Catalysts* 8 (2018) 203-221.

[36] Q. Guo, Y. Liu. MnO_x modified Co_3O_4-CeO_2 catalysts for the preferential oxidation of CO in H_2-rich gases. *Applied Catalysis B: Environmental* 82 (2008) 19-26.

[37] Z. Zhao, T. Bao, Y. Li, X. Min, D. Zhao, T. Muhammad. The supported CeO_2/Co_3O_4–MnO_2/CeO_2 catalyst on activated carbon prepared by a successive-loading approach with superior catalytic activity and selectivity for CO preferential oxidation in H_2-rich stream. *Catalysis Communications* 48 (2014) 24-28.

[38] S. Lu, F. Wang, C. Chen, F. Huang, K. Li. Catalytic oxidation of formaldehyde over CeO_2-Co_3O_4 catalysts. *Journal of Rare Earths* 35 (2017) 867-874.

[39] G. Li, L. Li, Y. Yuan, J. Shi, Y. Yuan, Y. Li, W. Zhao, J. Shi. Highly efficient mesoporous Pd/CeO_2 catalyst for low temperature CO oxidation especially under moisture condition. *Applied Catalysis B: Environmental* 158-159 (2014) 341-347.

[40] Y. Liu, B. C. Liu, Q. Wang, C. Y. Li, W. T. Hu, Y. X Liu, P. Jing, W. Z. Zhao, J. Zhang. Three-dimensionally ordered macroporous Au/CeO_2-Co_3O_4 catalysts with mesoporous walls for enhanced CO preferential oxidation in H_2-rich gases. *Journal of Catalysis* 296 (2012) 65-76.

[41] C-F. Yan, H. Chen, R-R. Hu, S. Huang, W. Luo, C. Guo, M. Li, W. Li. Synthesis of mesoporous CoeCe oxides catalysts by glycine-nitrate combustion approach for CO preferential oxidation reaction in excess H_2. *International Journal of Hydrogen Energy* 39 (2014) 18695-18701.

[42] C-W. Tang, C-C. Kuo, M-C. Kuo, C-B. Wang, S-H. Chien. Influence of pretreatment conditions on low-temperature carbon monoxide oxidation over CeO_2/Co_3O_4 catalysts. *Applied Catalysis A: General* 309 (2006) 37-43.

[43] S. Varghese, M. G. Cutrufello, E. Rombi, C. Cannas, R. Monaci, I. Ferino. CO oxidation and preferential oxidation of CO in the presence of hydrogen over SBA-15-templated $CuO-Co_3O_4$ catalysts. *Applied Catalysis A: General* 443-444 (2012) 161-170.

[44] X. Chen, H. Zou, S. Chen, X. Dong, W. Lin. Selective oxidation of CO in excess H_2 over Ru/Al_2O_3 catalysts modified with metal oxide. *Journal of Natural Gas Chemistry* 16 (2007) 409-414.

[45] L. E. Go´mez, E. E. Miro, A. V. Boix. Spectroscopic characterization of Mn-Co-Ce mixed oxides, active catalysts for COPROX reaction. *International Journal of Hydrogen Energy* 38 (2013) 5645-5654.

[46] S. Varghese, M. G. Cutrufello, E. Rombi, C. Cannas, R. Monaci, I. Ferino. CO oxidation and preferential oxidation of CO in the presence of hydrogen over SBA-15-templated $CuO-Co_3O_4$ catalysts. *Applied Catalysis A: General* 443-444 (2012) 161-170.

[47] O. Pozdnyakova, D. Teschner, A. Wootsch, J. Krohnert, B. Steinhauer, H. Sauer, L. Toth. Preferential CO oxidation in hydrogen (PROX) on ceria-supported catalysts, part II: Oxidation states and surface species on Pd/CeO_2 under reaction conditions, suggested reaction mechanism. *Journal of Catalysis* 237 (2006) 17-28.

[48] F. Marino, F. Descorme, D. Dupre. Noble metal catalysts for the preferential oxidation of carbon monoxide in the presence of hydrogen (PROX). *Applied Catalysis B: Environmental* 54 (2004) 59-66.

[49] T-S. Nguyen, V. Morfin, V. Aouine, V Bosset, J-L. Rousset and L. Piccolo. Trends in the CO oxidation, PROX performances of the platinum-group metals supported on ceria. *Catalysis Today* 253 (2015) 106-114.

[50] D. Gamarra, A. Martínez-Arias. Preferential oxidation of CO in rich H_2 over CuO/CeO_2: Operando-DRIFTS analysis of deactivating effect of CO_2 and H_2O. *Journal of Catalysis* 263 (2009) 189-195.

[51] L. Pia, N. Yanga, W. Hanc, W. Xiao, D. Wang, Y. Xiong, M. Zhoua, H. Hou, X. Maoa. Heterogeneous activation of peroxy mono carbonate by Co-Mn oxides for

the efficient degradation of chlorophenols in the presence of a naturally occurring level of bicarbonate. *Chemical Engineering Journal* 334 (2018) 1297-1308.

CHAPTER 6

GENERAL CONCLUSIONS

This chapter presents the main conclusions on the preparation methods, effect of the reducing agent, effect of calcination temperature, effect of a promoter of the supported metal-based catalysts, and evaluation of the supported Pd metal-based catalyst in the conversion of CO in H_2 rich gas stream at 40 to 220 ^oC. The chapter also present the recommendation on the future research work.

6.1 PREPARATION OF THE CATALYSTS AND THEIR CATALYTIC EVALUATION

The Co_3O_4 and Co_3O_4(H) catalysts were successfully prepared by precipitation method. Both catalysts were reduced by 5% H_2/He to CoO and CoO(H). The Pd species was introduced on different Co_3O_4 by improved wet impregnation method. The XRD and TPR of Co_3O_4(H) catalyst indicated that a surface transformation occurred, as confirmed by an increase in the BET surface area. Although an in-situ reduction has occurred prior to calcination of CoO_xH_y(H), the FTIR data did not show peak ratio differences, which indicates that a usual amount of Co^{3+} and Co^{2+} were formed; which is consistent with the XRD, XPS and TPR data. Introduction of Pd species on the cobalt oxide did not change the structure of Co_3O_4 as indicated by XRD, XPS and TEM data, however, an increased in surface area was observed.

The PROX activity of the catalysts increased with CO/O_2 ratio (λ), and the formation of moisture was observed at higher CO/O_2 ratio (λ). The catalyst activity increased with temperature, especially within the fuel cells temperature window. This activity correlates with the surface properties of the catalyst and showed a very low moisture formation at temperatures above 120 ^oC. The PROX data of Co_3O_4(H) catalyst gave 85% CO conversion (with good selectivity) at 100 ^oC under dry conditions, which remained stable for 21 h. The Co_3O_4 catalyst is unstable and deactivated with time on stream at 100 ^oC. The PROX activity of Co_3O_4(H) catalyst in the presence of moisture deactivated from 100 to 70% and remained fluctuating steadily for almost 21 h. The Co_3O_4(H) produced almost 75% CO conversion in the presence of CO_2, which deactivate as time increased. The CoO(H) catalyst showed higher PROX activity at low temperature range, which could be due to the formation of Co^{3+} species as confirmed by TPR and XRD data.

The addition of Pd species on Co_3O_4(H) suppressed the activity of the catalyst in CO conversion, favour conversion of H_2 and formation of moisture. A decrease in CO conversion from 85% (over Co_3O_4(H)) to 51% (over 1wt.%Pd on Co_3O_4(H)) at 100 ^oC was observed, and the activity increased with time on stream for 21 h, due to water gas shift of the accumulated moisture. Similarly, the catalyst showed better stability under both moisture and CO_2 conditions for 21 h.

The 2wt.% metal oxides (CeO_2, MnO_2, MgO, Cr_3O_4, and TiO_2) on cobalt, and Pd supported on CeO_2-Co_3O_4 and MnO_2-Co_3O_4 were successfully prepared by co-precipitation method. The XRD data shows that introduction of the metal oxide on Co_3O_4 did not alter its structural phase, except for the composite with TiO_2 species. All samples showed good thermal stability as confirmed by TGA. The 2wt.%CeO_2-Co_3O_4 composite showed an improved surface area of 81.8 m^2/g compared to Co_3O_4(H). A decreased surface area to 70.9 m^2/g was observed when 0.5wt.%Pd is introduced. The presence of Pd species on the catalyst decreased the XPS intensity peaks, which suggest an increase in the Co^{3+}/Co^{2+} atomic ratio. A decrease in BET surface area of MnO_2-Co_3O_4 catalyst was observed with increased concentration of MnO_2. And a further decrease in surface area to 63.1 m^2/g was observed when 0.5wt.%Pd is introduced on 7wt.%MnO_2-Co_3O_4.

Although, 2wt.%MnO_2 on Co_3O_4(H) showed higher activity of 99.3% at 80 ^oC in PROX, both MnO_2 and CeO_2 improved the activity of Co_3O_4(H) at 100 ^oC. The higher activity of MnO_2 is attributed to the higher surface area of the composite catalyst (i.e., 249 m^2/g), in relation to ceria composite catalyst (i.e., 81.8 m^2/g). Although the MnO_2 species transformed the structure of Co_3O_4 by lowering the oxidation state to Co^{2+}, the spent catalyst showed transformation from Co^{2+} to Co^{3+} during PROX, as confirmed by TPR data.

An optimum activity in PROX was observed over 2wt.%CeO_2-Co_3O_4 compared to other ceria loadings (i.e., 3, 5, 8, 10, 15, 30wt.%CeO_2). However, the catalyst activity decreased slightly at 100 ^oC in the presence of 0.5wt.%Pd, which could be associated with a decrease in the surface area. The 0.5wt.%Pd-2wt.%CeO_2 species on Co_3O_4 lowered H_2 conversion, and the creation of oxygen vacancies by ceria species resulted in redox reaction of Co^{2+} to Co^{3+} as confirmed by XPS. Although its activity is lower,

the catalyst has shown good stability in dry, moisture and CO_2 conditions at 100 ^oC for 21 h.

The introduction of 7wt.%MnO_2 species on Co_3O_4 catalyst improved the activity at 60 ^oC, however, the catalyst could not improve the activities at higher temperatures. The lower activity could be due to a decreased surface area as concentration of MnO_2 increases. A further increase in activity at lower temperature was observed over 0.5wt.%Pd-7wt.%MnO_2/Co_3O_4 catalyst, which could be due to reduction of Co^{3+} to Co^{2+} in the presence of Pd, as confirmed by XPS data. The catalyst has shown good stability in dry, moisture and CO_2 conditions at 100 ^oC for 21 h. The hydrazine treated cobalt-based catalysts in the presence of palladium and manganese oxide is the promising catalysts for proton exchange membrane fuel cells technology.

6.2 RECOMMENDATIONS

The reductive pre-treatment, the presence of a metal oxide, and the Pd species play an important role in the activity of the catalyst in CO PROX reaction. However, the CO PROX depends on the preparation method than the surface area and the crystallite sizes of the materials. The preparation of the catalyst using different surfactant can improve the activity and selectivity of the materials in CO PROX reaction at lower reaction temperature. The study on the activity and selectivity of the materials in CO PROX reaction, in the presence of both CO_2 and moisture, has to be conducted at different temperatures.

APPENDIXES

Appendix A The chromatogram results of the CO, O_2 and H_2 feed obtained by by-passing the reactor before the catalytic test of 0.5wt.%Pd/-7wt.%MnO_2/Co_3O_4(H).

	Reten. Time (min)	**Area (mV.s)**	**Height (mV)**	**Area (%)**	**Height (%)**	**WO5 (min)**	**Compound name**
1	0.707	6.930	2.496	78.3	91.9	0.05	H_2
2	1.343	0.662	0.149	7.5	5.5	0.08	O_2
3	6.987	1.256	0.070	14.2	2.6	0.29	CO
	Total	8.848	2.715	100.0	100.0		

Reten = Retention.

Appendix B The chromatogram results of CO PROX over 0.5wt.%Pd-7wt.%MnO_2/Co_3O_4 (H) catalyst at 40 ^oC.

	Reten. Time (min)	**Area (mV.s)**	**Height (mV)**	**Area (%)**	**Height (%)**	**WO5 (min)**	**Compound name**
1	0.707	6.931	2.517	21.5	91.8	0.05	H_2
2	1.347	0.453	0.102	1.4	3.7	0.8	O_2
3	1.817	24.042	0.078	74.7	2.9	0.20	CO_2
4	6.980	0.762	0.045	2.4	1.6	0.28	CO
	Total	32.188	2.742	100.0	100.0		

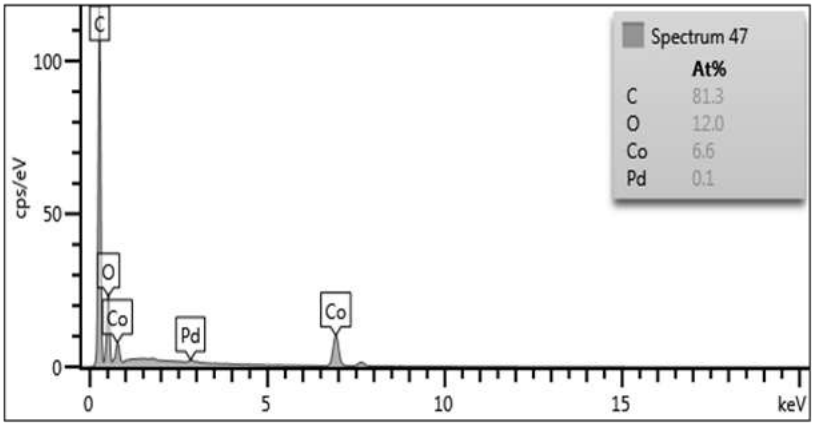

Appendix C The EDS analysis of 2wt.%Pd/(Co_3O_4(H)) sample.

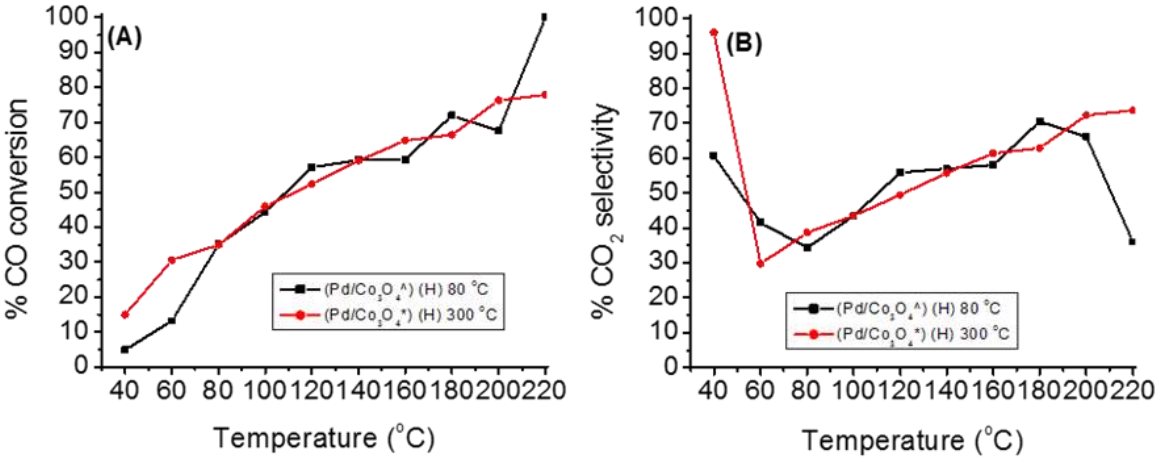

Appendix D The CO conversion (A), and CO_2 selectivity (B) of (a) (2wt.%Pd/Co_3O_4^) (H) 80 °C (■) and (b) (2wt.%Pd/Co_3O_4*) (H) 300 °C (●).

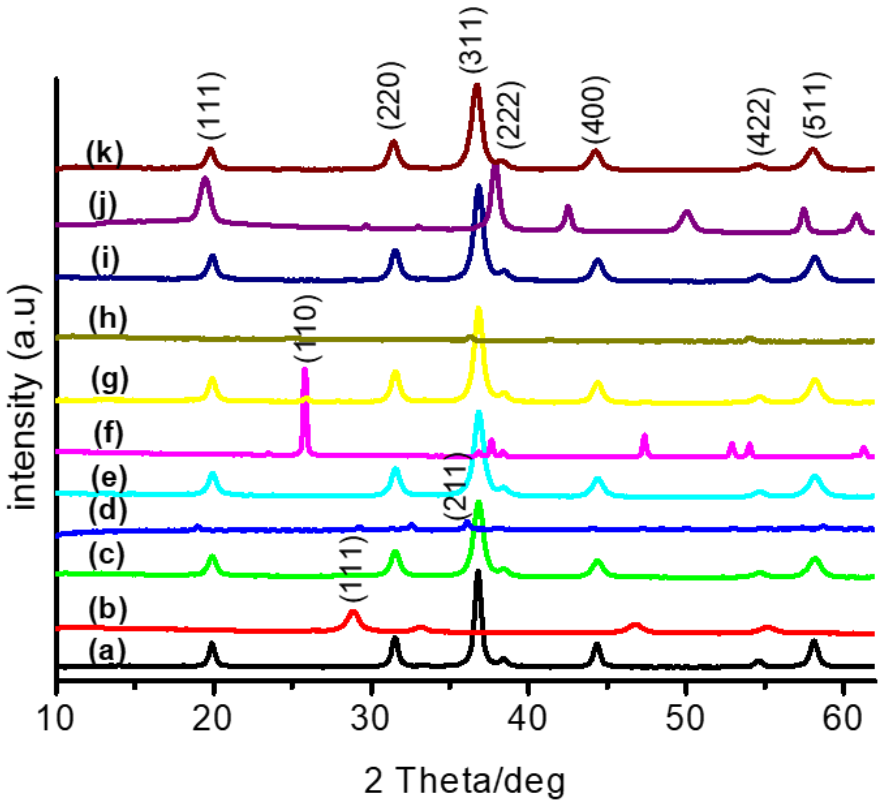

Appendix E The XRD patterns of (a) Co_3O_4 (H), (b) CeO_2, (c) 2%CeO_2-Co_3O_4(H), (d) MnO_2, (e) 2%MnO_2-Co_3O_4(H), (f) TiO_2, (g) 2%TiO_2-Co_3O_4(H), (h) MgO, (i) 2%MgO-Co_3O_4(H), (j) Cr_3O_4, and (k) 2%Cr_3O_4-Co_3O_4(H), catalysts.

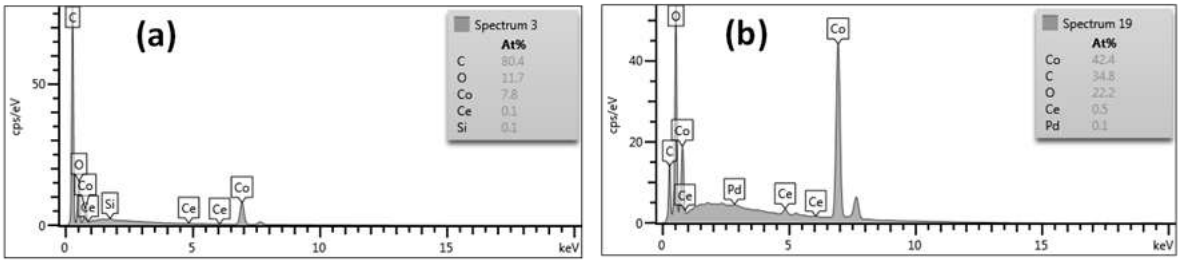

Appendix F The EDS analysis of (a) 2wt.%CeO_2-Co_3O_4(H), and (b) 0.5wt.%Pd-2wt.%CeO_2/Co_3O_4(H) samples.

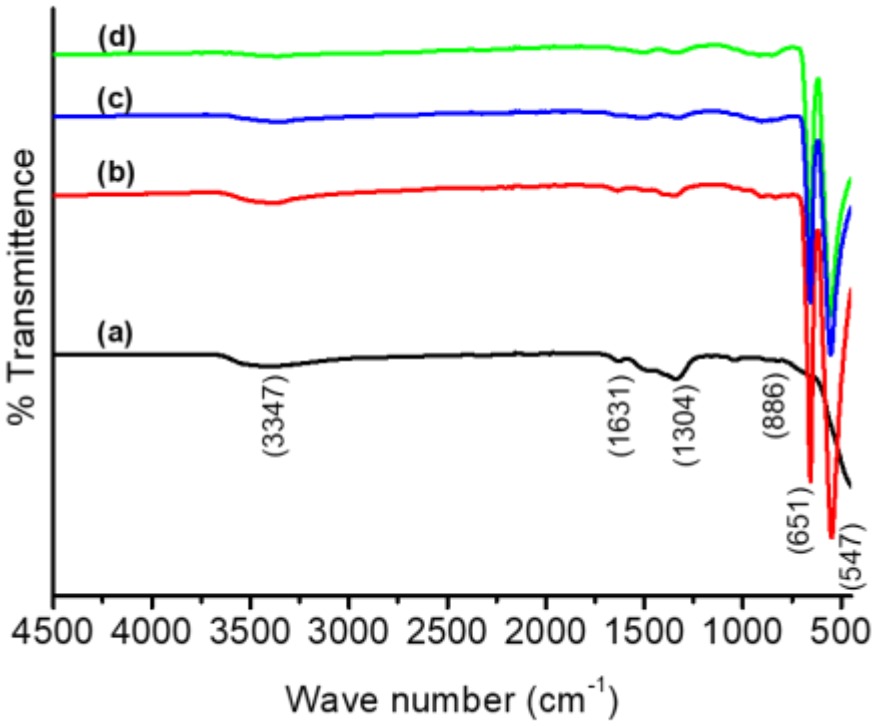

Appendix G The FTIR spectra of (a) CeO_2, (b) Co_3O_4 (H), (c) 2wt.%CeO_2-Co_3O_4(H), and (d) 0.5wt.%Pd-2wt.%CeO_2/Co_3O_4(H), catalysts.

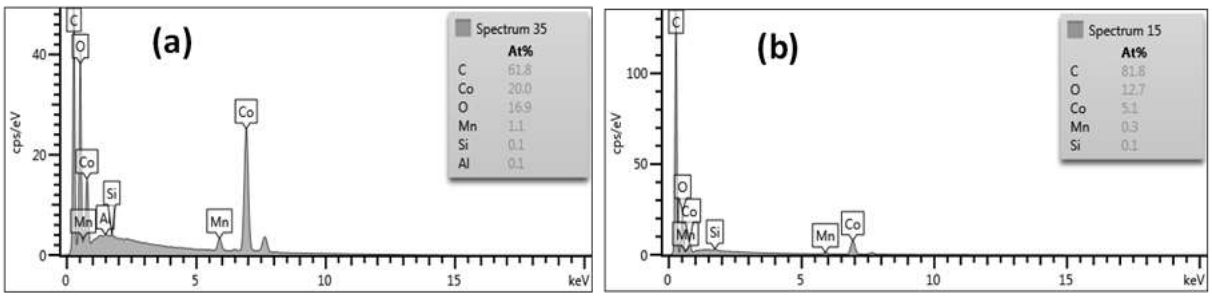

Appendix H The EDS analysis of (a) 7wt.%MnO_2-Co_3O_4(H), and (b) 0.5wt.%Pd-7wt.%MnO_2/Co_3O_4(H) samples.

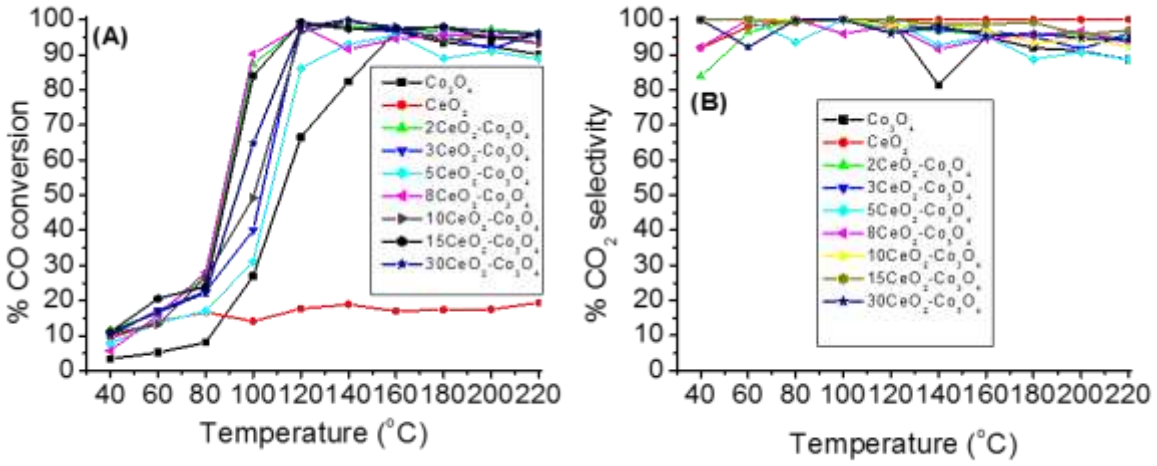

Appendix I The effect of ceria on PROX of CO over; (a) Co_3O_4 (■), (b) CeO_2 (●), (c) 2wt.%CeO_2-Co_3O_4 (▲), (d) 3wt.%CeO_2-Co_3O_4 (▼), (e) 5wt.%CeO_2-Co_3O_4 (♦), (f) 8wt.%CeO_2-Co_3O_4 (◀), (g) 10wt.%CeO_2-Co_3O_4 (▶), (h) 15wt.%CeO_2-Co_3O_4 (⬣), and (i) 30wt.%CeO_2-Co_3O_4 (★), catalysts.

Appendix J The effect of ceria load on CeO_2-Co_3O_4 in CO PROX reaction at temperature range of 40-240 °C at dry condition.

Catalyst	**CO conversion at 100 °C**	**T_{max}(°C)[a]**	**Maximum CO conversion (%)[a]**
3wt.%CeO_2-Co_3O_4	40.1	120	99.0
5wt.%CeO_2-Co_3O_4	31.1	160	95.7
8wt.%CeO_2-Co_3O_4	90.2	120	98.2
10wt.%CeO_2-Co_3O_4	49.2	140	99.5
15wt.%CeO_2-Co_3O_4	84.0	120	99.3

[a] T_{max} is the temperature achieving the maximum CO conversion.

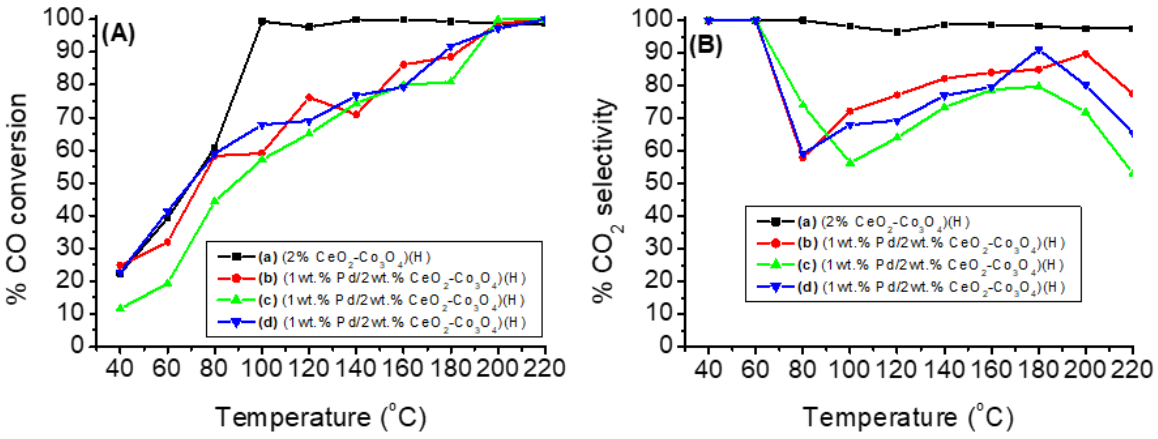

Appendix K The effect of introduction of Pd species on 2wt.%CeO_2-Co_3O_4 catalyst on PROX of CO; (a) (2wt.%CeO_2-Co_3O_4)(H) (■), (b) 1wt.%Pd/2wt.%CeO_2-Co_3O_4(H) impregnation (●), (c) 1wt.%Pd/2wt.%CeO_2-Co_3O_4(H) deposition (▲), and (d) 1wt.%Pd/2wt.%CeO_2-Co_3O_4(H) precipitation (▼), catalysts.